

Dissertation
submitted to the
Combined Faculties for Natural Sciences and for Mathematics
of the Ruperto-Carola University of Heidelberg, Germany
for the degree of
Doctor of Natural Sciences

presented by
Kathrin Leppek, M.Sc. Molecular Biosciences
born in Heidelberg, Germany
Oral examination on 10.03.2014

RNA Affinity Purification and Characterization of Roquin Proteins in CDE-mediated mRNA Decay

Referees: Prof. Dr. Bernd Bukau
PD Dr. Georg Stoecklin

It's Not Lupus.
- Dr. House

I hereby declare that I have written the submitted dissertation myself and in this process have used no other sources or material than those explicitly indicated.

The work was carried out at the German Cancer Research Center (DKFZ) in Heidelberg in the group "*Posttranscriptional Control Of Gene Expression*" of Dr. Georg Stoecklin.

I was granted permission from Cell Press (Elsevier) and Oxford University Press to reproduce material from two publications, of both of which I am first author. The respective License Agreements are stated in the Appendix.

Heidelberg, December 2013

Kathrin Leppek

Contents

Abstract	1
List of Figures	5
List of Tables	7
1 Introduction	9
1.1 The Cytokine Tumor Necrosis Factor- α	9
1.1.1 TNF α in Inflammation and Cancer	10
1.1.2 Macrophages are a Major Source of TNF α	11
1.1.3 Function of TNF α Protein	12
1.1.4 Regulation of TNF α Expression	13
1.2 Posttranscriptional Control of TNF α mRNA Expression	15
1.2.1 3'UTR Elements that Mediate TNF α mRNA Decay	15
1.3 mRNA Decay Machineries	23
1.3.1 The Major Eukaryotic Deadenylation Complexes	23
1.3.2 Exosome-mediated 3'-5' mRNA Degradation	24
1.3.3 Decapping and 5'-3' mRNA Degradation	25
1.3.4 P-bodies as Sites of mRNA Decay and Storage	26
1.4 The Roquin Protein Family	28
1.4.1 Immunological Relevance of Roquin and ICOS	28
1.4.2 Roquin and Roquin2 Knockout Mouse Models	29
1.4.3 Function of Roquin Proteins	30
1.5 mRNP Affinity Purification Techniques	32
1.5.1 Protein- and RNA-centric Purification Approaches	32
1.5.2 Bacteriophage RNA-protein Systems	33
1.5.3 RNA Aptamers for Purification	35
1.6 Aim of the Study	36
2 Results	37
2.1 An Optimized RNA Aptamer for mRNP Purification	37
2.1.1 Development of the RNA Aptamer S1m	37
2.1.2 Comparison to the PP7 and MS2 Systems	40
2.1.3 Higher Affinity of S1m for Streptavidin	43
2.1.4 Elution with Biotin and RNase	43

2.1.5	Purification of ARE-associated Proteins via 4xS1m . . .	45
2.1.6	Confirmation of Rbms1 and Roxan as Novel ARE-BPs . .	48
2.2	Roquin-mediated Constitutive Decay of CDE-containing mRNAs	52
2.2.1	The CDE is a Conserved Stem-Loop Motif	52
2.2.2	The P2-L2 Stem-Loop is Sufficient for CDE-mediated mRNA Decay	54
2.2.3	Identification of CDE-binding Proteins	57
2.2.4	Roquin and Roquin2 Specifically Bind to the CDE . . .	59
2.2.5	Roquin and Roquin2 Promote CDE-mediated mRNA Decay	65
2.2.6	Roquin Promotes CDE-mRNA Deadenylation by Recruitment of Ccr4-Caf1-Not	69
2.2.7	ICOS mRNA Contains a Functional CDE	69
2.2.8	Roquin Recognizes a Conserved Class of CDE-containing mRNAs	71
2.2.9	Interference with CDE-Roquin Binding Alleviates TNF α Suppression	74
3	Discussion	79
3.1	An Optimized RNA Aptamer for mRNP Purification	79
3.1.1	The 4xS1m Aptamer is More Efficient than S1	79
3.1.2	Successful 4xS1m-mediated RNP Purification	81
3.1.3	4xS1m Pulldown of Established and Novel ARE-BPs . .	82
3.1.4	Confirmation of Rbms1 and Roxan as ARE-BPs	83
3.1.5	Understanding mRNPs Through RNA Affinity Purification	83
3.2	Roquin-mediated Constitutive Decay of CDE-containing mRNAs	85
3.2.1	The CDE in the TNF α 3'UTR	85
3.2.2	The CDE is not a miRNA Binding Site	86
3.2.3	Established Structured RNA Degradation Motifs	86
3.2.4	The CDE Folds into a Conserved Stem-Loop Motif . . .	88
3.2.5	Roquin and Roquin2 Specifically Bind to the CDE . . .	89
3.2.6	Roquin is a Suppressor of TNF α Expression	90
3.2.7	Roquin Recruits the Ccr4-Caf1-Not Complex for mRNA Deadenylation	91
3.2.8	Structure-Function Analysis of Roquin Domains	92
3.2.9	Roquin Recognizes a Conserved Class of CDE-containing mRNAs	93
3.2.10	Physiological Consequences of the Roquin-CDE Interaction	93
3.3	Summary and Model	95
3.4	Outlook	97

3.4.1	S1m is a Powerful Tool for mRNP Analysis	97
3.4.2	The Roquin-CDE Complex and Roquin/2 Targets	97
3.4.3	Regulation of Roquin Proteins	99
3.4.4	Regulatory RNA Structures in Mammals	100
4	Materials and Methods	101
4.1	Materials	101
4.2	Methods	101
4.2.1	Cell Culture and Transfection	101
4.2.2	Plasmid Construction	102
4.2.3	Oligo Phosphorylation and Ligation	107
4.2.4	Polymerase Chain Reaction (PCR)	107
4.2.5	mRNA Decay Assay	107
4.2.6	Northern Blot Analysis	108
4.2.7	Western Blot Analysis	109
4.2.8	Antibodies	109
4.2.9	Recombinant Protein Purification	110
4.2.10	Cellular RNP Purification via S1/S1m Aptamers	110
4.2.11	Cellular RNP Purification via GST	111
4.2.12	<i>In vitro</i> Transcription	111
4.2.13	<i>In vitro</i> RNP Purification via S1m	112
4.2.14	<i>In vitro</i> RNP Purification via S1m and Biotin Elution	114
4.2.15	Mass Spectrometry	114
4.2.16	In-Line Probing	115
4.2.17	Quantitative RT-PCR	116
4.2.18	Protein-IP	116
4.2.19	RNA-IP	117
4.2.20	Electromobility Shift Assay (EMSA)	118
4.2.21	Knockdown by siRNA	119
4.2.22	Enzyme-linked Immunosorbent Assay (ELISA)	120
4.2.23	Morpholino Delivery	120
4.2.24	Data Sources for Sequence Alignments	121
4.2.25	RNA-IP, Library Preparation, Deep Sequencing and Data Analysis	122
4.2.26	Accession Numbers	122
	Abbreviations	123
	Publications	127
	Acknowledgments	129
	Bibliography	131

5	Supplemental Data	167
5.1	Supplemental Figures	167
5.2	Supplemental Tables	176
5.3	Roquin Protein Sequence Alignment	180
6	Appendix	185
6.1	Materials Used in this Study	185
6.1.1	Disposable Material and Kits	185
6.1.2	Chemicals and Enzymes	186
6.1.3	Technical Equipment	189
6.1.4	Antibodies	191
6.1.5	Plasmids	192
6.1.6	DNA Oligonucleotides	196
6.2	Permission Statements	199
6.2.1	Permission from Cell Press, Elsevier	200
6.2.2	Permission from Oxford University Press	203

Abstract

Tumor necrosis factor (TNF)- α is the most potent pro-inflammatory cytokine in mammals. The degradation of TNF α mRNA is critical for restricting TNF α synthesis and involves an AU-rich element (ARE) and a constitutive decay element (CDE) in the 3' untranslated region (UTR) of the mRNA. In the first part of my thesis, I optimized an RNA-based method to identify RNA-binding proteins (BPs) associated with TNF α mRNA. For this, I developed a modified streptavidin-binding RNA aptamer termed S1m. It has improved affinity for streptavidin and I found a four-fold repeat (4xS1m) to be most efficient. I then used TNF α ARE-4xS1m RNA to purify ARE-BPs from cellular extracts. By this, I found the majority of established ARE-BPs and confirmed Rbms1 and Roxan as novel ARE-BPs. The optimized 4xS1m aptamer therefore provides a powerful tool for the discovery of ribonucleoprotein (RNP) components.

In the second part of my thesis, I investigated the TNF α CDE in detail and found that the CDE is a 17 nucleotide long structured motif. Structural probing and mutagenesis provide evidence that it folds into a short RNA stem-loop in its active conformation. Using my 4xS1m protocol, I then identified CDE-associated proteins by mass spectrometry. Thereby, I found that the CCCH-type zinc and RING finger proteins Roquin (Rc3h1) and its paralog Roquin2 (Rc3h2) are stem-loop specific CDE-BPs. Next, I confirmed that the ROQ domain of Roquin specifically and directly binds to the CDE stem-loop. I could further show that Roquin is required for CDE-mediated mRNA decay and suppression of TNF α production in macrophages. TNF α expression was also increased by introduction of a morpholino that interferes with CDE-Roquin binding. My data provide evidence that Roquin proteins promote mRNA degradation by recruiting the Ccr4-Caf1-Not deadenylase complex. CDE motifs are highly conserved and are found in over 50 vertebrate mRNAs, many of which encode regulators of development and inflammation. In macrophages, I confirmed that CDE-containing mRNAs are the primary targets of Roquin on a transcriptome-wide scale. Thus, Roquin proteins act broadly as mediators of mRNA deadenylation by recognizing a conserved class of stem-loop RNA degradation motifs. In all, I unraveled a mechanism that adds an important component to the complex network that governs posttranscriptional control of gene expression.

Zusammenfassung

Tumor Nekrose Faktor (TNF)- α ist das wirksamste pro-inflammatorische Zytokin in Säugetieren. Der Abbau der TNF α mRNA ist entscheidend für die begrenzte Herstellung von TNF α und schließt ein AU-reiches Element (ARE) und ein konstitutives Abbauelement (CDE) in der 3' untranslatierten Region (UTR) der mRNA ein. Im ersten Teil meiner Doktorarbeit optimierte ich eine RNA-basierte Methode um RNA-Bindeproteine (BP), die mit der TNF α mRNA assoziiert sind, zu identifizieren. Dazu entwickelte ich ein modifiziertes Streptavidin-bindendes RNA Aptamer, genannt S1m. Es hat eine verbesserte Affinität zu Streptavidin, und ich fand heraus, dass eine vierfache Verkettung (4xS1m) am effizientesten ist. Dann verwendete ich TNF α ARE-4xS1m RNA, um ARE-BPe aus zellulären Extrakten zu reinigen. Dadurch fand ich die meisten etablierten ARE-BPe und bestätigte Rbms1 und Roxan als neue ARE-BPe. Das optimierte 4xS1m Aptamer stellt damit ein leistungsstarkes Hilfsmittel dar, um Ribonukleinsäure-Protein (RNP) Komponenten zu entdecken.

Im zweiten Teil meiner Doktorarbeit untersuchte ich das TNF α CDE im Detail und fand heraus, dass das CDE ein 17 Nukleotid-langes strukturiertes Motif ist. Strukturanalyse und Mutagenese zeigten, dass es sich in seiner aktiven Konformation in einen kurzen RNA Stem-Loop faltet. Indem ich das 4xS1m Protokoll anwendete, identifizierte ich dann CDE-assoziierte Proteine durch Massenspektrometrie. Dadurch fand ich, dass die CCCH-Typ Zink und RING Finger Proteine Roquin (Rc3h1) und dessen Paralog Roquin2 (Rc3h2) Stem-Loop-spezifische CDE-BPe sind. Anschließend bestätigte ich, dass die ROQ Domäne von Roquin spezifisch und direkt an den CDE Stem-Loop bindet. Ich zeigte weiterhin, dass Roquin notwendig ist für CDE-vermittelten mRNA Abbau und für die Suppression der TNF α Produktion in Makrophagen. TNF α Expression stieg durch das Einbringen eines Morpholinos an, das mit der CDE-Roquin Bindung interferiert. Meine Daten zeigen, dass Roquin Proteine mRNA Abbau fördern, indem sie den Ccr4-Caf1-Not Deadenylase Komplex rekrutieren. CDE Motive sind hochkonserviert in Vertebraten und finden sich in über 50 mRNAs, von denen viele für Entwicklungs- und Entzündungsregulatoren kodieren. Ich bestätigte CDE-enthaltende mRNAs als primäre Zielgruppe von Roquin auf Transkriptom-weiter Ebene in Makrophagen. Folglich agieren Roquin Proteine weitgehend als Vermittler von mRNA Deadenylierung indem sie eine konservierte Klasse von Stem-Loop RNA Abbaumotiven erken-

nen. Insgesamt entschlüsselte ich einen Mechanismus, der dem komplexen System, das die posttranskriptionelle Kontrolle von Genexpression steuert, eine wichtige Komponente hinzufügt.

List of Figures

1.1	TLR4-signaling and the TNF α Response upon LPS-activation of Macrophages.	14
1.2	Regulation of TNF α mRNA Expression upon LPS-stimulation.	19
1.3	Cytoplasmic Eukaryotic mRNA Degradation, Decay and Quality Control.	27
1.4	Roquin Regulation of ICOS Expression.	31
2.1	Improved Streptavidin-binding Efficiency of the S1m Aptamer.	38
2.2	The S1m Aptamer Does Not Interfere with ARE-mRNA Decay.	40
2.3	Recombinant Protein Purification and PP7cp Sequence Alignment.	41
2.4	Binding Efficiencies of the MS2 and PP7 Systems.	42
2.5	Binding Affinities of the S1 and S1m Aptamers.	44
2.6	Elution of the S1 and S1m Aptamers.	46
2.7	Schematic Representation of S1m-mediated <i>in vitro</i> RNP Purification.	47
2.8	Identification of ARE-BPs by 4xS1m RNA Affinity Purification.	49
2.9	Rbms1 and Roxan Specifically Bind to the TNF α ARE.	50
2.10	Mapping of the Mouse TNF α CDE.	53
2.11	The Active TNF α CDE is a Conserved RNA Stem-Loop Motif.	55
2.12	Mutational Analysis of the Mouse TNF α CDE.	56
2.13	Mutational Analysis of the TNF α CDE Stem-Loop.	58
2.14	CDE RNA Affinity Purification of CDE-BPs Enriches for Roquin and Roquin2.	60
2.15	Roquin Binding and Overexpression Analysis of CDE-mutants M7 and M9.	61
2.16	Specific Binding of Roquin to the CDE Inside Cells.	63
2.17	Specific Binding of Roquin to the CDE <i>in vitro</i>	64
2.18	Roquin Overexpression Accelerates CDE-mediated mRNA Degradation.	66
2.19	Roquin is Required for CDE-mediated mRNA Degradation.	67
2.20	The CDE Induces Caf1-dependent mRNA Deadenylation.	70
2.21	ICOS mRNA Contains a Functional CDE.	72
2.22	Genome-wide Identification of CDEs and Roquin Target mRNAs.	73
2.23	Confirmation of CDE-containing mRNAs as Roquin Targets.	75

2.24	Interference with CDE-Roquin Binding Elevates TNF α Expression.	76
3.1	Schematic Comparison of <i>in vitro</i> and <i>in vivo</i> S1m-mediated RNP Purification.	84
3.2	Roquin Promotes Constitutive Decay of CDE-containing mRNAs.	95
3.3	Characteristics of CCCH-type Zinc Finger Proteins in mRNA Decay.	99
5.1	S1m Sequence and pSP73-4xS1m Plasmid Map.	168
5.2	Sequence of the pSP73-4xS1m Plasmid.	169
5.3	Secondary Structure Determination and Comparison of TNF α CDE Variants.	170
5.4	Purification of Recombinant Roquin-N.	171
5.5	Knockdown of Roquin and Roquin2 Prevents CDE-mRNA Degradation.	172
5.6	Reproducibility of Roquin-IPs for RNA-Seq.	174
5.7	Induction of mRNAs Containing Putative CDEs and Roquin Target mRNA Validation.	175

List of Tables

4.1	List of Cell Lines.	101
4.2	List of Generated Stable Cell Lines.	103
4.3	PCR Reaction.	108
4.4	PCR Program.	108
4.5	<i>In vitro</i> Transcription Reaction.	112
4.6	RT Reaction for cDNA Synthesis.	116
4.7	qPCR Program.	117
4.8	List of RNA Oligonucleotides.	119
4.9	List of siRNAs.	120
4.10	List of Morpholinos.	121
5.1	CDE Sequences and Globin Reporter mRNA Half-lives in NIH3T3 Cells.	177
5.2	mRNAs Significantly Enriched by Roquin-IP.	178
6.1	List of Disposable Material and Kits.	185
6.2	List of Chemicals and Enzymes.	186
6.3	List of Technical Equipment.	189
6.4	List of Antibodies.	191
6.5	List of Generated Plasmids.	192
6.6	List of DNA Oligonucleotides.	196

1 Introduction

The ability of cells to rapidly alter their gene expression program depends on multiple mechanisms. The lifespan of messenger RNAs (mRNAs) is increasingly recognized as an important determinant in this respect. Despite the fact that cellular mRNAs share a common set of important structural features like the 5' cap and poly(A) tail, mRNA half-life can vary largely, spanning from less than one hour to >24 hours in mouse cells [1]. Short half-lives are particularly important for dynamically regulated transcripts whose expression needs to be rapidly turned on and off despite ongoing transcription. This includes mRNAs encoding transcription factors (TF), signaling components, cell cycle proteins and regulators of immune responses [2, 3, 4]. Particularly in the context of the immune system, a major focus of this study, posttranscriptional dampening of protein expression can actively promote the resolution of inflammation and is required to prevent autoimmune diseases and chronic inflammation [5]. In fact, the largest group of labile mRNAs in mammals encode pro-inflammatory cytokines. Most factors that mediate mRNA decay and translation repression bind to multiple *cis*-elements in the 5' or 3' untranslated region (UTR) of mRNAs. Together with translation and protein stability control, the cell is equipped to fine-tune gene expression according to environmental changes.

A classic example for highly integrated posttranscriptional expression control is the most potent pro-inflammatory cytokine in mammals, Tumor Necrosis Factor- α (TNF α), the main focus of this study. I will first introduce regulatory 3'UTR elements and decay machineries as mediators of mRNA decay in the context of TNF α regulation. Moreover, I will present the Roquin family of proteins. Finally, I will describe messenger ribonucleoprotein (mRNP) purification approaches that aim at identifying novel RNA-binding proteins (RNA-BPs) as regulators of TNF α .

1.1 The Cytokine Tumor Necrosis Factor- α

TNF α undergoes extensive transcriptional and posttranscriptional control [6, 7]. While the local production of TNF α at sites of injury or infection is important to trigger an immune response, its systemic or chronic release has detrimental consequences by causing septic shock and chronic inflammatory

diseases [8, 9]. Hence, immune cells need to maintain strict control over the expression of TNF α .

1.1.1 TNF α in Inflammation and Cancer

In response to bacterial components, especially lipopolysaccharide (LPS), TNF α is secreted by macrophages, a major source of this cytokine. Together with other cytokines, TNF α induces the acute-phase response of the immune system in the liver and changes cell metabolism to provide energy for fever and inflammation. In inflammation, TNF α plays a crucial role in the vasculature to locally contain infections. Initially, TNF α increases vascular permeability and blood flow, which enhances invasion of the infected site by immune cells. Later, small blood vessel clotting blocks systemic infection via the blood stream and thereby prevents septic shock. The pivotal role of TNF α in septic shock highlights its potent physiological and pathological capacity. On the one hand, during septic shock, excess TNF α is secreted by macrophages leading to increased systemic vascular permeability, plasma loss and reduced perfusion, which results in multiple organ failure. On the other hand, chronically decreased or increased TNF α also leads to numerous deleterious inflammatory and autoimmune diseases [10, 11]. Transgenic mice overproducing TNF α suffer from multi-organ or tissue-specific inflammation, leading to a spontaneous pathology resembling rheumatoid arthritis [12, 13]. Dysregulation of TNF α expression has been linked to chronic inflammatory arthritis, rheumatoid arthritis, inflammatory bowel disease, multiple sclerosis, asthma, cardiovascular diseases, type II diabetes, psoriasis, systemic lupus erythematosus, inflammatory Crohn's disease [8, 9, 14], as well as differential susceptibility to infectious diseases including tuberculosis and cerebral malaria [15, 16]. Importantly, restricted expression of TNF α by either macrophages or T lymphocytes is sufficient to induce intestinal inflammation [17].

The role of TNF α in cancer is less clear. Originally, TNF α was discovered as an activity that causes tumor remission upon bacterial infection, hence its name [18]. Later, the connection between LPS, macrophages and TNF α itself was discovered, which is responsible for this anti-cancer effect. This effect is primarily caused by the ability of TNF α to enhance tumor vasculature destruction and necrosis of malignant cells. However, due to its severe systemic toxicity and the risk of septic shock, therapeutic application of TNF α is restricted to individual extremities [18]. In contrast, tumors themselves secrete TNF α which promotes tumor growth, metastasis, DNA damage and neo-angiogenesis [18]. TNF α is also produced by adipocytes and is involved in adipose tissue regulation, energy mobilization and insulin resistance linking diseases like obesity and type II diabetes [19]. Numerous processes, pathways and deleterious

functions have been assigned to TNF α action which calls for a tight regulatory network balancing TNF α expression.

1.1.2 Macrophages are a Major Source of TNF α

The innate immune system is the first line of defense against pathogens which mediates a rapid, unspecific response to invaders. TNF α is mainly produced by macrophages primarily in response to bacterial and inflammatory stimuli like LPS [6]. It is expressed by many cells of the immune system, such as T and B lymphocytes and mast cells, but also by endothelial cells and neuronal tissues [20]. Macrophages have remarkable plasticity that allows them to alter their phenotype and physiology in response to immune signals [21]. Initially, detection of gram-negative bacteria by macrophages involves binding of the outer-wall component LPS to its cognate receptor complex, comprising the pattern recognition receptor (PRR) Toll-like receptor 4 (TLR4), as well as CD14 and MD2 [22] (**Figure 1.1A**). LPS-induced formation of this complex elicits different intracellular pathways directly activated by TLR4. As a consequence, indirect autocrine and paracrine signaling events are induced to initiate an innate immune response [23]. There are two main groups of macrophages, M1 and M2. The classically activated macrophages of the M1 “killer” type, stimulated via TLRs and interferon- γ (IFN γ), exhibit enhanced killing of microorganisms, increased expression of co-stimulators and elevated secretion of chemokines, cytokines like TNF α , and other communication signals to coordinate inflammation.

The well-characterized TLR protein family consists of membrane bound PRRs expressed by various cell types either located at the cellular surface (TLR1, 2, 4, 5, 6, 10) or in endosomes (TLR3, 7, 8, 9). There are in total 10 and 12 functional TLRs identified in human and mouse, respectively [22]. They detect a variety of extra- and intracellular pathogens or damage-associated molecular patterns [24, 25, 26]. Recognition of LPS by the TLR4/MD2 receptor complex leads to dimerization of TLR4 and downstream signaling via recruitment of the adaptors MyD88, TRIF, and TRAM. MyD88 orchestrates this early response which leads to activation of the I κ B/Nuclear Factor (NF) κ B (NF κ B) pathway as well as mitogen-activated protein kinase (MAPK) members p38, ERK1/2, and JNK. In activated macrophages and T-cells, NF κ B shuttles from the cytoplasm to the nucleus and binds to promoters of inflammatory effector proteins [27]. Signaling pathways elicited by LPS are summarized in **Figure 1.1A**. LPS-signaling then leads to rapid transcriptional and translational induction of AU-rich element (ARE)-mRNAs encoding pro-inflammatory proteins (such as TNF α , interleukin-1 β (IL-1 β), IL-6, cyclooxygenase 2 (COX-2), and IFN γ) [5].

For their primary function of rapid cytokine and chemokine secretion, activated macrophages dramatically increase their exocytotic trafficking activity. This promotes efficient vesicle transport to and fusion with the cell membrane [28]. Within 2 hours of LPS-stimulation, the newly synthesized transmembrane TNF α precursor accumulates in the perinuclear Golgi complex [29, 30], is packaged and is released in small vesicles from the *trans*-Golgi network. From there, it is delivered to sites of phagocytic cup formation [28].

Macrophages release pro- as well as anti-inflammatory mediators. Once activated, they are subject to tight control to prevent an overshoot. The release of the anti-inflammatory cytokine IL-10, the most potent inhibitor of macrophage activation, is one of the most critical anti-inflammatory feedback loops. Macrophage-derived IL-10 suppresses the expression of many cytokines (e.g. TNF α , IL-1, IL-6, IL-12, GM-CSF, IFN γ), several chemokines, and COX-2, during resolution of inflammation [31]. IL-10 further inhibits the differentiation of neighboring cells into activated macrophages. Most of this inhibitory effect of IL-10 appears to occur at the transcriptional level involving STAT3-signaling. The suppressive effect of IL-10 on TNF α expression depends on the TNF α 3'UTR [32]. IL-10 also reduces TNF α translation through inhibition of the p38-MAPK-MK2 pathway [33].

1.1.3 Function of TNF α Protein

TNF α is a type II transmembrane protein, whose ectodomain can be cleaved by the metalloprotease TNF α converting enzyme (TACE or ADAM17) [34], which is activated upon immune challenge. This releases a homotrimeric soluble form, sTNF α , into the blood stream [35]. The ubiquitously expressed TNF α receptor TNFR1 is fully activated by soluble and membrane-integrated TNF α . In contrast, a second receptor, TNFR2, is mainly expressed on hematopoietic cells and is primarily activated by membrane-bound TNF α . Both TNF α receptors trimerize upon ligand binding and trigger signaling pathways that involve the adaptor protein TRADD as a major mediator. Depending on the cellular context, TNF α can stimulate three different cascades [18, 35, 36] given in **Figure 1.1B**. One leads to the activation of the TF AP1 via induction of the MAPK pathway involving JNK-, p38-MAPK-, and ERK-signaling. Thereby, TNF α stimulates differentiation, proliferation and apoptosis. A second pathway results in activation of the TF NF κ B that shuttles to the nucleus and induces transcription of anti-apoptotic factors and mediators of cell survival, proliferation and inflammation. A third pathway induces caspase-mediated apoptosis, though it is antagonized by the anti-apoptotic function of TNF α -induced NF κ B. Signaling through TNFR1 mainly activates pro-inflammatory, cytotoxic and apoptotic responses. However, TNFR2, which lacks an intracel-

lular death domain, promotes cellular activation, proliferation and migration [37]. Additionally, cleaved TNFRs can competitively bind to TNF α [18] displaying reverse signaling and TNF α neutralization. This represents a complex signaling network that involves extensive crosstalk.

1.1.4 Regulation of TNF α Expression

Potentially harmful factors like TNF α are expressed in a regulated pulse. Regulation on multiple levels includes mRNA transcription, splicing, export, stability, and translation. Posttranslational control includes control of protein stability and activity by cleavage. These regulatory mechanisms are activated by LPS or TNF α itself. Upon LPS-stimulation, coordinate transcriptional control is accomplished by TFs selectively recognizing TNF α promoter elements [38]. Thereby, TNF α mRNA is transcribed within minutes independently of *de novo* protein synthesis [39]. This involves enhanceosomes [40]. The conserved proximal core promoter ~200 nt upstream the transcription start site is sufficient for transcription in response to LPS [41, 42, 43, 44]. This core promoter includes a TATA box and multiple *cis*-acting TF elements such as six NFAT binding sites, an Egr binding site, and a cyclic AMP response element (CRE). Numerous TFs induce TNF α mRNA synthesis, such as LITAF (LPS-induced TNF-alpha factor) and particularly NF κ B [45].

In the following, I give an overview of the main posttranscriptional mechanisms that regulate TNF α , as not all of them will be presented in further detail later. In lymphocytes, splicing of stored TNF α pre-mRNA occurs through a PKR-dependent 3'UTR element upon activation [46]. Export of mature TNF α mRNA from the nucleus in macrophages requires activation of the Tpl2 and ERK kinases [47], whereas spliced TNF α mRNA is retained nuclear in non-stimulated macrophages [47]. It was suggested that tethering of exon junction complex proteins to spliced TNF α mRNA facilitates ERK/ARE-dependent nuclear export [48]. In the cytoplasm, both translation and degradation of TNF α mRNA are extensively regulated [49, 50]. In particular, TNF α expression is fine-tuned by control of translation initiation and polyadenylation [49, 51]. Translation regulation includes the JNK pathway and particularly the p38-MAPK-MK2 pathway in the context of ARE-mediated mRNA stability control [52, 53, 54], as described later. Inhibition of JNKs blocks TNF α mRNA translation in LPS-stimulated macrophages [55]. PKR and its substrate fascin are also involved in 3'UTR-dependent regulation of TNF α and IL-6 translation upon LPS-stimulus [56]. Further, ARE-binding proteins (ARE-BPs) such as TTP, TIA-1, TIAR and FXR-1, also serve as repressors of TNF α mRNA translation via the ARE in macrophages. Tight posttranscriptional control of TNF α also involves several regulatory elements in the 3'UTR.

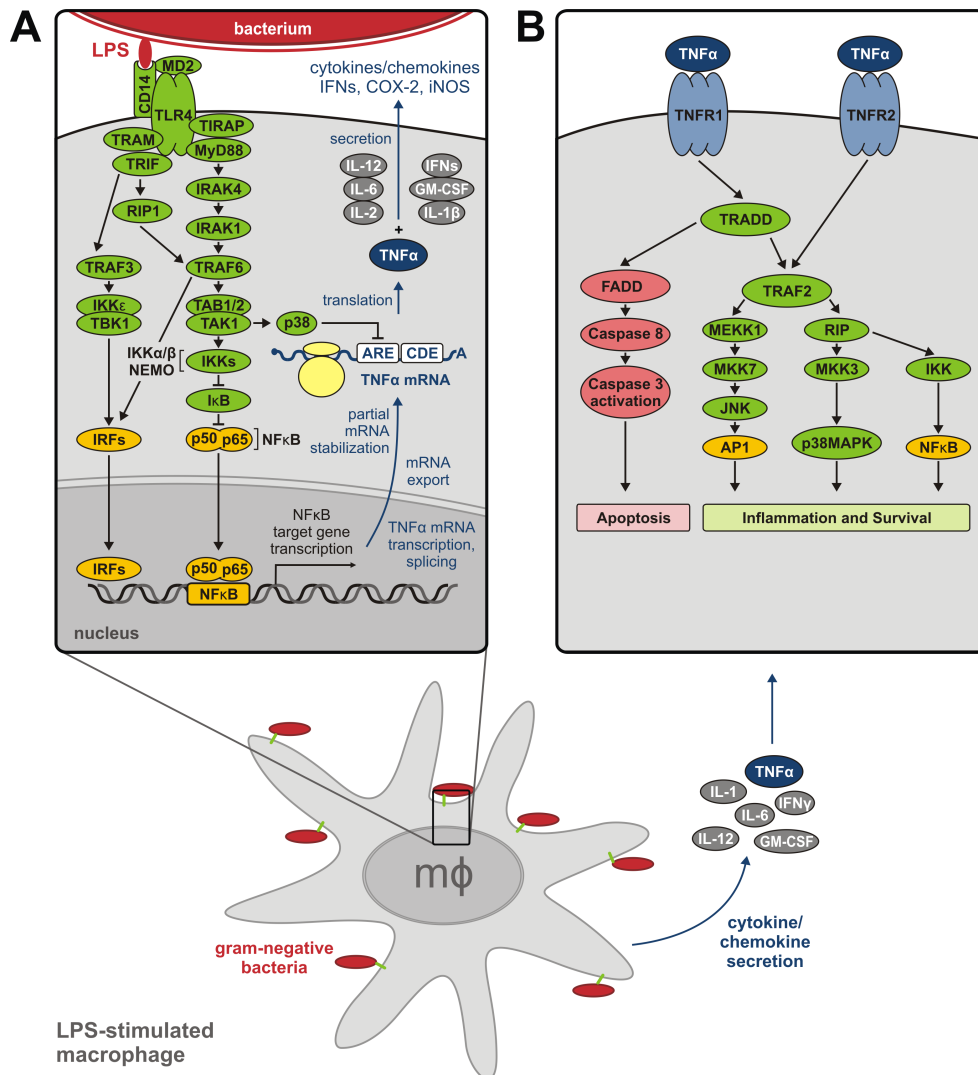


Figure 1.1: TLR4-signaling and the TNF α Response upon LPS-activation of Macrophages. (A) TLR4-signaling. LPS-stimulation of TLR4 triggers the association of MyD88 which recruits IRAK4 and IRAK1. Downstream signaling involves phosphorylation of IRAK1, TAB2, and TAK1. TAK1 phosphorylates the NF κ B-inhibitor complex IKK (IKK1, IKK2, NEMO). IKK then phosphorylates I κ B, which is ubiquitinated and degraded. NF κ B translocates to the nucleus and induces target transcription. In parallel, TRAF3 activates nuclear translocation of IRF TFs. This induces TNF α mRNA transcription, splicing, export, and partial mRNA stabilization via p38-MAPK. This leads to enhanced translation and secretion of TNF α . (B) TNF α -signaling. TNFR activation leads to the recruitment of adaptor proteins to activate multiple pathways. TNFR1 activation can have two different cellular context-dependent results. The default pathway is induction of genes involved in inflammation and cell survival. TNFR1-TNF α binding induces a range of inflammatory mediators and growth factors through activation of the AP1 TF or I κ B kinases (IKKs) that activate NF κ B. Alternatively, if NF κ B activation is inadequate, apoptosis is mediated through caspase 8 and others. This is a late response to TNF α . Figure adapted from: Schott and Stoecklin 2010, Balkwill 2009 [57, 18].

1.2 Posttranscriptional Control of TNF α mRNA Expression

Posttranscriptional control includes regulation of an mRNA's life from nuclear transcription to its degradation in cytosolic processing bodies (P-bodies). Several quality control mechanisms have evolved in parallel, and many were linked to TNF α mRNA. The ones not associated with TNF α mRNA regulation so far include nonsense-mediated decay (NMD), no-go (NGD), and non-stop (NSD) decay. These are means to detect and degrade aberrant transcripts harboring a premature stop codon, no start codon, or no stop codon, respectively. Thereby, these translation-dependent mechanisms mediate mRNA surveillance and ensure translational fidelity to protect the cell from potentially toxic proteins. An attempt to present all aspects of this field can only be incomplete without compromising to abstraction. This is why I will focus on important posttranscriptional mechanisms in the context of TNF α mRNA regulation [58].

1.2.1 3'UTR Elements that Mediate TNF α mRNA Decay

The regulation of some mRNAs requires the activity of several regulatory elements in the same UTR. Importantly, tight stability control of mRNAs encoding cytokines and chemokines is mediated by many 3'UTR destabilizing elements [57, 59, 5] (**Figure 1.2**). These are recognized by *trans*-acting factors and thus serve as platforms for the recruitment of the decay machinery. A prominent example is the ARE, a divergent and potent class of 3'UTR destabilizing sequences that controls the degradation and translational repression of many cytokine and TF mRNAs [60]. microRNA (miRNA) binding sites also contribute to mRNA decay. They are recognized by miRNAs whereby imperfect base-pairing leads to recruitment of argonaute (Ago) and TNRC6 proteins. This in turn causes translation repression and/or mRNA degradation [61]. A third instability element that so far is exclusive for the TNF α 3'UTR is the constitutive decay element (CDE) [62], the major focus of this study.

1.2.1.1 miRNA Binding Sites Induce miRNA-mediated Decay

miRNAs contribute to the posttranscriptional regulation of immune function [57]. Overall, small non-coding RNAs regulate the majority of eukaryotic genes by inducing translational repression and/or decay [63, 64]. miRNAs are ~22 nucleotide (nt) long single-stranded RNAs that are processed from longer precursors. This involves cleavage and export from the nucleus (reviewed by [64]). In short, a precursor pri-miRNA is transcribed from miRNA genes or

generated from introns (miRtrons) and is processed by the RNase III type endonuclease Drosha-DGCR8 complex to ~70 nt pre-miRNA hairpins. In mammals, the pre-miRNA is exported via exportin 5/Ran-GTP, associates with the endoribonuclease Dicer in complex with TRBP and Argonaute 2 (Ago2), and is cleaved by Dicer to obtain a mature miRNA. While one strand (passenger strand) of the miRNA duplex is degraded, the other (guide strand) functions as miRNA. It is bound by Ago proteins and confers target mRNA specificity to the RNA-induced silencing complex (RISC). As part of the RISC, the miRNA binds to partially complementary sequences mostly in the 3'UTR of target mRNAs. While the small interfering RNA (siRNA) pathway leads to direct endonucleolytic cleavage of base-paired miRNA-target site duplexes (RNA interference) [65], miRNAs mostly target an mRNA with imperfect base-pairing for which the context of the miRNA target sequence is crucial [66]. This includes a nucleating 5' seed region, a bulged mismatched central region and perfect complementarity to the miRNA 3' half to stabilize the interaction [67, 68]. mRNA-binding by RISC first leads to translational silencing followed by mRNA degradation via deadenylation [69, 70]. Here, the RISC component GW182 has a key role in recruiting both deadenylase complexes, PAN2-PAN3 and Ccr4-Not, to the target mRNA [71]. At the same time, GW182 promotes dissociation of poly(A) binding protein (PABP) from the poly(A) tail which inhibits translation [72, 73]. For silencing, miRNA-bound transcripts are delivered to P-bodies [74].

miRNA Binding Sites in the TNF α 3'UTR

The miRNA miR-125b participates in dampening TNF α expression [75, 76]. In resting macrophages, miR-125b binds to the TNF α 3'UTR and reduces its expression. In activated macrophages, miR-125b is downregulated, and TNF α mRNA becomes derepressed [75]. It is not yet clear whether miR-125b affects mRNA stability or translation. With no direct binding site predicted, miR-155, which is induced in LPS-stimulated macrophages [77, 76], enhances TNF α production by indirectly regulating mRNA stability or translation. Thus, the LPS-induced upregulation of miR-155 together with suppression of miR-125b allows for efficient induction of TNF α . Moreover, miR-369-3 is required for starvation-induced translational activation of TNF α by binding to the TNF α ARE [78].

1.2.1.2 AU-Rich Elements Induce ARE-mediated Decay

In the 1980s, AREs were discovered in the 3'UTR of many labile mRNAs coding for cytokines, proto-oncogenes and TFs in mammals [79, 80, 81, 82, 83, 84]

(reviewed by [85, 86]). AREs serve as binding sites for *trans*-acting ARE-BPs and miRNAs that cause mRNA decay and translation repression [87, 5, 82, 83, 84]. In case of TNF α mRNA, a strong ARE suppresses translation and causes rapid mRNA decay in the cytoplasm and thus prevents chronic inflammation [13]. Thereby, the ARE ensures low expression levels of potentially harmful proteins [88, 89, 90, 91]. This is reflected by the association of pathological states such as cancer, chronic inflammation and autoimmune diseases to deregulation of ARE-mediated decay (AMD) (reviewed by [92, 93]).

AREs are typically ~50 nt long sequences of high uracil and adenine content [2, 94]. They mostly contain multiple repeats of a canonical AUUUA pentamer, which is why cooperative binding of several factors in close proximity has been proposed [87]. Due to variation in copy-number, sequence and position of pentanucleotides among ARE-mRNAs, AREs were sorted into three different classes: Class I with one to three scattered AUUUAs and class II with at least two overlapping copies of the UUAUUUA(U/A)(U/A) nonamers. Class II AREs enhance deadenylation [95, 96, 97] and can contain a cluster of four to seven partially overlapping AUUUAs within a U-rich context. Class III AREs contain no AUUUAs, but a U-rich region [85]. Importantly, there is no strict consensus sequence for any ARE class. The Stoecklin lab has developed the AREScore algorithm to identify AREs genome-wide [98]. Most class II AREs are present in cytokine mRNAs, including TNF α , whereas TFs and cell cycle regulators mostly contain class I and III AREs. AREs are very common regulating 5-8% of all human mRNAs [99, 100, 81]. They are conserved in 75% of mammalian ARE-containing mRNAs comparing human, rat and mouse transcripts [101]. Among these, genes that regulate normal development or processes like adhesion, growth, differentiation, and apoptosis, are overrepresented.

ARE-mRNA stability is mainly regulated by altering mRNP composition that either promotes or represses decay and/or translation. Numerous studies focused on ARE-BPs that bind to AREs [84, 100]. Only in rare cases, the ARE itself can directly recruit the exosome [102]. The large number of ARE-BPs identified includes tristetraprolin (TTP), butyrate response factor 1 and 2 (BRF1, BRF2), AU-rich binding factor-1 (AUF1 or hnRNP D), KH splicing regulatory protein (KSRP), RHAU, Human antigen R (HuR) and other members of the embryonic lethal abnormal vision (ELAV) protein family, T cell intracellular antigen-1 (TIA-1), TIA-1-related protein (TIAR), and Fragile X mental retardation syndrome related 1 (FXR1) (for summary see [60]). ARE-BPs are evolutionarily conserved from yeast to mammals, exemplified by Cth2, the yeast ortholog of TTP, that globally regulates the expression of ARE-mRNAs in response to nutritional stress [103]. Several protein domains are able to specifically bind AREs, including the RNA recognition motif (RRM, found in TIA-1, TIAR, CUGBP2, HuR, AUF1 and AUF2), the zinc

finger (ZF) domain (TTP, BRF1 and BRF2) and the K-homology (KH) domain (FXR1 and KSRP). Each of these proteins can individually affect the translation and/or decay of ARE-mRNAs: Generally, TIA-1 [104], TIAR [104], FXR1 [105] and CUGBP2 [106] inhibit translation; TTP [107], BRF1 [108], BRF2 [108] and KSRP [109, 110] promote decay; AUF1 either promotes or inhibits decay [111, 112, 113, 114]; and HuR inhibits decay [115, 116] and either promotes [117] or inhibits [118] translation.

The ARE in the TNF α 3'UTR

The class II TNF α ARE of nine successive AUUUA motifs triggers a rapid, asynchronous and processive shortening of the poly(A) tail. Its crucial function for limiting TNF α overexpression *in vivo* was impressively illustrated in knock-in mice by deletion of the ARE in one of the TNF α alleles (TNF α Δ ARE) [13]. Even heterozygous animals developed chronic inflammatory arthritis and Crohn's-like inflammatory bowel disease. This was due to TNF α overproduction as shown in macrophages and synovial fibroblasts of these mice, which recapitulates the pathology in patients with rheumatoid arthritis [13]. In addition, analysis of autoimmunity-prone mice showed that they contained a spontaneous dinucleotide insertion in the TNF α ARE, which paradoxically correlated with reduced levels of TNF α and contributed to their development of lupus autoimmunity [119]. In line with this, TNF α transgenic mice suffer from inflammatory arthritis [12]. These results imply that posttranscriptional control is essential for to prevent spontaneous inflammatory diseases.

The destabilizing effect of the TNF α ARE is mainly mediated by the ARE-BPs TTP, BRF1 and BRF2, as well as KSRP and AUF1 [120, 113], whereas HuR and Hel-N1 are stabilizing ARE-BPs that competitively antagonize TTP [87, 116]. This illustrates the complexity of AMD. Moreover, the ARE also represses translation [49] via TTP, as well as TIA-1 and TIAR, which mediate translational silencing specifically in macrophages [121, 104, 122, 123, 124]. Upon stress, TIA proteins associate with translation initiation components and are directed to stress granules (SGs) [125]. HuR overexpression in macrophages correlates with reduced TNF α levels due to a strong translational block, along increased mRNA stability, which requires TIA-1 [118]. FXR1 represses translation of TNF α via the ARE in LPS-activated macrophages [105]. It also increases translation of an ARE-containing reporter mRNA upon serum starvation and cell cycle arrest [126]. Thus, environmental cues might convert the ARE from a repressor to an activator of translation, which correlates with the recruitment of FXR1 and Ago2 by the ARE, involving miR369-3 [126, 78]. Indeed, macrophages lacking FXR1 produce more TNF α than wild type (WT) controls, a consequence of enhanced translation [105].

The ARE-BP TTP is a Major Regulator of TNF α Expression

TTP, BRF1 and BRF2 comprise a family of related proteins with ZF domains for RNA recognition [128]. As a major regulator of TNF α mRNA, TTP is one of the best studied ARE-BPs [129]. TTP also destabilizes mRNAs encoding other inflammatory modulators, including granulocyte-macrophage colony-stimulating factor (GM-CSF), IL-2, IL-6, c-Fos, inducible nitric oxide (iNOS), COX-2, chemokine (C-C motif) ligand 2 (CCL2), CCL3, CXC-chemokine ligand 1 (CXCL1), IFN γ and IL-10 (reviewed by [130]). With regard to TNF α , TTP promotes rapid mRNA decay by binding to its ARE [107] and recruitment of the Ccr4-Caf1-Not deadenylase complex [131], the decapping enzyme Dcp2 [132] and the exosome [120, 133].

Similar to mice lacking the TNF α ARE, the phenotype of TTP-knockout mice indicates that its main function is to dampen inflammation. These mice develop cachexia, spontaneous arthritis, dermatitis, and neutrophilia [134, 107, 135]. They show chronic overproduction of TNF α as a result of increased stability and derepression of translation of TNF α mRNA, and exhibit severe signs of systemic inflammation [135, 134]. Treatment of these mice with TNF α -specific antibodies reverses almost all of the pathology, implicating TNF α to be the principal cause of this phenotype. This was confirmed by breeding TTP-deficient mice with mice lacking TNFR1 or TNFR2. Whereas TTP^{-/-}TNFR1^{-/-} mice did not develop cachexia or arthritis, TTP^{-/-}TNFR2^{-/-} developed more severe arthritis than mice lacking TTP alone [135]. This showed that TNF α binding to TNFR1 causes the described pathology.

In activated macrophages, the p38/MAP-kinase pathway is induced which leads to inactivation of TTP through direct phosphorylation by MAPK p38-MAPK-activated kinase 2 (MK2) on multiple serines and threonines [53, 54]. This triggers binding of 14-3-3 protein which blocks interactions with the decay machinery [136]. This inactivation of TTP contributes to the stabilization of TNF α mRNA [136] and translation derepression of TNF α and other targets. Paradoxically, macrophage stimulation also induces TTP expression [107]. Upon stimulation, ARE-mediated translational silencing of TNF α is overcome via an MK2-dependent pathway [52]. As a component of an alternative p38-activated translational regulatory pathway, MAPK signal-integrating kinase (Mnk) Mnk1 selectively promotes the translation of TNF α transcripts by phosphorylation of the translational silencer hnRNP A1 and its release from the TNF α ARE [137]. Recently, it was shown that TNF α mRNA translation at the ER requires HuR with either p38 MAPK/MK2 pathway activity or in absence of TTP [138]. MK2-phosphorylated TTP has decreased affinity to the ARE, is unable to replace HuR from the ARE, and thus allows for HuR-mediated TNF α translation initiation. This is also part of a feedback loop increasing TTP's own phosphorylation-regulated translation. In later stages

of inflammation, TTP is dephosphorylated by the phosphatase PP2A, which restores TTP activity [139]. This allows for immediate cytokine synthesis upon infection, yet ensures limited expression. In addition, stimuli like LPS and TNF α itself induce TTP transcription [140] as part of a feedback loop that dampens cytokine expression to promote resolution of inflammation [107].

It has also been controversially discussed whether miRNA and ARE function is integrated to control the expression of immune mediators [141, 142] (reviewed by [143]). It was proposed that in *Drosophila*, Dicer1, Ago1 and Ago2, in human cells only Dicer, are required for decay of TNF α ARE-containing mRNA reporters involving miR-16 [141]. The miR-16 seed sequence is only partially complementary to its proposed target site in the TNF α ARE, which makes it unlikely to efficiently target the ARE. It was claimed that an indirect interaction of miR-16 with TTP in complex with Ago proteins is required to assist in ARE-targeting. Presumably, TTP compensates for the weak complementarity of miR-16 to the ARE. Another report demonstrated that recognition of an ARE by miRNA-loaded RISC, in association with FXR-1, activates mRNA translation in quiescent cells [126, 78]. Contradictory, there is evidence that tethering of TTP to non-ARE transcripts alone can induce degradation. This demonstrates the ability of TTP to directly recruit the decay machinery without the need for miRNAs [133]. A more recent study used Dicer-knockout MEFs and knockdown of Dicer and Ago proteins in *Drosophila* cells to show that there is no general requirement of miRNAs for ARE function [142]. Hence, while involvement of miRNAs in regulating the expression of immune mediators is well established [57], their role in AMD is controversial.

Interestingly, while TTP targets like GM-CSF mRNA become fully stabilized in LPS-stimulated macrophages, TNF α mRNA stays labile [62]. This effect on TNF α mRNA can be assigned to the presence of a second element, the constitutive decay element (CDE) [62].

1.2.1.3 The Constitutive Decay Element

The CDE was previously described as a second destabilizing element in the TNF α 3'UTR [62]. Whereas AMD is transiently blocked during macrophage activation, the CDE was found to cause constitutive mRNA decay. Thereby, the CDE limits TNF α expression by promoting mRNA decay also under pro-inflammatory conditions.

It was initially found that in AMD-deficient human fibrosarcoma HT1080 cells, an mRNA reporter containing the fulllength TNF α 3'UTR was still labile [144]. This suggested a second, ARE-independent pathway targeting the TNF α 3'UTR for decay. In a subsequent study, deletion mapping and actinomycin D (actD)-chase experiments in mouse macrophages and fibroblasts showed that

a 80 nt long region downstream of the ARE mediates this decay activity [62]. This region was later narrowed down to an active element of 40 nt ([145]; Bernd Rattenbacher and Christoph Moroni, personal communication). The CDE is highly conserved in ten mammalian species. Thus, all mutants tested containing largely altered sequence stretches or mutated nucleotides, abolished CDE decay activity [62]. Signaling pathways that abrogate AMD did not affect CDE-mediated mRNA decay. Precisely, CDE-harboring mRNA reporters were insensitive to all established AMD inhibitors tested, which included LPS, ionomycin or TPA, or transfection with constitutively active forms of PI3K, MEK6 or v-H-ras [62]. This led to the name Constitutive Decay Element or CDE. The CDE has dramatic consequences for TNF α abundance upon immune challenge. TNF α mRNA remains short-lived irrespective of AMD inhibition as the CDE constantly targets it for decay, while TTP inactivation can only partially stabilize the mRNA. This provides a safeguard mechanism to prevent fatal TNF α overexpression.

Later, a biased crosslinking approach identified nucleolin as a CDE-binding protein (CDE-BP) [145]. Nucleolin is a large and abundant nucleolar RNA-BP that functions in ribosome biogenesis. It has been linked to AMD as binding of nucleolin to the ARE stabilized bcl-2 mRNA [146]. However, besides binding the Nucleolin Recognition Element (NRE), nucleolin interacts with numerous highly diverse RNA sequence motifs and is more considered a general RNA-BP [147]. Together with the fact that I did not confirm the nucleolin-CDE interaction (data not shown), the specificity and relevance of this is questionable and was not further investigated.

1.2.1.4 Other Regulatory Elements in Cytokine UTRs

Several short hairpins involved in mRNA stability control in cytokine and early response genes [5, 84] are distinct from, though often adjacent to, the ARE. Examples of such structured motifs are the CDE (TNF α , this thesis), SLDE (G-CSF), 2-APRE (TNF α), and a pseudoknot (IFN γ). Regulatory RNA structures in bacteria, e.g. riboswitches or thermosensors, are well-known as remnants of an ancient RNA world [148, 149], but are also present in modern genomes of higher eukaryotes [150, 151]. This is demonstrated by the increasing list of diverse roles of RNA structures in eukaryotic gene expression, including short and long non-coding RNAs, riboswitches, and structured motifs in mRNAs [152]. Most families of human regulatory RNA elements identified so far consist of short hairpins [153] which are the most wide-spread among known regulatory RNA structures [154].

RNA structures in TNF α and IFN γ mRNAs strongly activate the RNA-dependent protein kinase PKR [46], a stress kinase that is activated by

double-stranded RNA (dsRNA). The *cis*-acting RNA element 2-APRE (2-aminopurine response element) in the human TNF α 3'UTR, upstream of the ARE, acts at the level of pre-mRNA splicing [46]. The 104 nt 2-APRE contains a stable 17 bp stem-loop which mimics viral RNA. It locally activates PKR more potently than dsRNA. Activated PKR inhibits translation by eIF2 α phosphorylation [155] which blocks translation. 2-APRE renders TNF α pre-mRNA splicing dependent on PKR activation and increases splicing efficiency by locally activating PKR, while it does not reduce TNF α translation [46]. It was named 2-APRE because mRNA splicing becomes sensitive to inhibition by the PKR inhibitor 2-aminopurine. In case of IFN γ , PKR activation is mediated by a type H RNA pseudoknot in the 5'UTR. This in turn induces eIF2 α phosphorylation and inhibits its own translation locally [156]. Downstream of the ARE, the TNF α 3'UTR contains a second conserved AU-rich region containing a single AUAUUUAU motif, the "ARE-like stability and efficiency element" (SEE) [127]. It was suggested to function in translation efficiency and is bound by at least seven macrophage proteins, some of which compete for ARE-binding. Stability of G-CSF mRNA involves a 3'UTR hairpin termed "stem-loop destabilizing element" (SLDE), which is functionally distinct from its ARE [157, 158]. The SLDE hairpin, which contains a trinucleotide loop and a less than 11 base-pairs long stem flanked by unpaired sequence, promotes mRNA deadenylation under conditions where the nearby ARE is inhibited [157, 158]. IL-6 mRNA also contains a predicted stem-loop upstream of a non-canonical ARE; both elements cooperatively regulate mRNA stability [159].

1.3 mRNA Decay Machineries

Most eukaryotic mRNAs have a 5' cap and a 3' poly(A) tail that promote mRNA translation and circularization. They also protect the ends from exonucleases. mRNA decay machineries enzymatically execute transcript degradation. In eukaryotes, deadenylation is the rate limiting step [60, 160]. Degradation of the mRNA body can then follow two distinct pathways, each of which is initiated by a gradual poly(A) tail shortening (**Figure 1.3**). Then, the mRNA is either decapped and degraded via the nuclease Xrn1 in 5'-3' direction or further deadenylated and degraded by the exosome in 3'-5' direction.

1.3.1 The Major Eukaryotic Deadenylase Complexes

The main eukaryotic deadenylases are PAN2 (poly(A) nuclease 2) in complex with its binding partner PAN3, the Ccr4-Not complex containing the deadenylase Caf1 (Pop2 in yeast), and the Pop2-related PARN (poly(A)-specific ribonuclease) (reviewed in [60, 161, 160, 162, 163]) (**Figure 1.3**). The poly(A)

tail is shortened in two consecutive steps: Initially, PAN2-PAN3 initiates poly(A) trimming to a length of ~ 50 As, which is stimulated by binding to PABP [164, 161]. In PAN2-PAN3, PAN2 is the catalytic deadenylase while the pseudokinase PAN3 is the regulatory subunit. The PAN2-PAN3 structure was solved recently [165]. In a second step, the conserved Ccr4-Not complex completes the trimming of the bulk poly(A) tail to a length of 10-15 As [166, 164, 60]. Ccr4-Not, the major cytoplasmic eukaryotic deadenylase [167], which also has a role in transcription, is a large conserved complex of nine proteins, five of which are the canonical subunits (Ccr4, Pop2/Caf1, Not1, Not2 and Not3/5). In Ccr4-Not, only Ccr4 and Caf1 have 3'-5' exonuclease activity [163]. They are docked onto the scaffold protein Not1 [168, 140]. Ccr4, whose activity is blocked by PABP, is tethered to the Ccr4-Not complex through Caf1. The structure of Caf1 is known [169, 170], as well as the one of Caf1 in complex with Not1 [171]. Similar to Ccr4, the activity of Caf1 is dependent on the poly(A) tail length [172]. Overall, the conserved core of Ccr4-Not consists of at least two modules: the NOT module and a catalytic module comprising both Ccr4 and Caf1. The recent structure of the Not1-Caf1-Ccr4 interaction shows that the N-terminal arm of Not1 forms a docking site [173]. The ternary Not-module, minimally consisting of the C-terminus of Not1, Not2 and Not5 in yeast [174] and of the Not1, Not2, and Not3 C-terminal regions in human [175], have recently been crystallized. In yeast, Ccr4 is the main deadenylase while in mammals, Caf1 seems to be dominant [176]. The nuclease PARN is unique in that its processivity is enhanced by the presence of and it directly binds to the 5' cap [177, 178], but is inhibited by cap-binding proteins. Unlike PAN2-PAN3 and Ccr4-Not, PARN is a single protein that has no counterparts in yeast or *Drosophila* [60]. Thus, it is not essential in all eukaryotes. It is a nucleo-cytoplasmic shuttling protein but is mainly nuclear [164], where it destabilizes ARE-mRNAs in resting cells [179].

1.3.2 Exosome-mediated 3'-5' mRNA Degradation

Upon deadenylation, the exosome complex is the major 3'-5' RNA degradation complex that catalyzes 3'-5' degradation of mRNAs [180, 181]. The yeast core exosome (Exo-10) is an RNase complex consisting of nine catalytically inert subunits (Exo-9) and a single active RNase, Rrp44, with endonuclease and 3'-5' exonuclease activity [182, 183]. It forms a huge barrel-shaped complex with nuclear and cytoplasmic forms. The crystal structure of the yeast exosome and the associated Ski complex required for cytoplasmic function were recently solved [184, 185, 186]. These show how single-stranded RNA is funnelled into the Exo-9 channel by an unwinding pore whereupon Rrp44 captures the RNA 3' end that exits from the side of Exo-9. While the cytoplasmic form appears to target only mRNAs, the nuclear exosome is involved in 3' end processing

of small nuclear RNAs (snRNAs), small nucleolar RNAs (snoRNAs) and 5.8S rRNA [187, 188, 189]. In addition, it degrades aberrant mRNAs that are products of miss-splicing or -processing in the nucleus. After 3'-5' exosomal degradation, the 5' cap is removed by the scavenger decapping enzyme DcpS that is specific for oligonucleotides [190, 191].

1.3.3 Decapping and 5'-3' mRNA Degradation

Usually, mRNA deadenylation precedes decapping which is the irreversible removal of the 5' 7-methyl-guanosine (7meG) cap [192, 193]. This is followed by exonucleolytic degradation of the residual mRNA body. Shortening of the poly(A) tail to fewer than ~12 nts prevents PABP binding which normally inhibits the activity of the heterodimer Dcp1-Dcp2 decapping complex. The displacement of PABP allows the recruitment of Pat1, an enhancer of decapping and a repressor of translation [60] in *S. cerevisiae* [194], *Drosophila* [195] and mammals [196, 197], as well as of the Lsm1-7 heptamer, seven SM-like proteins [198], to the mRNA 3' end. This blocks further trimming. The Pat1-Lsm1-7 complex [199, 200] preferentially binds short terminal oligo(A) and oligo(U) tracts [201] and stimulates decapping by recruiting Dcp1-Dcp2 [202]. This complex consists of the decapping activator Dcp1 and the decapping enzyme Dcp2 [203]. In *S. cerevisiae*, the dimer Dcp1p-Dcp2p is responsible for cap removal upon deadenylation [204, 60]. In higher eukaryotes, the additional component Hedls (Ge-1) has decapping stimulatory activity in the complex [60]. The accessory proteins enhancer of decapping 3 (Edc3) and DExD/H-box RNA helicase Dhh1 (RCK/p54) join for efficient decapping. Edc3 is proposed to serve as a scaffold which forms a complex with Dcp1, Dcp2 and Dhh1. Following cap removal, the accessible 5' end of the mRNA body can be degraded by the cytoplasmic 5'-3' exoribonuclease 1 (Xrn1) [205, 206] (**Figure 1.3**). Recently, it was shown that Dcp1 and Xrn1 directly interact which couples decapping to 5' exonucleolytic decay [207]. Alternatively, or in addition, deadenylation can continue degradation from the 3' end via the exosome. While several components of the Ccr4-Not complex, as well as Xrn1, Dcp1-Dcp2 and Pat1-Lsm1-7, all localize to P-bodies [208], at least some decapping and 5'-3' decay occurs in *S. cerevisiae* while mRNAs remain with translating ribosomes. This suggests that ribosome dissociation and mRNA localization to P-bodies are not prerequisites for deadenylation [209].

With regard to ARE-mRNAs in mammals, deadenylation initiates decay by either mediating processive (classes I and III) or distributive (class II) poly(A) shortening [85]. Once deadenylated, the ARE-mRNA undergoes rapid degradation through the exosome [120, 210]. Alternatively, ARE mRNAs can also be degraded through the 5'-3' decapping-Xrn1 pathway in P-bodies

[132, 211, 212, 213]. It is still not clear whether the 5'-3' or the 3'-5' direction is the preferential pathway for degradation of ARE-mRNAs. Moreover, it has recently been shown that a set of transcripts, including ARE-mRNAs encoding IL-6 and IL-12b, are specifically destabilized via endonucleolytic cleavage of a stem-loop in their 3'UTRs by the ZF ribonuclease Regnase-1 upon TLR-stimulation of macrophages [214, 215, 216, 217].

1.3.4 P-bodies as Sites of mRNA Decay and Storage

P-bodies and SGs are discrete cytoplasmic foci that are enriched in mRNA catabolizing enzymes and translational repressors [218, 219, 208]. Thus, they participate in the regulation of mRNA translation or decay [102]. SGs form when polysomes disassemble in cells exposed to stress; eIF2 α kinases are activated and translation is globally inhibited [102] (reviewed by [123]). Thus, SGs serve as specialized storage sites where untranslated mRNAs are kept under stress. P-bodies are related RNA granules found in both stressed and unstressed cells [219]. Their formation is stimulated by the release of mRNAs from polysomes [220, 221]. At least the final steps of mRNA degradation are thought to occur in P-bodies [102, 208]. Components of the main 5'-3' mRNA decay pathway are concentrated there together with factors involved in translation initiation, deadenylation including Ccr4-Not and PAN2-PAN3 [222], decapping, 5'-3' exonucleolytic decay, NMD and miRNA-mediated mRNA decay. Translation factors found in P-bodies excludes eIF4E indicating the presence of non-translating mRNPs only. Thus, mRNAs are either degraded or stored there in a translationally silent state [218, 219]. In stressed cells, SG and P-bodies interact, which is regulated by proteins like shuttling ARE-BPs [102]. Thereby, mRNAs destined for decay are sorted at the SG and delivered to the P-body for degradation. Notably, ARE-mRNA delivery to P-bodies and SGs is a reversible process. Several destabilizing proteins such as ARE-BPs directly bind to components of the degradation machinery, e.g. Ccr4-Not, to direct their associated mRNAs to P-bodies [131]. Consequently, bound regulatory factors can enhance mRNA decay in P-bodies.

Upon binding to the ARE, TTP directly recruits mRNA deadenylases and exosome components [131], and nucleates the formation of P-bodies [223]. TTP can be recruited to both P-bodies and SGs and delivers ARE-mRNAs to them [213, 223]. It also facilitates the transfer of selected mRNAs between these distinct classes of RNA granules [213] and promotes interactions between them. In its active form, TTP is recruited to SGs, but it is excluded from them in its inactive phosphorylated form [136], accumulating in the cytoplasm. While TTP preferentially mediates degradation of ARE-mRNAs by the exosome [120, 109], the exosome is found in neither P-bodies nor SGs.

1.3 mRNA Decay Machineries

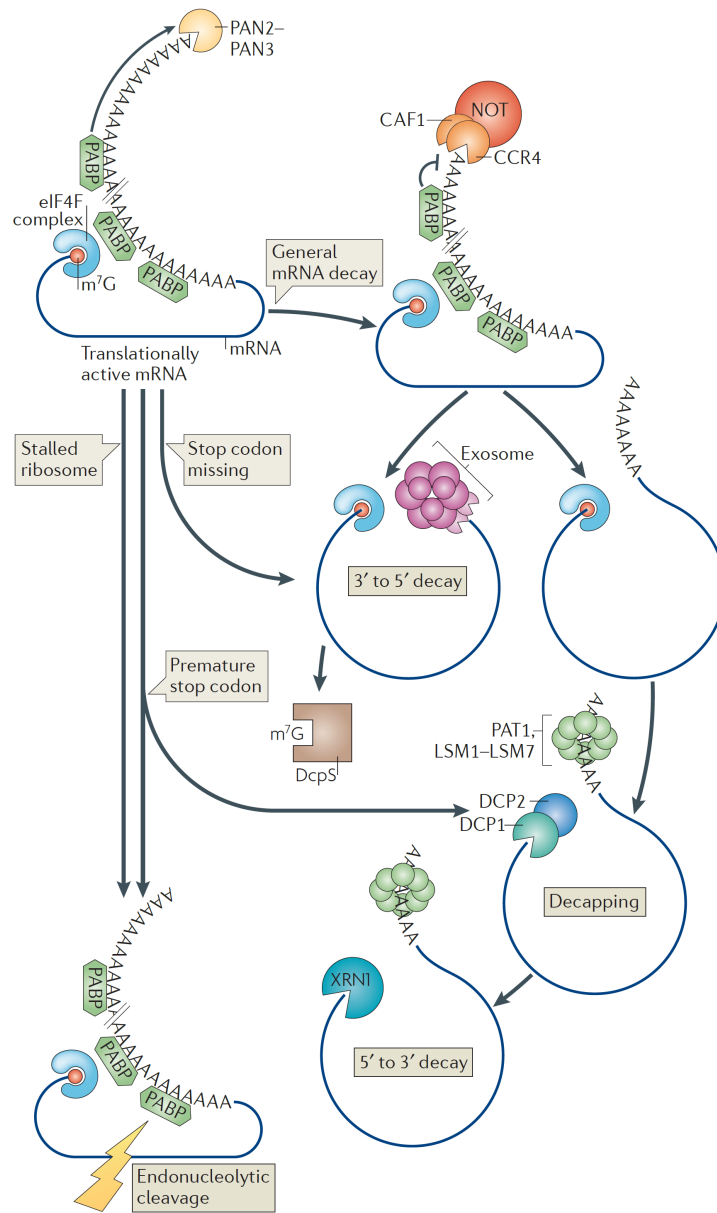


Figure 1.3: Cytoplasmic Eukaryotic mRNA Degradation, Decay and Quality Control. Most eukaryotic mRNAs undergo deadenylation-dependent decay. Initial poly(A) tail trimming by the PAN2–PAN3 deadenylase is stimulated by PABP. Default mRNA decay proceeds via further deadenylation by the Ccr4-Not complex, which is inhibited by PABP. It may be stimulated by RNA-BPs in an mRNA-specific manner. Trimming of the residual poly(A) tail yields a deadenylated intermediate that is no longer bound by PABP susceptible to both of two mechanisms: decay by further 3'-5' exonucleolysis by the exosome or, more frequently, by recruitment of the Pat1-Lsm1-Lsm7 complex, which stimulates decapping by Dcp1-Dcp2 and subsequent 5'-3' exonucleolysis by the exoribonuclease Xrn1. Several quality control mechanisms detect possible erroneous features of an mRNA leading to different outcomes. Upon exosome-mediated 3'-5' decay, the remaining cap is hydrolysed by DcpS. Figure modified from: Norbury 2013 [160].

1.4 The Roquin Protein Family

Roquin (Rc3h1) is a member of the Roquin protein family consisting of Roquin and its paralog Roquin2 (Rc3h2). Their names are due to their unique ROQ domain [224]. Roquin was previously found to suppress the expression of inducible T cell co-stimulator (ICOS), a co-stimulatory receptor on follicular T helper (TFH) cells, by accelerating ICOS mRNA degradation in T cells by targeting the ICOS 3'UTR [225, 226].

1.4.1 Immunological Relevance of Roquin and ICOS

In the *sanroque* mutant mouse (Roquin^{san/san}), that was identified in a random mutagenesis-based screen for autoimmunity phenotypes, the Roquin gene is exclusively affected harboring a point mutation. Homozygous *sanroque* mice contain a single amino acid substitution (M199R) in the ROQ domain of Roquin [227]. They display a severe, lupus-like autoimmune syndrome resembling systemic lupus erythematosus (SLE), autoantibody formation due to aberrant, excessive germinal center (GC) reactions [227], as well as intestinal inflammation in the small intestine but not the colon [228]. This phenotype results from an expansion of TFH cells with elevated ICOS levels due to its dysregulated expression based on Roquin's function as a repressor of ICOS [227, 225]. The M199R substitution in Roquin does not affect protein stability and is a rather hypomorphic mutation that only leads to intermediate upregulation of ICOS on the cell surface [227]. ICOS mRNA stabilization in cells expressing *sanroque* Roquin leads to enhanced T cell activation due to elevated ICOS co-stimulation, a common trigger of autoimmunity. Indeed, ICOS is associated with the pathogenesis of SLE: ICOS levels are elevated in SLE patients [229], and blockage of ICOS can prevent autoimmunity in mouse models of lupus [230]. Physiologically, ICOS is induced on activated T cells and is dependent on CD28 co-stimulation, while ectopic expression of ICOS on naïve T cells induces spontaneous differentiation and expansion of TFH cells [231]. ICOS binds to its ligand ICOSL, which is expressed on activated dendritic cells (DCs), monocytes, macrophages and B cells. It can also be induced on non-lymphoid tissues by inflammatory stimuli [232] (**Figure 1.4**). This plays a crucial role in TFH cell development, which is severely impaired in the absence of ICOS co-stimulation [233, 234]. Overexpression and deficiency of ICOS are both linked to autoimmune diseases. When naïve CD4+ T cells are stimulated with an antigen, they can further differentiate into several subsets depending on the context of activation. The formation of the TFH subset, which provides help to B cells in the GC reaction, is controlled by Roquin and supposedly miR-101 [227, 225]. Consistently, the ICOS repressor miR-

101 is highly expressed in naïve T cells, but downregulated in TFH cells. A second target of miR-101 and Roquin is neuropilin-1 [225], a surface protein that participates in the activation of T cells by mediating interactions between T cells and DCs [235]. Recently, in addition to ICOS mRNA, Ox40 mRNA was found to be specifically bound and regulated by Roquin and Roquin2 in a 3'UTR-dependent manner [226, 236]. INF γ mRNA was also reported to be destabilized by Roquin [237, 238]. Recently, Pratama *et al.* (2013) found that TNF α expression was increased in *sanroque* macrophages that show elevated inflammation in an arthritis model [239]. Icos originates from gene duplication of the more ancient but similar Cd28 gene that act via distinct pathways. It was suggested that Roquin ensures discrimination between ICOS and CD28 functions [240].

1.4.2 Roquin and Roquin2 Knockout Mouse Models

The complete knockout of Roquin causes perinatal lethality and malformations of the tail and spinal column, as well as insufficiently ventilated lungs [241]. However, the knockout of Roquin in the hematopoietic system did not cause autoimmunity, but a rather different, more inflammatory phenotype. A similar phenotype was observed for Roquin2 gene ablation in mice [236]. In comparison, heterozygous *sanroque* mice do not show autoimmunity but develop tumors resembling angioimmunoblastic T cell lymphoma (AITL) [242]. The effect of Roquin ablation in T cells was dominated by the expansion of eosinophilic granulocytes, macrophages and CD8+ effector-like T cells [241]. Mice with Roquin-deficient T cells showed increased ICOS levels on T cells and failed to elicit elevated numbers of TFH cells or anti-nuclear antibody responses [241]. In contrast, conditional deletion of Roquin2 did not lead to increased CD8+ effector-like T cells or ICOS or Ox40 induction [236]. In B cells, Roquin knockout led to impaired immune homeostasis; particularly expansion of total B, regulatory T, activated CD4+ and CD8+ T, and germinal center B cells [241]. Therefore, in the hematopoietic system, Roquin is required to maintain immune homeostasis, while loss of Roquin is not sufficient to cause autoimmunity. Thus, the conditional gene ablation of either Roquin [241] or Roquin2 [236] in mice did not recapitulate the phenotype of the *sanroque* mouse model. However, mice harboring the combined deletion of both paralogs in CD4+ T cells develop lymphadenopathy and splenomegaly with increased spleen weight, as well as cellularity with increased TFH cell and GC B cell numbers, which phenocopies *sanroque* mice [236]. Thus, on the one hand, this suggests a functional redundancy between Roquin and Roquin2 in the control of T cell activation and TFH cell differentiation [236]. It was proposed that the lack of compensation of Roquin-defects by Roquin2 in *sanroque* mice

may be due to the mutated protein retaining its scaffold position within RNA granules, preventing Roquin2 to access target mRNAs for regulation [239]. On the other hand, it is likely that the complex phenotypes of the hematopoietic Roquin knockout and *sanroque* mice may in fact arise from the simultaneous deregulation of multiple mRNAs encoding regulators of the immune system or of early development.

1.4.3 Function of Roquin Proteins

The Roquin protein family contains the two paralogs Roquin (Rc3h1) [227] and Roquin2 (Rc3h2, also membrane-associated nucleic acid binding protein, Mnab) [243]. They harbor a single C3H-type ZF, as found in the ZFP36 family including TTP, a RING (really interesting new gene) domain and an exclusive ROQ domain [224] (**Figure 1.4**). Roquin protein is highly conserved from humans to sponges (see alignment in the Supplemental Data) and is ubiquitously expressed in almost all tissues. Roquin2 is however generally lower expressed compared to Roquin, five-fold in T cells [236]. The two paralogs are very similar in primary sequence and domain organization, predominantly in the C-terminal portion, while Roquin2 has an extended C-terminus harboring a predicted hydrophobic patch. This was speculated to allow Roquin2 to insert into the plasma membrane [243]. Roquin2 was otherwise only known to be a nucleic acid binding protein [243]. Roquin instead has a C-terminal coiled-coil domain that might mediate oligomerization. Due to its N-terminal RING domain, Roquin was suggested to have RING-type E3 ubiquitin ligase activity [227]. While uninvestigated in mammals, the single Roquin protein homolog RLE-1 in *C. elegans* was shown to induce the degradation of the transcription activator DAF-16 by ubiquitination [244]. The RLE-1 C-terminus interacts with DAF-16 while the RING domain mediates DAF-16 ubiquitination for proteasomal degradation. The Foxo3a homolog DAF-16 is important for stress resistance and longevity. Thus, its RLE-1-mediated degradation shortens the worm's lifespan. Previous studies indicate that the ZF domain in Roquin/2 is not required for mRNA interaction but the ROQ domain is involved in RNA binding [226, 245]. Of note, the *sanroque* mutation did not interfere with RNA binding [245]. It was proposed that the putative Roquin/2 binding motif in the ICOS mRNA is located 100-200 nts downstream of the stop codon [226, 236], as was a short 47 nt long sequence adjacent to the miR-101 site at the 3' end of the 3'UTR [225]. Thus, the ICOS 3'UTR might contain several *cis*-acting elements.

1.4 The Roquin Protein Family

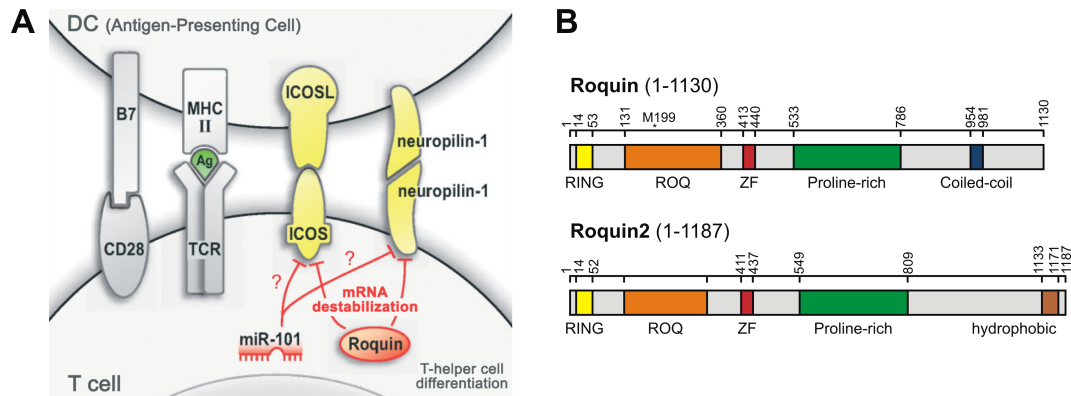


Figure 1.4: Roquin Regulation of ICOS Expression. (A) Roquin, possibly together with miR-101, destabilizes the ICOS and neuropilin-1 mRNAs in naïve CD4⁺ T cells. ICOS and neuropilin-1 are upregulated during differentiation into TFH cells and mediate interactions with dendritic cells (DC). Downstream ICOS-signaling is mediated via PI3K recruitment. (B) Domain architecture of Roquin family proteins Roquin and Roquin2. M199 indicates the position of the Roquin *sanroque* mutation. Figure A modified from: Schott and Stoecklin 2010 [57].

It was previously reported that Roquin suppresses ICOS mRNA expression via miRNAs [225]. In contrast to Yu *et al.* (2007), who proposed that Roquin destabilizes ICOS mRNA together with miR-101, a more recent study found that Roquin acts on ICOS mRNA independently of miRNAs [226]. We observed that CDE-mediated mRNA decay, which is caused by Roquin as demonstrated in this study, is Dicer-independent (Johanna Schott, data not shown, [246]). This also argues against the involvement of miRNAs in Roquin-mediated suppression. Glasmacher *et al.* (2010) also show that Roquin directly binds to ICOS mRNA via the 3'UTR without the need for miRNA interaction [226]. The Roquin mRNA 3'UTR might itself be regulated by miR-223, as shown in mouse colon intraepithelial lymphocytes [247]. Interestingly, the *sanroque* mutation M199R in ROQ does not impair Roquin binding to ICOS mRNA, but is rather likely to prevent the interaction with critical effector proteins [245]. Roquin-mediated repression requires functional RNA-independent cooperation with other decay-related proteins such as the decapping components Rck and Edc4 [226]. This suggests that Roquin causes ICOS mRNA degradation via the decapping pathway. Further studies are required to clarify the precise mechanisms by which Roquin recognizes its target mRNAs including characterization of a precise binding motif.

The etiology of the Roquin *sanroque* mutation-induced autoimmune syndrome has been linked to SGs [227, 225]. Roquin, *sanroque* Roquin and Roquin2 are cytoplasmic and localize to P-bodies or SGs while ICOS mRNA localizes to both SGs and P-bodies [227, 226, 245]. Hereby, the ROQ domain alone was

sufficient for SG localization [245], whereas a C-terminal deletion mutant was impaired in P-body localization [226]. Recently, analysis of a RING- and a ROQ-deletion mutant mice of Roquin and Roquin2 showed that both Roquin mutants disrupted ICOS mRNA regulation. While the ROQ mutant of Roquin still localized to SGs, RING-deficient Roquin failed to do so, which allowed Roquin2 to compensate in ICOS repression [239]. As Roquin shuttles between P-bodies and SGs in T cells upon stress [226], it was suggested that Roquin might cause mRNA degradation by directing translationally silenced mRNAs from SGs to P-bodies [225]. With the examples of the ZF proteins TTP, Regnase-1, and Roquin, a set of CCCH-type ZF and/or P-body proteins are recognized to have an important function as immune regulators that control RNA metabolism.

1.5 mRNP Affinity Purification Techniques

mRNAs are controlled by *trans*-acting factors at virtually every step of their complex lives [248, 249, 250]. The fate of any given mRNA is essentially determined by its mRNP complex, i.e. the ensemble of proteins and regulatory RNAs an mRNA interacts with. Although decades of research have uncovered specific functions of numerous RNA-BPs, surprisingly little is known about the composition, heterogeneity and dynamics of whole mRNPs.

1.5.1 Protein- and RNA-centric Purification Approaches

There are essentially two strategies to explore the content of mRNPs: protein-based or RNA-based methods [251]. On the one hand, protein-based approaches rely on the immunoprecipitation of a particular RNA-BP with an antibody together with all associated mRNAs, whose identity can be determined by cDNA cloning, microarray analysis (RIP-ChIP) or deep sequencing (RIP-Seq) [252]. RNA-sequencing technologies in combination with crosslinking protocols, e.g. (i)CLIP, PAR-CLIP and HITS-CLIP, recently emerged as efficient tools to identify protein recognition sites at a transcriptome-wide level [253, 254, 255, 256] (reviewed by [257]). These approaches are increasingly applied to investigate whole RNA interactomes for a specific protein. This is in line with deep sequencing becoming broadly available with decreasing cost and high throughput. Such protein-based approaches provide the spectrum of target mRNAs a particular RNA-BP interacts with. However, they do not reveal the complexity and dynamics of mRNPs. This means whether different proteins associate with the same mRNA in a cooperative, independent or competitive manner. These methods are technically challenging in addition. As

native protein-based purifications have previously been widely used to identify protein components of mRNPs (e.g. [258]), specific mRNAs cannot be assigned to interacting proteins, as indirect RNA interactions might be detected.

These limitations call for alternative, RNA-centric strategies for mRNP isolation. Here, a single mRNA species is purified together with its associated proteins and RNAs. These can be identified by mass spectrometry (MS) and RNA-Seq, respectively. The advantage of this alternative approach is that one obtains a less biased picture of the mRNP, including proteins that were not known to interact with a certain RNA. Ideally, RNA-based purification should reveal changes that occur during the lifetime of an mRNP or in response to signaling events. However, this approach faces major difficulties: finding a suitable way to purify a specific mRNA in the context of its chaperoning proteins as part of an intact mRNP; the generally low abundance of mRNAs compared to proteins in the cell; and the scale of purification needed for successful identification of proteins by MS. Moreover, some RNA-BPs bind to mRNAs only transiently with high off-rates in a regulatory manner. This calls for the need to crosslink prior to RNP-purification [259]. This freezes the mRNP in its current composition in the cell, a step that comes along with its own set of disadvantages. The two most prevalent principles for RNA-mediated mRNP purification either make use of RNA-protein interactions found in nature or of *in vitro* selected aptamers that exhibit high affinity for specific ligands.

1.5.2 Bacteriophage RNA-protein Systems

One way to purify endogenous RNA-protein complexes by using antisense oligonucleotides, as exemplified by the isolation of the telomerase RNP [260] or bulk poly(A)-mRNPs via oligo(dT) [261, 262]. A different approach exploits naturally occurring, bacteriophage-derived RNA-protein interactions of high specificity and affinity consisting of a bacteriophage RNA structure and an RNA-binding portion. One such example is the boxB RNA motif, which binds to the λ N peptide of the *Escherichia coli* (*E. coli*) bacteriophage λ antiterminator protein N [263, 264]. Another example is the coat protein (cp) from the single-stranded group I RNA bacteriophage MS2 of *E. coli*. As a dimer, MS2cp binds tightly to an 19 nt RNA stem-loop, termed operator hairpin or MS2 binding site (MS2bs), in the MS2 RNA. Precisely, the hairpin is at the 5' end of the viral replicase sequence encompassing the replicase start codon and thereby represses its translation [265, 266]. Upon cp aggregation for capsid assembly, translation repression is released. The MS2 protein-RNA interaction has been studied extensively and its crystal structure has been solved [267, 268, 269]. The *Pseudomonas aeruginosa* (*P. aeruginosa*) bacteriophage PP7cp binds with high specificity to a distinct stem-loop in the PP7 RNA

[270, 271]. Its recognition specificity differs substantially from the one of its distant relative coliphage MS2, as the cps only share 13% sequence identity [270, 271, 272]. The PP7cp dimer is also a translational repressor that binds a single translational operator hairpin in the replicase initiation site [270]. The PP7 binding site (PP7bs) has structural features that make it unrecognizable by the cps of other phages, which is beneficial for applications that use both systems simultaneously. The MS2 and PP7 RNA hairpins differ in the position of a bulged A as well as in the size and nucleotide composition of the loop [272].

These systems (λ N peptide, MS2cp and PP7cp) have proven powerful for visualizing RNAs in living cells [273]; and for tethering approaches whereby proteins of interest are fused to λ N, MS2cp or PP7cp, and are artificially attracted to reporter mRNAs bearing the respective recognition motifs inside cells [274, 275, 276, 196]. MS2 has also been used in a yeast three-hybrid system to identify RNA-BPs for regulatory RNAs [277]. With regard to RNP purification, the λ N peptide has been applied for coupling *in vitro* transcribed RNAs to a matrix with the aim of capturing RNA-associated proteins from cellular lysates [264]. MS2 was used for purification of highly stable RNPs such as the U1 snRNP [267], less stable mRNPs [278] from both yeast and mammalian cells, as well as RNPs associated with non-coding regulatory RNAs [279, 280, 281, 282]. Precisely, for the latter, MS2-tagged RNA was used to elucidate RNA-RNA and RNA-protein interactions, namely miRNAs with MS2bs-tagged long intergenic non-coding RNA-p21 [280], protein and RNA interactors of lncRNA-MS2bs in STAU1-mediated mRNA decay [281], and interacting proteins of bacterial small regulatory RNAs [282, 283, 284]. The MS2 system was also combined with stable isotope labeling of amino acids in cell culture (SILAC)-based quantitative MS to investigate viral non-coding RNA interactors as well as UV-crosslinked MS2-tagged RNPs in HEK cells [279, 285]. Similar to MS2, the PP7 system has been exploited for the isolation of both stable 7SK RNPs [286] and mRNPs [287], in this case *in vivo* assembled complexes of Upf1 on PP7bs-tagged mRNAs from HEK cells. For the isolation of human 7SK RNP, Hogg *et al.* (2007) combined two RNA aptamers, PP7bs and the tobramycin motif, to yield an RNA Affinity in Tandem (RAT) tag that allows sequential purifications [286]. Recently, the Csy4 endoribonuclease of the *P. aeruginosa* CRISPR system has been engineered for RNP affinity purification, making use of its catalytic activity for elution [288]. Here, an inactive biotinylated Csy4 nuclease associates with its target hairpin fused to an RNA of interest and is immobilized on an avidin-matrix. Upon RNP formation *in vitro*, addition of imidazole activates Csy4 to cleave the RNA for release of the RNP. This shows that bacteriophage-derived systems were successfully modified to be utilized for RNP purification in a variety of experimental settings.

1.5.3 RNA Aptamers for Purification

A further possibility is to use aptamers, structured RNA motifs selected *in vitro* for the ability to bind proteins or small molecule ligands. In contrast to bacteriophage systems, they do not require synthesis of recombinant proteins. Examples include a streptomycin-binding aptamer (StreptoTag), which was used for U1 snRNP isolation [289], and a tobramycin-binding aptamer that was used for purification of pre-spliceosomal RNP complexes [290]. Moreover, Srisawat and Engelke developed a streptavidin (SA)-binding aptamer termed S1 by which yeast and human RNase P-associated RNPs could be purified [291, 292]. S1 was selected *in vitro* by SELEX (Systematic Evolution of Ligands by Exponential Enrichment) from a random RNA library with SA as bait [291]. The S1 aptamer is advantageous as native complexes can be eluted from the SA-resin by biotin, which makes use of one of the strongest noncovalent and irreversible interactions in nature of biotin to SA (K_d 10^{-14} M), while S1 binds to SA with a K_d of 7×10^{-8} M [291]. Another advantage of this system is that biotinylated molecules in cellular lysates can be efficiently blocked by avidin [293] which has no affinity for the S1 aptamer [294].

Examples of successful mRNP recovery via S1 are limited. After UV-crosslinking of bound proteins to an S1-tagged mRNA inside human cells, the S1 aptamer was used for the isolation of an *in vivo* assembled ARE-mRNP that mediates translation activation upon starvation [126]. Beside this single example for S1-mediated mRNP purification from mammalian cells, the S1-tag was applied to isolate intact RNPs of the yeast snR30 small nucleolar RNA complex [295] and bacterial ribosomes via S1-tagged 23S rRNA [296]. Moreover, mRNA-interacting proteins of the Crb3 mRNA complex were affinity purified from human cells and *Drosophila* embryo extracts using *in vitro* transcribed RNAs attached to SA via the S1 tag [297, 298, 299]. Finally, when a SILAC-based RNA pulldown of S1-tagged RNAs was combined with PAR-CLIP, RNA-protein interactions were mapped in a quantitative MS approach [300, 301]. In a different setting which used a Cy3-labelled anti-S1 probe, S1-tagged yeast RNAs were localized *in vivo* by applying fluorescent *in situ* hybridization [302].

1.6 Aim of the Study

The principle aim of this study was to investigate CDE-mediated mRNA decay. So far, it was only known that the CDE in the 3'UTR conveys constitutive decay to the TNF α mRNA. This occurs in an apparently non-regulated fashion with respect to immune challenge, a condition that inhibits the neighboring ARE. This highlights the CDE's ability to serve as a robust safeguard signal against TNF α overshoot. The CDE employs an unknown mechanism, which contributes to dampening TNF α mRNA and protein levels upon stimulation.

The aim of my PhD thesis was to investigate the CDE RNA structure, to identify proteins that bind to the CDE and that are crucial for CDE activity, as well as to classify the mechanism of CDE function. For this, I established an optimized protocol to purify mRNP complexes from cells via RNA tags to enrich for specific RNA-interacting proteins. I also used this method to isolate well-known and novel ARE-BPs. Finally, this study also aimed at identifying CDE-like motifs in other mRNAs on a genome-wide scale, which allows me to characterize the CDE as a novel class of decay elements in mammals.

2 Results

2.1 An Optimized RNA Aptamer for mRNP Purification

The first aim of my PhD thesis was to develop an improved protocol for mRNP purification based on structured RNA aptamers that have affinity for specific matrices, which allows for RNA-based purification of RNA-protein complexes. For several reasons this has always been a challenging task. Its importance becomes evident as it offers the ability to study and understand processes in the cell that involve large RNA-protein complexes. Notably, the majority of crucial cellular machineries consist of RNA and protein. My goal was to use this technique to identify novel RNA-BPs as effectors of defined RNA elements. In this study, I first focused on improving a previously established streptavidin (SA)-binding RNA aptamer and applied my protocol to find unknown protein regulators of the ARE [303].

2.1.1 Development of the RNA Aptamer S1m

The S1 aptamer was originally developed by Srisawat and Engelke (2001) through *in vitro* selection of an SA-binding aptamer from a random RNA library by SELEX [291]. The minimal S1 motif consists of a 44 nt long structured RNA containing two double-stranded (ds) RNA helices, a 13 nt internal loop between the two helices, and a 9 nt terminal loop (**Figure 2.1A**) [294]. To test the efficiency of the S1 aptamer for mRNP purification, I introduced a single copy of S1 into the 3'UTR of a β -globin reporter gene that contains the 53 nt long ARE of mouse TNF α [304] (**Figure 2.1B**). The globin-ARE-1xS1 reporter gene was then transiently transfected into COS7 cells, which were harvested the following day by rapid freezing in liquid nitrogen. I prepared cellular lysates by detergent-free cryomilling as previously suggested for RNP purification [305]. Compared to detergent-based lysis, cryolysis was equally efficient with regard to RNA recovery (data not shown). After pre-clearing with avidin-beads that do not bind the aptamer [294] but remove biotin and biotinylated proteins due to the high affinity of egg white avidin for biotin, I incubated the lysates with SA Sepharose to capture the mRNP. Beads were

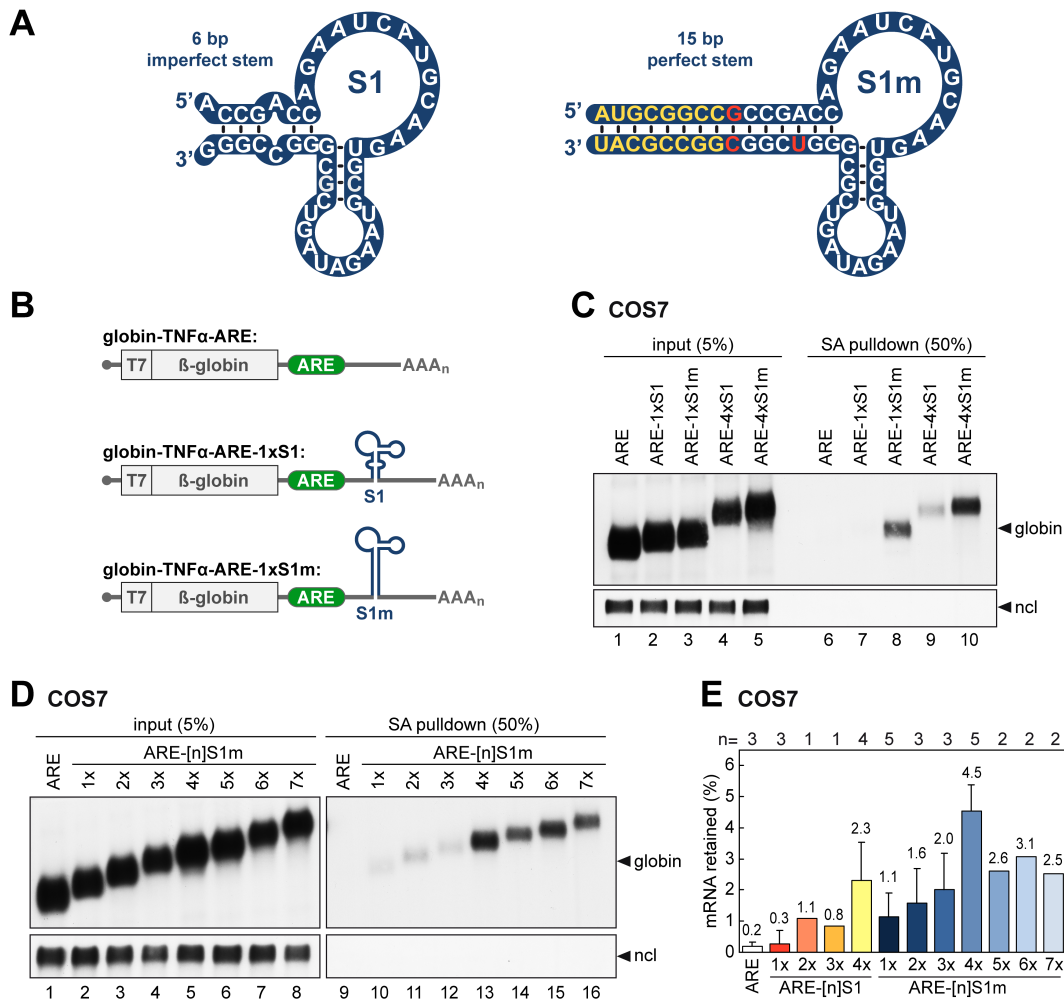


Figure 2.1: Improved Streptavidin-binding Efficiency of the S1m Aptamer.

(A) Left: secondary structure of S1 [291]. Right: secondary structure of the modified S1m. Nucleotides mutated (red) or added to prolong the stem (yellow) are highlighted. (B) Schematic representation of globin reporter mRNAs encoding rabbit β -globin fused to the T7 epitope. The TNF α ARE was inserted into the β -globin 3'UTR, upstream of S1 or S1m. (C) COS7 cells were transiently transfected with globin-TNF α -ARE, globin-TNF α -ARE-1xS1, -1xS1m, -4xS1 or -4xS1m. One day later, cells were lysed by cryomilling, and cleared supernatants were incubated with SA Sepharose beads. RNA was isolated from the cleared supernatants (input) and from the beads after five washing steps (SA pulldown). The RNA was resolved on 1.1% agarose gels, and subjected to Northern blot analysis using a β -globin probe against the globin reporter mRNA. Nucleolin (ncl) mRNA serves as a loading control. (D) COS7 cells were transiently transfected with globin reporter genes containing the TNF α ARE, or the ARE together with 1–7 copies of S1m. Retention of the mRNAs by SA pulldown was analyzed as in panel C. (E) Quantification of SA pulldown efficiencies. Different reporter mRNAs were expressed in COS7 cells as in panels C and D, and the amount of mRNA retained by SA Sepharose was expressed as % of input. Shown are average values \pm SD, n is indicated above the graph. Reproduced with permission from Nucleic Acids Research, Oxford Journals.

2.1 An Optimized RNA Aptamer for mRNP Purification

then washed and RNA was eluted by phenol/chloroform extraction to assess the efficiency of mRNP recovery. Northern blot analysis of input and purified (SA pulldown) RNA showed only minimal binding of globin-ARE-1xS1 mRNA (**Figure 2.1C**, lane 7). Quantification indicated that only 0.3% of globin-ARE-1xS1 mRNA was retained on SA Sepharose compared to 0.2% background binding of globin-ARE mRNA lacking the S1 aptamer (**Figure 2.1E**).

With the aim to improve binding efficiency, I generated a modified aptamer termed S1m (**Figure 2.1A** and **Suppl. Figure 5.1**) in which the terminal S1 RNA structure was stabilized by introducing perfect strand complementarity in the basal stem (shown in red), as was done previously for a modified S1 aptamer in the design of an RNA-based antibody mimic [306]. Similar to Xu and Shi (2009), I also extended the basal stem of S1, yet only by 8 base-pairs (**Figure 2.1A**, in yellow) to a total length of 15 base-pairs. When the modified S1m aptamer was inserted into the reporter mRNA (globin-TNF α -ARE-1xS1m), I observed 3–4 fold higher binding efficiency (**Figure 2.1C**, lane 8) with 1.1% of the mRNA retained on SA Sepharose (**Figure 2.1E**). I then introduced multiple copies of the S1m aptamer into the reporter gene, speculating that a synergistic effect might further increase binding efficiency. A linear 21 nt spacer sequence lacking secondary structure (**Suppl. Figure 5.2**) was inserted between the individual aptamers to increase flexibility between consecutive motifs. Indeed, I observed steadily increasing binding efficiencies with 2, 3 and 4 copies of S1m (**Figure 2.1D**, lanes 11–13). Additional copies of S1m (up to 7) did not further improve mRNA recovery; in fact, these longer repeats were less efficient than 4xS1m (lanes 14–16). Using 4 copies of the original S1 aptamer also improved RNA binding compared to the single copy 1xS1 construct (2.3 versus 0.3%, **Figures 2.1C** and **2.1E**). Quantification of several repeat experiments showed that of all constructs tested, 4xS1m had the highest binding efficiency: with 4.5% of mRNA retained on SA Sepharose, it was 15 times more efficient than the original S1 aptamer.

To assess functionality of the aptamer tagged mRNPs, I tested whether insertion of 4xS1m would interfere with ARE-mediated mRNA decay. NIH3T3 cells were stably transfected with globin-TNF α -ARE-4xS1m, globin-4xS1m or globin alone, and reporter mRNA stability was measured by actinomycin D (actD) chase experiments (**Figure 2.2A**). Northern blot analysis showed that the globin and globin-4xS1m control mRNAs were stable over time with half-lives >9 hours, whereas the globin-TNF α -ARE-4xS1m mRNA was rapidly degraded with a half-life of 1.9 ± 0.1 hours. As demonstrated in transiently transfected NIH3T3 cells (**Figure 2.2B**), there was no difference between the decay rate of globin-TNF α -ARE (1.8 ± 0.3 hours) and globin-TNF α -ARE-4xS1m (1.8 ± 0.5 hours). Thus, ARE-mRNA decay was not affected by placing 4xS1m in the vicinity of the ARE, a prerequisite for purifying mRNPs.

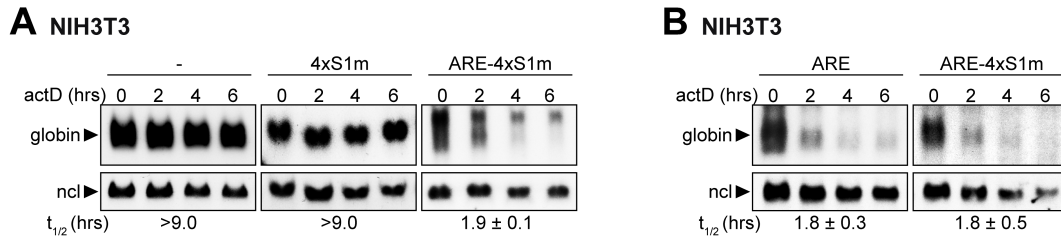


Figure 2.2: The S1m Aptamer Does Not Interfere with ARE-mRNA Decay.

(A) Globin reporter genes containing no insert in the 3'UTR (-), 4xS1m or ARE-4xS1m were stably transfected into NIH3T3 cells. Reporter mRNA decay was measured by treatment with actinomycin D (actD), extraction of total RNA at 2 hours intervals followed by Northern blot analysis. Globin mRNA signals normalized to nucleolin (ncl) were used for calculation of average mRNA half-lives ($t_{1/2}$) \pm SD, $n = 3$. (B) After transient transfection of NIH3T3 cells, the decay of globin-ARE and globin-ARE-4xS1m reporter mRNAs was measured as in panel A; shown are average mRNA half-lives ($t_{1/2}$) \pm SD, $n = 3$. Reproduced with permission from Nucleic Acids Research, Oxford Journals.

2.1.2 Comparison to the PP7 and MS2 Systems

My next goal was to compare the S1m aptamer with the PP7 and MS2 systems. To capture the globin reporter mRNAs that contained either the PP7bs or the MS2bs, PP7cp and MS2cp were expressed in *E. coli* as glutathione S transferase (GST)-fusion proteins (**Figure 2.3**). In addition, one or two cleavage sites for the Tobacco Etch Virus protease (TEV, T in **Figures 2.3A and 2.4A**) were engineered between GST and the coat proteins (**Figures 2.3A and 2.4A**). To this end, globin reporter mRNAs were generated by Georg Stoecklin containing the TNF α ARE and six copies of either the PP7bs or the MS2bs (**Figure 2.4A**). From tethering assays it is known that inserting 6–8 copies of the MS2bs strongly increases binding efficiency to the MS2cp [274].

The globin-TNF α -ARE-6xPP7bs and globin-TNF α -ARE-6xMS2bs reporter genes were transiently transfected into COS7 cells, and lysates were prepared by cryomilling as described for the S1 aptamer above. After pre-clearing with glutathione (GSH) Sepharose beads, I incubated the lysates with the recombinant GST-tagged coat proteins before capture on GSH Sepharose beads. Northern blot analysis showed that only 0.7% of globin-ARE-6xPP7bs mRNA was retained by GST-T-PP7cp on GSH Sepharose (**Figure 2.4B**, lane 6, quantification in **Figure 2.4C**). I also tested an optimized (o)PP7cp, a previously published PP7cp mutant containing two mutations to alanine (C68A, C73A; **Figure 2.3B**) that confer higher affinity to its cognate RNA and reduced tendency to multimerize [286]. With oPP7cp, 1.0% of the globin-ARE-6xPP7bs mRNA was retained on GSH Sepharose, slightly more than with the WT PP7cp protein.

2.1 An Optimized RNA Aptamer for mRNP Purification

MS2cp was either fused to GST directly, or via a linker containing two consecutive TEV protease cleavage sites (TT, **Figures 2.3A** and **2.4A**). With both GST-MS2cp and GST-TT-MS2cp, more globin-ARE-MS2bs mRNA was recovered than with PP7cp or oPP7cp (**Figure 2.4B**, lanes 9 and 10, quantification in **Figure 2.4C**). GST-MS2cp gave the best result with 3.2% of the input mRNA retained on the beads. When compared to the 4xS1m aptamer, however, the PP7 and MS2 systems performed less well, so I decided to pursue mRNP purification using 4xS1m.

2.1.3 Higher Affinity of S1m for Streptavidin

To further explore to which extent the S1m aptamer performs better than S1, I compared their binding affinities to SA *in vitro*. By electromobility shift assay (EMSA), I showed that one copy of S1 RNA binds to recombinant SA protein with an apparent dissociation constant (K_d) of 59 nM (**Figure 2.5A**), similar to the K_d of 70 nM reported previously [291, 292]. S1m showed a 2-fold higher affinity with an apparent K_d of 29 nM (**Figure 2.5A**). I noticed that a considerable amount of the RNA remained unbound even at high SA concentrations. This did not affect calculation of the K_d since I achieved saturated binding, but this suggested that a proportion of the RNA was incorrectly folded. An unrelated, unstructured 23 nt long ARE RNA did not form a complex with SA by EMSA (**Figure 2.5C**), confirming that the complex I observed between SA and S1/S1m was due to specific binding. Taken together, these data revealed that S1m has higher affinity towards SA than S1. This, together with the synergistic effect of connecting four copies of the aptamer, explained the improved efficiency of the 4xS1m tag in capturing a cellular mRNA (**Figure 2.1C–E**).

2.1.4 Elution with Biotin and RNase

Next, I wanted to compare the ability of biotin to elute 4xS1- and 4xS1m-tagged RNAs from SA Sepharose in the presence of a cellular lysate. ARE-4xS1 and ARE-4xS1m RNAs as well as the control RNAs 4xS1 and 4xS1m, as depicted in **Figure 2.6A**, were transcribed *in vitro*, subjected to a folding step and coupled to SA beads (**Figure 2.6B**). As expected from the higher affinity of S1m, binding of ARE-4xS1m (59%, input minus unbound) was more efficient than binding of ARE-4xS1 (27%). The RNA affinity resin was then incubated with a highly concentrated pre-cleared NIH3T3 cell extract (30-50 mg/ml), washed three times and eluted with 10 mM biotin. Residual RNA on the beads was recovered by a second elution using Trizol. This analysis

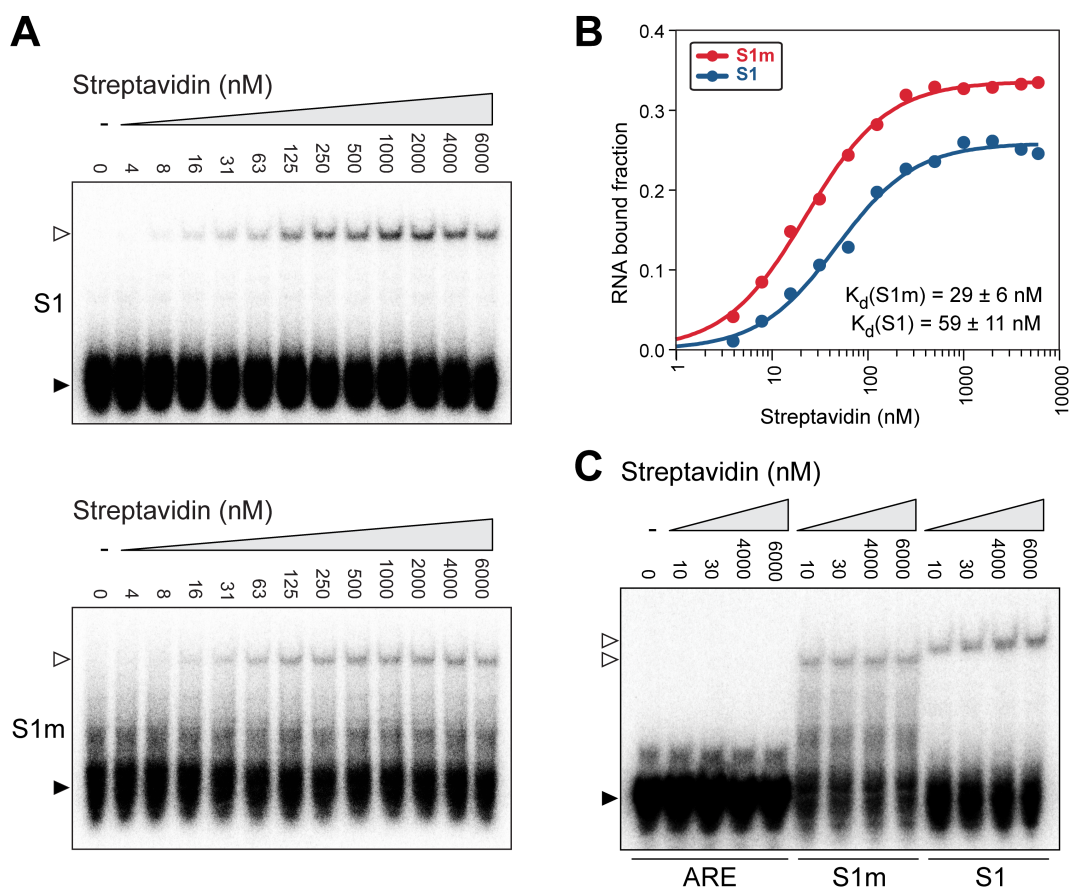


Figure 2.5: Binding Affinities of the S1 and S1m Aptamers. (A) *In vitro* binding of recombinant SA protein to S1 and S1m RNA was measured by electromobility shift assay (EMSA). Radiolabeled S1 and S1m RNAs were incubated with increasing concentrations of SA. Free RNA (black arrow) was separated from RNA-protein complexes (white arrow) by native 6% PAGE. (B) The apparent dissociation constant $K_d \pm \text{SD}$ was calculated from quantification of three independent experiments. (C) *In vitro* binding of SA protein to S1 and S1m RNA was compared to that of a 23 nt long control ARE RNA by EMSA. Radiolabeled ARE, S1 and S1m RNAs were incubated with increasing concentrations of SA along the range shown in A. Reproduced with permission from Nucleic Acids Research, Oxford Journals.

2.1 An Optimized RNA Aptamer for mRNP Purification

showed that 70% of the bound ARE-4xS1 RNA and 47% of the bound ARE-4xS1m RNA was eluted with biotin (**Figure 2.6B**). 28% (ARE-4xS1) and 17% (ARE-4xS1m) of the RNA remained on the beads and was recovered only after Trizol elution.

As an alternative for eluting proteins bound to the captured RNA, I observed that RNase A degraded the SA-bound ARE-4xS1 and ARE-4xS1m RNAs completely (**Figure 2.6C**). I also saw that RNase A was efficient in eluting protein from mRNPs recovered from intact cells (data not shown). Thus, cellular proteins did not interfere with access of the RNase to RNA-protein complexes. I then examined the release of proteins bound to the RNA by RNase A elution (**Figure 2.6D**). HuR, a well-established ARE-BP, was captured specifically by ARE-4xS1 and ARE-4xS1m, but not by the corresponding control RNAs lacking the ARE. RNase A was able to release most of the bound HuR, whereas only small amounts remained bound to the SA beads, visualized by SDS elution. Notably, ARE-4xS1m RNA was able to recover more HuR protein than ARE-4xS1. G3BP, an RNA-BP not associated to AREs, did not interact with any of the RNA-affinity resins, demonstrating specificity of my purification method. In all, this was a first indication that an ARE-BP can be specifically purified via 4xS1m-tagged ARE-RNA.

Taken together, elution with biotin appears somewhat less efficient, releasing only about half of the bound ARE-4xS1m RNA, yet might be chosen as an alternative if the goal is to recover native RNP complexes from the column i.e. for a second purification step. However, my results suggested that elution by RNase A is the method of choice if the goal is to recover proteins from the RNA-affinity column.

2.1.5 Purification of ARE-associated Proteins via 4xS1m

In my initial experiments, I attempted to identify proteins associated with the globin-ARE-4xS1m mRNA stably expressed in NIH3T3 cells. However, I mostly detected cytoskeletal proteins in both the ARE and control purifications, and I was not able to capture specific RNA-BPs (data not shown). Therefore I turned to the *in vitro* RNA affinity chromatography approach established in **Figure 2.6B–D** (schematically depicted in **Figure 2.7**), and optimized the protocol (details are given in the Methods section).

The ARE-4xS1m and negative control 4xS1m RNAs were transcribed *in vitro*, refolded and coupled to SA beads. In this approach, RNA binding to the column was found to be highly efficient (77–95%, **Figure 2.8A**). Then, highly concentrated cell extracts (70 mg protein/ml) were obtained by cryomilling of NIH3T3 cells, cleared from cellular debris by centrifugation at 17.000 x g, pre-blocked with avidin and SA beads, and incubated with the RNA affinity

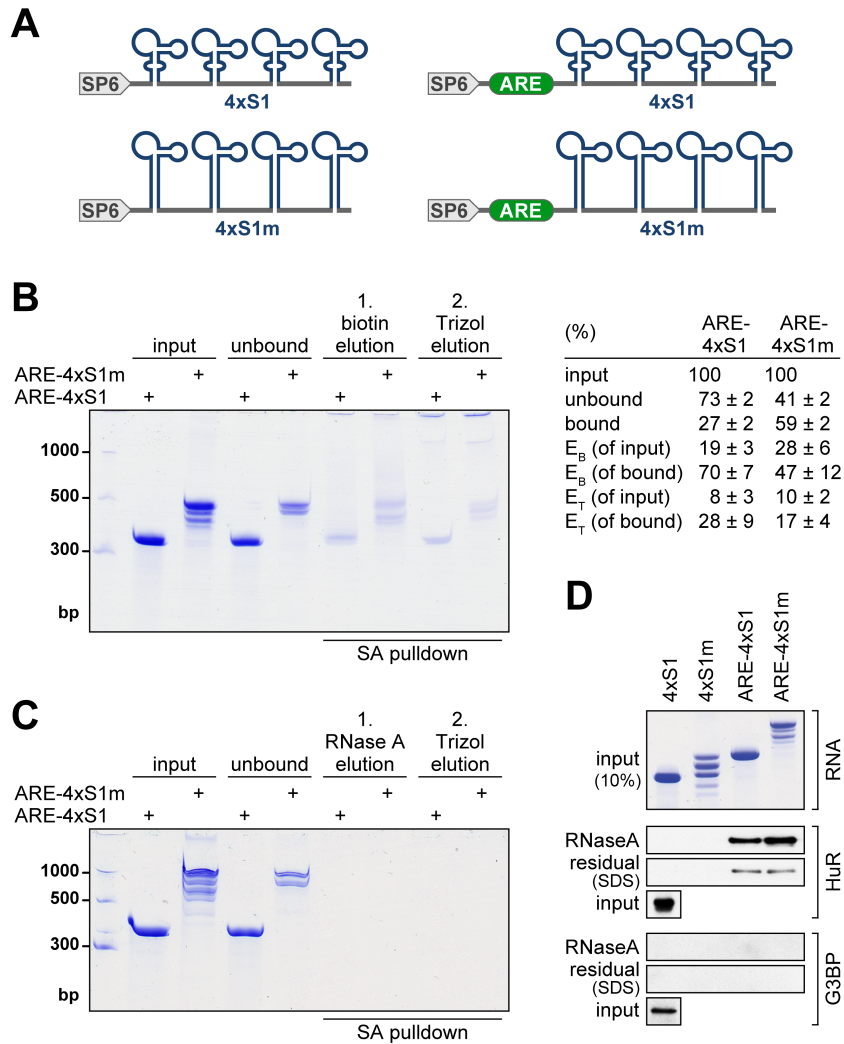


Figure 2.6: Elution of the S1 and S1m Aptamers. (A) Schematic representation of DNA templates used for *in vitro* transcription of 4xS1, 4xS1m, ARE-4xS1 and ARE-4xS1m RNAs. (B) Left: elution by biotin was examined by *in vitro* SA pulldown. *In vitro* transcribed RNAs were coupled to SA Sepharose beads, incubated with NIH3T3 cell extracts, washed and eluted using 10 mM biotin (E_B). Residual RNA bound to beads was subsequently eluted with Trizol (E_T). RNA was resolved by 6% denaturing urea-PAGE and visualized by methylene blue staining. Each lane represents 20% of the starting amount. Reference: Low Range ssRNA Ladder (NEB). Right: the percentage of RNA recovered at each step was quantified based on three independent repeat experiments, average values \pm SD. (C) The same experiment as in B, except that the first elution was carried out with 0.05 μ g/ μ l RNase A. (D) Upon RNA affinity purification using an NIH3T3 cell lysate as in B, proteins were eluted with RNase A followed by elution with SDS to determine residual protein bound to the beads. Upper panels: 10% of each RNA fraction was resolved by denaturing urea-PAGE and stained with methylene blue. Bottom panels: 23% of the RNase A and SDS eluates was resolved by PAGE and proteins were monitored by Western blot analysis. ARE-BP HuR, positive control; G3BP, negative control. Reproduced with permission from Nucleic Acids Research, Oxford Journals.

2.1 An Optimized RNA Aptamer for mRNA Purification

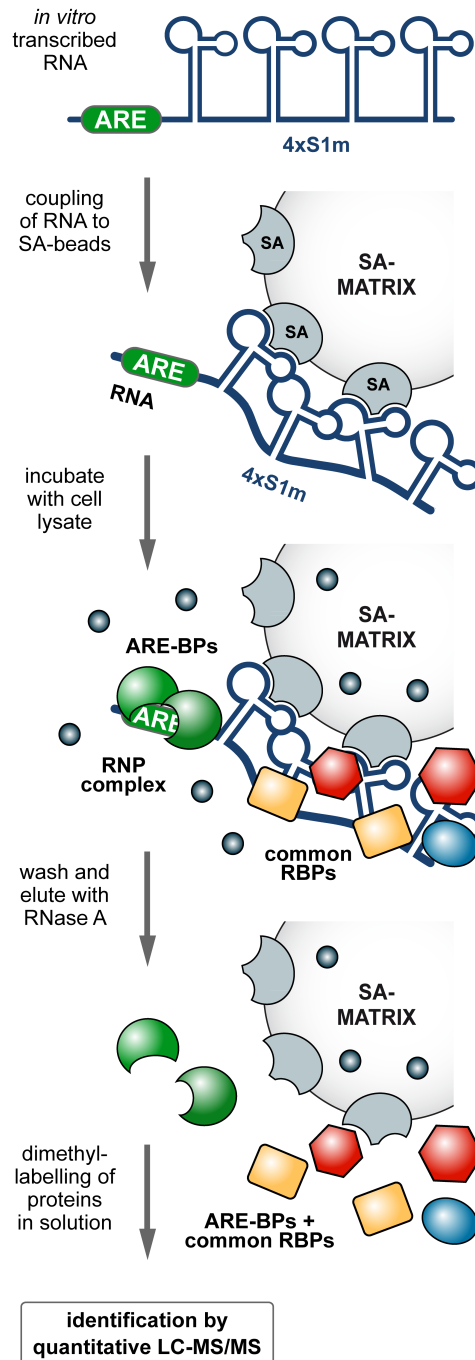


Figure 2.7: Schematic Representation of S1m-mediated *in vitro* RNP Purification. *In vitro* transcribed ARE-4xS1m and control 4xS1m RNAs are coupled to SA Sepharose beads and incubated with a highly concentrated cellular extract. RNP complexes formed contain proteins specific to the ARE, as well as RNA-BPs that interact with aptamers and linkers. Following high salt washes, elution by RNase A releases RNA-associated proteins. Proteins enriched in the ARE-4xS1m eluate over the 4xS1m eluate are identified by quantitative MS using dimethyl labeling after tryptic digestion. Reproduced with permission from Nucleic Acids Research, Oxford Journals.

columns. After washing with a buffer containing 300 mM NaCl, proteins bound to the RNA were eluted with RNase A. One third of the eluate was resolved by PAGE and visualized by colloidal Coomassie blue staining (**Figure 2.8B**, left panel). Subsequent elution of the columns with SDS showed that vast amounts of protein adhered unspecifically to the SA Sepharose resin (right panel), whereas RNA-associated proteins represented a minority. Thus, elution by RNase provides an important advantage in the purification scheme because many of the unspecifically bound proteins remain on the column.

Two thirds of the RNase A eluates were vacuum-concentrated and resolved by PAGE over a short distance (**Figure 2.8C**). The pattern of protein bands was very similar in the 4xS1m and ARE-4xS1m samples, suggesting that most of the purified proteins were associated with the 4xS1m aptamer or the spacer sequence. To detect ARE-specific proteins enriched in the ARE-4xS1m sample, I therefore used quantitative MS with the help of the ZMBH Mass Spectrometry (MS) Core Facility. The two lanes were cut into four slices each and proteins were in-gel digested with trypsin, followed by peptide dimethyl labeling [307] using either formaldehyde (4xS1m sample, light) or deuterated formaldehyde (ARE-4xS1m sample, medium). The light and medium samples were then combined for liquid chromatography-MS/MS analysis. This approach allowed for calculation of the enrichment of low abundance proteins in one sample despite the presence of highly abundant proteins in both samples.

The table in **Figure 2.8D** lists proteins that were enriched by >8-fold in the ARE-4xS1m sample. Notably, my purification yielded most of the established ARE-BPs (in green) including HuR (Elav1), BRF2 (Zfp36L2), TIAR (Tial1), BRF1 (Zfp36L1) and AUF1 (Hnrnpd). I also found two proteins (in blue), Fubp3 and Dazap1, which had previously been purified with the TNF α ARE [308, 309], although their function in regulating ARE-mRNAs has not been established. An additional five RNA-BPs (in yellow) were specifically enriched in the ARE-4xS1m purification including two proteins of the U2 snRNP (A' and B''), a general snRNP protein (Sm-D2), an RRM-containing protein (Rbms1) and a ZF protein termed Roxan (Zc3h7b).

2.1.6 Confirmation of Rbms1 and Roxan as Novel ARE-BPs

To confirm binding of novel candidate ARE-BPs, I chose Rbms1 and Roxan from the list of enriched proteins (**Figure 2.8D**), both of which had previously not been associated with the ARE. Rbms1 (RNA-binding motif, single-stranded-interacting protein 1), also known as MSSP (c-myc single-strand binding protein), contains two RNA recognition motif (RRM) domains. It was initially identified as a DNA-binding protein that interacts with a region upstream of the c-Myc gene [310] and was proposed to function in DNA repli-

2.1 An Optimized RNA Aptamer for mRNP Purification

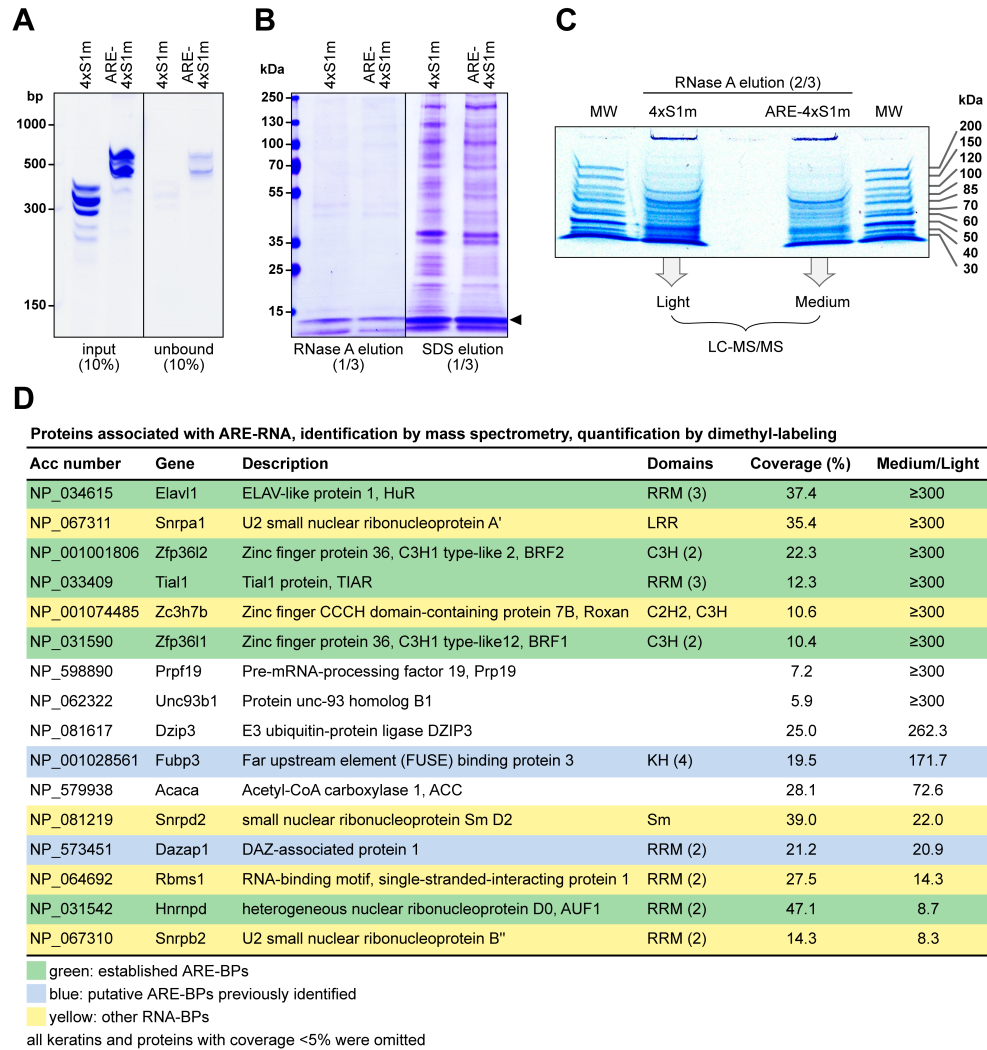


Figure 2.8: Identification of ARE-BPs by 4xS1m RNA Affinity Purification.

(A) *In vitro* transcribed RNAs were coupled to SA-beads. To monitor coupling efficiency, 10% of the input and unbound RNA fraction were resolved on a 6% polyacrylamide/TBE/urea gel and stained with methylene blue. Reference: Low Range ssRNA Ladder (NEB). (B) NIH3T3 cell extracts were incubated with the RNA-coupled SA-beads, washed and eluted using RNase A. SDS was used for a second elution of the beads. 1/3 of the eluates was resolved on a 5-20% polyacrylamide gradient gel and proteins were stained with colloidal Coomassie blue. Black arrow: RNase A. (C) 2/3 of the RNase A elution samples were resolved over a short distance on a 10% polyacrylamide gel and stained with colloidal Coomassie blue. Lanes including the wells were cut into four gel slices and in-gel trypsin-digested. Peptides from the 4xS1m (Light) and ARE-4xS1m (Medium) eluate were differentially dimethyl-labeled and processed for MS; MW, molecular weight marker. (D) List of proteins identified by MS in ARE-RNPs purified via 4xS1m. The ratio of Medium/Light reflects the specific enrichment of proteins in ARE-4xS1m over 4xS1m. All proteins enriched >8-fold are depicted and categorized as established ARE-BPs (green), putative ARE-BPs identified previously (blue) or other RNA-BPs (yellow). Reproduced with permission from Nucleic Acids Research, Oxford Journals.

cation [311]. Rbms1 was further shown to bind to the c-Myc protein and stimulate its transforming activity [312], yet the RNA-binding properties of Rbms1 have not been investigated so far. The second candidate, Roxan (rotavirus X protein associated with NPS3), also termed Zc3h7b (zinc finger CCCH-type containing 7B), is a 110 kDa cellular protein of unknown function that was shown to bind the rotavirus nonstructural protein NSP3. NSP3 interacts with both the 3' consensus sequence of non-polyadenylated viral mRNAs and eukaryotic translation initiation factor eIF4GI, suggesting that Roxan may function in the regulation of viral mRNA translation [313]. Moreover, Roxan was shown to interact with poly(A)-binding protein (PABP-C1) and to promote its nuclear localization during rotavirus infection [314].

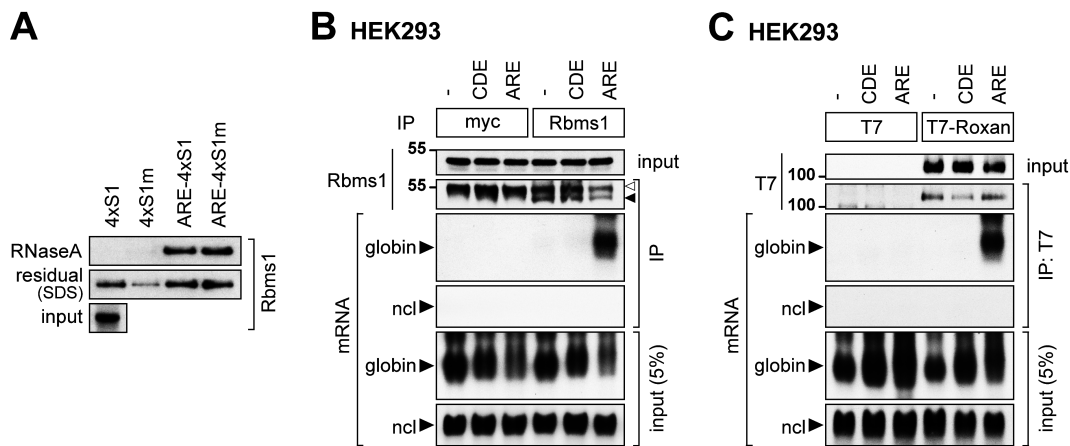


Figure 2.9: Rbms1 and Roxan Specifically Bind to the TNF α ARE. (A) Binding of Rbms1 to the ARE was analyzed by *in vitro* SA pulldown, as in in Figure 2.6D. Rbms1 was detected using an antibody against endogenous Rbms1. (B) Binding of endogenous Rbms1 to the TNF α ARE was analyzed by RNA-IP. HEK293 cells were transiently transfected with the globin reporter lacking an insert (-), globin-TNF α -CDE or globin-TNF α -ARE. After IP of endogenous Rbms1 with an Rbms1-specific antibody, the protein was monitored by Western blot analysis. White arrow: immunoglobulin heavy chain; black arrow: Rbms1. Anti-myc antibody was used for the negative control IP. Globin reporter mRNAs were visualized by Northern blot analysis, ncl mRNA serves as negative control. (C) Binding of Roxan to the TNF α ARE was analyzed by RNA-IP. HEK293 cells were transiently transfected with T7 or T7-Roxan together with the globin reporters as in B. After IP with anti-T7 antibody, T7-Roxan was monitored by Western blot analysis. Reproduced with permission from Nucleic Acids Research, Oxford Journals.

First, I confirmed the specific interaction of Rbms1 with the ARE in an *in vitro* SA pulldown experiment (as in **Figure 2.6D**) using an antibody against endogenous Rbms1 (**Figure 2.9A**). Indeed, Rbms1 was found to be specifically enriched by RNase A elution in the ARE-4xS1 and ARE-4xS1m samples.

2.1 An Optimized RNA Aptamer for mRNP Purification

Notably, the second elution with SDS revealed additional, unspecific binding of Rbms1 to the beads, underlining the importance of elution by RNase. By an inverse approach, i.e. RNA-immunoprecipitation (IP) of endogenous Rbms1 from HEK293 cells, I confirmed that Rbms1 strongly associates with globin-TNF α -ARE mRNA but not with globin mRNA alone (**Figure 2.9B**). Likewise, Rbms1 did not bind globin-TNF α -CDE mRNA, which contains the CDE, a stem-loop motif that confers ARE-independent TNF α mRNA decay [246]. Since a negative control antibody against myc did not pull down any of the reporter mRNAs, this experiment demonstrated that Rbms1 is a specific ARE-BP.

To assess binding of Roxan to ARE-RNA, RNA-IP was then carried out with T7-tagged Roxan transiently expressed in HEK293 cells. Similar to Rbms1, I observed that T7-Roxan specifically interacts with globin-TNF α -ARE, but not with the globin or globin-TNF α -CDE mRNAs (**Figure 2.9C**). The T7-tag alone did not bind to any of the reporter mRNAs. These results illustrated that 4xS1m-mediated RNA affinity chromatography and quantitative MS successfully identified at least two novel ARE-BPs in addition to a large number of known ARE-BPs.

2.2 Roquin-mediated Constitutive Decay of CDE-containing mRNAs

The stability of TNF α mRNA is determined by 3'UTR-residing elements such as miRNA binding sites, the ARE, as well as the CDE. So far, the active CDE mediating constitutive decay of this mRNA has been mapped to an element downstream of the ARE (**Figure 2.10A**). However, no further characterization had been performed. Thus, in my PhD thesis I aimed at identifying and characterizing CDE-interacting proteins to unravel the underlying mechanism that the CDE employs for its function [246].

2.2.1 The CDE is a Conserved Stem-Loop Motif

Previously, the CDE had been mapped to an 80 nt long sequence in the mouse TNF α 3'UTR by Stoecklin *et al.* (2003) [62], which was named K Δ AU. In his PhD thesis, B. Rattenbacher [145] was able to narrow down the element to a 37 nt long fragment using decay assays with globin-TNF α reporter transcripts which I reproduced in stably transfected NIH3T3 cells (**Figure 2.10A**). I referred to that element as CDE₃₇ which corresponds to the 3' most portion of the 80 nt-long K Δ AU element (**Figure 2.10B**). When I compared TNF α CDE sequences from 19 mammalian species as annotated in NCBI, the CDE₃₇ region was found to be especially highly conserved in primary sequence (**Figure 2.11A**).

When I cloned CDE₃₇ in different sequence and structure contexts I observed that this strongly influenced the decay activity of the respective variants (compare version V2 and V3 in **Suppl. Figure 5.3A and B**, and **Suppl. Table 5.1**), suggesting that the CDE might be a structured element. To address its structure experimentally, I collaborated with the Ming Hammond lab at UC Berkeley to subject these varying RNAs to in-line probing [315]. This is an RNA cleavage assay in which base-paired or structurally constrained nucleotides are protected from spontaneous phosphodiester bond hydrolysis. The cleavage reaction (**Suppl. Figure 5.3C**) revealed that the highly active CDE₃₇-V3 RNA folds into a P2-L2 stem-loop, which is flanked by an internal L1 loop followed by a P1 stem (**Figure 2.11B**, **Suppl. Figure 5.3C**, middle panel). Regions protected from cleavage precisely correspond to the base-paired regions of the P1 and P2 stems, whereas cleavage sites (circled in **Figure 2.11B**) were observed at most nucleotides in the L1 and L2 loops. This is in well agreement with the Mfold bioinformatic structure prediction [316] I performed for the mouse CDE (**Figure 2.11B**). In contrast, the less active CDE₃₇-V2 RNA, in which a 2 nt insertion disrupted the continuity between the cloning stem and P1, showed a diffuse cleavage pattern that could

2.2 Roquin-mediated Constitutive Decay of CDE-containing mRNAs

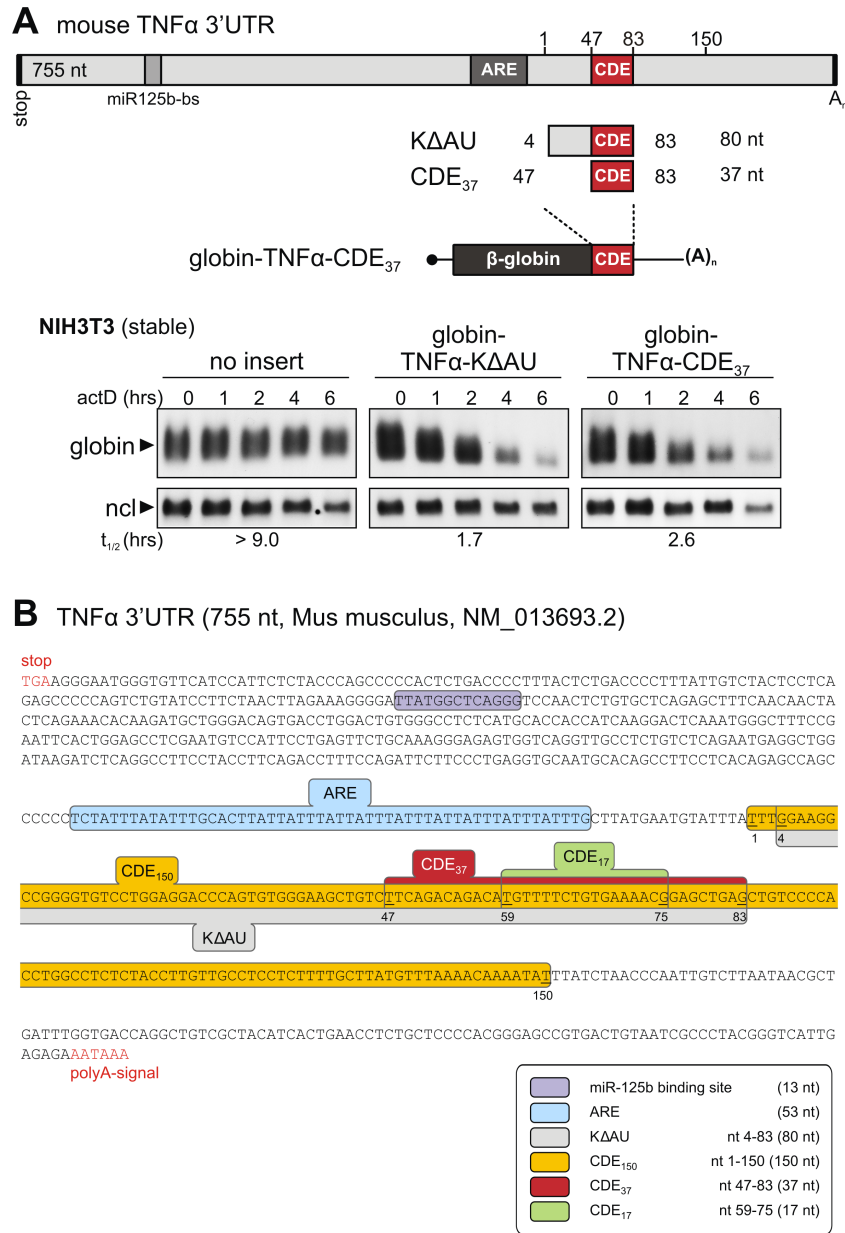


Figure 2.10: Mapping of the Mouse TNF α CDE. (A) Schematic representation of the mouse TNF α 3'UTR. CDE-containing TNF α sequences were inserted into the 3'UTR of a globin reporter gene. Reporter genes were stably transfected into NIH3T3 cells, and degradation of the reporter mRNAs was measured upon treatment with 5 μ g/ml actD. Total RNA was extracted at regular time intervals, resolved on 1.1% agarose gels, and subjected to Northern blot analysis. Globin mRNA signals normalized to nucleolin (ncl) mRNA were used for calculation of mRNA half-lives ($t_{1/2}$). (B) Sequence of the mouse TNF α 3'UTR (755 nt). Regulatory elements are highlighted in color: miR-125b binding site (purple), ARE (blue), CDE₁₅₀ (yellow), K Δ AU (grey), CDE₃₇ (red) and the minimal CDE₁₇ stem-loop (green). The stop-codon and the poly(A)-signal are marked in red. Nucleotides are numbered according to the CDE₁₅₀ fragment (nt 1-150). Reproduced with permission from Cell, Elsevier.

not be assigned to a predominant structure (**Suppl. Figure 5.3C**, right panel). Ming Hammond then performed in-line probing of a 150 nt long RNA containing the CDE in its native TNF α sequence context (CDE₁₅₀). This also resulted in a diffuse cleavage pattern (**Suppl. Figure 5.3C**, left panel). Like CDE₃₇-V2, CDE₁₅₀ was less active in mediating mRNA decay than CDE₃₇-V3 (**Suppl. Figure 5.3B**). The stem-loop structures in both CDE₃₇-V2 and CDE₁₅₀ also provide a much smaller decrease in free energy (ΔG , kcal/mol) as compared to CDE₃₇-V3 (**Suppl. Figure 5.3A**), which is indicative of a less strong tendency to contain structured regions. I concluded that the highly active CDE₃₇-V3 adopts a stable structure, whereas the less active CDE₃₇-V2 and CDE₁₅₀ appear to fluctuate between alternative or unstructured conformations.

Importantly, I found that the human CDE sequence can fold into a similar P1-L1-P2-L2 structure that differs primarily in the P1-L1 region when bioinformatically predicted with Mfold (**Figure 2.11C**). Like the mouse CDE, it causes rapid degradation of reporter mRNAs at a comparable rate (**Figure 2.11D**). Based on the TNF α CDE alignment of 19 mammalian species I could show that the P2-L2 stem-loop is conserved to nearly 100% with few variations in the lower P2 and only one C/U variation in L2 (red in **Figure 2.11A**), whereas the P1 and L1 sequences are more divergent (**Figure 2.11A**).

2.2.2 The P2-L2 Stem-Loop is Sufficient for CDE-mediated mRNA Decay

Next, I investigated sequence substitution analysis in which I mutated nucleotides along the CDE structure on one side or on both sides of a stem to disrupt or reconstitute the stem, respectively. This approach tested whether the CDE requires structure only or sequence specificity as well. Similarly, nucleotides in the loop regions were exchanged to analyze their contribution for CDE decay activity. These CDE-mutants were generated and tested with contribution of Sonja Reitter. The mutagenesis results are summarized in **Suppl. Table 5.1**. This analysis revealed that mutations within the P1 stem or the L1 loop did not affect CDE-mRNA decay (**Figure 2.12A–C**). In contrast, all mutations disrupting P2 or L2 inactivated the CDE, pointing towards the importance of the highly conserved P2-L2 stem-loop.

I then tested by mutagenesis whether the CDE's ability to fold into a stem-loop is required for mRNA decay. All mutations disrupting the P2 stem (M16, M19, M21, M22) abrogated CDE₃₇ activity (**Figures 2.12D and 2.13A**). While compensatory mutations restoring the apical part of P2 remained inactive (M23, M27), compensatory mutations in the basal part of the stem rescued CDE₃₇ activity (M20, M26; **Figure 2.12D**). Importantly, the compensatory

2.2 Roquin-mediated Constitutive Decay of CDE-containing mRNAs

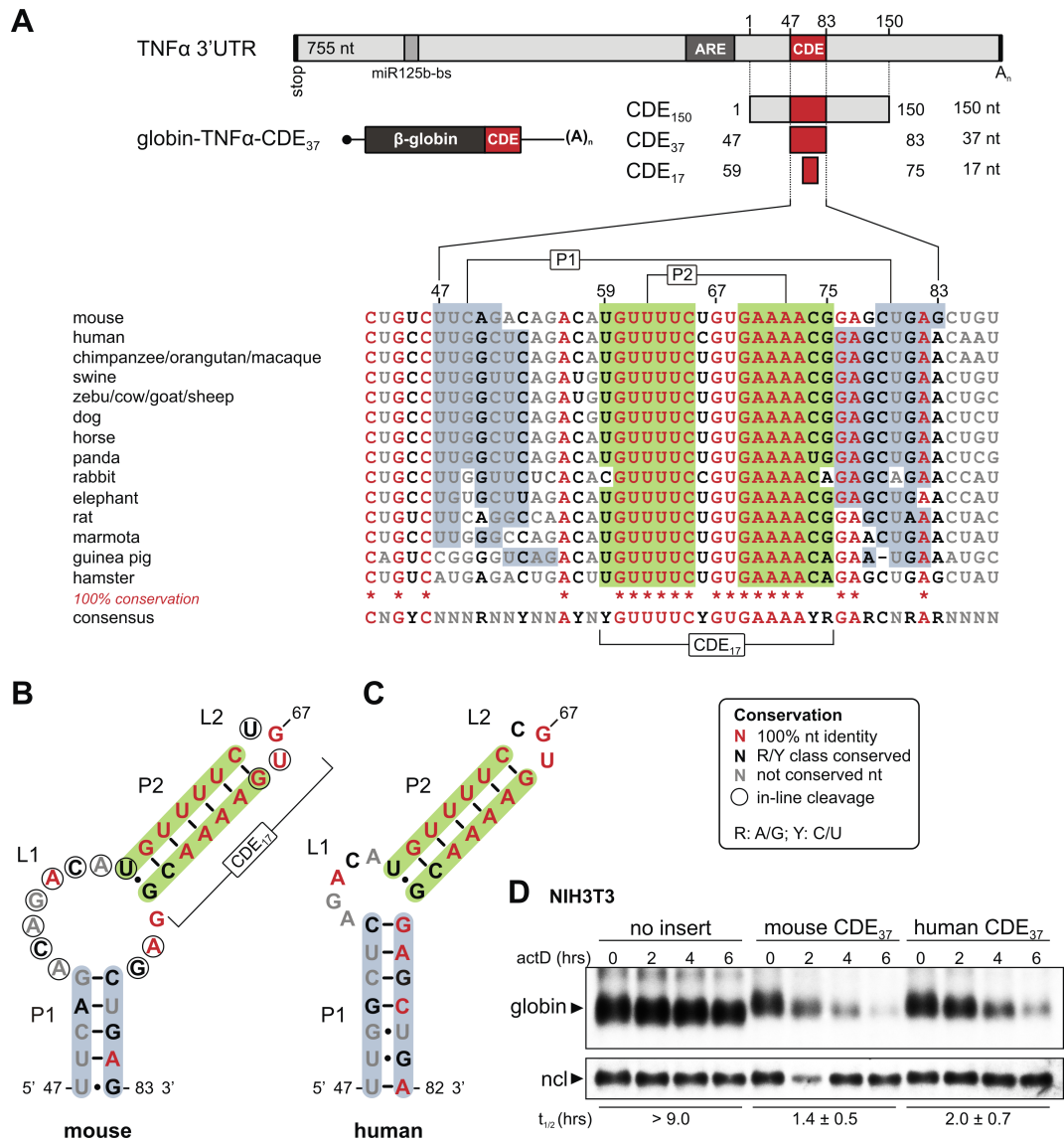


Figure 2.11: The Active TNFα CDE is a Conserved RNA Stem-Loop Motif.

(A) Schematic representation of the mouse TNFα 3'UTR along with an alignment of 19 mammalian TNFα CDE sequences. Nucleotides are color-coded according to conservation as indicated in the box; R, purine; Y, pyrimidine. Numbers refer to nucleotide positions within the CDE₁₅₀ fragment. (B) Secondary structure model of the mouse TNFα CDE₃₇ RNA derived from in-line probing. Nucleotides 5' to cleavage sites are circled, pairing elements P1 and P2 are shaded in blue and green, respectively, and nucleotides are color-coded according to conservation. (C) Secondary structure model predicted for the human TNFα CDE₃₇ RNA by thermodynamic modeling. (D) Globin reporter genes containing no insert in the 3'UTR, mouse CDE₃₇-V3 or human CDE₃₇-V3 were transiently transfected into NIH3T3 cells. Upon treatment with actD, total RNA was extracted at 2 hour intervals, resolved on 1.1% agarose gels, and subjected to Northern blot analysis. Globin mRNA signals normalized to nucleolin (ncl) were used for calculation of average mRNA half-lives (t_{1/2}) ± SD, n ≥ 3. Reproduced with permission from Cell, Elsevier.

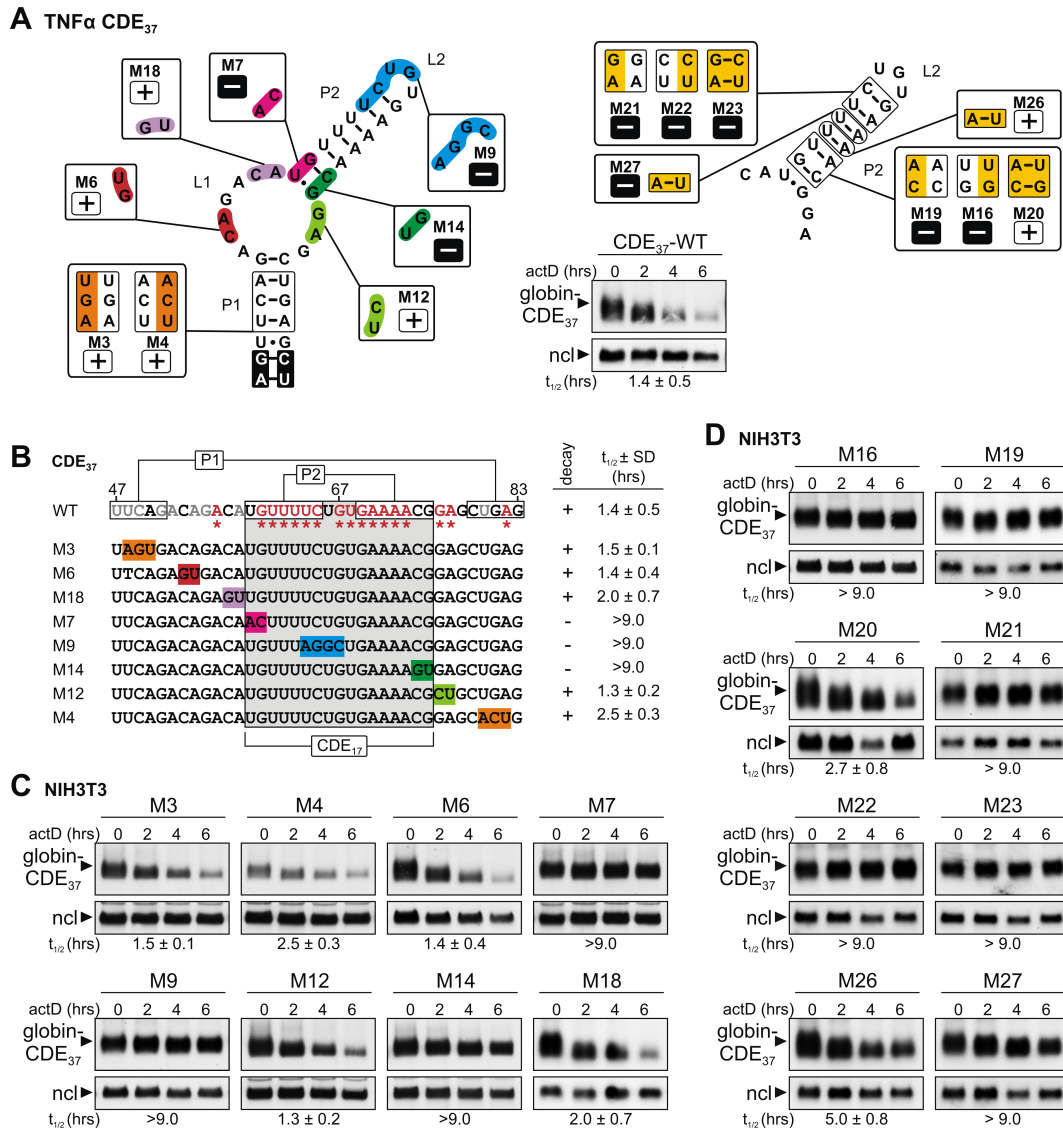


Figure 2.12: Mutational Analysis of the Mouse TNF α CDE. (A) Schematic representation of substitution mutations mapped onto the mouse TNF α CDE structure. CDE₃₇ mutants active in mRNA decay ($t_{1/2} < 6.0$ hrs) are labeled "+", inactive mutants ($t_{1/2} > 9.0$ hrs) are labeled "-". For comparison, decay of globin-CDE₃₇-WT-V3 was measured in transiently transfected NIH3T3 cells. (B) The same substitution mutations as in the left panel of A were mapped onto the linear TNF α CDE, $t_{1/2} \pm$ SD ($n \geq 3$) of the reporter mRNAs is given. (C) The effect of the CDE₃₇ mutations (in the V3 cloning context) on mRNA degradation was measured by transient transfection of the globin reporter genes into NIH3T3 cells. (D) P2 stem mutations were introduced into the TNF α CDE₃₇-V3, either in one strand to disrupt P2, or as compensatory mutations in both strands to restore P2. Globin reporter mRNA decay was measured in transiently transfected NIH3T3 cells by Northern blot analysis, average $t_{1/2} \pm$ SD, $n \geq 3$. Northern blot analysis was carried out as in Figure 2.11D. The mutagenesis analysis was performed with the assistance of Sonja Reitter. Reproduced with permission from Cell, Elsevier.

mutation M20 was also able to restore the activity of CDE₁₅₀ (**Figure 2.13B**), demonstrating the existence of a functional P2 stem in the context of the native TNF α 3'UTR. Taken together, both stem structure and nucleotide identity in the apical three base-pairs of P2 are essential for CDE activity, whereas base-pairing alone is sufficient in the basal part of P2.

Analysis of the trinucleotide L2 loop revealed that changing its middle position (nt 67) from G to A did not abrogate CDE₃₇ activity (M24, **Figure 2.13C**). Variation is also tolerated at position 66, where the human CDE has a C as opposed to a U in the mouse L2 loop (**Figure 2.11B–D**). Indeed, position 66 is the only nucleotide in the upper P2-L2 that is not 100% conserved among the mammalian TNF α sequences analyzed, differing, for instance, between the closely related human and chimpanzee. However, decay activity was lost when the entire UGU loop was replaced by ACA (M25, **Figure 2.13C**), indicating that the CDE allows only for limited nucleotide variation in the L2 loop.

Interestingly, the P2-L2 stem-loop in isolation was sufficient to promote rapid mRNA degradation when I provided an open, single-stranded (ss) conformation at the base of the P2 stem (CDE₁₇-ss, **Figure 2.13D**). In CDE₁₇-ss flanking *XbaI*-*AgeI* sites mimic the open conformation of the L1 loop. In contrast, the CDE was inactive when I terminally elongated the P2 stem by base-pairing sequence (CDE₁₇-ds), suggesting that the L1 loop at the base of P2 is also an important structural feature of the active CDE providing unpaired sequences in the natural context of the TNF α 3'UTR. From these experiments I concluded that the 17 nt long P2-L2 stem-loop with unpaired flanking nucleotides is the minimal element sufficient to induce CDE-mediated mRNA decay.

2.2.3 Identification of CDE-binding Proteins

As demonstrated in the previous chapter, I developed 4xS1m-mediated mRNP purification with the aim to identify specific RNA-BPs to RNA elements of interest. One major motivation for this project was to find CDE-binding proteins (CDE-BPs), as functional interaction partners were previously not known. Thus, I applied my optimized technique to the CDE by constructing 4xS1m-tagged CDE₃₇ RNAs for protein pulldown. Importantly, prior to up-scaled purifications, I confirmed that 4xS1m alone in context of an mRNA reporter does not induce mRNA decay. It does also not interfere with CDE-mRNA decay in transiently and stably transfected NIH3T3 cells (**Figure 2.14A**). Next, *in vitro* transcribed CDE₃₇-4xS1m and control 4xS1m RNAs were coupled to SA for affinity purification of proteins from NIH3T3 cell lysates (**Figure 2.14B**). While most purified proteins were associated with both RNAs, I was able to identify proteins specifically enriched with CDE₃₇-4xS1m by MS based on peptide counts (**Figure 2.14C**). Strongest peptide enrichment was ob-

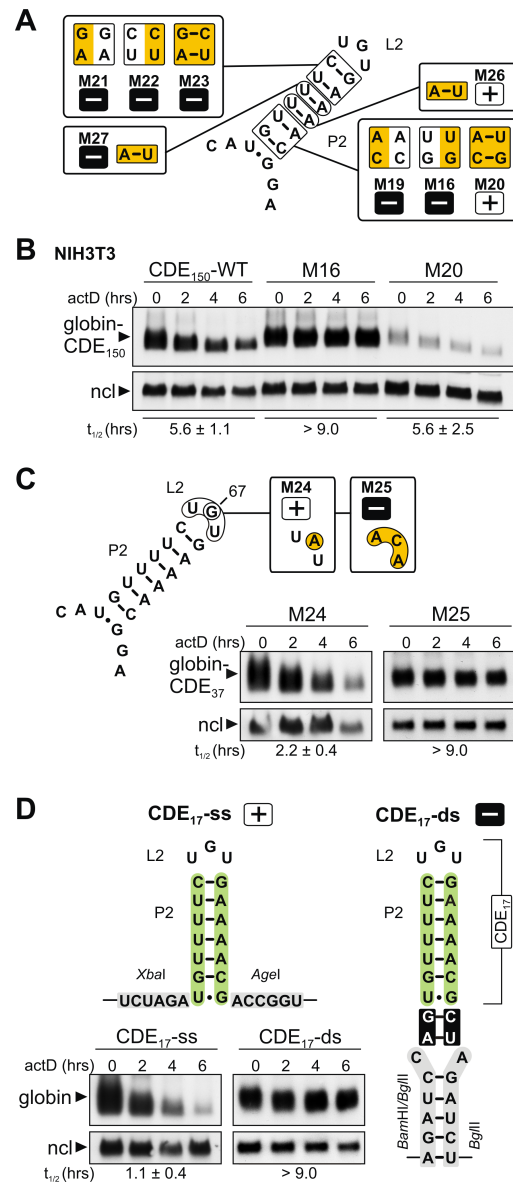


Figure 2.13: Mutational Analysis of the TNF α CDE Stem-Loop. (A) Summary of P2 stem mutations introduced into the TNF α CDE, either to disrupt or compensate P2 structure as in Figure 2.12. The mutated CDE₃₇ in the V3 context were cloned into the globin reporter gene 3'UTR, and mRNA decay was measured in transiently transfected NIH3T3 cells, average $t_{1/2} \pm SD$, $n \geq 3$. (B) P2 disrupting mutation M16 and compensatory mutation M20 were introduced into globin-TNF α -CDE₁₅₀, and mRNA decay was measured in transiently transfected NIH3T3 cells by Northern blot analysis, average $t_{1/2} \pm SD$, $n \geq 3$. (C) L2 loop mutations were introduced into globin-TNF α -CDE₃₇-V3, and mRNA half-lives (average $t_{1/2} \pm SD$, $n = 4$) were measured as in B. (D) The TNF α P2-L2 stem loop (CDE₁₇) was tested in two different cloning contexts that provide a ss or ds conformation at the base of P2. Reporter mRNA half-lives (average $t_{1/2} \pm SD$, $n = 3$) were measured as in B. The mutagenesis analysis was performed with the assistance of Sonja Reitter. Reproduced with permission from Cell, Elsevier.

served for Roquin (Rc3h1, RING finger and CCCH zinc finger protein 1). Its paralog Rc3h2, which I refer to as Roquin2, was also purified specifically with CDE₃₇-4xS1m. Roquin has previously been described as a protein that prevents autoimmunity by destabilizing the mRNA encoding ICOS [225] and thus seemed to be a very promising candidate regulator important for CDE-mediated mRNA decay.

2.2.4 Roquin and Roquin2 Specifically Bind to the CDE

I obtained a plasmid encoding EGFP-Roquin from the Vigo Heissmeyer group. In parallel, Sonja Reitter generated the according EGFP-Roquin2 plasmid based on a cDNA clone. With these tools on hand I performed RNA-IP. By RNA-IP using EGFP-binder beads, I could show that EGFP-Roquin strongly associated with globin-CDE₃₇ reporter mRNA, but not with the globin mRNA alone (**Figure 2.15B**). I obtained the same results with EGFP-Roquin2. I then investigated the two inactive CDE₃₇-mutants M7 and M9 in EGFP-Roquin RNA-IP (**Figure 2.15B**). M7 was bound equally well compared to the WT CDE₃₇, while M9 did not interact. In M7, base-pairing of 2 nts is disrupted in the basal part of the P2 stem. Roquin seemed to still be able to associate with this mutant. The M9, in which a 4 nt mutation affects the apical P2 stem and the L2 loop however, is altered too much to be recognized. Of note, both CDE₃₇-M7 and -M9 did not induce mRNA decay in the absence of exogenous Roquin in NIH3T3 cells as seen in the EGFP control (**Figure 2.15C**). Interestingly, decay of the CDE₃₇-M7 mRNA was activated by co-expression of EGFP-Roquin, whereas the CDE₃₇-M9 mRNA remained stable. This suggested that Roquin may interact with the apical part of P2-L2, and that overexpression of EGFP-Roquin might be sufficient to stabilize M7 in the active conformation.

By RNA-IP, I verified that EGFP-Roquin and -Roquin2 strongly associate with globin-CDE₁₅₀ reporter mRNA as well (**Figure 2.16A**). Disrupting the P2 stem in the CDE mutant M16 in context of CDE₁₅₀ dramatically reduced binding to EGFP-Roquin, while restoring the stem through a compensatory mutation in M20 rescued Roquin-binding (**Figure 2.16A**). Thus, this showed that Roquin recognizes the CDE as a stem-loop motif. It also indicated that the CDE stem-loop forms in context of its native UTR sequence which is bound by Roquin. Additionally, Fabian Pötz could show by *in vivo* crosslinking, subsequent EGFP-Roquin-IP and urea washes that the Roquin-CDE association occurs inside cells [246].

Roquin has been reported to localize in P-bodies in T cells [226], cytoplasmic foci in which most enzymes required for mRNA degradation are concentrated [219]. By immunofluorescence microscopy, Sonja Reitter could clearly visualize

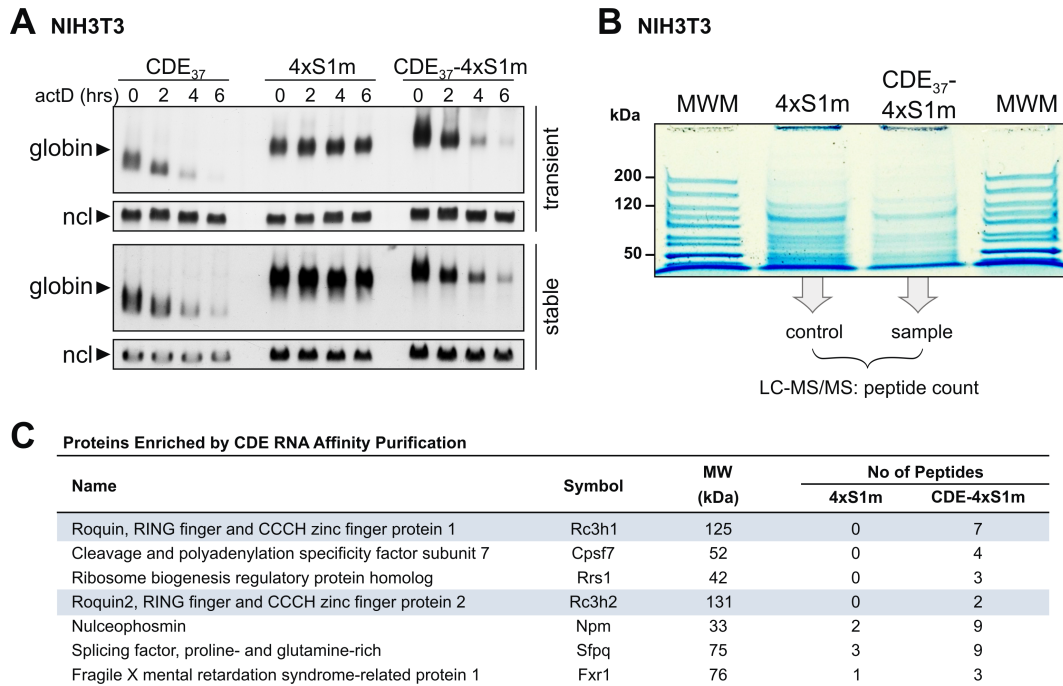


Figure 2.14: CDE RNA Affinity Purification of CDE-BPs Enriches for Roquin and Roquin2. (A) NIH3T3 cells were transiently (upper panel) and stably (lower panel) transfected with globin reporter genes containing either the TNF α CDE₃₇, the improved SA-binding aptamer 4xS1m, or both, in their 3'UTR. Reporter mRNA decay measurements by Northern blot analysis was done as in Figure 2.11D. (B) For purification of CDE-BPs, RNAs containing the 4xS1m alone or CDE₃₇-4xS1m were transcribed *in vitro*, coupled to SA Sepharose beads, and incubated with cytoplasmic NIH3T3 cell extracts. After washing, proteins were eluted from the matrix using RNase A, resolved by PAGE and visualized by colloidal Coomassie blue staining. MWM, molecular weight marker. (C) Out of the 252 proteins identified by MS, I only list those for which the peptide count in the CDE-4xS1m purification was ≥ 3 times higher than in the control 4xS1m. Reproduced with permission from Cell, Elsevier.

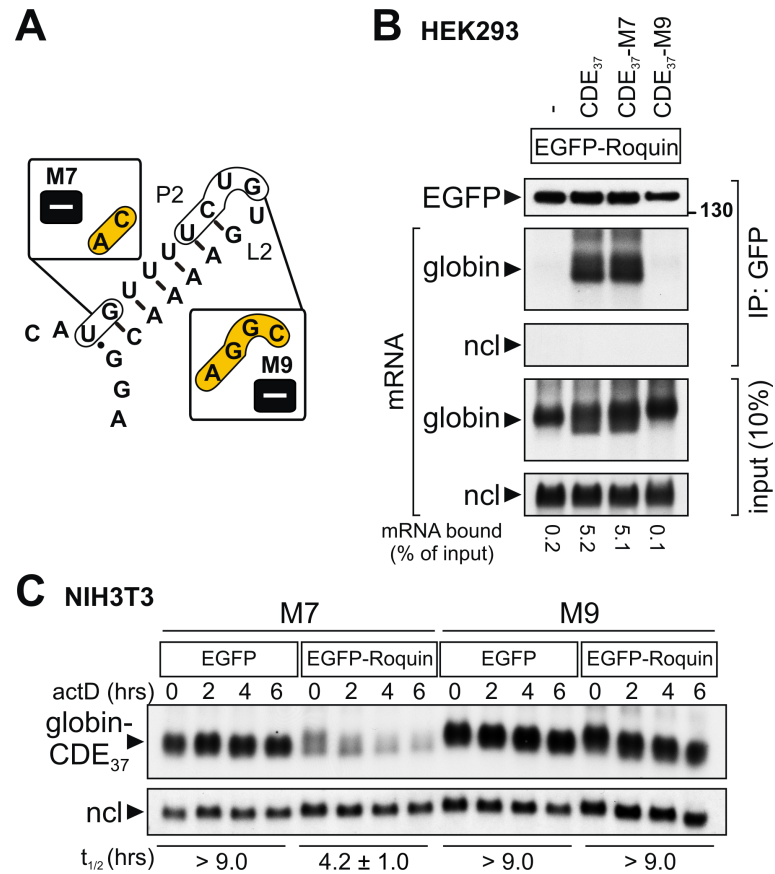


Figure 2.15: Roquin Binding and Overexpression Analysis of CDE-mutants M7 and M9. (A) Schematic representation of mouse TNF α CDE-mutants M7 and M9 mapped onto the CDE₃₇ stem-loop structure. (B) Binding of Roquin to CDE₃₇-M7 and -M9 was analyzed by RNA-IP as in Figure 2.6A showing that the CDE₃₇-M7 reporter mRNA binds to Roquin almost as efficiently as the WT CDE₃₇ reporter mRNA while CDE₃₇-M9 does not bind. (C) The effect of EGFP-Roquin overexpression on degradation of the control globin reporter mRNA lacking an insert (-) as well as mutant globin-TNF α -CDE₃₇-M7 and -M9 mRNA was examined by transient transfection in NIH3T3 cells, as described in Figure 2.11D. mRNA half-lives are given as average values \pm SD, n = 3.

co-localization of EGFP-Roquin and EGFP-Roquin2 with the P-body marker Rck in distinct cytoplasmic foci in HeLa, NIH3T3 and Huh7 cells (**Figure 2.16C**). In the meantime, this finding has been confirmed in HEK cells by others [239]. Roquin-induced mRNA deadenylation may thus be linked to relocalization of targeted mRNAs to P-bodies.

Roquin contains a RING finger, a ROQ domain, a ZF and a poorly defined C-terminal, proline-rich domain (**Figure 2.16B**). Since ZFs are frequently involved in RNA binding, as seen for many well-studied RNA-BPs like TTP [129], Sonja Reitter examined if the Roquin ZF domain is important for its function. She was able to show that mutation of the ZF domain in Roquin (C419R) [246] and Roquin2 (C416R) did neither alter their ability to associate with globin-CDE₃₇ mRNA to accelerate CDE mRNA degradation, nor their localization to P-bodies. Fabian Pötz then conducted domain-function analyses by investigating Roquin deletion mutants (**Figure 2.16B**). While deletion of the RING domain (Δ RING) had no effect compared to the WT, deletion of the ROQ domain (Δ ROQ) prevented binding to the CDE₃₇ reporter mRNA, decay activity and P-body localization. In line with this result, Roquin N-term as well as the ROQ domain alone were able to associate with globin-CDE₃₇ mRNA, whereas Roquin C-term was not. Of all these truncation mutants only Δ RING was found to localize in P-bodies. I also tested the activity of fulllength Roquin containing the *sanroque* mutation harboring a single amino acid substitution (M199R) due to which *sanroque* mice display a lupus-like autoimmune syndrome [227]. This is believed to be caused by increased ICOS mRNA expression due to impaired Roquin function while RNA binding activity does not change [245]. With regard to RNA-IP and decay promoting activity, Roquin-M199R interacted with the CDE and mediated decay as WT Roquin (data not shown). Thus, I did not further investigate the *sanroque* mutation. These results are summarized in the table in **Figure 2.16C**.

By EMSA, I then examined whether Roquin interacts directly with the CDE RNA *in vitro*. First, I purified recombinant Roquin-N protein (amino acids 2–440, **Suppl. Figure 5.4A**) already described in Glasmacher *et al.* (2010), which could be obtained in a highly pure form (**Suppl. Figure 5.4B**). Roquin-N was found to efficiently bind to a 23 nt long CDE stem-loop RNA (CDE₂₃), which consists of the P2-L2 stem-loop plus three adjacent nucleotides of L1 at each end, with an apparent K_d of 92 nM (**Figure 2.17**). In contrast, the mutant CDE₂₃-M23 harboring a compensatory 2 base-pair mutation in the functionally important apical part of P2 did not associate with Roquin-N, and an unstructured ARE RNA of identical length did not bind either (**Figure 2.17**). In summary, from these experiments I concluded that Roquin recognizes the CDE stem-loop with high specificity both *in vitro* and inside cells.

2.2 Roquin-mediated Constitutive Decay of CDE-containing mRNAs

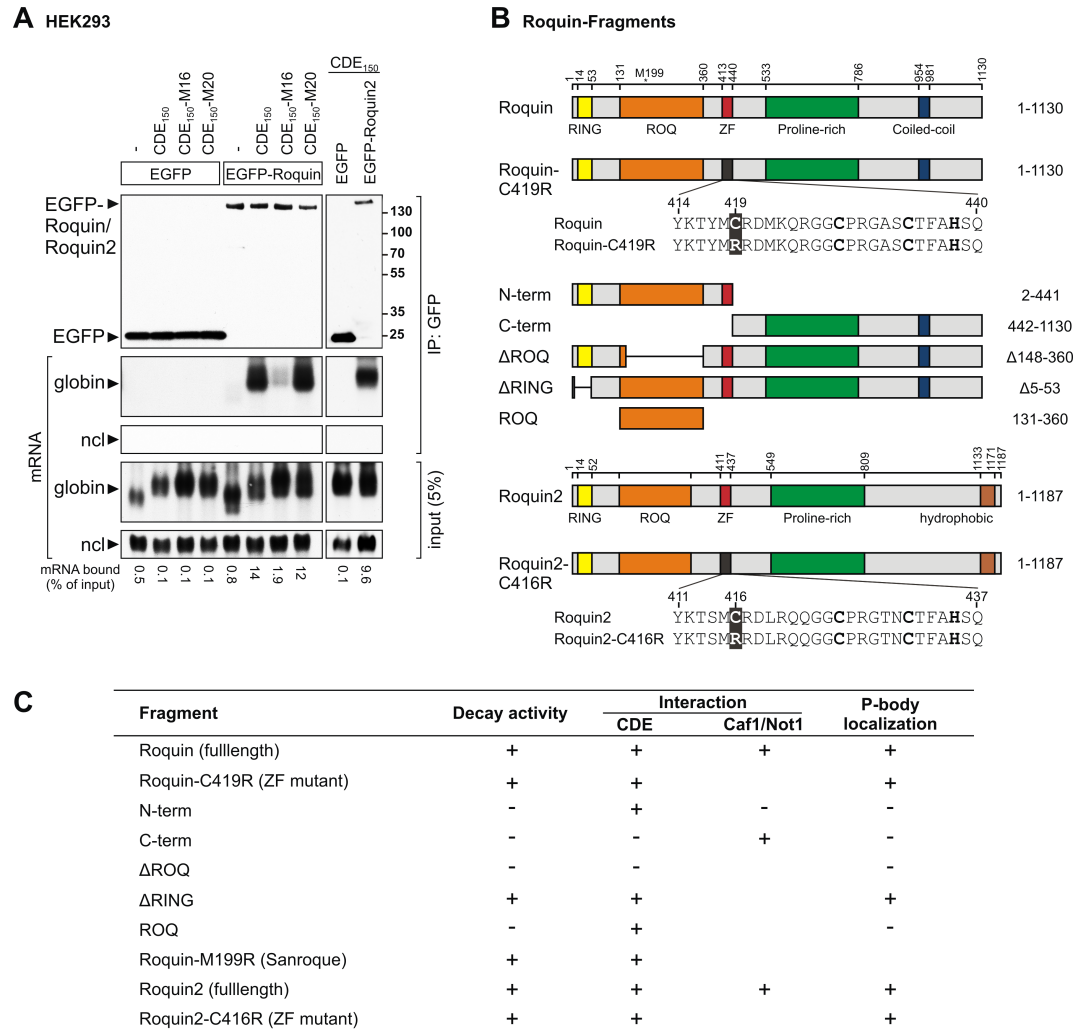


Figure 2.16: Specific Binding of Roquin to the CDE Inside Cells. (A) Binding of Roquin to the mouse TNF α CDE₁₅₀ was analyzed by RNA-IP. HEK293 cells were transiently transfected with EGFP, EGFP-Roquin or -Roquin2 together with a globin reporter lacking an insert (-), globin-TNF α -CDE₁₅₀, or the corresponding M16 and M20 mutants. Upon IP, EGFP-tagged proteins were monitored by anti-GFP Western blot analysis. Associated reporter mRNAs were visualized by Northern blot analysis, ncl mRNA serves as negative control. The fraction of mRNA bound by IP is given as % of the input. (B) Schematic representation of mouse Roquin domains; ZF, zinc finger. Deletion mutants are depicted below the fulllength protein. Numbers indicate amino acid positions, M199 refers to the position mutated to R in *sanroque* mice. (C) Table summarizing structure-function analysis of Roquin fulllength and fragments with respect to CDE decay activity as well as CDE and Caf1/Not1 interaction. The majority of the domain analysis was performed by Fabian Pötzt, while ZF mutants and Roquin2 construct generation, as well as localization analysis was done by Sonja Reitter. Reproduced with permission from Cell, Elsevier.

2.2.5 Roquin and Roquin2 Promote CDE-mediated mRNA Decay

As a first test for Roquin function, EGFP-Roquin or -Roquin2 were ectopically expressed (**Figure 2.18**) in HeLa and NIH3T3 cells to examine whether Roquin and Roquin2 are important for CDE-mediated mRNA decay. By Western blot analysis (**Figure 2.18A**), I showed that in both cell lines, the amount of overexpressed EGFP-Roquin is highly increased with respect to endogenous Roquin levels. Roquin2 could not be detected due to lack of a specific antibody. I found both overexpressed EGFP-Roquin and -Roquin2 to accelerate degradation of globin-CDE₁₅₀ mRNA up to 4-fold compared to the EGFP control in NIH3T3 cells (**Figure 2.18B**). This effect was less pronounced for globin-CDE₃₇ mRNAs as its decay in the absence of excess Roquin was already very fast. The reporter mRNA lacking a CDE remained stable (**Figure 2.18C**). In HeLa cells, that generally do not mediate CDE mRNA decay, elevated expression of Roquin accelerated CDE-mediated mRNA decay even more strongly. Degradation of globin-CDE₃₇ (**Figure 2.18D**) and globin-CDE₁₅₀ (**Figure 2.18E**) reporter mRNA was induced by overexpression of EGFP-Roquin and -Roquin2. Hereby, Roquin2 appeared to be less effective in decay induction, possibly because EGFP-Roquin2 is expressed at lower levels than EGFP-Roquin in HeLa cells with identical amounts of plasmid transfected (**Figure 2.18A**). This analysis indicated that in both NIH3T3 and HeLa cells, mRNA decay of CDE-containing mRNAs can be accelerated by ectopical overexpression of Roquin and Roquin2.

Taking the opposite approach, I then examined the effect of knocking down Roquin and Roquin2. In NIH3T3 cells, knockdown (kd) of either protein alone (**Suppl. Figure 5.5A**) caused a modest 2-fold stabilization of globin-CDE₃₇ mRNA, whereas the simultaneous kd of both proteins led to a 7-fold stabilization (**Figure 2.19A** and **Suppl. Figure 5.5B**). Fabian Pötz then constructed an siRNA-resistant Roquin cDNA that cannot be recognized by siRNA Roquin (B) (si(B)-res) and thus rescues Roquin expression after si-Roquin (B) kd in HEK and NIH3T3 cells as validated by Western blot analysis (**Suppl. Figure 5.5C**). Expression of si(B)-res Roquin cDNA restored degradation of the CDE₃₇ reporter mRNA after kd of endogenous Roquin and Roquin2 (**Figure 2.19B**), demonstrating the specificity of the Roquin kd effect on CDE mRNA decay.

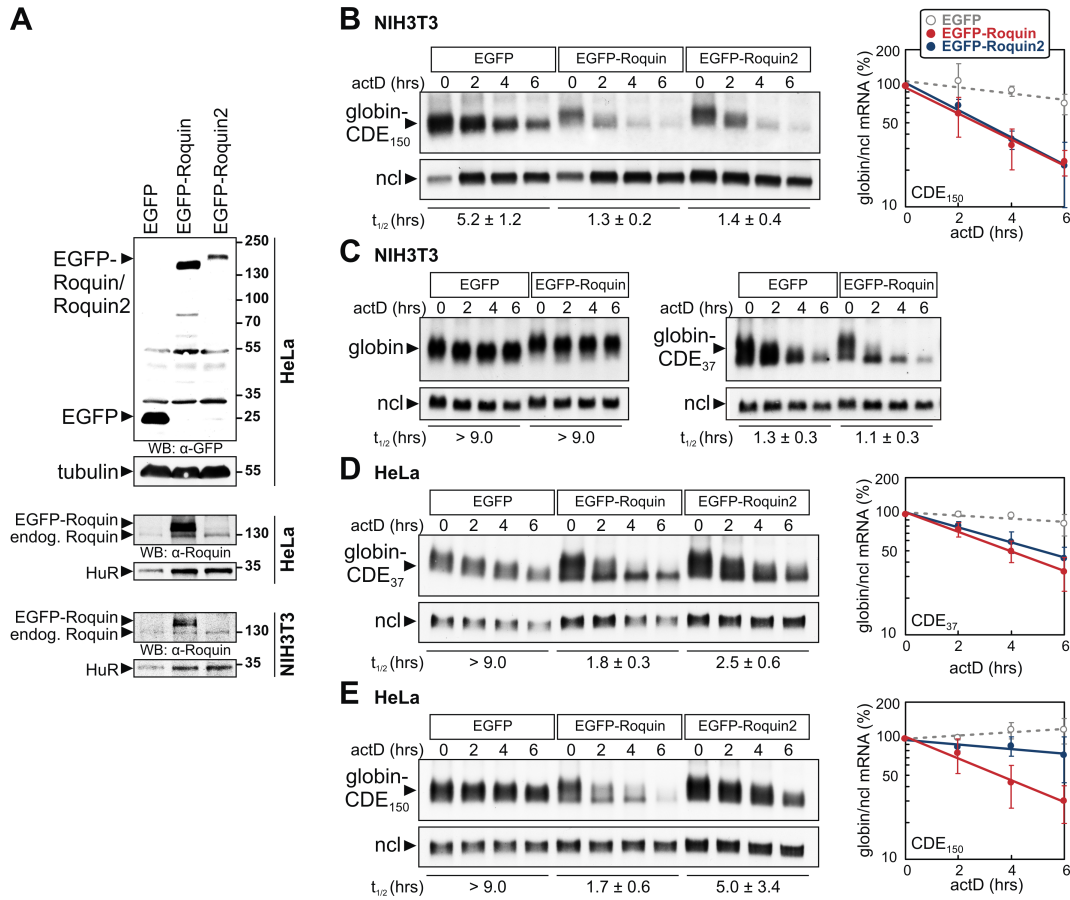


Figure 2.18: Roquin Overexpression Accelerates CDE-mediated mRNA Degradation. (A) Equal amounts of plasmid encoding EGFP, EGFP-Roquin or EGFP-Roquin2 were transiently transfected into HeLa and NIH3T3 cells, corresponding to the amounts used for the experiments in B-E. Upper panel, proteins were detected by anti-GFP Western blot analysis, tubulin serves as a loading control; middle panel, endogenous Roquin and EGFP-Roquin were detected using an anti-Roquin antibody, HuR serves as a loading control; bottom panel, same analysis in NIH3T3 cells. (B) NIH3T3 cells were transiently transfected with EGFP, EGFP-Roquin or -Roquin2 together with globin-TNF α -CDE₁₅₀. Reporter mRNA degradation was measured as in Figure 2.11D, average $t_{1/2} \pm$ SD, $n \geq 3$. Right panel, decay curves show average globin reporter mRNA levels normalized to ncl mRNA as % of the initial value (\pm SD), plotted against time. (C) The effect of EGFP-Roquin overexpression on degradation of the control globin reporter mRNA as well as globin-TNF α -CDE₃₇-V3 mRNA was examined by transient transfection in NIH3T3 cells, as described in Figure 2.11D, average $t_{1/2} \pm$ SD, $n = 3$. (D) HeLa cells were transiently transfected with EGFP, EGFP-Roquin or EGFP-Roquin2 together with globin-TNF α -CDE₃₇-V3. Left panel, degradation of the reporter mRNA was measured as in Figure 2.11D, average $t_{1/2} \pm$ SD, $n \geq 3$. Right panel, decay curves as in B. (E) The same analysis as in D with the globin-TNF α -CDE₁₅₀ reporter. Overexpression analysis was performed with the assistance of Sonja Reitter. Reproduced with permission from Cell, Elsevier.

2.2 Roquin-mediated Constitutive Decay of CDE-containing mRNAs

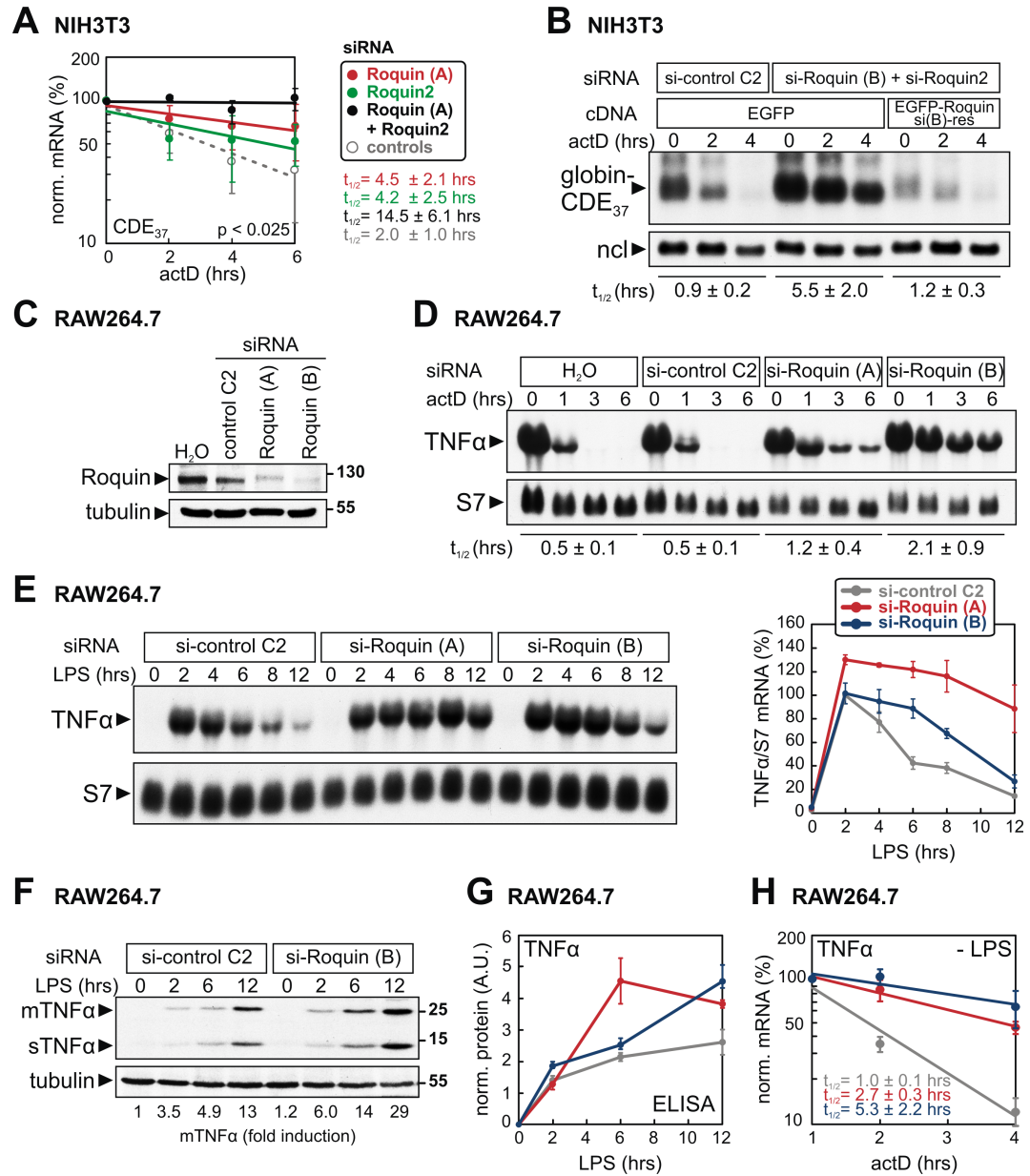


Figure 2.19: Roquin is Required for CDE-mediated mRNA Degradation. (A)

Knockdown of Roquin and Roquin2, either alone or in combination, and transient expression of globin-TNF α -CDE₃₇-V3 in NIH3T3 cells. Reporter mRNA decay rates were quantified from Northern blots (depicted in Suppl. Figure 5.6B), average $t_{1/2} \pm$ SD, $n \geq 3$. The p-value (one-sided T-test) is given for $t_{1/2}$ of double Roquin/Roquin2 kd and combined controls. (B) EGFP or EGFP-Roquin-si(B)-res was transfected into NIH3T3 cells one day after transfection of control siRNA C2 or Roquin-siRNA (B). Degradation of globin-TNF α -CDE₃₇-V3 reporter mRNA was measured on day 2 as in Figure 2.11D. (C) RAW264.7 cells were transfected twice over a period of 2 days with water (H₂O), control siRNA (C2), or two different siRNAs against Roquin (Roquin (A) and Roquin (B)). Roquin protein levels were assessed by Western blot analysis. (Figure legend continued on next page)

Figure legend continued: **(D)** RAW264.7 cells were transfected with siRNAs as in C, and stimulated with LPS (100 ng/ml) for 2 hours prior to addition of actD. Endogenous TNF α mRNA decay was measured by Northern blot analysis, ribosomal protein S7 mRNA serves as loading control; average $t_{1/2} \pm SD$, $n = 3$. **(E)** TNF α mRNA expression in response to LPS was analyzed by Northern blot in RAW264.7 cells subjected to Roquin or control kd. Right panel, quantification of average TNF α mRNA levels normalized to S7 mRNA ($\pm SD$, $n = 3$). **(F)** Synthesis of mTNF α and sTNF α in response to LPS was analyzed by Western blot in RAW264.7 cells subjected to Roquin or control kd. Quantification of mTNF α normalized to tubulin is shown. **(G)** TNF α secretion was measured by ELISA in the supernatants of RAW264.7 cells treated as in E. The graph shows normalized TNF α levels (average $\pm SE$, $n = 3$). **(H)** Degradation of TNF α mRNA was measured in resting RAW264.7 macrophages by RT-qPCR after normalization to NupL1 mRNA. Shown are average values $\pm SD$, $n = 3$. Data in H was obtained by Sonja Reitter. Reproduced with permission from Cell, Elsevier.

These results were corroborated in LPS-stimulated RAW264.7 macrophages, where kd of Roquin by two different siRNAs ((A) and (B)), as monitored by Western blot analysis (**Figure 2.19C**), led to a 2- to 4-fold stabilization of endogenous TNF α mRNA (**Figure 2.19D**) as shown by Northern blot analysis. Importantly, Roquin kd by siRNA (A) and (B) prevented rapid clearance of TNF α mRNA during prolonged exposure of macrophages to LPS up to 12 hours (**Figure 2.19E**). In stimulated macrophages, after a sharp early increase, TNF α mRNA levels would normally decrease with time due to activated anti-inflammatory pathways as seen for the si-C2 control. When I examined TNF α protein levels, I observed that Roquin kd caused elevated levels of both membrane-bound (m) and secreted (s)TNF α , as shown by Western blot analysis and ELISA (**Figures 2.19F–G**). Of note, the simultaneous kd of Roquin and Roquin2, as seen to be necessary for a full response in NIH3T3 cells before, did not cause a further increase in TNF α mRNA (**Suppl. Figure 5.5D**) or protein (**Suppl. Figure 5.5E**) levels in macrophages as compared to kd of Roquin alone. This was presumably because Roquin depletion was less efficient in the double kd condition (**Suppl. Figure 5.5F**). In addition, Sonja Reitter detected that in unstimulated macrophages, TNF α mRNA was also stabilized upon kd of Roquin (**Figure 2.19H**). Taken together, these results demonstrate that Roquin, by binding to the CDE and accelerating mRNA decay, is crucial for limiting TNF α production in both resting and activated macrophages.

2.2.6 Roquin Promotes CDE-mRNA Deadenylation by Recruitment of Ccr4-Caf1-Not

To further explore the mechanism of Roquin-induced mRNA decay, Sonja Reitter stably expressed EGFP, EGFP-Roquin and EGFP-Roquin2 in HEK293 cells and affinity-purified them via the GFP-binder. By MS, this revealed Not1 to be strongly associated with both Roquin and Roquin2 [246]. Not1 is the scaffold subunit of the Ccr4-Caf1-Not complex, a major deadenylase in eukaryotic cells [317, 163]. Indeed, virtually all the other subunits of the complex including Not2, Not3, Not10, TAB182, Ccr4b, Caf1a and Caf1b were enriched in the Roquin and Roquin2 purifications. By co-IP, I confirmed that EGFP-Roquin and -Roquin2 interact with endogenous Not1 and Caf1a (**Figure 2.20A**), which Fabian Pötz also confirmed to be occurring in an RNA-independent manner [246]. He also found that it is the C-terminal domain of Roquin that associates with Not1 and Caf1a (**Figure 2.16C**, [246]).

A previous study suggested that Roquin may activate ICOS mRNA degradation by interacting with enhancers of mRNA decapping [226]. However, and in line with the finding that Roquin interacts with the deadenylase complex, I noticed that EGFP-Roquin primarily enhanced deadenylation of a CDE-containing mRNA (**Figure 2.18C**). I thus tested Caf1a-AA, a dominant-negative mutant of the deadenylase Caf1a, generated in the Stoecklin lab before [131]. I found that its overexpression fully blocked both deadenylation and degradation of globin-CDE₃₇ mRNA as observed on higher resolution Northern blots (**Figure 2.20B**). As opposed to Caf1a-AA, overexpression of neither Caf1a-WT (**Figure 2.20C**) nor of the dominant-negative decapping enzyme Dcp2-AA (**Figure 2.20B**) affected CDE-mRNA decay showing that CDE reporter mRNA is deadenylated before the body of the mRNA is degraded. The strong inhibitory effect of dominant-negative Caf1a-AA indicated that deadenylation is the first step in CDE-mediated mRNA degradation. These data provide strong evidence that Roquin recruits the Ccr4-Caf1-Not complex and thereby induces rapid deadenylation and subsequent degradation of its target mRNAs.

2.2.7 ICOS mRNA Contains a Functional CDE

Roquin was reported to enhance the degradation of ICOS mRNA [227, 225], yet the exact binding motif was unknown. By empirically inspecting the ICOS sequence, I found a highly conserved CDE-like element in the 3'UTR of human and mouse ICOS (**Figure 2.21A**), as well as other mammals, as annotated in NCBI (**Figure 2.21B**). I saw that while the stem in the ICOS element is 2 base-pairs shorter than the P2 stem in the TNF α CDE, the functionally

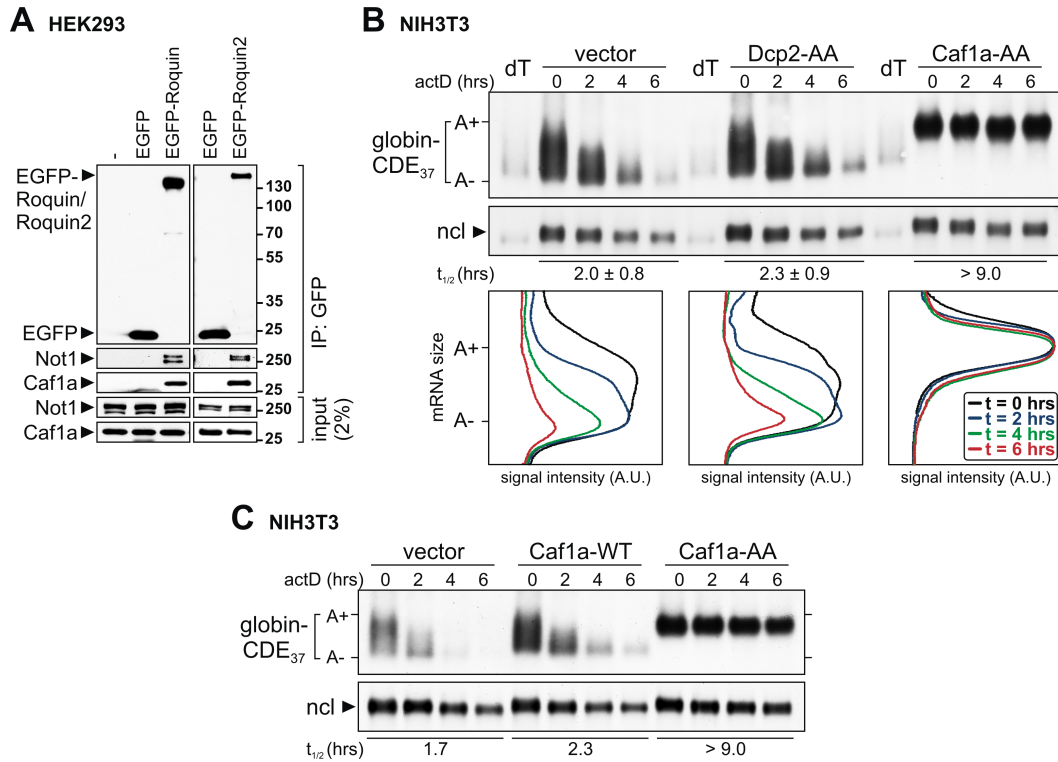


Figure 2.20: The CDE Induces Caf1-dependent mRNA Deadenylation. (A) HEK293 cells were transiently transfected with EGFP, EGFP-Roquin or -Roquin2. After EGFP-IP from cytoplasmic lysates endogenous Not1 and Caf1a were detected by Western blot analysis. (B) NIH3T3 cells were transiently transfected with globin-TNF α -CDE₃₇-V3 together with a vector control, dominant-negative Dcp2-AA or dominant-negative Caf1a-AA. Reporter mRNA degradation was analyzed as in Figure 2.11D, except that RNA was resolved on a higher resolution 1.6% agarose gel. dT, treatment of RNA with oligo-dT and RNase H to remove poly(A) tails, average $t_{1/2} \pm SD$, $n = 3$. Bottom panel, deadenylation was visualized by quantifying the signal intensity (A.U., arbitrary units) of the reporter mRNA along the length of the signal, plotted against mRNA size; A+, polyadenylated; A-, deadenylated mRNA. (C) NIH3T3 cells were transiently transfected with globin-TNF α -CDE₃₇-V3 together with either vector control, WT Caf1a or Caf1a-AA. mRNA degradation was analyzed as in B. Reproduced with permission from Cell, Elsevier.

important apical part of the stem is identical in sequence. When I cloned it into the ss globin 3'UTR context, ICOS CDE₁₇-ss induced reporter mRNA decay, which was further accelerated by overexpression of EGFP-Roquin (**Figure 2.21C**). These results imply that Roquin recognizes the ICOS mRNA via a functional CDE-like stem-loop motif.

2.2.8 Roquin Recognizes a Conserved Class of CDE-containing mRNAs

With the aim to predict CDE-containing mRNAs genome-wide, Johanna Schott combined our experimental mutagenesis data and derived a structure- and sequence-based CDE consensus motif (**Figure 2.22A**). CDEs were defined by a trinucleotide pyrimidine-purine-pyrimidine loop and a 5–8 base-pairs long stem whose apical 3 base-pairs match the consensus in the TNF α and ICOS CDE. For bioinformatics analyses, her CDE conservation criteria only classified detected stem-loops as CDEs that were conserved in >10/46 vertebrate species based on the UCSC 46 vertebrate genome alignment [318]. When she searched all 3'UTRs of the mouse transcriptome, she identified 109 putative CDEs in 108 genes [246]. Notably, 56 of the identified CDEs were highly conserved in >10 out of 46 vertebrate species (**Figure 2.22C**, [246]). She further showed that the corresponding genes are preferentially associated with regulation of development, transcription, nucleic acid metabolism and T cell differentiation based on Gene Ontology (GO)-term analysis [246].

I next aimed at experimentally determining Roquin target mRNAs. Thus, I immunoprecipitated endogenous Roquin from cytoplasmic lysates of LPS-stimulated macrophages (**Figure 2.22B**) and identified Roquin-associated mRNAs (**Suppl. Table 5.2**) by deep sequencing of RNA samples. The bioinformatics analysis of deep sequencing data was all performed by Johanna Schott. Importantly, the three biological replicates were highly reproducible (**Suppl. Figure 5.6**). Remarkably, 15 mRNAs with conserved CDEs in the 3'UTR, based on our criteria, showed a strong and highly significant enrichment in the Roquin-IP (red in **Figure 2.22D**, frequency of association in **Figure 2.22C**). There were four mRNAs enriched that contain a CDE in the ORF, as well as additional 76 enriched mRNAs that lack a CDE. However, the group of mRNAs that were highest enriched were at the same time the ones harboring conserved CDEs. This major finding strongly supported our previous data and demonstrated that Roquin target mRNAs preferentially contain a conserved and thus putative functional CDE.

For the highest enriched Roquin target mRNA candidates, I derived a secondary structure consensus for their respective CDEs based on conservation data provided in the UCSC Genome alignment (**Figure 2.23A**). The top

2.2 Roquin-mediated Constitutive Decay of CDE-containing mRNAs

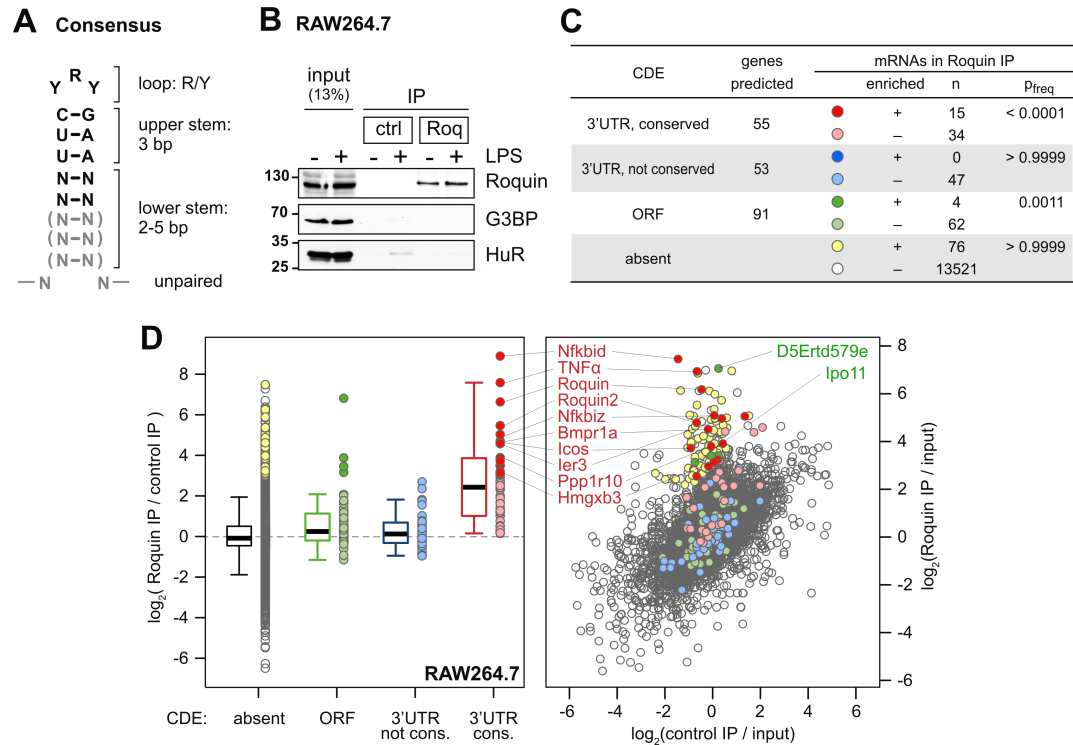


Figure 2.22: Genome-wide Identification of CDEs and Roquin Target mRNAs.

(A) Consensus CDE stem-loop motif used for bioinformatics prediction of CDE-containing mRNAs generated by Johanna Schott. (B) Endogenous Roquin (Roq) was immunoprecipitated from cytoplasmic lysates of RAW264.7 macrophages \pm stimulation with LPS (100 ng/ml) for 2 hours. HA-antibody was used for control (ctrl) IP. Roquin-IP was monitored by Western blot analysis, RNA-binding proteins G3BP and HuR serve as controls for specificity. (C) Numbers of genes predicted to contain a CDE and corresponding mRNAs significantly enriched by Roquin-IP from LPS-stimulated RAW264.7 macrophages. Significant enrichment is defined by a p-value ≤ 0.005 (Roquin-IP vs control-IP) and fold enrichment (Roquin-IP / control-IP) > 8.0 . P_{freq} represents the hypergeometric probability of randomly finding the observed number of mRNAs enriched by Roquin-IP in each of the four groups of mRNAs, given the overall frequency of 95 significantly enriched mRNAs in a total of 13,759 mRNAs. Analysis performed by Johanna Schott. (D) mRNAs associated with Roquin in LPS-stimulated RAW264.7 macrophages were recovered by RNA-IP and identified by RNA-Seq, $n = 3$. Left: average enrichment (Roquin-IP / control-IP) is plotted for all RefSeq-annotated transcripts that were identified, grouped according to the bioinformatics prediction of CDEs. Right: enrichment over input is depicted for the same transcripts. The color code refers to C. Analysis performed by Johanna Schott. Reproduced with permission from Cell, Elsevier.

Roquin target (475-fold enrichment) was Nfkbid mRNA, which also represents the only mouse transcript that contains a tandem CDE stem-loop motif in its 3'UTR (**Figure 2.23A**). The mRNAs encoding Roquin and Roquin2 themselves contain conserved CDEs and were enriched by Roquin-IP, suggesting that Roquin proteins may regulate their own mRNAs as part of a feedback loop. Consistent with my previous results, TNF α and ICOS mRNA were strongly enriched by Roquin-IP. Thus, an unbiased RNA-IP approach provided compelling evidence that CDE-containing mRNAs are the primary targets of Roquin.

I then verified binding of several mRNAs containing conserved CDEs (**Figure 2.23A**) by IP of endogenous Roquin from macrophages followed by RT-qPCR. TNF α mRNA was found to associate with Roquin to a similar degree in resting and stimulated macrophages (**Figure 2.23B**, left panel). Like TNF α mRNA, several of the candidate CDE mRNAs, especially immune regulators as Nfkbiz and Ier3, were induced in expression upon LPS treatment of macrophages and were hardly detected in resting cells (**Suppl. Figure 5.7A**). In contrast to four control mRNAs lacking a CDE, six out of seven mRNAs with conserved CDEs were strongly enriched (≥ 20 -fold) by Roquin-IP from LPS-stimulated RAW264.7 macrophages (**Figure 2.23B**, right panel). For target mRNAs detectable also in resting macrophages, all data are summarized in **Suppl. Figure 5.7B**. Together, these data suggested that all putative Roquin targets tested could be confirmed to specifically associate with Roquin in RAW264.7 cells.

I further investigated, with the help of Johanna Schott, whether Roquin controls the degradation of newly identified, CDE-containing target mRNAs. Indeed, kd of Roquin and Roquin2 led to the stabilization of Nfkbiz, Ier3, Ppp1r10 and Hmgxb3 mRNA in NIH3T3 cells while ectopic expression of siRNA-resistant Roquin impressively restored the degradation of these mRNAs (**Figure 2.23C**). Nfkbid mRNA could not be analyzed in NIH3T3 cells due to its low expression level in these cells, but was as well found to be stabilized by kd of Roquin in RAW264.7 macrophages (**Figure 2.23D**). These results demonstrate that Roquin not only associates with CDE mRNAs but in fact regulates the degradation of numerous mRNAs containing CDE stem-loop motifs.

2.2.9 Interference with CDE-Roquin Binding Alleviates TNF α Suppression

Finally, I explored whether Roquin-mediated mRNA regulation could be blocked with a *trans*-acting antisense morpholino (MO) that interferes with CDE stem-loop formation. CDE-MO-1 and -2 were designed to base-pair with

2.2 Roquin-mediated Constitutive Decay of CDE-containing mRNAs

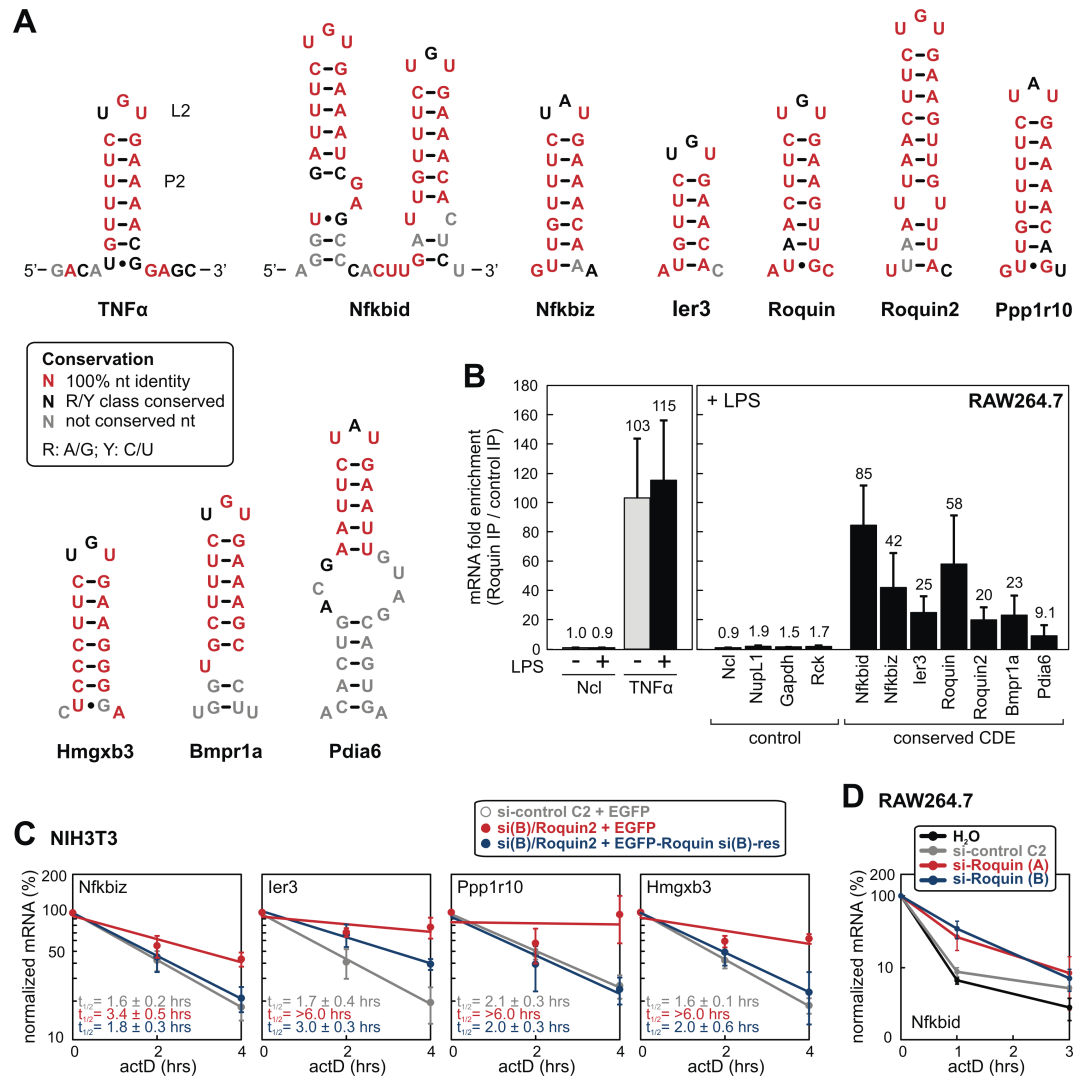


Figure 2.23: Confirmation of CDE-containing mRNAs as Roquin Targets. (A)

Secondary structures predicted for conserved CDEs representing the mouse CDE. Nucleotides are color-coded according to conservation (UCSC genome alignment) as in Figure 2.11. (B) Binding of mRNAs by Roquin RNA-IP. Left: TNF α mRNA was quantified by RT-qPCR after IP of Roquin from RAW264.7 macrophages \pm stimulation with LPS (100 ng/ml) for 2 hours. The signal was divided by the amount of TNF α mRNA in the control IP, and expressed as fold enrichment (average \pm SE, $n \geq 7$). Right: average enrichment \pm SE ($n \geq 3$) of 4 control mRNAs and 7 mRNAs containing conserved CDEs. (C) Degradation of the CDE-containing Nfkbiz, Ier3, Ppp1r10 and Hmgxb3 mRNAs was measured by RT-qPCR in NIH3T3 cells after control kd (siRNA C2), kd of Roquin/Roquin2, and rescue by siRNA-resistant Roquin. All mRNA levels were normalized to NupL1 mRNA, average $t_{1/2} \pm$ SE, $n = 3$. (D) Degradation of the tandem CDE-containing Nfkbid mRNA was measured by RT-qPCR in RAW264.7 macrophages after stimulation with LPS (100 ng/ml) for 2 hours. Nfkbid mRNA levels were normalized to NupL1 mRNA, average $t_{1/2} \pm$ SE, $n = 3$. Data in C and D were generated with the assistance of Johanna Schott and Sonja Reitter. Reproduced with permission from Cell, Elsevier.

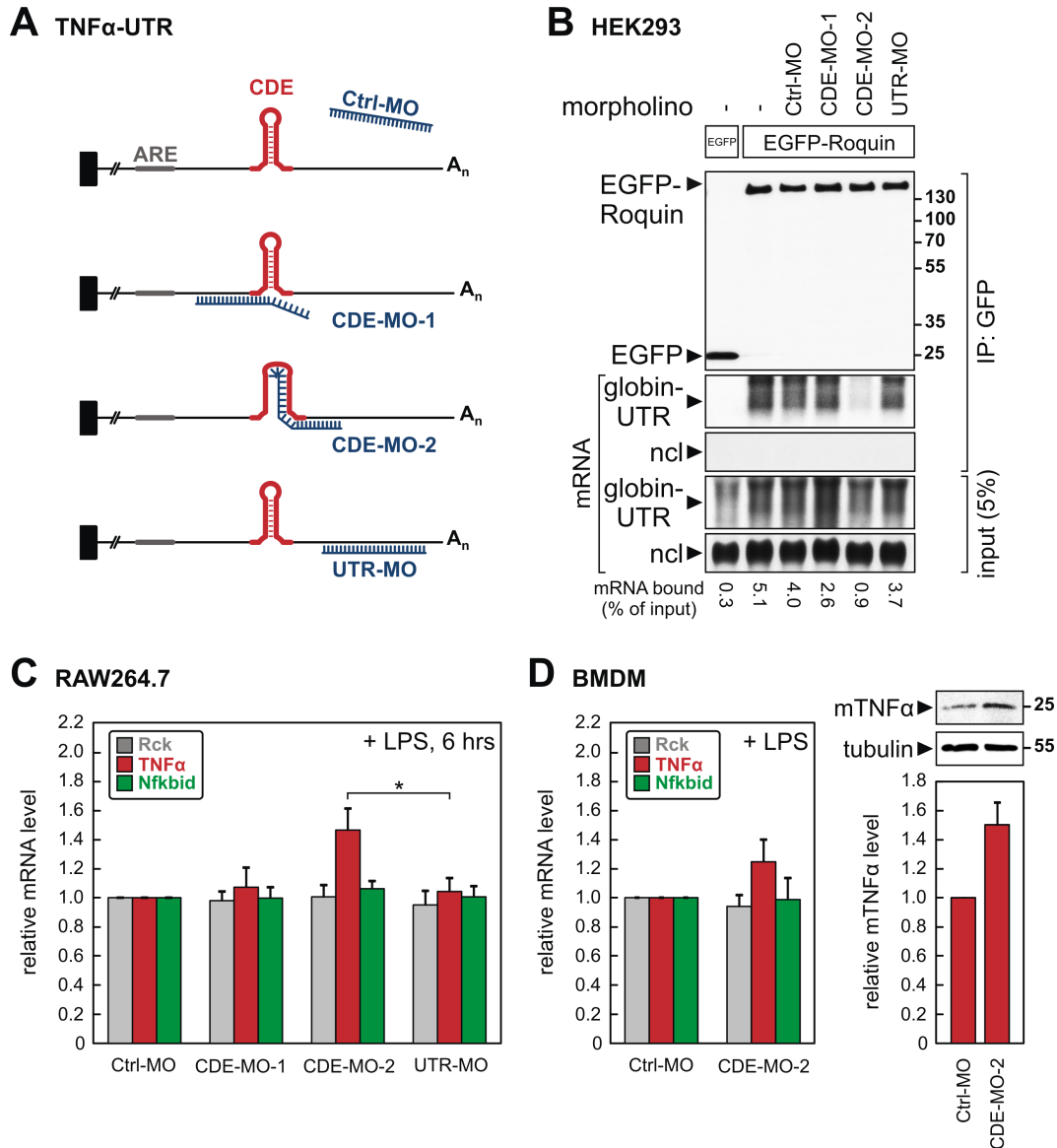


Figure 2.24: Interference with CDE-Roquin Binding Elevates TNF α Expression. (A) Schematic representation of antisense morpholinos Ctrl-MO, CDE-MO-1, CDE-MO-2 and UTR-MO interacting with the TNF α 3'UTR. (B) MOs were transfected into HEK293 cells together with EGFP-Roquin and globin-TNF α -UTR containing the entire mouse TNF α 3'UTR. Proteins were monitored after EGFP-IP by anti-GFP Western blot analysis. Reporter mRNA binding was monitored as in Figure 2.15A. (C) One day after MO delivery into RAW264.7 macrophages using 2 μ M Endo-Porter, cells were stimulated with LPS (100 ng/ml) for 6 hours. Rck, TNF α and Nfkbid mRNA levels were measured by RT-qPCR and normalized to NupL1; average values \pm SE, $n \geq 6$; * indicates $p < 0.05$ by two-tailed, paired T-test. (D) Ctrl-MO and CDE-MO-2 were delivered into primary mouse BMDM as in C. Left: average mRNA values \pm SE, normalized to NupL1, $n = 9$, were measured by RT-qPCR. Right: mTNF α protein was assessed by Western blot analysis; quantification of mTNF α normalized to tubulin is depicted below the blot, average values \pm SE, $n = 6$. Reproduced with permission from Cell, Elsevier.

the left and right arm of the TNF α CDE stem-loop, respectively (**Figure 2.24A**). As controls, I used a provided Ctrl-MO lacking any target sequence and UTR-MO, a morpholino designed to base-pair with the TNF α 3'UTR downstream of the CDE. RNA-IP of EGFP-Roquin in HEK cells showed that CDE-MO-2 reduces binding of Roquin to the 3'UTR of TNF α mRNA by 4-fold (**Figure 2.24B**). In contrast, CDE-MO-1 was not able to compete with CDE-Roquin binding, presumably because the portion that needs to invade the P2-L2 stem-loop is shorter in CDE-MO-1 (7 nt) than in CDE-MO-2 (11 nt). When introduced into RAW264.7 macrophages and upon LPS stimulation for 6 hours, I saw that CDE-MO-2 specifically increased the expression of endogenous TNF α mRNA by 1.5-fold (**Figure 2.24C**), whereas it did not affect two control mRNAs: *Rck*, which does not contain a CDE, and *Nfkbid*, whose tandem CDEs lack sequence complementarity to CDE-MO-2 outside of the stems. The extent to which CDE-MO-2 increased TNF α mRNA expression was similar to the effect of Roquin kd on TNF α mRNA steady-state levels (1.7-fold, [246]). Importantly, CDE-MO-2 also elevated expression of TNF α mRNA and protein in mouse primary bone marrow-derived macrophages (BMDM, **Figure 2.24D**). Since the morpholino approach was effective in primary cells, interfering with structured RNA motifs in *trans* may represent a future strategy to influence inflammatory responses in a therapeutic setting.

3 Discussion

In my PhD thesis, I unravelled the mechanism of how Roquin proteins regulate decay of CDE-containing mRNAs [246]. For that, I first improved an *in vitro* approach for mRNP purification. I developed the optimized SA-binding RNA aptamer 4xS1m and demonstrated that it is successful in purifying novel ARE-BPs [303]. With this method, I identified Roquin and Roquin2 to specifically recognize the CDE. I found that the CDE is a structured RNA motif that folds into a stem-loop. Roquin then attracts the Ccr4-Caf1-Not deadenylase complex to degrade the mRNA from the 3' end. Initially discovered in the TNF α mRNA 3'UTR [62], I now show that functional CDEs represent a whole class of novel decay elements in the 3'UTR of many mRNAs of physiological importance. This demonstrates the importance of regulatory RNA structures bound by RNA-BPs in mammals for the control of critical processes like the immune response. Additionally, the ability to interfere with the Roquin-CDE interaction using a morpholino approach provides a means of possible applicability in a therapeutic setting. By this, I hope to initiate future investigations that discover and decipher the function of regulatory mRNA structures in higher eukaryotes to highlight their contribution to posttranscriptional control of gene expression.

3.1 An Optimized RNA Aptamer for mRNP Purification

The ability to capture a snapshot of an mRNP's composition remains a challenge but offers important insight into how complex cellular machineries work. Here, I present an *in vitro* purification approach that makes use of the optimized SA-aptamer tag 4xS1m developed herein [303].

3.1.1 The 4xS1m Aptamer is More Efficient than S1

In this study I improved a structured SA-binding RNA aptamer. RNA structure is critical for aptamer function as the tag might adopt flexible conformations that do not recognize its target. For S1m, I aimed at stabilizing the

terminal S1 RNA structure by elongating the basal stem of the original S1 aptamer [291] by eight base-pairs (in yellow) (**Figure 2.1A**). I also stabilized its structure by point mutations (in red) similar to the design in Xu *et al.* (2009) that cause perfect strand complementarity [306]. Thereby, the SA-binding portion of the aptamer would further protrude from the mRNP into the cytoplasm. I chose to introduce the aptamer 3' to the reporter gene and regulatory element instead of internally, as previously reported [126, 291], in order not to disrupt RNA structure. When I inserted multiple consecutive copies of S1m into the reporter gene, I included a 21 nts long linear linker sequence in between individual motifs to prevent structural hindrance. Thereby, a synergistic avidity effect of the elements may further increase binding efficiency. For 4xS1m, I concatemerized four aptamers in a single tag.

With the optimized 4xS1m aptamer, the recovery of a reporter mRNA expressed in cells was increased by 15-fold (**Figure 2.1**). In my hands, 4xS1m was also more efficient than the MS2 and PP7 systems (**Figure 2.4**). SA-binding aptamers offer several advantages such as straight-forward one-step purification without the need for recombinant protein production, readily available matrices, no restrictions regarding antibody availability, the applicability to any RNP complex, as well as the possibility for scaled-up approaches. Moreover, the user has the option to either tag *in vitro* transcribed RNAs or RNAs expressed in cells. A previous report has compared S1 to the use of internally biotin-labelled ribonucleotides, and addition of biotin-ATP or biotin-dATP, respectively, and found the S1 aptamer to be superior [300]. In addition, S1-attachment to an RNA element results in identical bait RNAs. Other investigators also found that elongating the basal stem of S1 increases binding to SA [306, 296]. Moreover, stabilizing S1 by adding a tRNA scaffold increased binding efficiency 10-fold [298]. This tRNA-modified S1 tag proved useful for identification of RNA-BPs and miRNA-RNA interactions from lysates [319]. However, Iioka *et al.* (2011) also tested six tandemly repeated S1 motifs, yet found the 6-fold repeat to be much less efficient than a single S1 aptamer. In contrast, my most efficient construct, 4xS1m, clearly benefits from an avidity effect. Additionally, in an *in vitro* EMSA approach, the S1m RNA as a single motif bound with 2-fold higher affinity to SA than the original S1 aptamer (**Figure 2.5**). Thus, elongation of the basal stem in S1m might induce a sterically favorable conformation that stabilizes the apical binding portion of the aptamer. This helps the binding portion to further protrude from the mRNP: both would facilitate retention on SA Sepharose beads.

3.1.2 Successful 4xS1m-mediated RNP Purification

I established an improved purification protocol that allows for proteome-wide discovery of RNA-BPs that recognize a specific RNA. This allows to further understand the function, composition and dynamics of RNPs. Optimized parameters include mechanical lysis with a tissue-lyser to avoid detergent in the lysis buffer [305], a pre-block step of the lysate with avidin-beads to remove biotinylated cell material [294, 320], as well as usage of RNA/DNA-low bind tubes to reduce unspecific RNA-binding to the tube walls.

With this on hand, my next goal was to purify mRNPs from stably transfected cells using 4xS1m. However, MS of these purifications showed high levels of contaminating proteins, mostly cytoskeleton components, and did not yield the expected pattern of RNA- and ARE-BPs (data not shown). One important limitation is that even with the optimized 4xS1m aptamer, I could only retrieve 4.5% of the tagged reporter mRNA from cells (**Figure 2.1E**). Overall, identification of protein components of endogenously assembled RNPs by RNA aptamers have only been used with limited success, especially for mRNA complexes [320]. I am aware of one example where the S1 aptamer was used successfully for purification of a cellular mRNP from transfected cells [126]. In that case, additional crosslinking to preserve an ARE RNP and gel filtration steps increased purification specificity. Here, reversible *in vivo* formaldehyde crosslinking [259] was necessary to identify specific interaction partners by MS. Of note, crosslinking can also cause artefacts when proteins are fixed non-specifically to mRNPs due to close proximity. I envision that the improved 4xS1m aptamer may also offer an advantage in such a combined protocol. Arguing in favor of crosslinking, the transient interactions of ARE-BPs can not only cause loss during purification from cells [321]. Limited ARE-BPs can also be competed off the ARE by other abundant RNA-BPs during lysis or along the purification procedure. It has indeed been reported that RNP composition can change post lysis [322].

With this in mind, I favored an *in vitro* approach. I was aware of the possibility that this protocol is partially limited by *in vitro* reconstruction of RNPs on pre-coupled RNA. They may not represent authentic RNPs as they exist in living cells. Synthetic RNA may not fold properly and non-specific RNA-protein interactions may form during cell lysis and purification. However, the example of the TNF α ARE purification provided evidence that this approach identified established RNA-protein interactions of biological importance, as well as new candidate RNA-BPs (**Figure 2.8D**). This strongly implicates non-artificial interactions while most of the highest enriched proteins are RNA-BPs.

I also decided to use the 4xS1m aptamer for purification of ARE-BPs from cellular extracts because the binding efficiency of *in vitro* transcribed 4xS1m RNA to SA was very high (**Figures 2.6B and 2.8A**). After incubating cell lysates

with the ARE-4xS1m-coupled matrix and subsequent washing, I eluted RNA-associated proteins with RNase A. This was more efficient than elution with biotin (**Figure 2.6B**). It was also much more specific than elution with SDS, which also released contaminating sticky proteins from the beads [323] (**Figure 2.8B**). Additionally, a near-complete but specific elution is crucial to obtain reasonable levels of protein for MS. Notably, even though I favored RNase A elution, the S1 aptamer-based approach alternatively allows for elution of S1-tagged RNPs with biotin as described before [300, 291, 294, 126, 299, 297]. This is as well possible with 4xS1m (**Figure 2.6B**). Despite its lower elution efficiency, this can be important for purifications that require an intact, native RNP conformation, investigate RNA components of a complex, or aim for a second purification step.

3.1.3 4xS1m Pulldown of Established and Novel ARE-BPs

On ARE-4xS1m RNA, in addition to specific ARE-BPs interacting with the ARE, the structured aptamers and linker sequences offer binding sites for general RNA-BPs recognizing certain sequence or double-stranded stretches. That is why 4xS1m alone is an important control which allows for discrimination of exclusively enriched proteins on ARE-4xS1m. Thus, key to successful identification of ARE-BPs was the direct comparison of the ARE-4xS1m and 4xS1m whole-protein samples by quantitative MS using differential dimethyl peptide-labeling [307]. This approach is advantageous over stringent washes followed by individual band isolation, as the latter favors identification bias of high-affinity and high-abundant binders visible on a gel. In my case, about 200 proteins were co-purified with similar efficiencies in both samples (enrichment 0.5–2.0-fold, peptide coverage >5%), which is also reflected in the similar patterns of protein bands in the eluates of the two purifications (**Figure 2.8C**). In contrast, only 16 proteins were enriched with the TNF α ARE (enrichment >8-fold, **Figure 2.8D**) including most of the established TNF α ARE-BPs: HuR, TIAR, AUF1, BRF1 and BRF2. I was surprised by the near complete list of known TNF α ARE-BPs that resulted from the ARE RNP purification, especially as highly dynamic ARE-BPs have rapid off-rates. In related terms, it would be interesting to investigate whether there is a quantitative correlation between the expression level of certain ARE-BPs and their enrichment on the ARE. This analysis would show how ARE-BPs compete for ARE-binding. This could unravel the impact of the different affinities of ARE-BPs to the ARE. Thereby, differential ARE-BP expression levels and affinities determine the overall ARE mRNA stability in a certain cell type. In fact, only two of the major TNF α ARE-BPs, TTP and KSRP, were not enriched in my purification. However, TTP expression is very low in resting NIH3T3 fibroblasts used [324]. It is only induced upon immune stimulation. Two additional proteins, FUBP3

3.1 An Optimized RNA Aptamer for mRNP Purification

and DAZAP1, had previously been purified with the TNF α ARE [308, 309]. However, their function in regulating ARE mRNAs has not been established. Thus, I am confident that this assay is able to identify crucial RNA regulators. Taken together, my results demonstrate that purification via 4xS1m was efficient at identifying specific, *bona fide* RNA-interacting proteins.

3.1.4 Confirmation of Rbms1 and Roxan as ARE-BPs

In addition to known ARE-BPs, I also identified five RNA-BPs that had previously not been associated with AREs. They included two proteins of the U2 snRNP (A' and B'') and a general snRNP protein (Sm-D2), suggesting that the ARE-4xS1m RNA might base-pair with U2 snRNA and retain U2 snRNPs. Alternatively, ARE-4xS1m may fold into a motif with similarity to U2 snRNA and thus binds U2-associated proteins directly. While the interaction of these proteins was not studied further, I confirmed binding of Rbms1 and Roxan to the ARE by RNA-IP (**Figure 2.9**). Rbms1 has so far not been studied with respect to its RNA-binding function. Yet, the reported connections to c-Myc [310, 312] pose the question whether Rbms1 might bind to the ARE located in the 3'UTR of c-Myc mRNA. Roxan has been implicated in rotavirus mRNA translation [313]. It will be interesting to determine whether Roxan might also contribute to the ability of AREs to repress translation of cellular mRNAs. Thereby, Roxan and Rbms1 represent novel ARE-BPs identified by S1m-mediated RNP purification. Additional proteins enriched in the ARE RNP remain to be confirmed as true ARE-BPs, which will further increase the repertoire of functional ARE regulators.

3.1.5 Understanding mRNPs Through RNA Affinity Purification

I have demonstrated that *in vitro* 4xS1m purification can successfully identify relevant RNA-BPs for a regulatory RNA element. It is still unclear, however, to which extent an *in vitro* assembled RNP on synthetic RNA resembles the respective endogenous mRNP formed *in vivo* (**Figure 3.1**). Besides specific RNA-BPs recognizing the fused RNA motif of choice, the *in vitro* RNP bound to SA via 4xS1m contains common RNA-BPs and RNAs that interact with aptamers and linkers which can be discriminated due to the 4xS1m control. The endogenous mRNP however, beside all these factors, contains additional cellular RNA-BPs and RNAs, regulatory proteins and miRNAs, as well as translating ribosomes and protein nascent chains bound by associated factors. Moreover, the UTR regions, as well as the cap and the poly(A)-tail, harbor their own set of regulatory components. This highlights that a cellular mRNP

is much more complex and dynamic than an *in vitro* reconstituted RNP. This is especially the case as external and internal stimuli such as e.g. stress, nutrient availability, or cell cycle stage, can influence and demand mRNP reorganization in order for the cell to adapt. Thus, to capture a snapshot of a dynamic mRNP, crosslinking may be required.

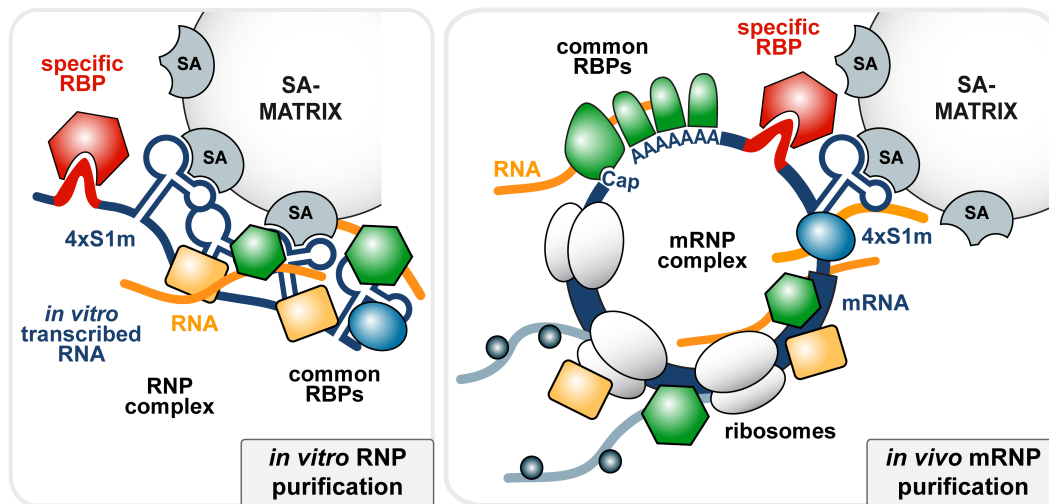


Figure 3.1: Schematic Comparison of *in vitro* and *in vivo* S1m-mediated RNP Purification. Left: *In vitro* transcribed 4xS1m-tagged RNAs are coupled to SA Sepharose beads and incubated with a highly concentrated cellular extract. RNP complexes formed contain RNA-BPs specific to the RNA element (red), as well as common RNA-BPs and RNAs that interact with aptamers and linkers. Right: *In vivo* formed mRNPs on endogenous 4xS1m-tagged mRNAs, harboring an RNA element of interest, contain all the components present in the *in vitro* RNP complex. In addition, they comprise factors such as translating ribosomes with nascent polypeptide chains, regulatory proteins and RNAs interacting with the poly(A)-tail, the cap, as well as the UTRs. The mRNP is much more complex and dynamic than the *in vitro* formed RNP.

Interestingly, the before mentioned study by Vasudevan *et al.* (2007) performed S1-pulldown of TNF α ARE mRNPs upon *in vivo* crosslinking from serum-starved cells [126]. Upon starvation-induced cell-cycle arrest, the ARE acts as a translation enhancer. They found the two proteins FXR1 and Ago2, which previously were considered effectors of translation repression, to exclusively associate with the ARE during translation activation upon starvation and to function together to activate translation. Important in this context is that they MS- or Western blot-identified enriched proteins bound to the ARE by analyzing extra bands on a gel compared to a control. This obtained JNK2, Tob1, GSTPI, FXR1, Ago2, as well as HuR and TTP [126]. This list is much shorter than the candidate ARE-BP list I obtained (**Figure 2.8D**) due to its limited resolution. A different study investigated ARE RNP complexes by

affinity purification of proteins on immobilized TNF α ARE RNA oligos from RAW macrophages and obtained a less biased list [308, 309]. This included TIA, TIAR, AUF1, several hnRNP proteins, as well as FUBP3 and DAZAP1, also found in my study. Notably, despite using RAW macrophages as protein source, they did not find HuR, BRF1 and BRF2 included in my purification, or TTP and KSRP. Thus, my presented technique is highly specific and is able to identify almost the complete set of well-known RNA-BPs for a certain RNA motif.

Recently, I applied 4xS1m-mediated RNA affinity chromatography to identify Roquin as the major protein that interacts with the CDE [246]. In the future, the optimized 4xS1m aptamer tag should also be applied for mRNP purification from cells with 4xS1m providing 15-fold higher binding efficiency than S1. In conclusion, I developed an improved technique for RNA-based identification of specific RNA-protein interactions from crude cell lysates in a one-step affinity purification approach [303]. I anticipate that 4xS1m will continue to be useful for identifying RNA-protein interactions to help uncover the intricate nature of mRNP complexes.

3.2 Roquin-mediated Constitutive Decay of CDE-containing mRNAs

In this study, I define CDEs as a novel class of regulatory motifs that mediate mRNA degradation through their interaction with Roquin proteins and provide a detailed analysis of the CDE RNA structure. I also present evidence for the physiological importance of the CDE for TNF α expression [246].

3.2.1 The CDE in the TNF α 3'UTR

The following presents the starting point for my study highlighting the importance to further investigate the CDE. TNF α plays a major role in mediating inflammation and immunity in the early response to infection. As its systemic secretion by LPS-stimulated macrophages can cause autoimmunity, septic shock and chronic inflammation [7, 325], TNF α synthesis is subject to tight control. Posttranscriptional regulation of this potentially harmful cytokine includes a variety of ARE-BPs [107] that bind the ARE in the TNF α 3'UTR. This orchestrates mRNA export, decay rate, and translation efficiency [326, 327, 328, 329]. Besides miRNA binding sites [76, 141], the TNF α 3'UTR harbors the CDE downstream of the ARE, that induces rapid mRNA decay [62]. Initially, Stoecklin *et al.* (2003) observed that the entire TNF α 3'UTR was still capable to stimulate mRNA decay in AMD-deficient mutant cells [62],

which proposed the existence of a second, AMD-independent mRNA decay pathway [145]. Importantly, the presence of more than one decay element and miRNA binding site in the TNF α 3'UTR allow for differential regulation under various physiological conditions. This highlights the need to understand the individual mechanistic contribution of the CDE to the overall TNF α mRNA stability.

3.2.2 The CDE is not a miRNA Binding Site

Many 3'UTRs are targets of miRNAs which leads to suppression of mRNA stability and/or translation [64]. Thus, it was initially tested whether the observed CDE-mediated mRNA decay activity was due to the CDE serving as a linear miRNA binding site, before even considering it to be a structured motif. Johanna Schott analyzed CDE-mediated mRNA decay in Dicer knockout ($^{-/-}$) mouse embryonic fibroblasts (MEFs) [226] generated in the Gregory Hannon lab (CSHL, USA). These MEFs express a truncated Dicer protein that lacks most of the RNase III domain and fail to generate mature miRNAs from pre-miRNA precursors, as exemplified for miR-16 [246]. A reporter mRNA containing green fluorescent protein (GFP) fused to globin and the TNF α CDE was degraded with similar half-lives in the Dicer $^{+/+}$ ($t_{1/2} = 2.2 \pm 0.2$ hours) and Dicer $^{-/-}$ MEFs ($t_{1/2} = 1.5 \pm 0.3$ hours) [246]. Almost all miRNAs require Dicer for their maturation. Since CDE-mRNA decay was not affected by knockout of Dicer, we concluded that the CDE is unlikely to represent a miRNA binding site.

Roquin was previously found to suppress the expression of ICOS mRNA by accelerating its degradation [226, 225]. Whereas Yu *et al.* (2007) proposed that Roquin suppresses ICOS mRNA in association with miR-101, Glasmacher *et al.* (2010) found that Roquin acts independently of miRNAs. Our observation that CDE-mediated mRNA decay is Dicer-independent would also argue against the involvement of miRNAs in Roquin-mediated suppression. This led to the idea that the CDE might fold into a specific structure that is important for its decay activity.

3.2.3 Established Structured RNA Degradation Motifs

There is a small but growing set of structured RNA elements that control mRNA stability in eukaryotes for which few examples exist. Beyond these individual examples, computational approaches suggest that structured mRNA motifs are more abundant and form large and distinct families [330, 153].

In histone mRNAs, a highly conserved stem-loop at the end of the 3'UTR is recognized by the stem-loop binding protein SLBP, which is required for rapid

histone mRNA degradation at the end of S-phase [331]. SLBP recruits factors for oligo(U) tail addition to histone mRNA 3' ends before mRNA degradation occurs through both 5'-3' and 3'-5' pathways [332]. However, oligouridylation initiates degradation, whereby the 3'-5' degradation machinery stalls [333]. It was recently shown that exoRNase Eri1 binds to the stem-loop and 3'-trims histone mRNAs. The oligo(U) tail of histone mRNAs is recognized by the Lsm1-7 heptamer which interacts with Eri1, whose catalytic activity is then able to stepwise degrade the stem-loop [334].

There are also stem-loop recognition elements in *Drosophila* maternal mRNAs that interact with Smaug which induces Ccr4-dependent transcript degradation [335]. This also regulates translation of nanos mRNA in flies [335]. Another example is Staufen, an RNA-BP that targets mRNAs for degradation by binding to long base-paired sequences [336, 337]. Hereby, STAU1 binds to dsRNA regions of the 3'UTR and interacts with the main NMD factor UPF1 to elicit mRNA decay. STAU1 binding sites are formed by imperfect base-pairing between a 3'UTR Alu element and another Alu element in a cytoplasmic, polyadenylated long non-coding RNA (lncRNA). Thereby, binding of STAU1 to mRNAs can be transactivated by lncRNAs [336].

A very direct mechanism for destabilizing mRNAs was discovered in IL-6 mRNA. A conserved stem-loop of about 30 nts within its 3'UTR is recognized by the endonuclease Regnase-1 (Zc3h12a), a ZF protein that directly cleaves its target mRNA [214, 215]. Interestingly, Regnase-1 binds to a similar stem-loop in its own mRNA as part of a negative feedback loop. Thereby, it prevents excessive translation of Regnase-1 and degradation of cytokine mRNAs [214, 338]. Initially, LPS-stimulated macrophages from Regnase-1^{-/-} mice showed increased production of IL-6 and IL-12b, but not TNF α . In accordance, IL-6 mRNA decay was severely impaired in these cells [214]. Regnase-1^{-/-} mice develop a severe systemic inflammation, characterized by production of autoantibodies. Thus, Regnase-1 exploits its RNase activity to cleave IL-6 mRNA by recognizing a stem-loop structure and thereby prevents autoimmunity [215].

As part of the regulatory circuit of the cellular iron metabolism, in iron-deficient cells, *cis*-regulatory hairpin structures, called iron-responsive elements (IREs), in the UTRs of mRNAs encoding proteins involved in iron transport and storage, are bound by iron regulatory protein 1 (IRP1) or IRP2 [339, 340]. The binding of IRPs to single IREs in the 5'UTR of target mRNAs inhibits their translation. However, IRP interaction with multiple 3'UTR IREs in the transferrin receptor 1 (TfR1) transcript increases its stability. As a consequence, TfR1-mediated iron uptake increases whereas iron storage in ferritin and export via ferroportin decrease [341].

3.2.4 The CDE Folds into a Conserved Stem-Loop Motif

The first indication that structure is important for CDE function arose from the observation that CDE activity was influenced by different cloning contexts it was inserted in. This either favored or prevented formation of base-paired regions (**Suppl. Figure 5.3**). The initial P1 stem was stabilized by two introduced base-pairing nucleotides which facilitated folding into an overall stabilized structure. By conservation analysis of mammalian TNF α 3'UTR sequences and thermodynamic modelling, I then derived a structure model for the CDE (**Figure 2.11**). This approach is challenging in higher eukaryotes. On the one hand, regulatory motifs acquire relatively minor sequence changes during evolution. This enhances their discovery by conservation-based bioinformatics approaches. On the other hand, co-evolution of primary sequence is not very frequent. This is in contrast to rapidly evolving bacterial genomes. This facilitates determination of conserved structures. This is exemplified by the rather straight-forward discovery of riboswitches in prokaryotes, regulatory RNA structures that control gene expression [148, 342]. Thus, due to the comparably small number of available mammalian genome sequences and more complex genomes, it is hard to identify functional RNA structures in higher eukaryotes. I suppose that regulatory RNA elements in mammals are more likely to rely on RNA-protein interactions rather than metabolite-binding due to the increased importance of proteins as gene expression regulators in higher eukaryotes.

The active CDE stem-loop motif was determined *in vitro* by in-line probing of variants that differ in their decay activity (**Suppl. Figure 5.3**) in the Hammond lab and by my functional analysis of compensatory mutations (**Figures 2.12D, 2.13A and 2.13B**). In fact, by thermodynamic modeling based on Mfold [316], we calculated a $\Delta G = -6.7$ kcal/mol for the mouse TNF α CDE₃₇ (**Figure 2.11B**) and a $\Delta G = -9.0$ kcal/mol for the human CDE₃₇ RNA (**Figure 2.11C**), whereas the lowest $\Delta G = -18.7$ kcal/mol was obtained for the mouse CDE₃₇-V3 (**Suppl. Figure 5.3A**). This indicated that the most active V3 variant also has the highest capacity to fold into the presented structure. Notably, the CDE stem-loop was not observed by in-line probing of the TNF α CDE₁₅₀ RNA, where the stem-loop is embedded in its natural sequence context (**Suppl. Figure 5.3C**). In fact, ΔG of the stem-loop in its natural context is predicted to be only -6.7 kcal/mol. This suggested that this region of the 3'UTR does not fold into a single structure, but samples different conformations. Inside cells, binding of Roquin is likely to stabilize the CDE in the stem-loop conformation. My finding that the CDE₃₇-M7 mutant, which has a destabilized P2 stem, can be activated by overexpression of Roquin (**Figure 2.15C**), supports the notion that binding of Roquin stabilizes the CDE in its active conformation.

Alternatively, RNA structure can be investigated by dimethyl sulphate (DMS) probing. This relies on *in vitro* transcription termination by ^{32}P -primer extension of an RNA whose unpaired As and Cs were *in vitro* or *in vivo* methylated by DMS beforehand. In addition, the SHAPE (selective 2'-hydroxyl acylation analyzed by primer extension) technique enables quantitative chemical probing of RNA structures in living cells. This reveals tertiary contacts and RNA-protein interactions [343, 344]. Recently, SHAPE was combined with RNA-Seq for high-throughput analysis [345]. These approaches allow to assess RNA structure inside cells to map native RNA-protein architectures.

Despite its low thermodynamic stability, the CDE bears features that are characteristic for trinucleotide hairpins. First, stable trinucleotide loops have a strong preference for Us at each position of the loop [346]. Indeed, UGU is by far the most frequently observed CDE loop according to our bioinformatics prediction [246]. Precisely, mutants and evolutionary sequence conservation revealed that the first nucleotide in the CDE loop is a pyrimidine, the second is a purine and the third nucleotide is U in all CDEs we tested (**Figures 2.11 and 2.13**). Although Johanna Schott allowed for either U or C in the bioinformatics search, all 56 highly conserved putative CDEs have a U at this position [246]. Second, the closing base-pair below the loop has an overwhelming preference for C–G in stable trinucleotide hairpins with a ΔG three times greater than that of the next best closing base-pair G–C [346]. Since the closing base-pair in the CDE needs to be C–G according to our mutational analysis (**Figures 2.12D and 2.13A**), it matches the thermodynamically most stable configuration of trinucleotide hairpins.

3.2.5 Roquin and Roquin2 Specifically Bind to the CDE

I applied the before mentioned 4xS1m tag fused to the CDE to find CDE-BPs by RNA affinity purification. This identified Roquin to be the highest enriched protein (**Figure 2.14C**). Interestingly, among other RNA-BP enriched >3-fold, Roquin2 was found at position four on that list. This already hinted at the Roquin family of proteins representing promising candidate CDE-BPs. A first indication of a specific Roquin-CDE interaction came from RNA-IP experiments (**Figures 2.15B and 2.16A**). They showed that EGFP-Roquin binds to CDE₃₇- and CDE₁₅₀-bearing reporter mRNAs in cells. I also confirmed specific binding of Roquin2 to CDE₃₇- and CDE₁₅₀-mRNAs. One concern is that RNP re-organization upon lysis can occur [322]. Thus, Fabian Pötts tested by *in vivo* crosslinking whether the Roquin-CDE association occurs inside cells, and not post-lysis [246]. This showed that in the absence of formaldehyde crosslinking, EGFP-Roquin associated with globin-CDE₃₇ mRNA under non-denaturing, but not under denaturing conditions (4 M urea). When cells

were crosslinked prior to lysis, globin-CDE₃₇ mRNA remained associated with EGFP-Roquin under denaturing conditions. Also, EGFP-Roquin did not bind globin mRNA lacking a CDE under either condition. In addition, my EMSA experiments showed that Roquin binds directly and with high specificity and affinity to the CDE stem-loop (**Figure 2.17**). Consistent with previous reports [245, 226], we saw that the ROQ domain is responsible for RNA binding (**Figure 2.16C**). Thus, these experiments demonstrated specific and direct association of Roquin with CDE-mRNA inside cells and *in vitro*.

3.2.6 Roquin is a Suppressor of TNF α Expression

While overexpression of Roquin or Roquin2 in NIH3T3 and HeLa cells accelerates CDE-mediated mRNA decay (**Figure 2.18**), the simultaneous kd of both proteins is necessary to effectively prevent CDE-mRNA degradation in NIH3T3 cells (**Figure 2.19A and Suppl. Figure 5.5B**). This indicates that the two proteins can induce mRNA degradation independently in these cells and therefore demonstrate a certain level of redundancy. It has recently been shown in T cells that Roquin and Roquin2 indeed have redundant functions in promoting mRNA decay and in controlling TFH cell differentiation [236]. In LPS-stimulated RAW264.7 macrophages, kd of Roquin alone is sufficient to cause stabilization and prolonged production of endogenous TNF α mRNA, which translates into elevated synthesis of TNF α (**Figure 2.19C–G**). In macrophages, double kd of Roquin and Roquin2 did not show a greater effect (**Suppl. Figure 5.5D–F**). This suggested that the relative importance of Roquin and Roquin2 may differ between cell types. By introducing an anti-sense morpholino that targets the TNF α CDE and interferes with Roquin binding *in trans*, I observed specifically elevated expression of TNF α mRNA and protein, not of any other CDE-containing mRNA, in RAW264.7 macrophages and primary BMDM (**Figure 2.24**). Taken together, these results demonstrate that Roquin acts through the CDE as a suppressor of TNF α expression in macrophages. This might be different in T cells, where overexpression of Roquin was found to cause elevated levels of numerous pro-inflammatory cytokines including TNF α [347].

In accordance with CDE activity, it was found that TNF α mRNA remains labile in LPS-stimulated macrophages [348, 104, 349]. In a mouse model [13], the ARE and the 18 nt AU-rich stretch of the fragment K was specifically deleted from the TNF α locus whereas K Δ AU was retained (TNF α - Δ ARE). Primary macrophages derived from these mice showed excessive TNF α mRNA and protein levels upon LPS-stimulation. Net mRNA levels suggested that the TNF α - Δ ARE transcript was stable in the presence of LPS, precluding the existence of a second, ARE-independent decay pathway. However, TNF α

ARE mRNA declined to baseline levels in 6 hours after accumulation. This is in agreement with the prolonged expression of TNF α mRNA in Roquin kd cells upon LPS stimulation (**Figure 2.19E**). This highlights the impact of the CDE on TNF α mRNA half-life rather than on steady-state levels. Also, ARE-dependent decay was inhibited in *trans* in TTP-knockout mice (TTP^{-/-}) [107, 350]. In TTP^{-/-}-mice, TNF α mRNA half-lives increased 2-fold in LPS-treated macrophages and a bit more than 2-fold in LPS-treated bone marrow stromal cells. The fact that TNF α mRNA was still fairly labile in TTP^{-/-} cells could be either due to the activity of TTP-related proteins, or to the CDE acting in an ARE-independent manner. Thus, the TTP knockout model is fully consistent with the CDE contributing to TNF α mRNA turnover. One interesting idea is that regulation of Roquin binding to the CDE is dependent on affinity: when TNF α mRNA levels increase upon stimulation, Roquin binding might be overcome as a result of titration, whereby the amount of Roquin protein present sets a dynamic threshold that determines the CDE-mRNA decay rate.

3.2.7 Roquin Recruits the Ccr4-Caf1-Not Complex for mRNA Deadenylation

My study also provided insight into the mechanism of CDE-dependent mRNA degradation. Previous work suggested that Roquin may activate ICOS mRNA degradation via interaction with decapping enhancers [226]. In contrast, by affinity purification of Roquin and Roquin2 from stably transfected HeLa cells, Sonja Reitter found that both proteins associate with the entire Ccr4-Caf1-Not complex [246]. We did not detect any decapping components. Co-IP experiments revealed that the interaction with Not1, the scaffold protein of the Ccr4-Caf1-Not deadenylation complex, and with the deadenylase Caf1a, is RNA-independent and occurs through the C-terminal region of Roquin (**Figure 2.20**, [246]). Importantly, a catalytically inactive Caf1a mutant was able to potently inhibit CDE-mRNA deadenylation and degradation. Thus, I propose that Roquin and Roquin2 serve as adaptor proteins that specifically recognize CDE-like RNA stem-loops via the ROQ domain. They destabilize their target mRNAs by recruitment of the Ccr4-Caf1-Not deadenylase complex (**Figure 2.20**), possibly through an interaction with Not1, via the C-terminal effector domain (**Figure 3.2**).

Several other mRNA decay pathways employ a similar mechanism. In case of TTP-bound ARE-mRNAs, TTP recruits the Ccr4-Caf1-Not complex to the mRNA through its association with Not1 [131]. miRNA-mediated mRNA degradation requires argonaute proteins to interact with TNRC6/GW182 adaptor proteins, which in turn recruits the Ccr4-Caf1-Not complex through direct association with Not1 [71, 351, 352]. Thus, Not1 may provide a plat-

form where mRNAs containing different destabilizing elements are regulated in a coordinated manner. Given that several immunity-related factors (e.g. TNF α , IL-6, VEGF and G-CSF) contain more than one destabilizing element in their mRNAs [57], it may be advantageous to coordinate access of RNA-BPs to the mRNA decay machinery.

3.2.8 Structure-Function Analysis of Roquin Domains

Fabian Pötzt examined the role of the RING and ROQ domains as well as of the N- and C-termini of Roquin, summarized in **Figure 2.16C**. Whereas deletion of the RING domain had no effect, the Roquin- Δ ROQ mutant was deficient in CDE RNA-binding [246], failed to accelerate CDE-mRNA decay upon overexpression and lost its ability to localize to P-bodies (**Figure 2.16**, [246]). Notably, the ROQ domain within the N-terminus of Roquin was sufficient to bind globin-CDE mRNA, whereas the C-terminal domain was found to associate with Not1 and Caf1a (**Figures 2.16C and 2.17**, [246]). When Fabian expressed the individual N-terminal domain, the C-terminal domain or the ROQ domain alone, this strongly reduced the degradation rate of the CDE reporter-mRNA in comparison to expression of EGFP alone. This suggested that these Roquin fragments have dominant-negative activity [246]. This could be explained by a competition of endogenous Roquin with the N-terminal ROQ domain for CDE-mRNA binding. Likewise, endogenous Roquin may compete with the C-terminal fragment for binding to the Ccr4-Caf1-Not complex. Taken together, these results demonstrate that the ROQ domain of Roquin is responsible for RNA-binding, whereas the C-terminal fragment contains the effector domain that recruits the Ccr4-Caf1-Not complex.

Localization of Roquin to P-bodies was found to be non-uniform in different cell types [226, 245]. When Sonja Reitter investigated P-body localization of Roquin and Roquin2, she found that both localize to P-bodies in HEK293, NIH3T3, as well as Huh7 cells (**Figure 2.16C**). For Roquin2, this had only recently been reported in HEK cells [239]. When she tested the ZF mutants of Roquin and Roquin2, she found that oth mutants efficiently localized to P-bodies. This was consistent with their CDE-binding activity and acceleration potential of CDE-decay upon overexpression compared to WT. Of the truncation mutants presented, only Roquin- Δ RING behaved as WT, while all others were found to be cytoplasmic or even reduced the P-body number per cell. This can be explained by either misfolding and inactivity of the protein domain, interference with function due to the attached EGFP-tag or an overall stress response of the cell to overexpression. All this can lead to mislocalization and can even induce a decrease in P-body numbers [353]. In all, this highlights that Roquin and Roquin2 localize to P-bodies, for which the ZF and RING

domain are not essential. Moreover, for efficient P-body localization, Roquin is likely to require both the N- and C-terminal domain.

3.2.9 Roquin Recognizes a Conserved Class of CDE-containing mRNAs

When Johanna Schott applied her consensus CDE sequence and structure model (**Figure 2.22A**) derived from our experimental data by searching all 3'UTRs of the mouse transcriptome, she identified 56 highly conserved CDEs in 55 vertebrate genes [246]. This identified a total 109 putative CDEs in 108 genes, and an additional 91 in ORFs. This was opposed to 55 CDEs that would have been expected to occur randomly. By an *in silico* approach, Parker *et al.* (2011) predicted novel families of structured motifs within mRNAs based on the conservation of potentially structured RNA sequences including several stem-loops that correspond to CDEs [153]. This provided independent evidence for the notion that the CDE is a widespread regulatory element. Through the genome-wide identification of Roquin target mRNAs by Roquin-IP and RNA-Seq (**Figure 2.22B–D**, **Suppl. Table 5.2**), we found that mRNAs with conserved CDEs are strongly enriched by Roquin-IP (**Figure 2.22C–D**). In fact, highest enrichment was observed for the only mouse mRNA (Nfkbid) that contains a tandem CDE motif in its 3'UTR. Similarly, the only two mouse mRNAs containing two CDEs in their ORF (D5Ert579e and Ipo11) showed strongest enrichment by Roquin-IP among all mRNAs with ORF CDEs. These results demonstrate that the CDE is the principal Roquin binding element.

3.2.10 Physiological Consequences of the Roquin-CDE Interaction

Roquin was previously found to suppress ICOS expression by accelerating its mRNA degradation [226, 225]. I could now show that a ICOS 3'UTR motif recognized by Roquin is indeed a conserved CDE-like motif (**Figure 2.21**). *Sanroque* mutant mice display a severe, lupus-like autoimmune syndrome due to the mutant Roquin protein which harbors a single amino acid substitution (M199R). This phenotype was shown to result from elevated ICOS expression [227]. I did not observe a difference between WT Roquin and the M199R mutant with regard to CDE-binding or acceleration of CDE-mRNA decay (**Figure 2.16C**). *Sanroque* Roquin has also been reported to not affect binding to the ICOS 3'UTR [245]. Also, a more recent study reported that the knockout of Roquin in the hematopoietic system did not cause autoimmunity, but a more inflammatory phenotype [241]. Our genome-wide iden-

tification of Roquin targets (**Suppl. Table 5.2**) revealed several immunity and inflammation-related mRNAs including TNF α and three regulators of the NF κ B-mediated transcription pathway: Nfkbid, a member of the I κ B family of NF κ B inhibitors, Nfkbiz, a nuclear member of the same family, and Ier3, a protein that suppresses activation of NF κ B by stabilization of I κ B α [354, 355]. Given that an estimated additional 50 mRNAs are likely to contain functional CDEs (**Suppl. Table 5.2**), and that 95 mRNAs were significantly enriched by Roquin-IP (**Suppl. Table 5.2**), I postulate that the complex phenotypes of the hematopoietic Roquin knockout and *sanroque* mice may in fact arise from the simultaneous deregulation of multiple mRNAs in the immune system.

In addition, the target spectrum detected from stimulated macrophages does not reflect the whole pool of Roquin target mRNAs, as only the transcripts expressed in that cell type can be found. Given that some of the Roquin-associated mRNAs were strongly induced by LPS whereas others were not (**Suppl. Figure 5.7**), Roquin appears to bind to both newly synthesized and constitutively expressed CDE-containing mRNAs. IP and RNA-Seq of ubiquitously expressed Roquin from different tissues will increase the number of specifically enriched transcripts. Moreover, we monitored 76 highly enriched mRNAs lacking a CDE which indicates, on the one hand, that our mutagenesis-derived criteria for functional CDEs was limited and highly restrictive. Thus, transcripts with more divergent CDE-like motifs were missed. On the other hand, these enriched mRNAs might contain additional common Roquin binding sites beside CDEs, representing a different class of Roquin recognition motifs. However, with respect to conservation, CDEs were the main class of conserved 3'UTR elements found.

The complete knockout of Roquin causes perinatal lethality and malformations of the tail and spinal column [241]. This phenotype may be linked to our observation that 13 mRNAs encoding regulators of development, including Wnt3a and the bone morphogenic protein receptor Bmpr1a, contain highly conserved CDEs [246]. Six of these mRNAs, including Bmpr1a, were also enriched by Roquin-IP (**Suppl. Table 5.2**). Interestingly, 10 of the CDEs we identified are conserved between fish and mammals, suggesting that Roquin-mediated mRNA regulation is maintained among vertebrates. Additionally, we found the Roquin protein to be present from human and mouse down to sponges (see the Roquin protein alignment in the Supplemental Data). The sequence alignment indicates a particular conservation of the N-terminal portion containing the RNA-binding domain. The high conservation of Roquin in lower and higher metazoans, together with CDEs in higher metazoans, hints at a potential conservation of the Roquin-CDE system as a decay signal and/or a function in development. Since Roquin homologs are found in all branches of metazoan evolution, Roquin-CDE interactions may have an ancient role in multicellular organisms.

3.3 Summary and Model

In this study, I describe the regulatory mechanism of CDE-mediated mRNA decay. I focused on identification and characterization of critical RNA-binding proteins that mediate CDE activity. For that, I first established an improved mRNP purification protocol [303] and identified novel protein regulators bound to the TNF α ARE. This included the development of a modified SA-binding aptamer, S1m, which has higher affinity for SA than the original S1, binds with highest avidity to SA in a four-repeat conformation (4xS1m), and is more efficient than the MS2 and PP7 systems. I applied the optimized 4xS1m tag fused to the ARE for purification of the ARE-RNP. This allowed me to detect most of the well-known ARE-BPs [87] and to determine novel ones. I confirmed Roxan and Rbms1 as new TNF α ARE-BPs, both of which have previously not been associated with AREs. Thereby, I established 4xS1m as an efficient and powerful tool for the isolation and identification of RNP-associated proteins.

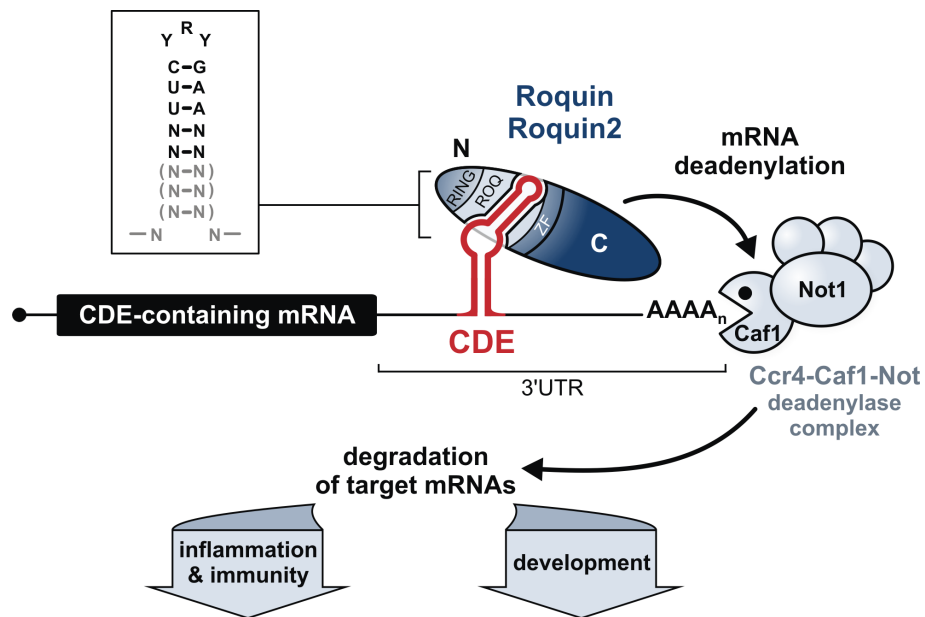


Figure 3.2: Roquin Promotes Constitutive Decay of CDE-containing mRNAs.

Model of CDE-mediated mRNA degradation. Roquin and Roquin2 bind to CDE RNA stem-loops via the ROQ domain. The Ccr4-Caf1-Not complex is recruited through the C-terminal effector domain. This causes Caf1a-dependent deadenylation and consecutive degradation of CDE-containing mRNAs, many of which encode proteins important for development as well as inflammation and immunity. Reproduced with permission from Cell, Elsevier.

Moreover, I demonstrate that the CDE is a structured motif that folds into an RNA stem-loop in its active conformation. The minimal active CDE forms a 17 nt hairpin with sequence and structure requirements for function. When I applied my optimized 4xS1m protocol to the TNF α CDE, I purified Roquin and its paralog Roquin2 as stem-loop specific CDE-binding proteins [246] (**Figure 3.2**). Roquin is required for CDE-mediated mRNA decay and suppression of TNF α production in macrophages. I further show that Roquin proteins cause mRNA deadenylation by recruiting the Ccr4-Caf1-Not complex. Here, the ROQ domain in the N-terminus provides the RNA-recognition site, while the C-terminus interacts with components of the decay machinery. Furthermore, I discovered target mRNAs of Roquin on a transcriptome-wide scale. Thereby, CDE-containing mRNAs were found to be the primary targets of Roquin in macrophages. These data provide evidence that Roquin controls the degradation of more than 50 vertebrate mRNAs with highly conserved CDE stem-loop motifs. Many of these transcripts encode regulators of development and inflammation. Finally, my data imply that morpholino-mediated interference with CDE structure formation alleviates TNF α suppression which represents a promising strategy for therapeutic applications.

My study defines CDEs as a conserved class of abundant regulatory RNA stem-loop motifs that mediate mRNA deadenylation through their association with Roquin proteins. This emphasizes the importance of structured RNA elements in the complex network of *cis*- and *trans*-acting factors regulating mRNA stability. As exemplified by TNF α , the presence of multiple regulatory elements in the same mRNA may allow for the integration of regulatory cues from various signaling pathways. Similar to promoter regions that offer binding sites for different TFs, the UTRs of mRNAs are increasingly recognized as versatile regulatory platforms. In all, comprehensive analysis of CDE-mediated mRNA decay provides a near complete picture of how the CDE conveys constitutive mRNA decay. This is important for limiting the TNF α -mediated inflammatory response and for the regulation of numerous CDE-containing mRNAs. This adds an important component to the regulation of posttranscriptional control of gene expression.

3.4 Outlook

3.4.1 S1m is a Powerful Tool for mRNP Analysis

Purification of intact mRNPs from cells has always been technically challenging. The improved 4xS1m aptamer offers an efficient tool to isolate complex RNPs via RNA. It has proven successful for retaining established and novel ARE-BPs on 4xS1m-tagged TNF α ARE RNA *in vitro* [303]. It remains to be investigated which function the confirmed, new ARE-BPs Roxan and Rbms1 have upon binding to the ARE. Other RNA-BPs enriched on the ARE also remain to be explored. In the future, I suspect a broad spectrum of applications for the 4xS1m-tag. These include identification of RNA-associated proteins important in RNA metabolism from splicing to decay, as well as interaction partners of non-coding RNAs. Besides, RNA components of an RNP can be assessed by RNA-Seq or microarray analysis upon biotin elution of 4xS1m. The biggest advantage of the presented *in vitro* pulldown approach is the available amount of *in vitro* transcribed RNA compared to the levels of mRNA expressed in cells. This is important for the detection of small amounts of RNA-BPs eluted by MS. While 30 μ g 4xS1m RNA and highly concentrated protein extracts were applied in an *in vitro* approach, I observed that a lysate of Cos7 cells transiently expressing 4xS1m-containing mRNAs of a confluent 10-cm dish yielded total 300 ng 4xS1m RNA (or 250,000 copies/cell). The large difference in numbers is critical for successful RNP isolation. This could explain the few reports for successful isolation of cellular mRNPs. Nonetheless, an approach employing cell lines stably expressing 4xS1m-containing RNAs would allow for purification of authentic endogenous mRNPs in their preserved composition upon formaldehyde crosslinking (**Figure 3.1**). Moreover, I find that with short RNA motifs, like the TNF α ARE (53 nt) [303] or CDE (37 nt) [246], one obtains a short list of specifically enriched RNA-BPs. These can be clearly discriminated from general RNA-BPs by comparison to the important aptamer-only control. Affinity purification of long RNAs will increase the total number of enriched RNA-BPs, which impedes determination of crucial regulators. I therefore recommend to previously map an RNA element to its core activity. With the interest shown by many labs to date, I assume that the 4xS1m aptamer will be of broad use in many areas of RNA research in the future.

3.4.2 The Roquin-CDE Complex and Roquin/2 Targets

In my thesis, I define the minimal TNF α CDE as a 17 nt long stem-loop structure. I showed by RNA-IP and EMSA that the CDE is specifically and

directly recognized by the ROQ domain in the N-terminal portion of Roquin (**Figures 2.16** and **2.17**, [246]). The ROQ domain lacks an established RNA-recognition motif but represents a novel RNA-binding domain. It would be interesting to investigate the structure of the Roquin-CDE complex by crystallography or NMR in order to obtain a clear picture of how the ROQ domain recognizes the CDE hairpin. It has been reported that the ROQ domain binds the ICOS 3'UTR to suppress ICOS mRNA [245, 226]. Interestingly, the ICOS 3'UTR may contain multiple *cis*-acting Roquin binding sites. This includes a 47 nt long sequence adjacent to the miR-101 site at the 3' end of the 3'UTR [225, 245], and a 100 nt long sequence located 100-200 nts downstream of the stop codon [226, 236]. The CDE in the ICOS 3'UTR that I identified in my thesis does not overlap with any of these sites. Thus, it will be important to investigate whether Roquin has different binding sites that play distinct roles in target mRNA regulation. I suggest to obtain Roquin CLIP data in order to decipher its exact binding sites, which might reveal several recognition motifs in one mRNA.

It is not yet fully understood why the *sanroque* mutation in the ROQ domain induces autoimmunity by causing increased ICOS expression [227], while it does not affect ICOS 3'UTR binding [245]. In agreement with this, my EMSA data show that *sanroque* Roquin-N-M199R binds to the CDE with equal affinity as WT Roquin-N (data not shown). It was suggested that *sanroque* Roquin binding sequesters Roquin mRNA targets, but impairs their degradation, which hinders Roquin2 to compensate for Roquin activity [236, 239]. This results in Roquin/2 target mRNA stabilization and aberrant TFH cell development. However, I did not see a difference between *sanroque* and WT Roquin regarding their activity to accelerate CDE-mediated mRNA decay upon overexpression (**Figure 2.16**). It was shown that *sanroque* Roquin localizes to SGs and P-bodies [239]. It should be tested by FISH whether *sanroque* Roquin sequesters its target mRNAs and thereby blocks their degradation in P-bodies. Also, the structural change in *sanroque* Roquin that mediates its impaired activity should be addressed by crystallography or NMR. It will also be interesting to challenge the proposed redundancy of Roquin and Roquin2. They may have a different target mRNA spectrum in different cell types. This can be addressed by Roquin- and Roquin2-IP prior to RNA-Seq from cells of different tissues, as performed for Roquin from RAW macrophages in this study (**Figure 2.22**). I suspect that Roquin mRNA targets differ already from T cells to macrophages, as for example ICOS is not well expressed in macrophages in which TNF α is a more important target. I propose that the *sanroque* phenotype is a result of increased expression of many Roquin targets at the same time. This should also be studied in the context of the observed developmental defects of Roquin KO mice, such as tail and spinal column defects [241]. This is in agreement with our finding that regulators of development like Bmpr1a

mRNA contain conserved CDEs and are bound by Roquin (**Figure 2.22** and **2.23**).

3.4.3 Regulation of Roquin Proteins

Differential expression of Roquin/2 is important in the context of the proposed redundancy of Roquin and Roquin2 function in different tissues, as demonstrated in T cells [236, 239]. Both are expressed in many different tissues, while Roquin2 is mostly expressed at lower levels than Roquin [236]. By kd experiments, I observed that in NIH3T3 cells, Roquin/2 act in a redundant fashion to suppress CDE-containing mRNAs. In RAW264.7 macrophages, kd of Roquin alone is sufficient to stabilize them (**Figure 2.19** and **Suppl. Figure 5.5**). It will be interesting to see how Roquin proteins are regulated in different tissues, which is not known so far. Roquin protein levels remain unchanged upon LPS-stimulation of macrophages (data not shown). Also, CDE-containing reporter mRNAs were found to be resistant to AMD-inhibiting stimuli such as LPS, ionomycin or TPA, and constitutive active variants of PI3K, MEK6 or v-H-ras1 [62]. Therefore, I so far have no evidence that Roquin-mediated CDE-mRNA decay is regulated. Roquin and Roquin2 mRNAs themselves contain a CDE and were both enriched in the Roquin-IP from macrophages. This suggests a negative feedback loop wherein Roquin proteins destabilize their own transcripts to dampen their own expression. This needs to be studied further. Roquin is a new member to the set of CCCH-type ZF proteins, including Regnase-1 and TTP (**Figure 3.3**), that regulate mRNA decay of transcripts encoding cytokines and immune mediators. They all recognize different classes of RNA motifs and have a distinct immune-relevant phenotype in mice. Future investigation should aim at revealing whether Roquin proteins, as seen for Regnase-1 and TTP, are regulated by posttranslational modifications; a common means to regulate immune effectors essential for mRNA decay.

Features	Regnase-1	TTP	Roquin
Number of C3H-type ZFs	1	2	1
Recognition motif	stem-loop	ARE	CDE
Target mRNA	IL-6, IL-12p40, Regnase-1	TNF α , GM-CSF, IL-2, IL-6, IFN γ , IL-10, CCL2, CCL3, CXCL1, c-Fos, iNOS, COX2	ICOS, Ox40, TNFα, Nfkbid, Nfkbiz, Ier3, Roquin, Roquin2, Bmpr1a, >50 other
Modification	Phosphorylation by IKK β	Phosphorylation by MK2	?
Phenotype in mice	Overproduction of IL-6 Activated acquired immune cells	Overproduction of TNF α Development of arthritis	Overproduction of ICOS Spontaneous GC formation

Figure 3.3: Characteristics of CCCH-type Zinc Finger Proteins in mRNA Decay. Comparison of Regnase-1, TTP and Roquin features. Roquin features in bold are based on my thesis. Figure modified from Uehata and Akira 2013 [215].

Due to its RING domain, Roquin and Roquin2 are predicted E3 ubiquitin ligases. For the *C. elegans* Roquin homolog RLE-1, which initiates DAF-16-degradation by by ubiquitination [244], E3 ligase activity was shown. Based on my data, the RING domain in Roquin does not play a role in CDE-mRNA decay. It is possible that Roquin, in addition to its function in mRNA decay, mediates ubiquitination of substrate proteins which needs further investigation. I suggest to study in an *in vitro* setting whether Roquin is capable of autoubiquitination, commonly seen for E3 ligases. This would give a first hint for E3 ligase activity of the RING finger in Roquin.

3.4.4 Regulatory RNA Structures in Mammals

In addition to the CDEs representing a conserved class of structured elements in mammals, I speculate that there are many unknown classes of regulatory RNA structures in higher eukaryotes that may play a role in posttranscriptional control. High conservation on primary sequence in UTR regions is an important indicator for a potential regulatory element, a fact we used to search for CDEs bioinformatically [246]. Co-variation of sequences with respect to structure conservation can additionally help to identify functional motifs. With increasing importance of regulatory RNA-protein systems in vertebrates, complicated networks have evolved to control gene expression. These systems integrate inputs from different regulatory pathways. One may speculate that two or more distinct elements in one 3'UTR, as seen for the TNF α ARE and CDE, might also be functionally linked. As mentioned before, the ICOS 3'UTR is likely to even contain different Roquin binding motifs, including the CDE. Moreover, there is a class of mRNAs that are enriched in the Roquin-IP that do not contain a conserved CDE as we define it (**Figure 2.22**). This suggests that Roquin is able to bind other distinct recognition motifs or weaker CDEs. This can either be addressed experimentally by performing Roquin CLIP experiments or bioinformatically by determining a further common motif in these 3'UTRs.

4 Materials and Methods

4.1 Materials

Detailed lists of the materials, chemicals and technical equipment used in this study can be found in the Appendix.

4.2 Methods

All commercial kits and reagents were used according to the manufacturer's instructions unless otherwise stated.

4.2.1 Cell Culture and Transfection

Cell lines used in this study are listed in **Table 4.1**.

Table 4.1: Cell Lines Used in this Study.

Cell line	Description and ATCC Number
COS7	African green monkey (<i>Cercopithecus eathiops</i>) kidney fibroblast-like cell line (CRL-1651)
NIH3T3 B2A2	Mouse (<i>Mus musculus</i>) NIH 3T3 fibroblast clone B2A2 cell line (Ann-Bin Shyu lab, 1998) is a stable transfectant of plasmid pUHD15-1 (Prof. H. Bujard) encoding hybrid transactivator protein (tTA)
HeLa	Human (<i>Homo sapiens</i>) epithelial cervical adenocarcinoma cell line (CCL-2)
HEK293	Hypotriploid human embryonic kidney cell line (CRL-1573)
RAW264.7	Mouse Abelson murine leukemia virus transformed macrophage cell line (TIB-71)

COS7 as well as NIH3T3, HeLa, HEK293T and RAW264.7 cells were cultured in Dulbecco's Modified Eagle's Medium (DMEM, Gibco) supplemented

with 10% fetal calf serum (PAA Laboratories), 2 mM L-glutamine, 100 U/ml penicillin and 0.1 mg/ml streptomycin (all PAN Biotech) at 37°C in 5% CO₂. Cells were trypsinized using trypsin-EDTA (PAN biotech). BMDM were isolated from the femur and tibia of WT C57BL/6 mice as described previously [356]. BMDM were cultured for 10–12 days in DMEM supplemented with 10% fetal calf serum (Sigma), 20 mM HEPES (PAA), 2 mM L-glutamine (PAN Biotech) essential and nonessential amino acids (Invitrogen), 55 μM 2-mercaptoethanol (Sigma), 100 units/ml penicillin (PAN Biotech), 100 μg/ml streptomycin (PAN Biotech) and 20% conditioned medium from L929 cells as a source of macrophage colony-stimulating-factor. NIH3T3 B2A2 cells [357] were a generous gift from Ann-Bin Shyu (University of Texas-Houston Medical School). NIH3T3, HeLa, HEK293T cells were seeded in 10-cm dishes and transfected the following day with 9–12 μg of plasmid using polyethyleneimine (PEI, Polysciences Europe, 1 mg/ml, pH 7.0) at a ratio of 1:2 (DNA:PEI) in serum-free and antibiotic-free DMEM. In case Tet-inducible vectors were transfected, 6 μg pTet reporter plasmid was co-transfected with 3 μg pTet-Off (p2249), and media containing 10% (v/v) Tet-negative fetal calf serum (PAA) was used. The medium was changed to regular DMEM 4–6 hours after transfection. Stable NIH3T3 cell lines were generated by PEI transfection and subsequent selection with puromycin (4–6 μg/ml, Applichem) as given in **Table 4.2**. Mass cultures were used for mRNA decay assays. Where indicated, RAW264.7 cells were treated with LPS (100 ng/ml, Sigma, L2630, *E. coli* serotype O111:B4).

4.2.2 Plasmid Construction

The following plasmids have been described previously: pTet-7B-ARE (pTet-7B-TNF α -ARE₅₃, p2260) containing a Tet-inducible promoter and a T7-tagged rabbit β -globin reporter gene with the 53 nt ARE of mouse TNF α in its 3'UTR [136]; puroMX β globin (p2220, also referred to as puroMX β) containing the β -globin reporter gene driven by the Moloney murine leukemia virus (MMLV) promoter [304]; puroMX β -TNF α -ARE (p2225) [304]; puroMX β -TNF α -K Δ AU (p2230) [62]; pEGFP-N1 (Clontech/ BD Biosciences); pLNCX2-EGFP-Roquin (p2838) encoding EGFP-tagged full-length mouse Roquin and pETM11-Roquin-N (p2940) for expression of His-Roquin-N (aa 2-440) [226]; TOPuro-Caf1a-mycSG (p2485) and TOPuro-Caf1a-AA-mycSG (p2737) encoding human WT Caf1a and the dominant negative D40A/E42A mutant, respectively; pcDNA3-Flag (p2002) and pcDNA3-Flag-Dcp2-AA (p2798) harboring the E147A/E148A Dcp2 mutant [196]; as well as pCMV-Flag-Not1 (p2556) encoding Not1 [358]. pcDNA3-hygro-T7tag (p3203) and pcDNA3-hygro-T7tag-Roxan (p3204) [313] were kindly provided by Didier Poncet (CNRS, Gif sur Yvette, France), and pGEX-2T-MS2cp (p2809) was a kind

4.2 Methods

Table 4.2: Stable Cell Lines Generated in this Study. All cell lines were generated by PEI transfection and selection with puromycin to a mass culture stage.

Cell line	Plasmid	Selection
NIH3T3 B2A2-puroMX β	p2220	puromycin
NIH3T3 B2A2-puroMX β -CDE	p2812	puromycin
NIH3T3 B2A2-puroMX β -TNF-K Δ AU	p2230	puromycin
NIH3T3 B2A2-puroMX β -CDE ₃₇ -V1	p2813	puromycin
NIH3T3 B2A2-puroMX β -CDE ₃₇ -V2	p2814	puromycin
NIH3T3 B2A2-puroMX β -CDE ₃₇ -V3	p2818	puromycin
NIH3T3 B2A2-puroMX β -CDE ₃₇ -V3-M1	p2820	puromycin
NIH3T3 B2A2-puroMX β -CDE ₃₇ -V3-M2	p2821	puromycin
NIH3T3 B2A2-puroMX β -CDE ₃₇ -V3-M3	p2822	puromycin
NIH3T3 B2A2-puroMX β -CDE ₃₇ -V3-M4	p2823	puromycin
NIH3T3 B2A2-puroMX β -CDE ₃₇ -V3-M5	p2824	puromycin
NIH3T3 B2A2-puroMX β -CDE ₃₇ -V3-M6	p2825	puromycin
NIH3T3 B2A2-puroMX β -CDE ₃₇ -V3-M7	p2826	puromycin
NIH3T3 B2A2-puroMX β -CDE ₃₇ -V3-M8	p2827	puromycin
NIH3T3 B2A2-puroMX β -CDE ₃₇ -V3-M9	p2828	puromycin
NIH3T3 B2A2-puroMX β -CDE ₃₇ -V3-M10	p2829	puromycin
NIH3T3 B2A2-puroMX β -CDE ₃₇ -V3-M11	p2830	puromycin
NIH3T3 B2A2-puroMX β -CDE ₃₇ -V3-hCDE	p2831	puromycin
NIH3T3 B2A2-puroMX β -4xS1m	p2824	puromycin
NIH3T3 B2A2-puroMX β -TNF-ARE-4xS1m	p2891	puromycin
NIH3T3 B2A2-puroMX β -CDE ₃₇ -V3-4xS1m	p2856	puromycin
NIH3T3 B2A2-puroMX β -CDE ₃₇ -V3-M7-4xS1m	p2857	puromycin
NIH3T3 B2A2-puroMX β -CDE ₃₇ -V3-M9-4xS1m	p2858	puromycin

gift from Stephen Wax and Paul Anderson (Brigham and Women’s Hospital, Boston, USA). pTet-Off (p2249) was purchased from Clontech.

For the S1 and S1m-containing pTet-7B-TNF α -ARE reporter constructs, oligonucleotides containing the S1 (G1779/G1780) or S1m (G1850/G1851) aptamer sequence (see **Suppl. Figure 5.1A**, **Suppl. Table 5.7**, all oligonucleotides were purchased from Invitrogen or Eurofins MWG Operon) were annealed, concatemerized via their 5’ *Bam*HI- and 3’ *Bgl*II-compatible ends and ligated. Head-to-head and tail-to-tail conformations were suppressed by cleavage with *Bgl*II and *Bam*HI, while *Bgl*II/*Bam*HI fusion sites in head-to-tail conformations gave rise to multimers. Fragments containing 1 to 7 consecutive repeats of the S1 or S1m aptamer were then cloned into the *Bgl*II site of pTet-7B-ARE (p2260). Thereby, the following series of pTet vectors was generated: pTet-7B-TNF α -ARE-1xS1 (p2775), -2xS1 (p2776), -3xS1 (p2777), -4xS1

(p2778), -5xS1 (p2779), -6xS1 (p2780), -7xS1 (p2788); pTet-7B-TNF α -ARE-1xS1m (p2781), -2xS1m (p2782), -3xS1m (p2783), -4xS1m (p2784), -5xS1m (p2785), -6xS1m (p2786), -7xS1m (p2787). Plasmid puroMX β -4xS1m (p2824) was generated by PCR-amplifying 4xS1m from pTet-7B-TNF α -ARE-4xS1m (p2784) using the forward *Bgl*II-mismatch repair primer G1919, which reconstitutes a *Bgl*II site from the *Bgl*II/*Bam*HI fusion site, and reverse primer G1918. The amplicon was then digested with *Bgl*II and inserted into the *Bgl*II site of puroMX β (p2220). The same 4xS1m fragment was cloned into the *Bgl*II site of puroMX β -TNF α -ARE (p2225) to generate puroMX β -TNF α -ARE-4xS1m (p2891), and into the *Bgl*II site of pSP73 (Promega) to generate pSP73-4xS1m (p2880) (see **Suppl. Figure 5.1 and 5.2**). For pSP73-4xS1 (p3278), a 4xS1 fragment with flanking *Bgl*II sites was PCR-amplified from pTet-7B-TNF α -ARE-4xS1 (p2778) with primers G1919/G1918, *Bgl*II-digested, and cloned into the *Bgl*II site of pSP73. For pSP73-TNF α -ARE-4xS1m (p2881), the ARE-4xS1m fragment was PCR-amplified from puroMX β -TNF α -ARE-4xS1m (p2891) using the forward *Bam*HI-mismatch repair primer G2247, which reconstitutes a *Bam*HI site from the *Bgl*II/*Bam*HI fusion site, and reverse primer G2235. Thereupon, the 5' *Bam*HI- and 3' *Bgl*II-flanked insert was cloned into the *Bgl*II site of pSP73. In analogy, for pSP73-TNF α -ARE-4xS1 (p3279), an ARE-4xS1 fragment with flanking *Bam*HI/*Bgl*II sites was PCR-amplified from pTet-7B-TNF α -ARE-4xS1 (p2778) with primers G2247/G2235, *Bam*HI/*Bgl*II-digested, and inserted into the *Bgl*II site of pSP73. The PP7bs was synthesized by annealing oligonucleotides G95 and G96, and concatemerized using the same *Bam*HI/*Bgl*II strategy as described above for S1/S1m. A 6-fold head-to-tail repeat of PP7bs was then cloned into pSP73, and transferred as a *Bam*HI-*Bgl*II fragment into the *Bgl*II site of pTet-7B-ARE (p2260) [136] to generate pTet-7B-TNF α -ARE-6xPP7bs (p2259). For pTet-7B-TNF α -ARE-6xMS2bs (p2258), a 6-fold repeat of MS2bs was amplified by PCR using primers G37 and G38 from plasmid b-6bs [274] and cloned as a *Bam*HI-*Bgl*II fragment into the *Bgl*II site of pTet-7B-ARE (p2260) [136].

For the expression of GST-tagged recombinant proteins, a 5' *Bam*HI-, 3' *Eco*RI-linked TEV sequence encoding ENLYFQG was first synthesized by annealing oligos G1875/G1876, and ligated into the *Bam*HI/*Eco*RI sites of pGEX-4T-3 to generate pGEX-4T-3-TEV (p2772). The PP7cp sequence was then PCR-amplified with oligos G1859/G1860 from pc-HA-PP7cp (p2211) [197] and inserted into the *Eco*RI/*Xho*I sites of pGEX-4T-3-TEV (p2772) to generate pGEX-4T-3-TEV-PP7cp (p2773). Using the same strategy, oPP7cp [286] was PCR-amplified from pET28-ZZ-TEV-oPP7cp-His6 (p2770), a kind gift from Kathy Collins (University of California Berkeley, USA), using oligos G1860/G1861, and inserted into the *Eco*RI/*Xho*I sites of pGEX-4T-3-TEV (p2772) to generate pGEX-4T-3-TEV-oPP7cp (p2774). A TEV-linked version of GST-MS2cp was generated by inserting two consecutive *Bam*HI/*Bgl*II-

linked TEV sites (G1852/G1853) into the *Bam*HI site of pGEX-2T-MS2cp (p2809), resulting in pGEX-2T-TEV-TEV-MS2cp (p2810).

For pcDNA3-GF β (p2732), which encodes a GFP/ β -globin fusion protein, EGFP was amplified with primers G1612/G1613 and cloned as a *Hind*III–*Kpn*I fragment into the *Hind*III/*Kpn*I sites of pcDNA3-7B (p2308) [196]. pcDNA3-GF β -TNF α -CDE (p2730), was generated by insertion of annealed oligonucleotides spanning a 14 nt linker (*Nhe*I, *Age*I sites) and the 40 nt CDE of mouse TNF α (see **Suppl. Table 5.1** for all CDE inserts). The oligonucleotides were designed with *Bam*HI- and *Bgl*II-compatible ends, 5'-phosphorylated using T4 polynucleotide kinase (Promega) and annealed prior to ligation into the *Bgl*II site of pcDNA3-GF β (p2732), whereby a 5'-*Bam*HI/*Bgl*II fusion site (AGATCC) and a 3'-*Bgl*II site were created. For puroMX β -TNF α -CDE (p2812), the CDE was excised as an *Eco*RI–*Bgl*II fragment from pcDNA3-GF β -TNF α -CDE (p2730) and ligated into the *Eco*RI/*Bgl*II sites of puroMX β (p2220).

By the same *Bam*HI-*Bgl*II strategy, annealed oligonucleotides were inserted into the *Bgl*II-site of puroMX β (p2220) to generate the following plasmids: puroMX β -TNF α -CDE₃₇-V2 (p2814), -V3 (p2823), -V3-M1 (p2825), -V3-M2 (p2826), -V3-M3 (p2827), -V3-M4 (p2828), -V3-M5 (p2829), -V3-M6 (p2830), -V3-M7 (p2831), -V3-M8 (p2832), -V3-M9 (p2833), -V3-M10 (p2834), -V3-M11 (p2835), -V3-M12 (p2859), -V3-M13 (p2860), -V3-M14 (p2861), -V3-M15 (p2862), -V3-M16 (p2863), -V3-M17 (p2864), -V3-M18 (p2944), -V3-M19 (p2945), -V3-M20 (p2959), -V3-M21 (p2946), -V3-M22 (p2947), -V3-M23 (p2960), -V3-M24 (p2961), -V3-M25 (p2948), -V3-M26 (p2967), -V3-M27 (p2968), puroMX β -TNF α -CDE₁₇-ds (p2966) and puroMX β -human-TNF α -CDE₃₇-V3 (p2836). All CDE sequences and corresponding mRNA half-lives are summarized in **Suppl. Table 5.1**.

In order to generate puroMX β -TNF α -CDE₁₇-ss (p2965) and puroMX β -ICOS-CDE₁₇-ss (p2991), puroMX β was engineered to contain an *Xba*I, *Age*I and *Nhe*I site between the β -globin stop codon and the *Bgl*II site, and CDE₁₇-containing oligos with *Xba*I- and *Age*I-compatible ends were ligated into the *Xba*I/*Age*I sites. For puroMX β -TNF α -CDE₁₅₀ (p2969), a 150 nt fragment of the mouse TNF α 3'UTR containing the CDE in its center was amplified using *Bam*HI- and *Bgl*II-linkered primers (G2495/G2496) and cloned into the *Bgl*II site of puroMX β (p2220). Mutations in puroMX β -TNF α -CDE₁₅₀-M16 (p2970) and puroMX β -TNF α -CDE₁₅₀-M20 (p2972) were generated by the following PCR strategy: up- and downstream portions of the CDE₁₅₀ were amplified using mutation-bearing primers (G2495/G2498 and G2497/G2496 for M16, G2495/G2502 and G2501/G2496 for M20), annealed, and the full CDE₁₅₀ fragment was reamplified with G2495/G2496 prior to insertion into the *Bgl*II site of puroMX β (p2220). The TNF α mouse 3'UTR was ligated into

puroMX β (p2220) as a *SalI/BglIII* fragment from pBABEpuro-GFP-TNF α -UTR (G. Stoecklin, unpublished) to generate puroMX β -TNF α -3'UTR (p2914).

A point mutation in the Roquin2 cDNA obtained from Imagenes was replaced with a WT fragment amplified by PCR from mouse cDNA with primers G2421/G2427. The fulllength Roquin2 cDNA was then cloned as a *SalI/ClaI* fragment into pLNCX2 (Clontech) to generate pLNCX2-Roquin2 (p2984). For pLNCX2-EGFP-Roquin2 (p2985), EGFP was excised using *SalI* from pLNCX2-EGFP-Roquin (p2838) and inserted into the *SalI* site of pLNCX2-Roquin2 (p2984).

The Roquin and Roquin2 ZF mutants were generated replacing the first cysteine in the CCCH-type zinc finger domains of both proteins with an arginine, resulting in a RCCH motif (Roquin-C419R and Roquin2-C416R). Mutagenesis was carried out using a dual PCR approach, as follows: Two PCR fragments each were amplified for Roquin (G2623/G2577, G2576/G2579) and Roquin2 (G2556/G2555, G2554/G2622), annealed and used as DNA templates for a second PCR with the outer primer pairs (Roquin, G2623/G2579; Roquin2, G2622/G2556). The secondary PCR fragments spanning the mutations were exchanged with the original sequence by restriction digest and subsequent ligation. *DraIII* was used for pLNCX2-EGFP-Roquin-C419R (p3013), and *MfeI/BstXI* were used for pLNCX2-EGFP-Roquin2-C416R (p3014).

To facilitate cloning of Roquin fusion proteins, the EGFP coding sequence was excised from pLNCX2-EGFP-Roquin (p2838) using *SalI* and replaced by a PCR-amplified EGFP fragment containing a unique *AgeI* site downstream of the EGFP sequence, yielding pLNCX2-EGFPA-Roquin (p3090). For the plasmids encoding the N-terminal portion (N-term) of Roquin (pLNCX2-EGFPA-Roquin-2-441aa; p3124) or the ROQ-domain (pLNCX2-EGFPA-Roquin-131-360aa; p3153), the Roquin coding sequence was excised from p3090 as a *AgeI/ClaI* fragment and replaced with corresponding PCR-amplified inserts coding for N-term (G2788/G2840) or ROQ (G2855/G2856). For pLNCX2-EGFPA-Roquin-442-1130aa (p3125) encoding the Roquin C-terminus (C-term), a larger N-terminal portion of Roquin was excised as an *AgeI/PmlI* fragment from pLNCX2-EGFPA-Roquin (p3090) and replaced by a shorter PCR-amplified fragment (G2842/G2843). pLNCX2-EGFPA-Roquin-S060r (p3101) encoding an siRNA s060 (si-Roquin (B))-resistant version of Roquin was generated using the above described dual PCR approach with primers G2788/G2791, G2789/G2790 and G2788/G2789. The resulting fragment harboring four silent point mutations in the s060 seed sequence were cloned into the *AgeI/MfeI* sites of pLNCX2-EGFPA-Roquin (p3090). Flag-tagged Roquin-fusion constructs pCI-neo-Flag-Roquin (p3061), pCI-neo-Flag-Roquin- Δ RING (p3062), and pCI-neo-Flag-Roquin- Δ ROQ (p3063) were kindly provided by Nancy Kedersha and Paul Anderson (Harvard Medical School, Boston, MA).

4.2.3 Oligo Phosphorylation and Ligation

In case oligos were used as inserts for cloning, they were 5'-phosphorylated in a kination reaction using T4 polynucleotide kinase (PNK, NEB). A 20 μ L reaction contained oligonucleotides at a concentration of 20 pmol/ μ L, 1x T4 kinase buffer, 1 mM ATP and 5 U T4 PNK. After incubation at 37°C for 30 minutes, sense and antisense oligos were mixed for annealing. Upon heating at 95°C for 15 minutes for denaturation, the mixture was slowly cooled down by incubation in a beaker of 500 ml boiling water and cooled to RT. The annealed oligos were nucleotide-purified (Nucleotide Purification Kit, QIAgen), eluted in 30 μ l H₂O and ligated for 30 minutes at RT in a 40 μ l reaction applying 5 U T4 DNA ligase (Rapid DNA Ligation Kit, Fermentas) This generated head-to-tail linked oligo chains. After nucleotide removal and elution in 40 μ l H₂O, in cases where *Bam*HI- and *Bgl*III-sites were attached, the inserts were *Bgl*III/*Bam*HI-digested in a 50 μ l reaction using 1 U restriction enzyme (NEB) each, for 1 hour at 37°C. This prevented links other than head-to-tail. The samples were resolved on a 1% agarose gel and ligation products of correct size were gel-extracted (QIAquick Gel Extraction Kit, QIAgen) and eluted in 30 μ l H₂O. Inserts were further applied for ligation with plasmid DNA. Where only one copy of an oligo served as insert, annealed oligonucleotides were nucleotide-purified, digested with the respective enzymes to reverse multimerization, and again nucleotide-purified before subsection to plasmid ligation. All oligonucleotide sequences are provided in **Suppl. Table 5.1**. Mutations, cloning boundaries and coding sequences were systematically verified by DNA sequencing (GATC Biotech).

4.2.4 Polymerase Chain Reaction (PCR)

In case plasmid construction included insert amplification by PCR, a 100 μ l reaction was performed as given in **Table 4.3** with the PCR program given in **Table 4.4**. Screening of colonies upon *E. coli* transformation by colony PCR was performed as exemplified for puroMX β constructs using primers G1854/G1855 in a downscaled 25 μ l reaction in analogy to as presented in **Table 4.3**. For that cells of a single colony were picked and used as template, increasing the initial denaturation time to 10 minutes. 10 μ l of the PCR reaction was loaded onto a 1 or 2% agarose gel and analyzed with a UV Gel Documentation device.

4.2.5 mRNA Decay Assay

For mRNA decay experiments, NIH3T3 B2A2 or HeLa cells were stably or transiently transfected with puroMX β globin reporter plasmids. 24 hours post

Table 4.3: PCR Reaction.

Amount	Component
0.5-1 µg	plasmid DNA
10 µl	10x Taq polymerase buffer (QIAGEN)
200 nM	dNTPs (dATP, dTTP, dGTP, dCTP, Fermentas; 10 mM each)
400 nM	forward primer G1854 (40 mM)
400 nM	reverse primer G1855 (40 mM)
2 U	Taq polymerase (QIAGEN)
ad 100 µl	water

Table 4.4: PCR Program.

Temperature (°C)	Duration (minutes)	Cycles
95	3	1
95	0.5	35
55-60	0.5	
72	0.5-1.5	
72	10	1
4	∞	1

transfection, 5 µg/ml actinomycin D (actD, AppliChem, Cat. No. A1489) was added to the medium for the indicated time intervals before harvesting cells and extracting total RNA using the Genematrix universal RNA purification kit (Eura, Roboklon). RNA was extracted from Trifast (PeqLab) samples by phase-separation using chloroform and precipitated with isopropanol. The RNA pellet was washed with ice-cold 70% ethanol and resuspended in RNase-free water. RAW264.7 cells were stimulated for 2 hours with LPS (100 ng/ml) before addition of actD. mRNA levels were determined either by Northern blot or by quantitative reverse transcription (RT)-PCR analysis. mRNA half-lives were calculated assuming a first order decay rate. After background subtraction, mRNA signals were normalized to the signal of the loading control and plotted against time. Curves with the following equation were fitted to the data points by linear regression: $y = a \times e^{(b \times t)}$, where y stands for the relative mRNA signal and t for the time. mRNA half-lives were calculated as follows: $t_{1/2} = \ln(2) / \ln(b)$.

4.2.6 Northern Blot Analysis

5–15 µg of RNA was resolved by 1.1% agarose/2% formaldehyde/MOPS (morpho-linepropanesulfonic acid) gel electrophoresis and blotted over night

with 8x saline-sodium citrate (SSC) buffer (1x contains 0.15 M NaCl and 0.015 M sodium citrate) onto Hybond-N+ Nylon membranes (Amersham, GE Healthcare). Membranes were hybridized overnight at 55°C with digoxigenin-labelled RNA probes synthesized *in vitro* using Sp6 polymerase (Fermentas) and DIG RNA labelling mix (Roche). 500 ng RNA probe was diluted in 10 ml hybridization buffer containing 50% formamide, 5x SSC, 5x Denhard's solution, 5 mM EDTA, 10 mM PIPES pH 7.0 at 25°C, 0.4 mg/ml torula yeast RNA (US Biological) and 1% SDS. Membranes were washed twice with 2x SSC/ 0.1% SDS for 5 minutes, and twice with 0.5x SSC/ 0.1% SDS for 20 minutes at 65°C. Alkaline phosphatase-coupled anti-digoxigenin Fab fragments and CDP-Star substrate (both Roche) were used for detection according to the manufacturer's instructions. Templates for RNA probes were generated by PCR using the following primers: G1000/G1001 (probe against exon 1 and 2 of rabbit β -globin), G83/G1009 (probe against human nucleolin), G078/G1008 (probe against mouse S7), and G314/G316 (probe against mouse TNF α). Deadenylated mRNA was generated using RNase H (NEB) and oligo-dT as described [131]. 1.6% agarose gels were used to resolve poly(A) tails, and the corresponding signals were quantified using ImageJ software.

4.2.7 Western Blot Analysis

Proteins were resolved on 5–20% polyacrylamide gradient Tris-glycine gels and transferred onto 0.2 μ m pore size nitrocellulose membranes (PeqLab). Protein loading was assessed by Ponceau Red staining. Membranes were then blocked in phosphate buffered saline (PBS) containing 0.1% sodium azide and 5% horse serum or milk powder, incubated with antibodies diluted in the same solution for 1 hour at room temperature or over night at 4°C, and washed in 150 mM NaCl, 50 mM Tris-HCl (pH 7.5 at 25°C), 1% Tween-20. Horseradish peroxidase-coupled secondary antibodies (Jackson ImmunoResearch) in combination with Western Lightning enhanced chemiluminescence substrate (Perkin Elmer) and X-ray films (FujiFilm) were used for detection. Films were documented using an EPSON scanner. For the detection of Roquin and TNF α in RAW264.7 macrophages, cells were harvested, washed once in PBS, solubilized in RNA-IP lysis buffer, and cytoplasmic lysates were supplemented with 2x SDS sample buffer containing 100 mM Dithiothreitol (DTT) prior to Western blot analysis.

4.2.8 Antibodies

A list of all primary antibodies and dilutions used in this study for Western blot analysis can be found in the Appendix. Antibodies received from others

include polyclonal rabbit anti-GST antibody which was kindly provided by Ludger Hengst (Innsbruck Medical University, Austria) and Frauke Melchior (ZMBH, University of Heidelberg, Germany). Polyclonal rabbit anti-Caf1a antibody was kindly provided by Ann-Bin Shyu (University of Texas-Houston Medical School).

4.2.9 Recombinant Protein Purification

For expression of the recombinant fusion proteins GST-T-PP7cp, GST-T-oPP7cp, GST-MS2cp, and GST-TT-MS2cp, pGEX-based plasmids described above were transformed into BL21 (DE3) codon+ *E. coli*. Cells were cultured in 1 l Luria-Bertani medium supplemented with 100 µg/ml ampicillin at 37°C to an OD₆₀₀ of 0.5 and protein expression was induced by addition of 1 mM IPTG. The culture was incubated for additional 16 hours at 21°C before cells were collected at 4°C, washed once with ice-cold phosphate buffered saline (PBS), and resuspended in 10 ml PBS-MEC (PBS, 0.1% (v/v) β-mercaptoethanol (ME), 1 tablet/10 ml Mini Complete Protease Inhibitors, EDTA-free (Roche)) and lysed in PBS-ME using a microfluidizer (Emulsiflex, Avestin). The lysate was supplemented with 1% Triton-X-100, insoluble debris was removed by centrifugation and the supernatant was incubated under rotation with Glutathione (GSH) Sepharose High Performance 4B (GE Healthcare) beads for 1 hour at 4°C. Beads were washed five times for 10 minutes with PBS-ME and transferred to a Poly-Prep column (Biorad) with a frit. PBS-ME was drained by gravity, and recombinant protein was eluted in 2 ml of elution buffer (50 mM glutathione, 50 mM Tris-HCl (pH 8.0), 10% glycerol, 1 tablet/10 ml Mini Complete Protease Inhibitors, EDTA-free (Roche), 0.1% (v/v) β-ME) for 2 hours at 4°C under rotation. Eluted protein was dialyzed against dialysis buffer (50 mM Tris-HCl (pH 8.0), 0.1% (v/v) β-ME) for 6 hours at 4°C, exchanging the buffer every 2 hours. The eluate was recovered, supplemented with 20% glycerol, and protein concentration was determined by Nanodrop measurement and SDS-PAGE using a BSA standard.

4.2.10 Cellular RNP Purification via S1/S1m Aptamers

One day after transient transfection of 1.2x10⁶ COS7 cells per 10-cm dish, cells were washed once with PBS, and the cell pellet was snap frozen in liquid nitrogen. By addition of a 5 mm steel bead, the cell pellet was homogenized by cryomilling using a tissue lyser (QIAgen TissueLyser II) at 25 Hz for 15 seconds.

For SA-pulldown of S1 and S1m-tagged RNAs, the homogenate was solubilized in 500 µl ice cold SA-RNP lysis buffer (20 mM Tris-HCl (pH 7.5), 150 mM

4.2 Methods

NaCl, 1.5 mM MgCl₂, 2 mM DTT, 2 mM vanadylribonucleosid complex RNase inhibitor (NEB), 1 tablet/10 ml Mini Complete Protease Inhibitors, EDTA-free (Roche). Lysates were first incubated with avidin agarose beads (Thermo Pierce) for 10 minutes at 4°C as a blocking step before cell debris was removed by centrifugation for 5 minutes at 2000 rpm (~400 x g) at 4°C. The pre-cleared lysate was transferred to a fresh tube, and 1:10 was saved as RNA input, mixed with 500 µl TriFast (PeqLab) and stored at -20°C for later RNA extraction. Lysates were incubated with Streptavidin Sepharose High Performance (GE Healthcare) beads for 4 hours at 4°C under rotation before washing five times for 5 minutes at 4°C with SA-RNP wash buffer (20 mM Tris-HCl (pH 7.5), 300 mM NaCl, 5 mM MgCl₂, 2 mM DTT). For the last wash, beads were transferred to a fresh tube, and RNA was eluted from the beads using 500 µl TriFast reagent (PeqLab) according to the manufacturer's instructions. 15 µg GlycoBlue (Ambion) was added to the RNA samples prior to precipitation. Subsequently, RNA was resolved on denaturing agarose gels for Northern Blot analysis to determine RNA binding efficiency to SA-beads.

4.2.11 Cellular RNP Purification via GST

COS7 cells were transfected, harvested and homogenized as described for SA-pulldown above. Homogenates were solubilized in 500 µl ice cold GSH-RNP lysis buffer (50 mM Tris-HCl (pH 8.0 at 25°C), 150 mM NaCl, 1 mM MgCl₂, 10% v/v glycerol, 2 mM DTT, 1 tablet/10 ml Mini Complete Protease Inhibitors, EDTA-free (Roche), 2 mM vanadylribonucleosid complex RNase inhibitor (NEB)), tumbled for 10 minutes at 4°C and cell debris was removed by centrifugation. The lysate was transferred to a fresh tube, and 1:10 was saved for extraction of input RNA using TriFast (PeqLab). Lysates were pre-cleared with Glutathione Sepharose High Performance 4B (GE Healthcare) beads for 2 hours at 4°C. The supernatant was then transferred to a new tube, and 1:10 was saved for extraction of pre-clear RNA. 2 µg of recombinant GST-tagged proteins was added to the pre-cleared lysates for 3 hours at 4°C prior to incubation with Glutathione Sepharose High Performance 4B (GE Healthcare) for another 3 hours. The beads were then washed six times for 5 minutes at 4°C with GSH-RNP lysis buffer. For the last wash, beads were transferred to a fresh tube, and protein was eluted from 10% of the beads using SDS sample buffer. RNA was eluted from 90% of the beads using 500 µl TriFast (PeqLab).

4.2.12 *In vitro* Transcription

Four RNAs were synthesized by *in vitro* transcription: ARE-4xS1 and ARE-4xS1m RNA containing a single copy of the 53 nt long TNF α ARE attached

to 4 copies of the S1 or S1m aptamer, respectively, as well as 4xS1 and 4xS1m alone as negative control RNAs. Since amplification of the highly structured 4xS1 and 4xS1m tag by PCR was problematic, linearized pSP73 plasmids or excised fragments from plasmids containing the ARE and 4xS1/4xS1m sequences served as templates. To this end, plasmids pSP73-4xS1 (p3278), pSP73-4xS1m (p2880), pSP73-TNF α -ARE-4xS1 (p3279), and pSP73-TNF α -ARE-4xS1m (p2881) were linearized at the *EcoRV*-site downstream of the 4xS1m sequence, purified with the QIAquick PCR Purification Kit (QIAGEN) and used as DNA templates for run-off *in vitro* transcription using SP6 RNA polymerase. Alternatively, plasmids were digested for 6 hours with *NdeI* and *EcoRV* to release SP6-tagged DNA templates that were gel-extracted with the QIAquick Gel Extraction Kit (QIAGEN). A 50 μ l transcription reaction contained the components given in **Table 4.5**.

Table 4.5: *In vitro* Transcription Reaction.

Amount	Component
8 μ g	linear DNA template
1x	5x SP6 Transcription Buffer (Fermentas)
4 mM	NTPs (ATP, UTP, GTP, CTP, Fermentas, 10 mM each)
0.5 U	yeast pyrophosphatase (Sigma)
50 U	RNasin RNase inhibitor (Promega)
400 U	SP6 RNA Polymerase (Fermentas)
ad 50 μ l	water

After incubation for 4 hours at 37°C, DNA was digested by addition of 5 U RQ1 DNase (Promega) for 15 minutes at 37°C. In cases where higher RNA yields were needed, the MEGAscript SP6 Kit (Invitrogen, Life Technologies) was used for transcription and DNase digestion according to the manufacturer's instructions. Synthesized RNA was purified by gel filtration using pre-packed G-50 Mini Quick Spin Sephadex RNA columns (Roche) according to the manufacturer's instructions, and RNA concentration was determined by Nanodrop. One reaction typically yielded 25–50 μ g of RNA.

4.2.13 *In vitro* RNP Purification via S1m

For the following procedures, DNA/RNA LoBind tubes (Eppendorf) were used to reduce the degree of unspecific binding. Per sample, 100 μ l 50% slurry of Streptavidin Sepharose High Performance (GE Healthcare) beads were washed three times with 1 ml of SA-RNP lysis buffer (20 mM Tris-HCl (pH 7.5), 150 mM NaCl, 1.5 mM MgCl₂, 2 mM DTT, 2 mM vanadylribonucleosid complex RNase inhibitor (NEB), 1 tablet/10 ml Mini Complete Protease Inhibitors,

4.2 Methods

EDTA-free (Roche)). At each step, beads were gently pelleted at 500 rpm (~20 x g) for 1 minute at 4°C. 30 µg of the *in vitro* transcribed 4xS1m or ARE-4xS1m RNAs was renatured in 50 µl SA-RNP lysis buffer by heating at 56°C for 5 minutes, 10 minutes at 37°C and incubation at room temperature for several minutes to refold RNA structures. The RNA was added to the 100 µl SA Sepharose slurry together with 3 µl RNasin (120 U, Promega), and 10 µl of the supernatant (10%) was saved for extraction of input RNA using TriFast (PeqLab). The mixture was incubated at 4°C for 2–3 hours under rotation to permit binding of the RNA to the column. After that, beads were sedimented and a 10 µl sample of the supernatant (10%) was saved for extraction of unbound RNA using TriFast (PeqLab), while the remaining supernatant was discarded. Input and unbound RNA samples were compared side by side through 6% polyacrylamide/TBE/urea gel electrophoresis and methylene blue staining to assess the efficiency of RNA coupling.

Cellular extracts were prepared from 40 confluent 15-cm dishes of untransfected NIH3T3 B2A2 cells. A total of 3.5 g cells was collected, washed once in PBS, divided into 300 mg portions and aliquoted in 2 ml safe-lock tubes (Eppendorf). The cell pellets were then snap frozen in liquid nitrogen, homogenized by cryomilling after addition of a 5 mm steel bead using a tissue lyser (QIAGEN TissueLyser II) at 25 Hz for 15 seconds 4–6 times, and the powder was either processed directly or stored in liquid nitrogen. The frozen homogenate of one aliquot (300 mg) was solubilized by the addition of 300 µl ice-cold RNP lysis buffer and allowed to thaw for 5 minutes at room temperature. Cell debris was removed by centrifugation for 10 minutes at 17,000 x g at 4°C, resulting in a supernatant of ~500 µl. The protein concentration in the extract was determined by Nanodrop to be ~70 mg/ml.

Next, the extract (~500 µl) was pre-cleared by addition of 25 µl of a 50% slurry of Avidin Agarose (Thermo Pierce) beads and tumbling for 30 minutes at 4°C. The supernatant was transferred to a fresh tube and tumbled with 50 µl of a 50% slurry of SA Sepharose beads for an additional 2–3 hours. Beads were discarded, and the pre-cleared lysate was supplemented with 1.5 µl (60 U) of RNasin (Promega), added onto the freshly prepared, RNA-coupled SA Sepharose matrix and incubated at 4°C for 3–4 hours under rotation. Beads were washed 6 times for 2–5 minutes with 1 ml SA-RNP wash buffer (20 mM Tris-HCl (pH 7.5), 300 mM NaCl, 5 mM MgCl₂, 2 mM DTT) supplemented with 2 mM vanadylribonucleosid complex RNase inhibitor (NEB) and 1 tablet/50 ml Complete Protease Inhibitors, EDTA-free (Roche). After the last wash, beads were transferred to a fresh tube and RNA-bound proteins were eluted by addition of 5 µg RNase A (Genomed) in 100 µl Low Salt Buffer (20 mM Tris-HCl (pH 7.5), 30 mM NaCl, 5 mM MgCl₂, 2 mM DTT, 1 tablet/10 ml Mini Complete Protease Inhibitors, EDTA-free (Roche)) for 10 minutes at 4°C. The RNase A eluate was recovered and concentrated by vacuum centrifu-

gation from 100 μ l to 30 μ l. 10 μ l of the eluate was analyzed by SDS-PAGE and colloidal Coomassie staining while 20 μ l were used for subsequent LC-MS/MS analysis. After RNase A elution, the beads were extracted with 30 μ l 2x SDS sample buffer, 10 μ l of which were analyzed by SDS-PAGE.

4.2.14 *In vitro* RNP Purification via S1m and Biotin Elution

Where indicated, elution of RNA-protein complexes with biotin was carried out using 10 mM biotin (50 mM stock, Invitrogen, Life Technologies) in SA-RNP lysis buffer for 1 hour at 4°C. For initial small-scale experiments aimed at quantifying binding and elution efficiencies, (and protein analysis), 20% of the RNA at each step was analysed by 6% polyacrylamide/TBE/urea gel electrophoresis and methylene blue staining. For that, the before mentioned protocol was adjusted as follows. Per sample, 20 μ l (50 μ L) washed 50% slurry of Streptavidin Sepharose High Performance (GE Healthcare) beads were incubated with 5 μ g (15 μ g) of *in vitro* transcribed RNA and 0.5 μ l (2 μ l) RNasin (20 U, Promega) in 50 μ L SA-RNP lysis buffer. 10 μ l of the supernatant (20%) was saved as input RNA, the RNA was coupled to beads at 4°C for 1–2 hours under rotation, and 10 μ l of the supernatant (20%) was saved as unbound RNA. Cellular extracts of 30–50 mg/ml protein concentration were prepared from frozen NIH3T3 cell homogenates in ice-cold SA-RNP lysis buffer, pre-cleared with SA and avidin beads for 30 minutes at 4°C, and 50 μ l (250 μ l) lysate supplemented with RNasin was incubated with RNA-resins for 1–2 hours at 4°C. Upon three washes with SA-RNP lysis buffer (SA-RNP wash buffer when monitoring protein), RNA-protein complexes were eluted either with 10 mM biotin (50 mM stock, Invitrogen, Life Technologies) in 40 μ l lysis buffer for 1 hour at 4°C or with 1 μ g (2.5 μ g) RNase A (Genomed) in 40 μ l lysis buffer (50 μ L wash buffer) for 10 minutes at 4°C. 10 μ L (20%) of each biotin and RNase A elution sample was saved. Residual RNA on beads was extracted using TriFast (PeqLab). For protein analysis, after RNase A elution, the beads were extracted with 40 μ l 2x SDS sample buffer. 23% of RNase A elutions and SDS bead elutions was analyzed by SDS-PAGE and Western blot.

4.2.15 Mass Spectrometry

Mass spectrometry analysis was carried out at the Mass Spectrometry Core Facility of the ZMBH (Zentrum für Molekulare Biologie der Universität Heidelberg). Proteins eluted from the RNA affinity matrix were shortly run into a 10% polyacrylamide Tris-glycine gel (NuPAGE, Novex/Invitrogen), and proteins were stained by colloidal Coomassie blue. For each sample, the entire lane was cut into 3–4 gel slices including the wells. After in-gel digestion

with trypsin, the supernatant was dried in a speed vac and solubilized in 55 μl of dimethyl labeling reaction mixture (50 μl 100 mM TEAB, 2 μl 150 mM NaBH_3CN) and 2 μl formaldehyde for light labeling and 2 μl deuterated formaldehyde for medium labeling [307]. After 1 hour at 25°C, the reaction was stopped with 1.6 μl 5% NH_4OH and acidified with 4 μl 50% formic acid 10 minutes later. NanoUPLC-MS/MS analysis (LTQ Orbitrap XL, Thermo Scientific) was carried out as described in more detail previously [131]. Database search was done using Mascot in the framework of ProteomeDiscoverer (PD1.3; ThermoScientific) with carbamidomethyl cysteine as fixed modification, and deamidation (NQ) and oxidation (M) as variable modification against the NCBI database (taxonomy: mus). Light and medium dimethylation at K and the N-terminus were searched as static modifications in two different nodes of PD1.3.

4.2.16 In-Line Probing

In-line probing was performed as described previously [315]. Mouse $\text{TNF}\alpha$ -CDE RNA (CDE₃₇-V2, CDE₃₇-V3 and CDE₁₅₀) was transcribed *in vitro* using T7 RNA polymerase, dephosphorylated and radiolabelled with [γ -³²P]ATP. T7-linkered primers (G2234/G2235, **Suppl. Table 5.7**) were used to amplify the DNA sequence of $\text{TNF}\alpha$ -CDE₃₇-V2 (92 nt) and $\text{TNF}\alpha$ -CDE₃₇-V3 (94 nt) from plasmid templates. For the CDE₁₅₀ DNA template, primers G2332/G2333 and plasmid puroMX β - $\text{TNF}\alpha$ -3'UTR (p2914) containing the full-length 3'UTR of mouse $\text{TNF}\alpha$ were used. After gel-extraction of the DNA templates, RNAs were prepared by *in vitro* transcription using T7 RNA polymerase (NEB) in a solution containing 40 mM Tris-HCl (pH 7.9 at 25°C), 6 mM MgCl_2 , 2 mM spermidine, and 10 mM dithiothreitol (DTT). The transcription products were subjected to denaturing 8 M urea/6% polyacrylamide gel electrophoresis (PAGE) for purification. The RNA transcripts were dephosphorylated using calf intestinal phosphatase (Roche) and radiolabeled with [γ -³²P]ATP using T4 polynucleotide kinase (NEB) in 70 mM Tris-HCl (pH 7.6 at 25°C), 10 mM MgCl_2 , 5 mM DTT. The radiolabeled RNA was purified using denaturing 6% PAGE. The purified RNA was subsequently incubated for 45 hours at room temperature in a solution containing 50 mM Tris-HCl (pH 8.3 at 25°C), 20 mM MgCl_2 , and 100 mM KCl. Reactions were quenched with urea and EDTA prior to loading. Products of spontaneous in-line cleavage were resolved next to a no reaction (NR) control, a partial RNase T1 digest (T1), and a partial alkaline digest (-OH) of the same RNA by denaturing 10% urea PAGE. Gels were dried and visualized using a GE Typhoon laser scanner under the phosphorimager setting.

4.2.17 Quantitative RT-PCR

For reverse transcription-quantitative PCR (RT-qPCR) analysis, cDNA was synthesized from 1–2 μg of total RNA using random hexamer primers (Fermentas) and Transcriptor reverse transcriptase (Roche) according to the manufacturer's instructions in an RT reaction. Prior to RT, residual DNA was removed from RNA samples in a DNase treatment step. 16 μl total RNA in a 20 μl DNase reaction was incubated with 2 U RQ1 DNase (1 U/ μl) and 1x RQ1 DNase Buffer (both Promega) and incubated at 37°C for 30 minutes before inactivation of the DNase by addition of 2 μL RQ1 stop solution and incubation at 65°C for 10 minutes. DNase-treated RNA was then used for RT. The RT reaction mixture given in **Table 4.6** was incubated for 30 minutes at 55°C for cDNA synthesis and the reverse transcriptase was inactivated at 85°C for 5 minutes. The generated cDNA was diluted 1:5 in water prior to PCR. qPCR reactions were assembled in 384-well plates using 1:20 of a cDNA reaction, 400 nM of each target-specific primer and the DNA SYBR Green I Master kit (Roche) in a final volume of 10 μl per well. qPCR was performed on the Lightcycler 480 system (Roche) applying the program given in **Table 4.7**. Mouse gene-specific primer sequences used for detection of mRNAs encoding nucleolin (G1706/G1707), Ier3 (G1712/G1713), TNF α (G1844/G1845), Gapdh (G2053/G2054), Nfkbiz (G2181/G2182), Nfkbid (G2199/G2200), NupL1 (G2364/G2365), Roquin (G2392/G2393), Roquin2 (G2394/G2395), Ppp1r10 (G2592/G2593), Bmpr1a (G2723/G2724), Pdia6 (G2729/G2730), Hmgxb3 (G2737/G2738) and Rck (G2747/G2748) are given in **Suppl. Table 5.7**.

Table 4.6: RT Reaction for cDNA Synthesis.

Amount	Component
1–2 μg	total RNA (DNase-treated)
4 μl	5x Transcription Buffer (Roche)
2 μl	dNTPs (dATP, dTTP, dGTP, dCTP, Fermentas; 10 mM each)
2 μl	100 mM DTT
0.01 μg	Random hexamer primers (Fermentas)
1 μl	RNasin RNase inhibitor (Promega)
10 U	Transcriptor Reverse Transcriptase (Roche)
ad 20 μl	water

4.2.18 Protein-IP

HEK293T cells were transiently transfected 24 hours prior to lysis. Cells of a confluent 10-cm dish were washed once with PBS, collected in a 2 ml reaction

Table 4.7: qPCR Program.

Program	Target (°C)	Acquisit. Mode	Hold	Ramp Rate
Pre-Incubation	95	none	5 min	4.4
Amplification	95	none	10 sec	4.4
	55	none	15 sec	2.5
	72	single	25 sec	4.8
Melting curve	95	none	5 sec	4.8
	60	none	1 min	2.5
	97	continuous	-	0.11
Cooling	40	none	10 sec	2

tube, and the cell pellet was disrupted mechanically with a tissue lyser (QIAGEN TissueLyser II). The lysate was solubilized in 400 μ l ice-cold RNP lysis buffer (20 mM Tris-HCl (pH 7.5 at 25°C), 100 mM KCl, 1.5 mM MgCl₂, 1 mM DTT, 1 tablet/10 ml Mini Complete Protease Inhibitors, EDTA-free (Roche)), and cell debris was removed by centrifugation. 1:20 of the lysate was saved as input before EGFP-tagged proteins were purified using the GFP-binder as described previously [359]. Lysates were incubated with sepharose-coupled GFP-binder for 1–3 hours at 4°C, followed by two washes with lysis buffer and 3–4 washes with RNP wash buffer (20 mM Tris-HCl (pH 7.5 at 25°C), 150 mM KCl, 2.5 mM MgCl₂, 1 mM DTT). Proteins were eluted from the beads with 1% SDS-containing sample buffer.

4.2.19 RNA-IP

Cells grown in 10-cm dishes were mechanically disrupted as described above for protein-IP, and solubilized in 400 μ l RNA-IP lysis buffer (20 mM Tris-HCl (pH 7.5 at 25°C), 150 mM NaCl, 1.5 mM MgCl₂, 1 mM DTT, Mini Complete protease inhibitors (Roche), 2 mM vanadylribonucleosid complex RNase inhibitor (NEB) or 0.2 U/ml RNasin (Promega)). 1:13 of the lysate was saved as RNA input, 1:40 for protein input. For IP of EGFP-tagged proteins, lysates were bound to GFP-binder beads for 2–4 hours at 4°C before washing twice with RNA-IP lysis buffer and four times with RNA-IP wash buffer (20 mM Tris-HCl (pH 7.5 at 25°C), 300 mM NaCl, 2.5 mM MgCl₂, 1 mM DTT, 2 mM vanadylribonucleosid complex RNase inhibitor (NEB)). Protein was eluted from 1:5 of the beads using SDS sample buffer; RNA was eluted from 4:5 of the beads using 500 μ l TriFast reagent (PeqLab) according to the manufacturer's instructions. 15 μ g GlycoBlue (Ambion) was added to the RNA prior to precipitation.

For RNA-IP of endogenous Rbms1 from HEK293T, cell lysates were pre-

cleared with Protein A/G UltraLink Resin (Thermo Pierce) for 1 hour at 4°C. 3 µg of Rbms1 antibody (ab150353, Abcam) or myc control antibody (Santa Cruz sc-789) were added for 2 hours at 4°C prior to incubation with protein A/G beads for another 2 hours. For RNA-IP of T7-tagged Roxan, 1 µg of T7 antibody (Novagen, 69522-3) was used instead. For RNA-IP of endogenous Roquin from RAW264.7 macrophages, lysates were pre-cleared with Protein A/G UltraLink Resin (Thermo Pierce) for 1 hour at 4°C. 4 µg Roquin antibodies (rabbit polyclonal, Bethyl, 514A and 515A, 2 µg each) or HA control antibody (mouse monoclonal, Covance Innovative Antibodies MMS-101P) were added for 2 hours at 4°C prior to incubation with protein A/G beads for another 2 hours. Flag-IPs were carried out using Flag antibody (M2, F3165, Sigma). For qPCR analysis following RNA-IP, a fixed volume of RNA extracted from IP and input samples was used for RT.

4.2.20 Electromobility Shift Assay (EMSA)

To express a recombinant N-terminal His-tagged fragment of Roquin (aa 2-440, Roquin-N), plasmid pETM11-Roquin-N (p2940, a kind gift of Vigo Heissmeyer, Helmholtz Center Munich, Germany) was transformed into BL21 codon+ *E. coli* cells. Cells were cultured in LB medium at 37°C to an OD₆₀₀ of 0.5, and protein expression was induced by addition of 1 mM IPTG. The culture was then incubated for additional 16 hours at 21°C before cells were lysed using a microfluidizer (Emulsiflex, Avestin). The recombinant protein was purified on Ni-Sepharose 6FastFlow beads (GE-Healthcare) under non-denaturing conditions and eluted in elution buffer (20 mM Tris-HCl (pH 8.0 at 25°C), 1 mM MgCl₂, 200 mM NaCl, 270 mM imidazole (pH 8.0 at 25°C), 0.1 % NP-40, 10 % glycerol, 1 tablet/10 ml Mini Complete Protease Inhibitors, EDTA-free (Roche)). For S1/S1m EMSAs, recombinant streptavidin protein was purchased from Life Technologies (43-4301) and reconstituted to 1 mg/ml in PBS.

The EMSA was performed according to [360] with the following modifications: RNA was prepared by 5' end-labeling 200 pmol of commercially synthesized RNA oligonucleotides (23 nt, Biomers.net, Germany; or IDT Inc) with [γ -³²P]-ATP using T4 polynucleotide kinase (NEB) as described above for in-line probing. Labelled RNA was separated from unincorporated nucleotides by column purification (QIAquick Nucleotide Removal Kit, QIAGEN) and adjusted with H₂O to 1 pmol/µl. Prior to binding reactions, a mastermix containing 500 pM labeled RNA (10 fmol per 20 µl reaction), 1x binding buffer (20 mM Tris-HCl (pH 7.5 at 25°C), 50 mM KCl, 5 mM MgCl₂, 20 µM ZnSO₄, 10% glycerol), 2 mM DTT, 0.1 mg/ml BSA, 3.75 µg/ml tRNA and 5 µg/ml heparin was heated at 55°C for 3 minutes and cooled down at room temperature for 5

4.2 Methods

minutes to promote RNA folding. In parallel, a dilution series of 10x protein stocks was prepared in 1x protein dilution buffer (1x binding buffer, 5 μ g/ml heparin, 0.2 U/ml RNasin (Promega), 1 tablet/10 ml Mini Complete Protease Inhibitors, EDTA-free (Roche)). For each binding reaction, 2 μ l of the 10x protein stock was added to 18 μ l of the mastermix at room temperature for 10 minutes. Reactions were then supplemented with 4 μ l of 6x loading buffer (30% glycerol, bromphenol blue, xylene cyanol) and placed on ice. RNP complexes were resolved by non-denaturing PAGE (6% polyacrylamide, 0.5x TBE, 20 μ M ZnSO₄, 5% glycerol) in ice-cold 0.5x TBE buffer (2 mM EDTA, 20 μ M ZnSO₄) at 200 V for 40 minutes at 4°C. Gels were dried at 80°C for 30 minutes and exposed to a phosphor imager screen. For S1/S1m EMSAs the protocol was applied as described except that ZnSO₄ was omitted in the binding buffer, the polyacrylamide gel and the TBE running buffer.

To calculate the K_d , the fraction of Roquin-N-bound RNA (specific binding, y variable) was plotted against the initial concentration of Roquin-N (x variable). Using Graphpad Prism software, a curve with the following equation was fitted to the data points: $y = y_{\max}^h \times x^h / (K_d^h + x^h)$, whereby y_{\max} is the maximum specific binding, K_d the dissociation constant, and h the Hill coefficient.

The RNAs used for EMSA were commercially synthesized and correspond to the sequences given in **Table 4.8**.

Table 4.8: RNA Oligonucleotides Used in this Study.

Name	Length	Sequence
CDE ₂₃	23 nt	5'-ACAUGUUUUCUGUGAAAACGGAG-3'
CDE ₂₃ -M23	23 nt	5'-ACAUGUUUAGUGUCUAAACGGAG-3'
TNF α -ARE	23 nt	5'-AUUUUUUUUUUUUUUUUUUUUU-3'
S1	44 nt	5'-ACCGACCAGAAUCAUGCAAGUGCGU AAGAUAGUCGCGGGCCGGG-3'
S1m	60 nt	5'-AUGCGGCCGCGCCGACCAGAAUCAUGC AAGUGCGUAAGAUAGUCGCGGGUCGG CGGCCGCAU-3'

4.2.21 Knockdown by siRNA

NIH3T3 B2A2 cells were transfected twice with siRNAs at a final concentration of 100 nM over a time period of four days using Lipofectamine RNAiMAX (Invitrogen) and OptiMEM (Gibco) according to the manufacturer's instructions. The second siRNA transfection on the third day included plasmid DNA. For rescue experiments, NIH3T3 cells were transfected with siRNAs on the first

day, plasmids were transfected using PEI on the second day, and the mRNA decay assay was performed on the third day. RAW264.7 macrophages were transfected twice on two consecutive days with siRNAs at a final concentration of 100 nM over a time period of three days using Lipofectamine LTX (Invitrogen) and OptiMEM (Gibco) according to the manufacturer's instructions. Mouse siRNAs used in this study were synthesized by Eurofins MWG Operon. They correspond to the sequences (sense strand) given in **Table 4.9**.

Table 4.9: siRNAs Used in this Study.

Name	Target	Sequence
D0 (s015)	control	5'-GCAUUCACUUGGAUAGUAAAdTdT-3'
C2 (s014)	control	5'-GCAUUCACUUGGAUAGUAAAdTdT-3'
Roquin (A) (s051)	Roquin	5'-CCUUCUAUCUGCUGAAAGAdTdT-3'
Roquin (B) (s060)	Roquin	5'-CGCACAGTTACAGAGCTCAAdTdT-3'
Roquin2 (s055)	Roquin2	5'-GGACTTGGCTCATAAATCAAdTdT-3'

4.2.22 Enzyme-linked Immunosorbent Assay (ELISA)

After knockdown of Roquin in RAW264.7 macrophages, supernatants were collected from cells exposed to LPS (100 ng/ml) for different periods of time, and the concentration of secreted TNF α was measured using the murine TNF α ELISA development kit (PeproTech, 900-K54) according to the manufacturer's instructions. TNF α concentrations were normalized to the amount of total RNA extracted from the same cells, and the resulting ratio was expressed as arbitrary units (A. U.).

4.2.23 Morpholino Delivery

For delivery of antisense morpholino oligonucleotides, RAW264.7 cells or BMDM were seeded into 12-well plates one and 10–12 days prior to transfection, respectively. Morpholinos were stored at 4°C (-20°C for long term storage) and heated at 65°C for 5 minutes before use. Morpholinos were added to the medium at a final concentration of 2 μ M in the presence of 6 μ M Endo-Porter (Gene Tools, LLC) according to the manufacturer's protocol. 24 hours later, cells were stimulated with LPS (100 ng/ml) for 6 hours. Cells were washed with PBS and either collected by trypsinization for lysis (RAW264.7) or lysed directly on the dish (BMDM) for total RNA extraction using the Genematrix universal RNA purification kit (Eurx, Roboklon). For RNA-IP, HEK293T cells were transfected with 2 μ M morpholino and plasmid

simultaneously using Lipofectamine 2000 (Life Technologies) according to the manufacturer’s protocol. The 25-mer morpholinos were obtained from Gene Tools, LLC, and are listed in **Table 4.10**.

Table 4.10: Morpholinos Used in this Study.

Name	Target / Sequence
CDE-MO-1 (m001)	left arm of the TNF α CDE 5'-GAAAACATGTCTGTCTGAAGACAGC-3'
CDE-MO-2 (m002)	right arm of the TNF α CDE 5'-GGACAGCTCAGCTCCGTTTTTCACAG-3'
UTR-MO (m003)	TNF α 3'UTR sequence downstream of the CDE 5'-AGCCTGGTCACCAAATCAGCGTTAT-3'
Ctrl-MO (m004)	standard control oligo from Gene Tools 5'-CCTCTTACCTCAGTTACAATTTATA-3'

4.2.24 Data Sources for Sequence Alignments

For sequence conservation analysis of TNF α and ICOS CDEs, GenBank mRNA 3'UTR sequences were retrieved for different species from the NCBI database: TNF α : mouse (*Mus musculus*; accession number NM_013693), human (*Homo sapiens*; NM_000594), chimpanzee (*Pan troglodytes*; XM_001152827), orangutan (*Pongo abelii*; XM_002816720), macaque (*Macaca mulatta*; NM_001047149), swine (*Sus scrofa*; NM_214022), zebu (*Bos indicus*; AF011927), cow (*Bos taurus*; NM_173966), goat (*Capra hircus*; X14828), sheep (*Ovis aries*; NM_001024860), dog (*Canis lupus familiaris*; NM_001003244), horse (*Equus caballus*; NM_001081819), giant panda (*Ailuropoda melanoleuca*; XM_002930032), rabbit (*Oryctolagus cuniculus*; NM_001082263), african elephant (*Loxodonta africana*; XM_003422213), rat (*Rattus norvegicus*; NM_012675), marmot (*Marmota monax*; AF096268), guinea pig (*Cavia porcellus*; NM_001173025), and chinese hamster (*Cricetulus griseus*; XM_003508487); ICOS: mouse (*Mus musculus*; NM_017480), human (*Homo sapiens*; NM_012092), chimpanzee (*Pan troglodytes*; XM_001173460), orangutan (*Pongo abelii*; XM_002812772), macaque (*Macaca mulatta*; XM_001104581), swine (*Sus scrofa*; NM_001044546), and cow (*Bos taurus*; NM_001034275). CDE sequence conservation analysis of Nfkbid, Nfkbiz, Ier3, Roquin, Roquin2, Bmpr1a, Pdia6, Ppp1r10 and Hmgxb3, performed by Johanna Schott, was based on sequences retrieved from the UCSC whole-genome alignment of 46 vertebrate organisms [318].

For conservation analysis of Roquin, we retrieved the following protein sequences from NCBI and aligned them by ClustalW: mouse (*Mus muscu-*

lus; NP_001020123.1), chicken (*Gallus gallus*; XP_001234605.2), African clawed frog (*Xenopus laevis*; NP_001084548.1), zebrafish (*Danio rerio*; NP_001108155.1), lancelet (*Branchiostoma floridae*; XP_002588179.1), sea squirt (*Ciona intestinalis*; XP_002125601.1), sea urchin (*Strongylocentrotus purpuratus*; XP_780349.3), red flour beetle (*Tribolium castaneum*; EFA08769.1), fruit fly (*Drosophila melanogaster*; NP_648886.1), water flea (*Daphnia pulex*; EFX88973.1), tick (*Ixodes scapularis*; XP_002414149.1), roundworm (*Ascaris suum*; ADY40466.1; *Caenorhabditis elegans*, CCD31104.1), sea anemone (*Nematostella vectensis*, XP_001626669.1), hydra (*Hydra magnipapillata*; XP_002158024.1), and sponge (*Amphimedon queenslandica*; XP_003385928.1).

4.2.25 RNA-IP, Library Preparation, Deep Sequencing and Data Analysis

Endogenous Roquin was immunoprecipitated from lysates of RAW246.7 macrophages that had been grown in two 15-cm dishes and stimulated for 2 hours with LPS (100 ng/ml). Beads alone served as control-IP. The IP was performed as described in the RNA-IP section. RNA was then extracted from both the IP and input samples using TriFast (PeqLab). Library preparation was carried out with Illumina protocols using 50–100 ng RNA making use of the service of the BioQuant Deep Sequencing Core Facility at the University of Heidelberg. Sequencing was performed at the EMBL Genomics Core Facility, Heidelberg, on an Illumina HiSeq2000 instrument, which yielded a raw read length of 58 bases (52 bases for the fragment plus 6 bases for the barcode). All sequence analysis was performed by Johanna Schott. Reads were aligned to the *Mus musculus* genome (NCBI build 37), and differential expression was tested using Bioconductor software. A detailed description and references, as well as statistical procedures, can be found in the Extended Experimental Procedures of Leppek *et al.* (2013) [246].

4.2.26 Accession Numbers

RNA sequencing data from Roquin-IP experiments were deposited in the Gene Expression Omnibus under accession number GSE44775.

Abbreviations

The following abbreviations were used in this study:

Abbreviation	Expanded form
-/-	knockout
5' TOP	5' terminal oligopyrimidine tract
4EBP	eIF4E-binding protein
α	alpha
A	adenine
aa	amino acid
Ab	antibody
actD	actinomycin D
Ago	argonaute
AMD	adenylate/uridylylate-rich element-mediated mRNA decay
ARE	adenylate/uridylylate-rich element
ARE-BP	AU-rich element binding protein
β	beta
bp	base-paired
BRF1/2	butyrate response factor 1/2
bs	binding site
BSA	bovine serum albumin
C	cytosine
°C	degree celcius
Caf1	carbon catabolite repressor protein (CCR4)-associative factor 1
Ccr4	carbon catabolite repressor protein 4
Ccr4-Not	Ccr4-Not complex
CDE	constitutive decay element
cDNA	complementary/copy DNA
CIP	calf intestinal phosphatase
Co-IP	co-immunoprecipitation
COS7	African green monkey kidney
cp	coat protein
cpm	counts per minute
Da	Dalton
Dcp	decapping protein

Abbreviation	Expanded form
DMEM	Dulbecco's modified eagle's medium
DNA	desoxyribonucleicacid
ds	double stranded
DTT	dithiothreitol
<i>E. coli</i>	<i>Escherichia coli</i>
eIF	eukaryotic translation initiation factors
Edc	enhancer of mRNA decapping
ELAV	embryonic-lethal abnormal vision
EMSA	electrophoretic mobility shift assay
FCS	fetal calf serum
FISH	fluorescence in situ hybridization
Flag	hydrophilic 8 aminoacid peptide
FMRP	fragile X mental retardation protein
FXR1	fragile X mental retardation-related protein 1
γ	gamma
G	guanine
G3BP	RasGAP-SH3-binding protein
GFP	green fluorescent protein
GM-CSF	Granulocyte macrophage colony stimulating factor
HA	hemagglutinin
hDcp1	human decapping enzyme 1
hnRNP	heterogeneous nuclear ribonucleoprotein
His	histidine
HPLC	high performance liquid chromatography
HuR	human antigen R
ICOS	inducible T cell co-stimulator
IF	immunofluorescence
IgG	Immunoglobulin G
IKK	IκB kinase
IL	interleukin
INFγ	interferon gamma
IP	immunoprecipitation
JNK	c-jun-N-terminal kinase
κ	kappa
k	kilo
K_d	dissociation constant
kDa	kilo dalton
LPS	lipopolysaccharide
Lsm	Sm-like protein
mA	milli Ampere

Abbreviations

Abbreviation	Expanded form
MAPK	mitogen-activated protein kinase
MEF	mouse embryonic fibroblast
Mg²⁺	magnesium
miRNA	microRNA
MK2	MAPK-activated protein kinase-2
mM	milli molar
Mnab	membrane-associated nucleic acid binding protein, Roquin2
MO	morpholino
mRNA	messenger ribonucleic acid
mRNP	messenger ribonucleoprotein
MS2	bacteriophage MS2
NB	Northern blot
NGD	No-go mRNA decay
NF-κB	nuclear factor kappa beta
NMD	nonsense mediated decay
NMR	nuclear magnetic resonance
Not	negative regulator of transcription
Not1	negative on TATA, Ccr4-Not complex subunit 1
NSD	nonstop mRNA decay
nt	nucleotide
PABP	poly(A) binding protein
PAGE	polyacrylamide gel electrophoresis
PAMP	pathogen-associated molecular pattern
PAN	poly(A) nuclease
PARN	poly(A)-specific ribonuclease
PARP	poly ADP-ribose polymerase
P-body	processing body
PBS	phosphate buffered saline
PCR	polymerase chain reaction
Pol	Polymerase
poly(A)	poly adenosine
PP2A	protein phosphatase 2
PP7	bacteriophage PP7
PTC	premature stop codon
puro	puromycin
qPCR	quantitative PCR
RBD	RNA-binding domain
Rbms1	RNA binding motif, single stranded interacting protein 1
Rc3h1	RING finger and CCCH-type zinc finger domain-containing protein 1, Roquin

Abbreviation	Expanded form
Rc3h2	RING finger and CCCH-type zinc finger domain-containing protein 2, Roquin2
RING	really interesting new gene, protein domain
RISC	RNA-induced silencing complex
RNA	ribonucleic acid
RNAi	RNA interference
RNase	ribonuclease
rp	ribosomal protein
rpm	revolutions per minute
RRM	RNA recognition motif
RT	reverse transcription
S7	ribosomal protein S7
san	<i>sanroque</i> allele, Roquin mutation M199R
SD	standard deviation
SDS	sodium dodecyl sulfate
SE	standard error
SG	stress granule
siRNA	small interfering RNA
ss	single stranded
T	thymine
t_{1/2}	half-life
TCA	trichloroacetic acid
Tet	tetracycline
TEV	tobacco etch virus
TF	transcription factor
TFH	follicular helper T cells
TIA-1	T cell intracellular antigen-1
TIAR	T cell intracellular antigen-1-related
TNFα	tumor necrosis factor α
TNFR	tumor necrosis factor receptor
TRAF2	TNF α receptor associated factor 2
TTP	tristetraprolin
U	uracil
UTR	untranslated region
UV	ultraviolet
V	Volt
WB	Western blot
WT	wild type
XRN1	5'-3' exoribonuclease 1
ZF	zinc finger

Publications

The following publications were based on this study

1. **Leppek K**, Schott J, Reitter S, Poetz F, Hammond MC, Stoecklin G. Roquin promotes constitutive mRNA decay via a conserved class of stem-loop recognition motifs. *Cell* **2013**; 153:869-81.
2. **Leppek K** and Stoecklin G. An optimized streptavidin-binding RNA aptamer for purification of ribonucleoprotein complexes identifies novel ARE-binding proteins. *Nucl Acids Res* **2013**; 10.1093/nar/gkt956.

Other publications

3. **Leppek K***, Schott J*, Stoecklin G. Protein synthesis and translational control: at eye level with the ribosome. *EMBO Rep* **2011**; 12:1214-16.
4. Spasic M, Friedel CC, Schott J, Kreth J, **Leppek K**, Hofmann S, Ozgur S, Stoecklin G. Genome-wide assessment of AU-rich elements by the AREScore algorithm. *PLoS Genet* **2012**; 8:e1002433.

* authors contributed equally

Acknowledgements

I would like to thank

Dr. Georg Stoecklin for having me in the lab, for always being a supportive, enthusiastic and patient supervisor, for listening to my ideas and sharing his own with me, for scientific guidance, motivation and belief in my work.

Prof. Bernd Bukau (ZMBH) and **Prof. Matthias Hentze** (EMBL) for scientific support and for critical and encouraging comments in my TAC meetings.

Prof. Irmgard Sinning and **Prof. Oliver Gruss** for their interest, time and participation in the oral examination.

all members of the Stoecklin lab (former and current) for creating a pleasant, supportive and productive atmosphere in the lab, for technical help, scientific input and discussions, and for the memorable time, the great fun and many laughs we shared in and outside the lab, and the wonderful friendships. I will miss you all.

my **CDE subgroup** of Johanna, Sonja, and Fabian for their tremendous help, support and contribution in stressful times without whom the fight would have been a much tougher one.

Prof. Ming Hammond (UC Berkeley, USA) for having me in her lab, for the scientific support and encouragement, for performing in-lines for me and for helpful advice throughout.

Dr. Thomas Ruppert of the ZMBH Mass Spectrometry Core Facility for the extensive help and support with MS analysis.

Dr. David Ibberson and **Dr. Sasithorn Chotewutmontri** of the Heidelberg University Deep Sequencing Core Facility and the Genomics Core Facility at EMBL, Heidelberg.

Alexandra Kurz (DKFZ) for help with the ELISAs.

Dr. Bernd Rattenbacher and **Prof. Christoph Moroni** (University of Basel, Switzerland) for sharing unpublished information.

Dr. Vigo Heissmeyer (Helmholtz Center Munich, Germany); **Prof. Witold Filipowicz** (Friedrich Miescher Institute for Biomedical Research, Basel, Switzerland); **Prof. Ann-Bin Shyu** (University of Texas-Houston Medical School, USA); **Dr. Takbum Ohn**, **Dr. Nancy Kedersha**, **Dr. Stephen Wax** and **Prof. Paul Anderson** (Harvard Medical School, Boston, USA); **PD Dr. Adelheid Cerwenka** (DKFZ); **Prof. Kathleen Collins** (UC Berkeley, USA), **Prof. David Peabody** (University of New Mexico School of Medicine, USA), **Prof. Jens Lykke-Andersen** (UC San Diego, USA), **Dr. Didier Poncet** (CNRS, Gif sur Yvette, France); **Prof. Ludger Hengst** (Innsbruck Medical University, Austria); **Prof. Frauke Melchior** (ZMBH, University of Heidelberg, Germany) for cell lines, plasmids, antibodies or other reagents.

Prof. Ingrid Grummt (DKFZ), **Dr. Aurelio Teleman** (DKFZ), **Prof. Matthias Mayer** and **Prof. Christine Clayton** (both ZMBH) for critical reading and comments on the manuscripts.

Helmholtz International Graduate School for Cancer Research (DKFZ) for supporting me with a PhD stipend.

Nadine Hertrich for encouragement and motivation when needed, for listening and for the happy times we shared, but above all for being a loyal and wonderful friend from the beginning.

Sarah Hofmann for the tennis and squash sessions, the trips, shared laughs and for being more than a labmate but a great friend through it all.

Yaki and **Vanesa Lafarga** for the weekly walks in the forest, welcomed dog-sitting weekends getting me out of the lab and for being a great friend.

Friends, collaborators and colleagues on and off the Heidelberg Campus.

the **DKFZ tennis girls** for many shared hours on the court.

above all **my family** for their unconditional love and endless support, for their encouragement, motivation, patience and interest, and for listening and always being there for me.

Bibliography

- [1] **Sharova, L. V., Sharov, A. A., Nedorezov, T., Piao, Y., Shaik, N. and Ko, M. S. H.**, *Database for mRNA half-life of 19 977 genes obtained by DNA microarray analysis of pluripotent and differentiating mouse embryonic stem cells.*, DNA Res, Vol. 16, No. 1, pp. 45–58, Feb 2009.
- [2] **Hao, S. and Baltimore, D.**, *The stability of mRNA influences the temporal order of the induction of genes encoding inflammatory molecules.*, Nat Immunol, Vol. 10, No. 3, pp. 281–288, Mar 2009.
- [3] **Rabani, M., Levin, J. Z., Fan, L., Adiconis, X., Raychowdhury, R., Garber, M., Gnirke, A., Nusbaum, C., Hacohen, N., Friedman, N., Amit, I. and Regev, A.**, *Metabolic labeling of RNA uncovers principles of RNA production and degradation dynamics in mammalian cells.*, Nat Biotechnol, Vol. 29, No. 5, pp. 436–442, May 2011.
- [4] **Schwanhäusser, B., Busse, D., Li, N., Dittmar, G., Schuchhardt, J., Wolf, J., Chen, W. and Selbach, M.**, *Global quantification of mammalian gene expression control.*, Nature, Vol. 473, No. 7347, pp. 337–342, May 2011.
- [5] **Stoecklin, G. and Anderson, P.**, *Posttranscriptional mechanisms regulating the inflammatory response.*, Adv Immunol, Vol. 89, pp. 1–37, 2006.
- [6] **Beutler, B. and Cerami, A.**, *Cachectin and tumour necrosis factor as two sides of the same biological coin.*, Nature, Vol. 320, No. 6063, pp. 584–588, 1986.
- [7] **Tracey, K. J. and Cerami, A.**, *Tumor necrosis factor: a pleiotropic cytokine and therapeutic target.*, Annu Rev Med, Vol. 45, pp. 491–503, 1994.
- [8] **Bradley, J. R.**, *TNF-mediated inflammatory disease.*, J Pathol, Vol. 214, No. 2, pp. 149–160, Jan 2008.
- [9] **Apostolaki, M., Armaka, M., Victoratos, P. and Kollias, G.**, *Cellular mechanisms of TNF function in models of inflammation and autoimmunity.*, Curr Dir Autoimmun, Vol. 11, pp. 1–26, 2010.

-
- [10] **Feldmann, M.**, *Development of anti-TNF therapy for rheumatoid arthritis.*, Nat Rev Immunol, Vol. 2, No. 5, pp. 364–371, May 2002.
- [11] **Tracey, D., Klareskog, L., Sasso, E. H., Salfeld, J. G. and Tak, P. P.**, *Tumor necrosis factor antagonist mechanisms of action: a comprehensive review.*, Pharmacol Ther, Vol. 117, No. 2, pp. 244–279, Feb 2008.
- [12] **Keffer, J., Probert, L., Cazlaris, H., Georgopoulos, S., Kaslaris, E., Kioussis, D. and Kollias, G.**, *Transgenic mice expressing human tumour necrosis factor: a predictive genetic model of arthritis.*, EMBO J, Vol. 10, No. 13, pp. 4025–4031, Dec 1991.
- [13] **Kontoyiannis, D., Pasparakis, M., Pizarro, T. T., Cominelli, F. and Kollias, G.**, *Impaired on/off regulation of TNF biosynthesis in mice lacking TNF AU-rich elements: implications for joint and gut-associated immunopathologies.*, Immunity, Vol. 10, No. 3, pp. 387–398, Mar 1999.
- [14] **Aggarwal, B. B., Shishodia, S., Takada, Y., Jackson-Bernitsas, D., Ahn, K. S., Sethi, G. and Ichikawa, H.**, *TNF blockade: an inflammatory issue.*, Ernst Schering Res Found Workshop, , No. 56, pp. 161–186, 2006.
- [15] **Lou, J., Lucas, R. and Grau, G. E.**, *Pathogenesis of cerebral malaria: recent experimental data and possible applications for humans.*, Clin Microbiol Rev, Vol. 14, No. 4, pp. 810–20, table of contents, Oct 2001.
- [16] **Jacobs, M., Samarina, A., Grivennikov, S., Botha, T., Allie, N., Fremond, C., Togbe, D., Vasseur, V., Rose, S., Erard, F., Monteiro, A., Quesniaux, V. and Ryffel, B.**, *Reactivation of tuberculosis by tumor necrosis factor neutralization.*, Eur Cytokine Netw, Vol. 18, No. 1, pp. 5–13, Mar 2007.
- [17] **Kontoyiannis, D., Boulougouris, G., Manoloukos, M., Armaka, M., Apostolaki, M., Pizarro, T., Kotlyarov, A., Forster, I., Flavell, R., Gaestel, M., Tschlis, P., Cominelli, F. and Kollias, G.**, *Genetic dissection of the cellular pathways and signaling mechanisms in modeled tumor necrosis factor-induced Crohn’s-like inflammatory bowel disease.*, J Exp Med, Vol. 196, No. 12, pp. 1563–1574, Dec 2002.
- [18] **Balkwill, F.**, *Tumour necrosis factor and cancer.*, Nat Rev Cancer, Vol. 9, No. 5, pp. 361–371, May 2009.
- [19] **Cawthorn, W. P. and Sethi, J. K.**, *TNF-alpha and adipocyte biology.*, FEBS Lett, Vol. 582, No. 1, pp. 117–131, Jan 2008.
- [20] **Vassalli, P.**, *The pathophysiology of tumor necrosis factors.*, Annu Rev Immunol, Vol. 10, pp. 411–452, 1992.

- [21] **Mosser, D. M. and Edwards, J. P.**, *Exploring the full spectrum of macrophage activation.*, Nat Rev Immunol, Vol. 8, No. 12, pp. 958–969, Dec 2008.
- [22] **Akira, S. and Takeda, K.**, *Toll-like receptor signalling.*, Nat Rev Immunol, Vol. 4, No. 7, pp. 499–511, Jul 2004.
- [23] **Bode, J. G., Ehling, C. and Häussinger, D.**, *The macrophage response towards LPS and its control through the p38(MAPK)-STAT3 axis.*, Cell Signal, Vol. 24, No. 6, pp. 1185–1194, Jun 2012.
- [24] **Kawai, T. and Akira, S.**, *The roles of TLRs, RLRs and NLRs in pathogen recognition.*, Int Immunol, Vol. 21, No. 4, pp. 317–337, Apr 2009.
- [25] **O’Neill, L. A. J.**, *The interleukin-1 receptor/Toll-like receptor superfamily: 10 years of progress.*, Immunol Rev, Vol. 226, pp. 10–18, Dec 2008.
- [26] **Kawai, T. and Akira, S.**, *Toll-like receptors and their crosstalk with other innate receptors in infection and immunity.*, Immunity, Vol. 34, No. 5, pp. 637–650, May 2011.
- [27] **Müller, C. W.**, *DNA recognition by NF kappa B and STAT transcription factors.*, Ernst Schering Res Found Workshop, , No. 34, pp. 143–166, 2001.
- [28] **Murray, R. Z., Kay, J. G., Sangermani, D. G. and Stow, J. L.**, *A role for the phagosome in cytokine secretion.*, Science, Vol. 310, No. 5753, pp. 1492–1495, Dec 2005.
- [29] **Shurety, W., Merino-Trigo, A., Brown, D., Hume, D. A. and Stow, J. L.**, *Localization and post-Golgi trafficking of tumor necrosis factor-alpha in macrophages.*, J Interferon Cytokine Res, Vol. 20, No. 4, pp. 427–438, Apr 2000.
- [30] **Pagan, J. K., Wylie, F. G., Joseph, S., Widberg, C., Bryant, N. J., James, D. E. and Stow, J. L.**, *The t-SNARE syntaxin 4 is regulated during macrophage activation to function in membrane traffic and cytokine secretion.*, Curr Biol, Vol. 13, No. 2, pp. 156–160, Jan 2003.
- [31] **Moore, K. W., de Waal Malefyt, R., Coffman, R. L. and O’Garra, A.**, *Interleukin-10 and the interleukin-10 receptor.*, Annu Rev Immunol, Vol. 19, pp. 683–765, 2001.
- [32] **Denys, A., Udalova, I. A., Smith, C., Williams, L. M., Ciesielski, C. J., Campbell, J., Andrews, C., Kwaitkowski, D. and Foxwell, B. M. J.**, *Evidence for a dual mechanism for IL-10 suppression of TNF-alpha production that does not involve inhibition of*

- p38 mitogen-activated protein kinase or NF-kappa B in primary human macrophages.*, J Immunol, Vol. 168, No. 10, pp. 4837–4845, May 2002.
- [33] **Kontoyiannis, D., Kotlyarov, A., Carballo, E., Alexopoulou, L., Blackshear, P. J., Gaestel, M., Davis, R., Flavell, R. and Kollias, G.**, *Interleukin-10 targets p38 MAPK to modulate ARE-dependent TNF mRNA translation and limit intestinal pathology.*, EMBO J, Vol. 20, No. 14, pp. 3760–3770, Jul 2001.
- [34] **Black, R. A., Rauch, C. T., Kozlosky, C. J., Peschon, J. J., Slack, J. L., Wolfson, M. F., Castner, B. J., Stocking, K. L., Reddy, P., Srinivasan, S., Nelson, N., Boiani, N., Schooley, K. A., Gerhart, M., Davis, R., Fitzner, J. N., Johnson, R. S., Paxton, R. J., March, C. J. and Cerretti, D. P.**, *A metalloproteinase disintegrin that releases tumour-necrosis factor-alpha from cells.*, Nature, Vol. 385, No. 6618, pp. 729–733, Feb 1997.
- [35] **Locksley, R. M., Killeen, N. and Lenardo, M. J.**, *The TNF and TNF receptor superfamilies: integrating mammalian biology.*, Cell, Vol. 104, No. 4, pp. 487–501, Feb 2001.
- [36] **Wajant, H., Pfizenmaier, K. and Scheurich, P.**, *Tumor necrosis factor signaling.*, Cell Death Differ, Vol. 10, No. 1, pp. 45–65, Jan 2003.
- [37] **Grell, M., Becke, F. M., Wajant, H., Männel, D. N. and Scheurich, P.**, *TNF receptor type 2 mediates thymocyte proliferation independently of TNF receptor type 1.*, Eur J Immunol, Vol. 28, No. 1, pp. 257–263, Jan 1998.
- [38] **Falvo, J. V., Tsytsykova, A. V. and Goldfeld, A. E.**, *Transcriptional control of the TNF gene.*, Curr Dir Autoimmun, Vol. 11, pp. 27–60, 2010.
- [39] **Goldfeld, A. E., Flemington, E. K., Boussiotis, V. A., Theodos, C. M., Titus, R. G., Strominger, J. L. and Speck, S. H.**, *Transcription of the tumor necrosis factor alpha gene is rapidly induced by anti-immunoglobulin and blocked by cyclosporin A and FK506 in human B cells.*, Proc Natl Acad Sci U S A, Vol. 89, No. 24, pp. 12198–12201, Dec 1992.
- [40] **Carey, M.**, *The enhanceosome and transcriptional synergy.*, Cell, Vol. 92, No. 1, pp. 5–8, Jan 1998.
- [41] **Goldfeld, A. E., Doyle, C. and Maniatis, T.**, *Human tumor necrosis factor alpha gene regulation by virus and lipopolysaccharide.*, Proc Natl Acad Sci U S A, Vol. 87, No. 24, pp. 9769–9773, Dec 1990.
- [42] **Trede, N. S., Tsytsykova, A. V., Chatila, T., Goldfeld, A. E. and Geha, R. S.**, *Transcriptional activation of the human TNF-alpha*

- promoter by superantigen in human monocytic cells: role of NF-kappa B.*, J Immunol, Vol. 155, No. 2, pp. 902–908, Jul 1995.
- [43] **Yao, J., Mackman, N., Edgington, T. S. and Fan, S. T.**, *Lipopolysaccharide induction of the tumor necrosis factor-alpha promoter in human monocytic cells. Regulation by Egr-1, c-Jun, and NF-kappaB transcription factors.*, J Biol Chem, Vol. 272, No. 28, pp. 17795–17801, Jul 1997.
- [44] **Tsai, E. Y., Falvo, J. V., Tsytsykova, A. V., Barczak, A. K., Reimold, A. M., Glimcher, L. H., Fenton, M. J., Gordon, D. C., Dunn, I. F. and Goldfeld, A. E.**, *A lipopolysaccharide-specific enhancer complex involving Ets, Elk-1, Sp1, and CREB binding protein and p300 is recruited to the tumor necrosis factor alpha promoter in vivo.*, Mol Cell Biol, Vol. 20, No. 16, pp. 6084–6094, Aug 2000.
- [45] **Tang, X., Metzger, D., Leeman, S. and Amar, S.**, *LPS-induced TNF-alpha factor (LITAF)-deficient mice express reduced LPS-induced cytokine: Evidence for LITAF-dependent LPS signaling pathways.*, Proc Natl Acad Sci U S A, Vol. 103, No. 37, pp. 13777–13782, Sep 2006.
- [46] **Osman, F., Jarrous, N., Ben-Asouli, Y. and Kaempfer, R.**, *A cis-acting element in the 3'-untranslated region of human TNF-alpha mRNA renders splicing dependent on the activation of protein kinase PKR.*, Genes Dev, Vol. 13, No. 24, pp. 3280–3293, Dec 1999.
- [47] **Dumitru, C. D., Ceci, J. D., Tsatsanis, C., Kontoyiannis, D., Stamatakis, K., Lin, J. H., Patriotis, C., Jenkins, N. A., Copeland, N. G., Kollias, G. and Tschlis, P. N.**, *TNF-alpha induction by LPS is regulated posttranscriptionally via a Tpl2/ERK-dependent pathway.*, Cell, Vol. 103, No. 7, pp. 1071–1083, Dec 2000.
- [48] **Rousseau, S., Papoutsopoulou, M., Symons, A., Cook, D., Lucocq, J. M., Prescott, A. R., O'Garra, A., Ley, S. C. and Cohen, P.**, *TPL2-mediated activation of ERK1 and ERK2 regulates the processing of pre-TNF alpha in LPS-stimulated macrophages.*, J Cell Sci, Vol. 121, No. Pt 2, pp. 149–154, Jan 2008.
- [49] **Han, J., Brown, T. and Beutler, B.**, *Endotoxin-responsive sequences control cachectin/tumor necrosis factor biosynthesis at the translational level.*, J Exp Med, Vol. 171, No. 2, pp. 465–475, Feb 1990.
- [50] **Lindstein, T., June, C. H., Ledbetter, J. A., Stella, G. and Thompson, C. B.**, *Regulation of lymphokine messenger RNA stability by a surface-mediated T cell activation pathway.*, Science, Vol. 244, No. 4902, pp. 339–343, Apr 1989.
- [51] **Wang, E., Ma, W. J., Aghajanian, C. and Spriggs, D. R.**, *Post-transcriptional regulation of protein expression in human epithelial carci-*

- noma cells by adenine-uridine-rich elements in the 3'-untranslated region of tumor necrosis factor-alpha messenger RNA.*, Cancer Res, Vol. 57, No. 23, pp. 5426–5433, Dec 1997.
- [52] **Kotlyarov, A., Neininger, A., Schubert, C., Eckert, R., Birchmeier, C., Volk, H. D. and Gaestel, M.**, *MAPKAP kinase 2 is essential for LPS-induced TNF-alpha biosynthesis.*, Nat Cell Biol, Vol. 1, No. 2, pp. 94–97, Jun 1999.
- [53] **Cao, H., Deterding, L. J. and Blackshear, P. J.**, *Phosphorylation site analysis of the anti-inflammatory and mRNA-destabilizing protein tristetraprolin.*, Expert Rev Proteomics, Vol. 4, No. 6, pp. 711–726, Dec 2007.
- [54] **Sandler, H. and Stoecklin, G.**, *Control of mRNA decay by phosphorylation of tristetraprolin.*, Biochem Soc Trans, Vol. 36, No. Pt 3, pp. 491–496, Jun 2008.
- [55] **Swantek, J. L., Cobb, M. H. and Geppert, T. D.**, *Jun N-terminal kinase/stress-activated protein kinase (JNK/SAPK) is required for lipopolysaccharide stimulation of tumor necrosis factor alpha (TNF-alpha) translation: glucocorticoids inhibit TNF-alpha translation by blocking JNK/SAPK.*, Mol Cell Biol, Vol. 17, No. 11, pp. 6274–6282, Nov 1997.
- [56] **Kim, J.-K., Lee, S.-M., Suk, K. and Lee, W.-H.**, *A novel pathway responsible for lipopolysaccharide-induced translational regulation of TNF- α and IL-6 expression involves protein kinase C and fascin.*, J Immunol, Vol. 187, No. 12, pp. 6327–6334, Dec 2011.
- [57] **Schott, J. and Stoecklin, G.**, *Networks controlling mRNA decay in the immune system.*, Wiley Interdiscip Rev RNA, Vol. 1, No. 3, pp. 432–456, 2010.
- [58] **Stamou, P. and Kontoyiannis, D. L.**, *Posttranscriptional regulation of TNF mRNA: a paradigm of signal-dependent mRNA utilization and its relevance to pathology.*, Curr Dir Autoimmun, Vol. 11, pp. 61–79, 2010.
- [59] **Ronkina, N., Menon, M. B., Schwermann, J., Tiedje, C., Hitti, E., Kotlyarov, A. and Gaestel, M.**, *MAPKAP kinases MK2 and MK3 in inflammation: complex regulation of TNF biosynthesis via expression and phosphorylation of tristetraprolin.*, Biochem Pharmacol, Vol. 80, No. 12, pp. 1915–1920, Dec 2010.
- [60] **Garneau, N. L., Wilusz, J. and Wilusz, C. J.**, *The highways and byways of mRNA decay.*, Nat Rev Mol Cell Biol, Vol. 8, No. 2, pp. 113–126, Feb 2007.

- [61] **Huntzinger, E.** and **Izaurralde, E.**, *Gene silencing by microRNAs: contributions of translational repression and mRNA decay.*, Nat Rev Genet, Vol. 12, No. 2, pp. 99–110, Feb 2011.
- [62] **Stoecklin, G.**, **Lu, M.**, **Rattenbacher, B.** and **Moroni, C.**, *A constitutive decay element promotes tumor necrosis factor alpha mRNA degradation via an AU-rich element-independent pathway.*, Mol Cell Biol, Vol. 23, No. 10, pp. 3506–3515, May 2003.
- [63] **Eulalio, A.**, **Huntzinger, E.**, **Nishihara, T.**, **Rehwinkel, J.**, **Fauser, M.** and **Izaurralde, E.**, *Deadenylation is a widespread effect of miRNA regulation.*, RNA, Vol. 15, No. 1, pp. 21–32, Jan 2009.
- [64] **Filipowicz, W.**, **Bhattacharyya, S. N.** and **Sonenberg, N.**, *Mechanisms of post-transcriptional regulation by microRNAs: are the answers in sight?*, Nat Rev Genet, Vol. 9, No. 2, pp. 102–114, Feb 2008.
- [65] **Diederichs, S.** and **Haber, D. A.**, *Dual role for argonautes in microRNA processing and posttranscriptional regulation of microRNA expression.*, Cell, Vol. 131, No. 6, pp. 1097–1108, Dec 2007.
- [66] **Grimson, A.**, **Farh, K. K.-H.**, **Johnston, W. K.**, **Garrett-Engle, P.**, **Lim, L. P.** and **Bartel, D. P.**, *MicroRNA targeting specificity in mammals: determinants beyond seed pairing.*, Mol Cell, Vol. 27, No. 1, pp. 91–105, Jul 2007.
- [67] **Bartel, D. P.**, *MicroRNAs: target recognition and regulatory functions.*, Cell, Vol. 136, No. 2, pp. 215–233, Jan 2009.
- [68] **Doench, J. G.** and **Sharp, P. A.**, *Specificity of microRNA target selection in translational repression.*, Genes Dev, Vol. 18, No. 5, pp. 504–511, Mar 2004.
- [69] **Bazzini, A. A.**, **Lee, M. T.** and **Giraldez, A. J.**, *Ribosome profiling shows that miR-430 reduces translation before causing mRNA decay in zebrafish.*, Science, Vol. 336, No. 6078, pp. 233–237, Apr 2012.
- [70] **Djuranovic, S.**, **Nahvi, A.** and **Green, R.**, *miRNA-mediated gene silencing by translational repression followed by mRNA deadenylation and decay.*, Science, Vol. 336, No. 6078, pp. 237–240, Apr 2012.
- [71] **Braun, J. E.**, **Huntzinger, E.**, **Fauser, M.** and **Izaurralde, E.**, *GW182 proteins directly recruit cytoplasmic deadenylase complexes to miRNA targets.*, Mol Cell, Vol. 44, No. 1, pp. 120–133, Oct 2011.
- [72] **Braun, J. E.**, **Huntzinger, E.** and **Izaurralde, E.**, *The role of GW182 proteins in miRNA-mediated gene silencing.*, Adv Exp Med Biol, Vol. 768, pp. 147–163, 2013.

- [73] Zekri, L., Kuzuo?lu-Öztürk, D. and Izaurralde, E., *GW182 proteins cause PABP dissociation from silenced miRNA targets in the absence of deadenylation.*, EMBO J, Vol. 32, No. 7, pp. 1052–1065, Apr 2013.
- [74] Liu, J., Valencia-Sanchez, M. A., Hannon, G. J. and Parker, R., *MicroRNA-dependent localization of targeted mRNAs to mammalian P-bodies.*, Nat Cell Biol, Vol. 7, No. 7, pp. 719–723, Jul 2005.
- [75] Androulidaki, A., Iliopoulos, D., Arranz, A., Doxaki, C., Schworer, S., Zacharioudaki, V., Margioris, A. N., Tsihchlis, P. N. and Tsatsanis, C., *The kinase Akt1 controls macrophage response to lipopolysaccharide by regulating microRNAs.*, Immunity, Vol. 31, No. 2, pp. 220–231, Aug 2009.
- [76] Tili, E., Michaille, J.-J., Cimino, A., Costinean, S., Dumitru, C. D., Adair, B., Fabbri, M., Alder, H., Liu, C. G., Calin, G. A. and Croce, C. M., *Modulation of miR-155 and miR-125b levels following lipopolysaccharide/TNF-alpha stimulation and their possible roles in regulating the response to endotoxin shock.*, J Immunol, Vol. 179, No. 8, pp. 5082–5089, Oct 2007.
- [77] Ruggiero, T., Trabucchi, M., De Santa, F., Zupo, S., Harfe, B. D., McManus, M. T., Rosenfeld, M. G., Briata, P. and Gherzi, R., *LPS induces KH-type splicing regulatory protein-dependent processing of microRNA-155 precursors in macrophages.*, FASEB J, Vol. 23, No. 9, pp. 2898–2908, Sep 2009.
- [78] Vasudevan, S., Tong, Y. and Steitz, J. A., *Switching from repression to activation: microRNAs can up-regulate translation.*, Science, Vol. 318, No. 5858, pp. 1931–1934, Dec 2007.
- [79] Caput, D., Beutler, B., Hartog, K., Thayer, R., Brown-Shimer, S. and Cerami, A., *Identification of a common nucleotide sequence in the 3'-untranslated region of mRNA molecules specifying inflammatory mediators.*, Proc Natl Acad Sci U S A, Vol. 83, No. 6, pp. 1670–1674, Mar 1986.
- [80] Shaw, G. and Kamen, R., *A conserved AU sequence from the 3' untranslated region of GM-CSF mRNA mediates selective mRNA degradation.*, Cell, Vol. 46, No. 5, pp. 659–667, Aug 1986.
- [81] Khabar, K. S. A., *The AU-rich transcriptome: more than interferons and cytokines, and its role in disease.*, J Interferon Cytokine Res, Vol. 25, No. 1, pp. 1–10, Jan 2005.
- [82] Khabar, K. S. A., *Rapid transit in the immune cells: the role of mRNA turnover regulation.*, J Leukoc Biol, Vol. 81, No. 6, pp. 1335–1344, Jun 2007.

- [83] **Hamilton, T. A., Novotny, M., Datta, S., Mandal, P., Hartuppee, J., Tebo, J. and Li, X.**, *Chemokine and chemoattractant receptor expression: post-transcriptional regulation.*, J Leukoc Biol, Vol. 82, No. 2, pp. 213–219, Aug 2007.
- [84] **Anderson, P.**, *Post-transcriptional control of cytokine production.*, Nat Immunol, Vol. 9, No. 4, pp. 353–359, Apr 2008.
- [85] **Chen, C. Y. and Shyu, A. B.**, *AU-rich elements: characterization and importance in mRNA degradation.*, Trends Biochem Sci, Vol. 20, No. 11, pp. 465–470, Nov 1995.
- [86] **Wilson, G. M. and Brewer, G.**, *The search for trans-acting factors controlling messenger RNA decay.*, Prog Nucleic Acid Res Mol Biol, Vol. 62, pp. 257–291, 1999.
- [87] **Barreau, C., Paillard, L. and Osborne, H. B.**, *AU-rich elements and associated factors: are there unifying principles?*, Nucleic Acids Res, Vol. 33, No. 22, pp. 7138–7150, 2005.
- [88] **Crawford, E. K., Ensor, J. E., Kalvakolanu, I. and Hasday, J. D.**, *The role of 3' poly(A) tail metabolism in tumor necrosis factor-alpha regulation.*, J Biol Chem, Vol. 272, No. 34, pp. 21120–21127, Aug 1997.
- [89] **Espel, E., Garcia-Sanz, J. A., Aubert, V., Menoud, V., Sperisen, P., Fernández, N. and Spertini, F.**, *Transcriptional and translational control of TNF-alpha gene expression in human monocytes by major histocompatibility complex class II ligands.*, Eur J Immunol, Vol. 26, No. 10, pp. 2417–2424, Oct 1996.
- [90] **Herschman, H. R.**, *Primary response genes induced by growth factors and tumor promoters.*, Annu Rev Biochem, Vol. 60, pp. 281–319, 1991.
- [91] **Schiavi, S. C., Belasco, J. G. and Greenberg, M. E.**, *Regulation of proto-oncogene mRNA stability.*, Biochim Biophys Acta, Vol. 1114, No. 2-3, pp. 95–106, Dec 1992.
- [92] **Audic, Y. and Hartley, R. S.**, *Post-transcriptional regulation in cancer.*, Biol Cell, Vol. 96, No. 7, pp. 479–498, Sep 2004.
- [93] **Conne, B., Stutz, A. and Vassalli, J. D.**, *The 3' untranslated region of messenger RNA: A molecular 'hotspot' for pathology?*, Nat Med, Vol. 6, No. 6, pp. 637–641, Jun 2000.
- [94] **Raghavan, A., Ogilvie, R. L., Reilly, C., Abelson, M. L., Raghavan, S., Vasdewani, J., Krathwohl, M. and Bohjanen, P. R.**, *Genome-wide analysis of mRNA decay in resting and activated primary human T lymphocytes.*, Nucleic Acids Res, Vol. 30, No. 24, pp. 5529–5538, Dec 2002.

- [95] **Lagnado, C. A., Brown, C. Y. and Goodall, G. J.**, *AUUUA is not sufficient to promote poly(A) shortening and degradation of an mRNA: the functional sequence within AU-rich elements may be UUAU-UUA(U/A)(U/A).*, Mol Cell Biol, Vol. 14, No. 12, pp. 7984–7995, Dec 1994.
- [96] **Zheng, D., Ezzeddine, N., Chen, C.-Y. A., Zhu, W., He, X. and Shyu, A.-B.**, *Deadenylation is prerequisite for P-body formation and mRNA decay in mammalian cells.*, J Cell Biol, Vol. 182, No. 1, pp. 89–101, Jul 2008.
- [97] **Lai, W. S., Carrick, D. M. and Blackshear, P. J.**, *Influence of nonameric AU-rich tristetraprolin-binding sites on mRNA deadenylation and turnover.*, J Biol Chem, Vol. 280, No. 40, pp. 34365–34377, Oct 2005.
- [98] **Spasic, M., Friedel, C. C., Schott, J., Kreth, J., Leppek, K., Hofmann, S., Ozgur, S. and Stoecklin, G.**, *Genome-wide assessment of AU-rich elements by the AREScore algorithm.*, PLoS Genet, Vol. 8, No. 1, pp. e1002433, Jan 2012.
- [99] **Bakheet, T., Frevel, M., Williams, B. R., Greer, W. and Khabar, K. S.**, *ARED: human AU-rich element-containing mRNA database reveals an unexpectedly diverse functional repertoire of encoded proteins.*, Nucleic Acids Res, Vol. 29, No. 1, pp. 246–254, Jan 2001.
- [100] **Bakheet, T., Williams, B. R. G. and Khabar, K. S. A.**, *ARED 3.0: the large and diverse AU-rich transcriptome.*, Nucleic Acids Res, Vol. 34, No. Database issue, pp. D111–D114, Jan 2006.
- [101] **Halees, A. S., El-Badrawi, R. and Khabar, K. S. A.**, *ARED Organism: expansion of ARED reveals AU-rich element cluster variations between human and mouse.*, Nucleic Acids Res, Vol. 36, No. Database issue, pp. D137–D140, Jan 2008.
- [102] **Anderson, P. and Kedersha, N.**, *RNA granules.*, J Cell Biol, Vol. 172, No. 6, pp. 803–808, Mar 2006.
- [103] **Puig, S., Askeland, E. and Thiele, D. J.**, *Coordinated remodeling of cellular metabolism during iron deficiency through targeted mRNA degradation.*, Cell, Vol. 120, No. 1, pp. 99–110, Jan 2005.
- [104] **Pieczyk, M., Wax, S., Beck, A. R., Kedersha, N., Gupta, M., Maritim, B., Chen, S., Gueydan, C., Kruys, V., Streuli, M. and Anderson, P.**, *TIA-1 is a translational silencer that selectively regulates the expression of TNF-alpha.*, EMBO J, Vol. 19, No. 15, pp. 4154–4163, Aug 2000.
- [105] **Garnon, J., Lachance, C., Di Marco, S., Hel, Z., Marion, D., Ruiz, M. C., Newkirk, M. M., Khandjian, E. W. and Radzioch,**

- D., *Fragile X-related protein FXR1P regulates proinflammatory cytokine tumor necrosis factor expression at the post-transcriptional level.*, J Biol Chem, Vol. 280, No. 7, pp. 5750–5763, Feb 2005.
- [106] **Mukhopadhyay, D., Houchen, C. W., Kennedy, S., Dieckgraefe, B. K. and Anant, S.**, *Coupled mRNA stabilization and translational silencing of cyclooxygenase-2 by a novel RNA binding protein, CUGBP2.*, Mol Cell, Vol. 11, No. 1, pp. 113–126, Jan 2003.
- [107] **Carballo, E., Lai, W. S. and Blackshear, P. J.**, *Feedback inhibition of macrophage tumor necrosis factor- α production by tristetraprolin.*, Science, Vol. 281, No. 5379, pp. 1001–1005, Aug 1998.
- [108] **Stoecklin, G., Colombi, M., Raineri, I., Leuenberger, S., Mallaun, M., Schmidlin, M., Gross, B., Lu, M., Kitamura, T. and Moroni, C.**, *Functional cloning of BRF1, a regulator of ARE-dependent mRNA turnover.*, EMBO J, Vol. 21, No. 17, pp. 4709–4718, Sep 2002.
- [109] **Gherzi, R., Lee, K.-Y., Briata, P., Wegmüller, D., Moroni, C., Karin, M. and Chen, C.-Y.**, *A KH domain RNA binding protein, KSRP, promotes ARE-directed mRNA turnover by recruiting the degradation machinery.*, Mol Cell, Vol. 14, No. 5, pp. 571–583, Jun 2004.
- [110] **Chou, C.-F., Mulky, A., Maitra, S., Lin, W.-J., Gherzi, R., Kappes, J. and Chen, C.-Y.**, *Tethering KSRP, a decay-promoting AU-rich element-binding protein, to mRNAs elicits mRNA decay.*, Mol Cell Biol, Vol. 26, No. 10, pp. 3695–3706, May 2006.
- [111] **Laroia, G., Cuesta, R., Brewer, G. and Schneider, R. J.**, *Control of mRNA decay by heat shock-ubiquitin-proteasome pathway.*, Science, Vol. 284, No. 5413, pp. 499–502, Apr 1999.
- [112] **Lu, J.-Y., Bergman, N., Sadri, N. and Schneider, R. J.**, *Assembly of AUF1 with eIF4G-poly(A) binding protein complex suggests a translation function in AU-rich mRNA decay.*, RNA, Vol. 12, No. 5, pp. 883–893, May 2006.
- [113] **Lu, J.-Y., Sadri, N. and Schneider, R. J.**, *Endotoxic shock in AUF1 knockout mice mediated by failure to degrade proinflammatory cytokine mRNAs.*, Genes Dev, Vol. 20, No. 22, pp. 3174–3184, Nov 2006.
- [114] **Sarkar, B., Xi, Q., He, C. and Schneider, R. J.**, *Selective degradation of AU-rich mRNAs promoted by the p37 AUF1 protein isoform.*, Mol Cell Biol, Vol. 23, No. 18, pp. 6685–6693, Sep 2003.
- [115] **Fan, X. C. and Steitz, J. A.**, *Overexpression of HuR, a nuclear-cytoplasmic shuttling protein, increases the in vivo stability of ARE-containing mRNAs.*, EMBO J, Vol. 17, No. 12, pp. 3448–3460, Jun 1998.

- [116] Peng, S. S., Chen, C. Y., Xu, N. and Shyu, A. B., *RNA stabilization by the AU-rich element binding protein, HuR, an ELAV protein.*, EMBO J, Vol. 17, No. 12, pp. 3461–3470, Jun 1998.
- [117] Galbán, S., Kuwano, Y., Pullmann, Jr, R., Martindale, J. L., Kim, H. H., Lal, A., Abdelmohsen, K., Yang, X., Dang, Y., Liu, J. O., Lewis, S. M., Holcik, M. and Gorospe, M., *RNA-binding proteins HuR and PTB promote the translation of hypoxia-inducible factor 1alpha.*, Mol Cell Biol, Vol. 28, No. 1, pp. 93–107, Jan 2008.
- [118] Katsanou, V., Papadaki, O., Milatos, S., Blackshear, P. J., Anderson, P., Kollias, G. and Kontoyiannis, D. L., *HuR as a negative posttranscriptional modulator in inflammation.*, Mol Cell, Vol. 19, No. 6, pp. 777–789, Sep 2005.
- [119] Jacob, C. O. and Tashman, N. B., *Disruption in the AU motif of the mouse TNF-alpha 3' UTR correlates with reduced TNF production by macrophages in vitro.*, Nucleic Acids Res, Vol. 21, No. 11, pp. 2761–2766, Jun 1993.
- [120] Chen, C. Y., Gherzi, R., Ong, S. E., Chan, E. L., Raijmakers, R., Pruijn, G. J., Stoecklin, G., Moroni, C., Mann, M. and Karin, M., *AU binding proteins recruit the exosome to degrade ARE-containing mRNAs.*, Cell, Vol. 107, No. 4, pp. 451–464, Nov 2001.
- [121] Gueydan, C., Droogmans, L., Chalon, P., Huez, G., Caput, D. and Kruys, V., *Identification of TIAR as a protein binding to the translational regulatory AU-rich element of tumor necrosis factor alpha mRNA.*, J Biol Chem, Vol. 274, No. 4, pp. 2322–2326, Jan 1999.
- [122] Anderson, P. and Kedersha, N., *Visibly stressed: the role of eIF2, TIA-1, and stress granules in protein translation.*, Cell Stress Chaperones, Vol. 7, No. 2, pp. 213–221, Apr 2002.
- [123] Kedersha, N. and Anderson, P., *Stress granules: sites of mRNA triage that regulate mRNA stability and translatability.*, Biochem Soc Trans, Vol. 30, No. Pt 6, pp. 963–969, Nov 2002.
- [124] Yamasaki, S., Stoecklin, G., Kedersha, N., Simarro, M. and Anderson, P., *T-cell intracellular antigen-1 (TIA-1)-induced translational silencing promotes the decay of selected mRNAs.*, J Biol Chem, Vol. 282, No. 41, pp. 30070–30077, Oct 2007.
- [125] Gilks, N., Kedersha, N., Ayodele, M., Shen, L., Stoecklin, G., Dember, L. M. and Anderson, P., *Stress granule assembly is mediated by prion-like aggregation of TIA-1.*, Mol Biol Cell, Vol. 15, No. 12, pp. 5383–5398, Dec 2004.

- [126] **Vasudevan, S. and Steitz, J. A.**, *AU-rich-element-mediated upregulation of translation by FXR1 and Argonaute 2.*, Cell, Vol. 128, No. 6, pp. 1105–1118, Mar 2007.
- [127] **Hel, Z., Di Marco, S. and Radzioch, D.**, *Characterization of the RNA binding proteins forming complexes with a novel putative regulatory region in the 3'-UTR of TNF-alpha mRNA.*, Nucleic Acids Res, Vol. 26, No. 11, pp. 2803–2812, Jun 1998.
- [128] **Hudson, B. P., Martinez-Yamout, M. A., Dyson, H. J. and Wright, P. E.**, *Recognition of the mRNA AU-rich element by the zinc finger domain of TIS11d.*, Nat Struct Mol Biol, Vol. 11, No. 3, pp. 257–264, Mar 2004.
- [129] **Brooks, S. A. and Blackshear, P. J.**, *Tristetraprolin (TTP): interactions with mRNA and proteins, and current thoughts on mechanisms of action.*, Biochim Biophys Acta, Vol. 1829, No. 6-7, pp. 666–679, 2013.
- [130] **Anderson, P.**, *Post-transcriptional regulons coordinate the initiation and resolution of inflammation.*, Nat Rev Immunol, Vol. 10, No. 1, pp. 24–35, Jan 2010.
- [131] **Sandler, H., Kreth, J., Timmers, H. T. M. and Stoecklin, G.**, *Not1 mediates recruitment of the deadenylase Caf1 to mRNAs targeted for degradation by tristetraprolin.*, Nucleic Acids Res, Vol. 39, No. 10, pp. 4373–4386, May 2011.
- [132] **Fenger-Grøn, M., Fillman, C., Norrild, B. and Lykke-Andersen, J.**, *Multiple processing body factors and the ARE binding protein TTP activate mRNA decapping.*, Mol Cell, Vol. 20, No. 6, pp. 905–915, Dec 2005.
- [133] **Lykke-Andersen, J. and Wagner, E.**, *Recruitment and activation of mRNA decay enzymes by two ARE-mediated decay activation domains in the proteins TTP and BRF-1.*, Genes Dev, Vol. 19, No. 3, pp. 351–361, Feb 2005.
- [134] **Taylor, G. A., Carballo, E., Lee, D. M., Lai, W. S., Thompson, M. J., Patel, D. D., Schenkman, D. I., Gilkeson, G. S., Broxmeyer, H. E., Haynes, B. F. and Blackshear, P. J.**, *A pathogenetic role for TNF alpha in the syndrome of cachexia, arthritis, and autoimmunity resulting from tristetraprolin (TTP) deficiency.*, Immunity, Vol. 4, No. 5, pp. 445–454, May 1996.
- [135] **Carballo, E. and Blackshear, P. J.**, *Roles of tumor necrosis factor-alpha receptor subtypes in the pathogenesis of the tristetraprolin-deficiency syndrome.*, Blood, Vol. 98, No. 8, pp. 2389–2395, Oct 2001.

- [136] Stoecklin, G., Stubbs, T., Kedersha, N., Wax, S., Rigby, W. F. C., Blackwell, T. K. and Anderson, P., *MK2-induced tristetraprolin:14-3-3 complexes prevent stress granule association and ARE-mRNA decay.*, EMBO J, Vol. 23, No. 6, pp. 1313–1324, Mar 2004.
- [137] Buxadé, M., Parra, J. L., Rousseau, S., Shpiro, N., Marquez, R., Morrice, N., Bain, J., Espel, E. and Proud, C. G., *The Mnks are novel components in the control of TNF alpha biosynthesis and phosphorylate and regulate hnRNP A1.*, Immunity, Vol. 23, No. 2, pp. 177–189, Aug 2005.
- [138] Tiedje, C., Ronkina, N., Tehrani, M., Dhamija, S., Laass, K., Holtmann, H., Kotlyarov, A. and Gaestel, M., *The p38/MK2-driven exchange between tristetraprolin and HuR regulates AU-rich element-dependent translation.*, PLoS Genet, Vol. 8, No. 9, pp. e1002977, Sep 2012.
- [139] Sun, L., Stoecklin, G., Van Way, S., Hinkovska-Galcheva, V., Guo, R.-F., Anderson, P. and Shanley, T. P., *Tristetraprolin (TTP)-14-3-3 complex formation protects TTP from dephosphorylation by protein phosphatase 2a and stabilizes tumor necrosis factor-alpha mRNA.*, J Biol Chem, Vol. 282, No. 6, pp. 3766–3777, Feb 2007.
- [140] Chen, Y.-L., Huang, Y.-L., Lin, N.-Y., Chen, H.-C., Chiu, W.-C. and Chang, C.-J., *Differential regulation of ARE-mediated TNFalpha and IL-1beta mRNA stability by lipopolysaccharide in RAW264.7 cells.*, Biochem Biophys Res Commun, Vol. 346, No. 1, pp. 160–168, Jul 2006.
- [141] Jing, Q., Huang, S., Guth, S., Zarubin, T., Motoyama, A., Chen, J., Di Padova, F., Lin, S.-C., Gram, H. and Han, J., *Involvement of microRNA in AU-rich element-mediated mRNA instability.*, Cell, Vol. 120, No. 5, pp. 623–634, Mar 2005.
- [142] Helfer, S., Schott, J., Stoecklin, G. and Förstemann, K., *AU-rich element-mediated mRNA decay can occur independently of the miRNA machinery in mouse embryonic fibroblasts and Drosophila S2-cells.*, PLoS One, Vol. 7, No. 1, pp. e28907, 2012.
- [143] von Roretz, C. and Gallouzi, I.-E., *Decoding ARE-mediated decay: is microRNA part of the equation?*, J Cell Biol, Vol. 181, No. 2, pp. 189–194, Apr 2008.
- [144] Stoecklin, G., Ming, X. F., Looser, R. and Moroni, C., *Somatic mRNA turnover mutants implicate tristetraprolin in the interleukin-3 mRNA degradation pathway.*, Mol Cell Biol, Vol. 20, No. 11, pp. 3753–3763, Jun 2000.

- [145] **Rattenbacher, B.**, Mechanisms of CDE-dependent mRNA decay., Ph.D. thesis, University of Berne, Switzerland, 2007, Dissertation.
- [146] **Sengupta, T. K., Bandyopadhyay, S., Fernandes, D. J. and Spicer, E. K.**, *Identification of nucleolin as an AU-rich element binding protein involved in bcl-2 mRNA stabilization.*, J Biol Chem, Vol. 279, No. 12, pp. 10855–10863, Mar 2004.
- [147] **Ginisty, H., Sicard, H., Roger, B. and Bouvet, P.**, *Structure and functions of nucleolin.*, J Cell Sci, Vol. 112 (Pt 6), pp. 761–772, Mar 1999.
- [148] **Winkler, W. C. and Breaker, R. R.**, *Regulation of bacterial gene expression by riboswitches.*, Annu Rev Microbiol, Vol. 59, pp. 487–517, 2005.
- [149] **Kortmann, J. and Narberhaus, F.**, *Bacterial RNA thermometers: molecular zippers and switches.*, Nat Rev Microbiol, Vol. 10, No. 4, pp. 255–265, Apr 2012.
- [150] **Kaempfer, R.**, *RNA sensors: novel regulators of gene expression.*, EMBO Rep, Vol. 4, No. 11, pp. 1043–1047, Nov 2003.
- [151] **Wachter, A.**, *Riboswitch-mediated control of gene expression in eukaryotes.*, RNA Biol, Vol. 7, No. 1, pp. 67–76, 2010.
- [152] **Wan, Y., Kertesz, M., Spitale, R. C., Segal, E. and Chang, H. Y.**, *Understanding the transcriptome through RNA structure.*, Nat Rev Genet, Vol. 12, No. 9, pp. 641–655, Sep 2011.
- [153] **Parker, B. J., Moltke, I., Roth, A., Washietl, S., Wen, J., Kellis, M., Breaker, R. and Pedersen, J. S.**, *New families of human regulatory RNA structures identified by comparative analysis of vertebrate genomes.*, Genome Res, Vol. 21, No. 11, pp. 1929–1943, Nov 2011.
- [154] **Svoboda, P. and Di Cara, A.**, *Hairpin RNA: a secondary structure of primary importance.*, Cell Mol Life Sci, Vol. 63, No. 7-8, pp. 901–908, Apr 2006.
- [155] **Sonenberg, N. and Hinnebusch, A. G.**, *Regulation of translation initiation in eukaryotes: mechanisms and biological targets.*, Cell, Vol. 136, No. 4, pp. 731–745, Feb 2009.
- [156] **Ben-Asouli, Y., Banai, Y., Pel-Or, Y., Shir, A. and Kaempfer, R.**, *Human interferon-gamma mRNA autoregulates its translation through a pseudoknot that activates the interferon-inducible protein kinase PKR.*, Cell, Vol. 108, No. 2, pp. 221–232, Jan 2002.
- [157] **Brown, C. Y., Lagnado, C. A. and Goodall, G. J.**, *A cytokine mRNA-destabilizing element that is structurally and functionally distinct*

- from *A+U-rich elements.*, Proc Natl Acad Sci U S A, Vol. 93, No. 24, pp. 13721–13725, Nov 1996.
- [158] **Putland, R. A., Sassinis, T. A., Harvey, J. S., Diamond, P., Coles, L. S., Brown, C. Y. and Goodall, G. J.**, *RNA destabilization by the granulocyte colony-stimulating factor stem-loop destabilizing element involves a single stem-loop that promotes deadenylation.*, Mol Cell Biol, Vol. 22, No. 6, pp. 1664–1673, Mar 2002.
- [159] **Paschoud, S., Dogar, A. M., Kuntz, C., Grisoni-Neupert, B., Richman, L. and Kühn, L. C.**, *Destabilization of interleukin-6 mRNA requires a putative RNA stem-loop structure, an AU-rich element, and the RNA-binding protein AUF1.*, Mol Cell Biol, Vol. 26, No. 22, pp. 8228–8241, Nov 2006.
- [160] **Norbury, C. J.**, *Cytoplasmic RNA: a case of the tail wagging the dog.*, Nat Rev Mol Cell Biol, Vol. 14, No. 10, pp. 643–653, Oct 2013.
- [161] **Schoenberg, D. R. and Maquat, L. E.**, *Regulation of cytoplasmic mRNA decay.*, Nat Rev Genet, Vol. 13, No. 4, pp. 246–259, Apr 2012.
- [162] **Arraiano, C. M., Mauxion, F., Viegas, S. C., Matos, R. G. and Séraphin, B.**, *Intracellular ribonucleases involved in transcript processing and decay: precision tools for RNA.*, Biochim Biophys Acta, Vol. 1829, No. 6-7, pp. 491–513, 2013.
- [163] **Wahle, E. and Winkler, G. S.**, *RNA decay machines: deadenylation by the Ccr4-not and Pan2-Pan3 complexes.*, Biochim Biophys Acta, Vol. 1829, No. 6-7, pp. 561–570, 2013.
- [164] **Yamashita, A., Chang, T.-C., Yamashita, Y., Zhu, W., Zhong, Z., Chen, C.-Y. A. and Shyu, A.-B.**, *Concerted action of poly(A) nucleases and decapping enzyme in mammalian mRNA turnover.*, Nat Struct Mol Biol, Vol. 12, No. 12, pp. 1054–1063, Dec 2005.
- [165] **Christie, M., Boland, A., Huntzinger, E., Weichenrieder, O. and Izaurralde, E.**, *Structure of the PAN3 pseudokinase reveals the basis for interactions with the PAN2 deadenylase and the GW182 proteins.*, Mol Cell, Vol. 51, No. 3, pp. 360–373, Aug 2013.
- [166] **Meyer, S., Temme, C. and Wahle, E.**, *Messenger RNA turnover in eukaryotes: pathways and enzymes.*, Crit Rev Biochem Mol Biol, Vol. 39, No. 4, pp. 197–216, 2004.
- [167] **Wiederhold, K. and Passmore, L. A.**, *Cytoplasmic deadenylation: regulation of mRNA fate.*, Biochem Soc Trans, Vol. 38, No. 6, pp. 1531–1536, Dec 2010.
- [168] **Tucker, M., Valencia-Sanchez, M. A., Staples, R. R., Chen, J., Denis, C. L. and Parker, R.**, *The transcription factor associated*

- Ccr4 and Caf1 proteins are components of the major cytoplasmic mRNA deadenylase in Saccharomyces cerevisiae.*, Cell, Vol. 104, No. 3, pp. 377–386, Feb 2001.
- [169] **Thore, S., Mauxion, F., Séraphin, B. and Suck, D.**, *X-ray structure and activity of the yeast Pop2 protein: a nuclease subunit of the mRNA deadenylase complex.*, EMBO Rep, Vol. 4, No. 12, pp. 1150–1155, Dec 2003.
- [170] **Horiuchi, M., Takeuchi, K., Noda, N., Muroya, N., Suzuki, T., Nakamura, T., Kawamura-Tsuzuku, J., Takahashi, K., Yamamoto, T. and Inagaki, F.**, *Structural basis for the antiproliferative activity of the Tob-hCaf1 complex.*, J Biol Chem, Vol. 284, No. 19, pp. 13244–13255, May 2009.
- [171] **Petit, A.-P., Wohlbold, L., Bawankar, P., Huntzinger, E., Schmidt, S., Izaurralde, E. and Weichenrieder, O.**, *The structural basis for the interaction between the CAF1 nuclease and the NOT1 scaffold of the human CCR4-NOT deadenylase complex.*, Nucleic Acids Res, Vol. 40, No. 21, pp. 11058–11072, Nov 2012.
- [172] **Schwede, A., Ellis, L., Luther, J., Carrington, M., Stoecklin, G. and Clayton, C.**, *A role for Caf1 in mRNA deadenylation and decay in trypanosomes and human cells.*, Nucleic Acids Res, Vol. 36, No. 10, pp. 3374–3388, Jun 2008.
- [173] **Basquin, J., Roudko, V. V., Rode, M., Basquin, C., Séraphin, B. and Conti, E.**, *Architecture of the nuclease module of the yeast Ccr4-not complex: the Not1-Caf1-Ccr4 interaction.*, Mol Cell, Vol. 48, No. 2, pp. 207–218, Oct 2012.
- [174] **Bhaskar, V., Roudko, V., Basquin, J., Sharma, K., Urlaub, H., Séraphin, B. and Conti, E.**, *Structure and RNA-binding properties of the Not1-Not2-Not5 module of the yeast Ccr4-Not complex.*, Nat Struct Mol Biol, Vol. 20, No. 11, pp. 1281–1288, Nov 2013.
- [175] **Boland, A., Chen, Y., Raisch, T., Jonas, S., Kuzuoğlu-Öztürk, D., Wohlbold, L., Weichenrieder, O. and Izaurralde, E.**, *Structure and assembly of the NOT module of the human CCR4-NOT complex.*, Nat Struct Mol Biol, Vol. 20, No. 11, pp. 1289–1297, Nov 2013.
- [176] **Bianchin, C., Mauxion, F., Sentis, S., Séraphin, B. and Corbo, L.**, *Conservation of the deadenylase activity of proteins of the Caf1 family in human.*, RNA, Vol. 11, No. 4, pp. 487–494, Apr 2005.
- [177] **Gao, M., Fritz, D. T., Ford, L. P. and Wilusz, J.**, *Interaction between a poly(A)-specific ribonuclease and the 5' cap influences mRNA deadenylation rates in vitro.*, Mol Cell, Vol. 5, No. 3, pp. 479–488, Mar 2000.

- [178] **Dehlin, E., Wormington, M., Körner, C. G. and Wahle, E.**, *Cap-dependent deadenylation of mRNA.*, EMBO J, Vol. 19, No. 5, pp. 1079–1086, Mar 2000.
- [179] **Lai, W. S., Kennington, E. A. and Blackshear, P. J.**, *Tristetraprolin and its family members can promote the cell-free deadenylation of AU-rich element-containing mRNAs by poly(A) ribonuclease.*, Mol Cell Biol, Vol. 23, No. 11, pp. 3798–3812, Jun 2003.
- [180] **Lykke-Andersen, S., Brodersen, D. E. and Jensen, T. H.**, *Origins and activities of the eukaryotic exosome.*, J Cell Sci, Vol. 122, No. Pt 10, pp. 1487–1494, May 2009.
- [181] **Chlebowski, A., Lubas, M., Jensen, T. H. and Dziembowski, A.**, *RNA decay machines: the exosome.*, Biochim Biophys Acta, Vol. 1829, No. 6-7, pp. 552–560, 2013.
- [182] **Lebreton, A., Tomecki, R., Dziembowski, A. and Séraphin, B.**, *Endonucleolytic RNA cleavage by a eukaryotic exosome.*, Nature, Vol. 456, No. 7224, pp. 993–996, Dec 2008.
- [183] **Raijmakers, R., Schilders, G. and Pruijn, G. J. M.**, *The exosome, a molecular machine for controlled RNA degradation in both nucleus and cytoplasm.*, Eur J Cell Biol, Vol. 83, No. 5, pp. 175–183, Jul 2004.
- [184] **Makino, D. L., Halbach, F. and Conti, E.**, *The RNA exosome and proteasome: common principles of degradation control.*, Nat Rev Mol Cell Biol, Vol. 14, No. 10, pp. 654–660, Oct 2013.
- [185] **Makino, D. L., Baumgärtner, M. and Conti, E.**, *Crystal structure of an RNA-bound 11-subunit eukaryotic exosome complex.*, Nature, Vol. 495, No. 7439, pp. 70–75, Mar 2013.
- [186] **Halbach, F., Reichelt, P., Rode, M. and Conti, E.**, *The yeast ski complex: crystal structure and RNA channeling to the exosome complex.*, Cell, Vol. 154, No. 4, pp. 814–826, Aug 2013.
- [187] **Allmang, C., Kufel, J., Chanfreau, G., Mitchell, P., Petfalski, E. and Tollervey, D.**, *Functions of the exosome in rRNA, snoRNA and snRNA synthesis.*, EMBO J, Vol. 18, No. 19, pp. 5399–5410, Oct 1999.
- [188] **Assenholt, J., Mouaikel, J., Andersen, K. R., Brodersen, D. E., Libri, D. and Jensen, T. H.**, *Exonucleolysis is required for nuclear mRNA quality control in yeast THO mutants.*, RNA, Vol. 14, No. 11, pp. 2305–2313, Nov 2008.
- [189] **Sloan, K. E., Schneider, C. and Watkins, N. J.**, *Comparison of the yeast and human nuclear exosome complexes.*, Biochem Soc Trans, Vol. 40, No. 4, pp. 850–855, Aug 2012.

- [190] **Liu, H., Rodgers, N. D., Jiao, X. and Kiledjian, M.**, *The scavenger mRNA decapping enzyme DcpS is a member of the HIT family of pyrophosphatases.*, EMBO J, Vol. 21, No. 17, pp. 4699–4708, Sep 2002.
- [191] **Li, Y. and Kiledjian, M.**, *Regulation of mRNA decapping.*, Wiley Interdiscip Rev RNA, Vol. 1, No. 2, pp. 253–265, 2010.
- [192] **Coller, J. and Parker, R.**, *Eukaryotic mRNA decapping.*, Annu Rev Biochem, Vol. 73, pp. 861–890, 2004.
- [193] **Arribas-Layton, M., Wu, D., Lykke-Andersen, J. and Song, H.**, *Structural and functional control of the eukaryotic mRNA decapping machinery.*, Biochim Biophys Acta, Vol. 1829, No. 6-7, pp. 580–589, 2013.
- [194] **Decker, C. J., Teixeira, D. and Parker, R.**, *Edc3p and a glutamine/asparagine-rich domain of Lsm4p function in processing body assembly in Saccharomyces cerevisiae.*, J Cell Biol, Vol. 179, No. 3, pp. 437–449, Nov 2007.
- [195] **Haas, G., Braun, J. E., Igreja, C., Tritschler, F., Nishihara, T. and Izaurralde, E.**, *HPat provides a link between deadenylation and decapping in metazoa.*, J Cell Biol, Vol. 189, No. 2, pp. 289–302, Apr 2010.
- [196] **Ozgun, S., Chekulaeva, M. and Stoecklin, G.**, *Human Pat1b connects deadenylation with mRNA decapping and controls the assembly of processing bodies.*, Mol Cell Biol, Vol. 30, No. 17, pp. 4308–4323, Sep 2010.
- [197] **Ozgun, S. and Stoecklin, G.**, *Role of Rck-Pat1b binding in assembly of processing-bodies.*, RNA Biol, Vol. 10, No. 4, pp. 528–539, Apr 2013.
- [198] **Tharun, S. and Parker, R.**, *Targeting an mRNA for decapping: displacement of translation factors and association of the Lsm1p-7p complex on deadenylated yeast mRNAs.*, Mol Cell, Vol. 8, No. 5, pp. 1075–1083, Nov 2001.
- [199] **Sharif, H., Ozgun, S., Sharma, K., Basquin, C., Urlaub, H. and Conti, E.**, *Structural analysis of the yeast Dhh1-Pat1 complex reveals how Dhh1 engages Pat1, Edc3 and RNA in mutually exclusive interactions.*, Nucleic Acids Res, Vol. 41, No. 17, pp. 8377–8390, Sep 2013.
- [200] **Sharif, H. and Conti, E.**, *Architecture of the lsm1-7-pat1 complex: a conserved assembly in eukaryotic mRNA turnover.*, Cell Rep, Vol. 5, No. 2, pp. 283–291, Oct 2013.
- [201] **Chowdhury, A., Mukhopadhyay, J. and Tharun, S.**, *The decapping activator Lsm1p-7p-Pat1p complex has the intrinsic ability to distinguish between oligoadenylated and polyadenylated RNAs.*, RNA, Vol. 13, No. 7, pp. 998–1016, Jul 2007.

- [202] **Bergman, N., Moraes, K. C. M., Anderson, J. R., Zaric, B., Kambach, C., Schneider, R. J., Wilusz, C. J. and Wilusz, J.,** *Lsm proteins bind and stabilize RNAs containing 5' poly(A) tracts.*, Nat Struct Mol Biol, Vol. 14, No. 9, pp. 824–831, Sep 2007.
- [203] **Tharun, S., He, W., Mayes, A. E., Lennertz, P., Beggs, J. D. and Parker, R.,** *Yeast Sm-like proteins function in mRNA decapping and decay.*, Nature, Vol. 404, No. 6777, pp. 515–518, Mar 2000.
- [204] **Wilusz, C. J. and Wilusz, J.,** *Bringing the role of mRNA decay in the control of gene expression into focus.*, Trends Genet, Vol. 20, No. 10, pp. 491–497, Oct 2004.
- [205] **Parker, R. and Song, H.,** *The enzymes and control of eukaryotic mRNA turnover.*, Nat Struct Mol Biol, Vol. 11, No. 2, pp. 121–127, Feb 2004.
- [206] **Nagarajan, V. K., Jones, C. I., Newbury, S. F. and Green, P. J.,** *XRN 5'→3' exoribonucleases: structure, mechanisms and functions.*, Biochim Biophys Acta, Vol. 1829, No. 6-7, pp. 590–603, 2013.
- [207] **Braun, J. E., Truffault, V., Boland, A., Huntzinger, E., Chang, C.-T., Haas, G., Weichenrieder, O., Coles, M. and Izaurralde, E.,** *A direct interaction between DCP1 and XRN1 couples mRNA decapping to 5' exonucleolytic degradation.*, Nat Struct Mol Biol, Vol. 19, No. 12, pp. 1324–1331, Dec 2012.
- [208] **Eulalio, A., Behm-Ansmant, I. and Izaurralde, E.,** *P bodies: at the crossroads of post-transcriptional pathways.*, Nat Rev Mol Cell Biol, Vol. 8, No. 1, pp. 9–22, Jan 2007.
- [209] **Hu, W., Sweet, T. J., Chamnongpol, S., Baker, K. E. and Collier, J.,** *Co-translational mRNA decay in Saccharomyces cerevisiae.*, Nature, Vol. 461, No. 7261, pp. 225–229, Sep 2009.
- [210] **Mukherjee, D., Gao, M., O'Connor, J. P., Raijmakers, R., Pruijn, G., Lutz, C. S. and Wilusz, J.,** *The mammalian exosome mediates the efficient degradation of mRNAs that contain AU-rich elements.*, EMBO J, Vol. 21, No. 1-2, pp. 165–174, Jan 2002.
- [211] **Gao, M., Wilusz, C. J., Peltz, S. W. and Wilusz, J.,** *A novel mRNA-decapping activity in HeLa cytoplasmic extracts is regulated by AU-rich elements.*, EMBO J, Vol. 20, No. 5, pp. 1134–1143, Mar 2001.
- [212] **Stoecklin, G., Mayo, T. and Anderson, P.,** *ARE-mRNA degradation requires the 5'-3' decay pathway.*, EMBO Rep, Vol. 7, No. 1, pp. 72–77, Jan 2006.
- [213] **Kedersha, N., Stoecklin, G., Ayodele, M., Yacono, P., Lykke-Andersen, J., Fritzler, M. J., Scheuner, D., Kaufman, R. J.,**

- Golan, D. E.** and **Anderson, P.**, *Stress granules and processing bodies are dynamically linked sites of mRNP remodeling.*, J Cell Biol, Vol. 169, No. 6, pp. 871–884, Jun 2005.
- [214] **Matsushita, K., Takeuchi, O., Standley, D. M., Kumagai, Y., Kawagoe, T., Miyake, T., Satoh, T., Kato, H., Tsujimura, T., Nakamura, H. and Akira, S.**, *Zc3h12a is an RNase essential for controlling immune responses by regulating mRNA decay.*, Nature, Vol. 458, No. 7242, pp. 1185–1190, Apr 2009.
- [215] **Uehata, T. and Akira, S.**, *mRNA degradation by the endoribonuclease Regnase-1/ZC3H12a/MCPIP-1.*, Biochim Biophys Acta, Vol. 1829, No. 6-7, pp. 708–713, 2013.
- [216] **Uehata, T., Iwasaki, H., Vandenbon, A., Matsushita, K., Hernandez-Cuellar, E., Kuniyoshi, K., Satoh, T., Mino, T., Suzuki, Y., Standley, D. M., Tsujimura, T., Rakugi, H., Isaka, Y., Takeuchi, O. and Akira, S.**, *Malt1-induced cleavage of regnase-1 in CD4(+) helper T cells regulates immune activation.*, Cell, Vol. 153, No. 5, pp. 1036–1049, May 2013.
- [217] **Akira, S.**, *Regnase-1, a Ribonuclease Involved in the Regulation of Immune Responses.*, Cold Spring Harb Symp Quant Biol, Oct 2013.
- [218] **Sheth, U. and Parker, R.**, *Decapping and decay of messenger RNA occur in cytoplasmic processing bodies.*, Science, Vol. 300, No. 5620, pp. 805–808, May 2003.
- [219] **Parker, R. and Sheth, U.**, *P bodies and the control of mRNA translation and degradation.*, Mol Cell, Vol. 25, No. 5, pp. 635–646, Mar 2007.
- [220] **Stoecklin, G. and Anderson, P.**, *In a tight spot: ARE-mRNAs at processing bodies.*, Genes Dev, Vol. 21, No. 6, pp. 627–631, Mar 2007.
- [221] **Kulkarni, M., Ozgur, S. and Stoecklin, G.**, *On track with P-bodies.*, Biochem Soc Trans, Vol. 38, No. Pt 1, pp. 242–251, Feb 2010.
- [222] **Cougot, N., Babajko, S. and Séraphin, B.**, *Cytoplasmic foci are sites of mRNA decay in human cells.*, J Cell Biol, Vol. 165, No. 1, pp. 31–40, Apr 2004.
- [223] **Franks, T. M. and Lykke-Andersen, J.**, *TTP and BRF proteins nucleate processing body formation to silence mRNAs with AU-rich elements.*, Genes Dev, Vol. 21, No. 6, pp. 719–735, Mar 2007.
- [224] **Heissmeyer, V. and Vogel, K. U.**, *Molecular control of Tfh-cell differentiation by Roquin family proteins.*, Immunol Rev, Vol. 253, No. 1, pp. 273–289, May 2013.

- [225] Yu, D., Tan, A. H.-M., Hu, X., Athanasopoulos, V., Simpson, N., Silva, D. G., Hutloff, A., Giles, K. M., Leedman, P. J., Lam, K. P., Goodnow, C. C. and Vinuesa, C. G., *Roquin represses autoimmunity by limiting inducible T-cell co-stimulator messenger RNA.*, Nature, Vol. 450, No. 7167, pp. 299–303, Nov 2007.
- [226] Glasmacher, E., Hoefig, K. P., Vogel, K. U., Rath, N., Du, L., Wolf, C., Kremmer, E., Wang, X. and Heissmeyer, V., *Roquin binds inducible costimulator mRNA and effectors of mRNA decay to induce microRNA-independent post-transcriptional repression.*, Nat Immunol, Vol. 11, No. 8, pp. 725–733, Aug 2010.
- [227] Vinuesa, C. G., Cook, M. C., Angelucci, C., Athanasopoulos, V., Rui, L., Hill, K. M., Yu, D., Domaschensz, H., Whittle, B., Lambe, T., Roberts, I. S., Copley, R. R., Bell, J. I., Cornell, R. J. and Goodnow, C. C., *A RING-type ubiquitin ligase family member required to repress follicular helper T cells and autoimmunity.*, Nature, Vol. 435, No. 7041, pp. 452–458, May 2005.
- [228] Schaefer, J. S., Montufar-Solis, D., Nakra, N., Vigneswaran, N. and Klein, J. R., *Small intestine inflammation in Roquin-mutant and Roquin-deficient mice.*, PLoS One, Vol. 8, No. 2, pp. e56436, 2013.
- [229] Hutloff, A., Büchner, K., Reiter, K., Baelde, H. J., Odendahl, M., Jacobi, A., Dörner, T. and Kroczeck, R. A., *Involvement of inducible costimulator in the exaggerated memory B cell and plasma cell generation in systemic lupus erythematosus.*, Arthritis Rheum, Vol. 50, No. 10, pp. 3211–3220, Oct 2004.
- [230] Iwai, H., Abe, M., Hirose, S., Tsushima, F., Tezuka, K., Akiba, H., Yagita, H., Okumura, K., Kohsaka, H., Miyasaka, N. and Azuma, M., *Involvement of inducible costimulator-B7 homologous protein costimulatory pathway in murine lupus nephritis.*, J Immunol, Vol. 171, No. 6, pp. 2848–2854, Sep 2003.
- [231] Linterman, M. A., Rigby, R. J., Wong, R. K., Yu, D., Brink, R., Cannons, J. L., Schwartzberg, P. L., Cook, M. C., Walters, G. D. and Vinuesa, C. G., *Follicular helper T cells are required for systemic autoimmunity.*, J Exp Med, Vol. 206, No. 3, pp. 561–576, Mar 2009.
- [232] Nurieva, R. I., Liu, X. and Dong, C., *Yin-Yang of costimulation: crucial controls of immune tolerance and function.*, Immunol Rev, Vol. 229, No. 1, pp. 88–100, May 2009.
- [233] Akiba, H., Takeda, K., Kojima, Y., Usui, Y., Harada, N., Yamazaki, T., Ma, J., Tezuka, K., Yagita, H. and Okumura, K.,

- The role of ICOS in the CXCR5+ follicular B helper T cell maintenance in vivo.*, J Immunol, Vol. 175, No. 4, pp. 2340–2348, Aug 2005.
- [234] **Bossaller, L., Burger, J., Draeger, R., Grimbacher, B., Knoth, R., Plebani, A., Durandy, A., Baumann, U., Schlesier, M., Welcher, A. A., Peter, H. H. and Warnatz, K.**, *ICOS deficiency is associated with a severe reduction of CXCR5+CD4 germinal center Th cells.*, J Immunol, Vol. 177, No. 7, pp. 4927–4932, Oct 2006.
- [235] **Tordjman, R., Lepelletier, Y., Lemarchandel, V., Cambot, M., Gaulard, P., Hermine, O. and Roméo, P.-H.**, *A neuronal receptor, neuropilin-1, is essential for the initiation of the primary immune response.*, Nat Immunol, Vol. 3, No. 5, pp. 477–482, May 2002.
- [236] **Vogel, K. U., Edelmann, S. L., Jeltsch, K. M., Bertossi, A., Heger, K., Heinz, G. A., Zöller, J., Warth, S. C., Hoefig, K. P., Lohs, C., Neff, F., Kremmer, E., Schick, J., Repsilber, D., Geerlof, A., Blum, H., Wurst, W., Heikenwälder, M., Schmidt-Supprian, M. and Heissmeyer, V.**, *Roquin paralogs 1 and 2 redundantly repress the Icos and Ox40 costimulator mRNAs and control follicular helper T cell differentiation.*, Immunity, Vol. 38, No. 4, pp. 655–668, Apr 2013.
- [237] **Lee, S. K., Silva, D. G., Martin, J. L., Pratama, A., Hu, X., Chang, P.-P., Walters, G. and Vinuesa, C. G.**, *Interferon- γ excess leads to pathogenic accumulation of follicular helper T cells and germinal centers.*, Immunity, Vol. 37, No. 5, pp. 880–892, Nov 2012.
- [238] **Chang, P.-P., Lee, S. K., Hu, X., Davey, G., Duan, G., Cho, J.-H., Karupiah, G., Sprent, J., Heath, W. R., Bertram, E. M. and Vinuesa, C. G.**, *Breakdown in repression of IFN- γ mRNA leads to accumulation of self-reactive effector CD8+ T cells.*, J Immunol, Vol. 189, No. 2, pp. 701–710, Jul 2012.
- [239] **Pratama, A., Ramiscal, R. R., Silva, D. G., Das, S. K., Athanasiopoulos, V., Fitch, J., Botelho, N. K., Chang, P.-P., Hu, X., Hogan, J. J., Maña, P., Bernal, D., Korner, H., Yu, D., Goodnow, C. C., Cook, M. C. and Vinuesa, C. G.**, *Roquin-2 shares functions with its paralog Roquin-1 in the repression of mRNAs controlling T follicular helper cells and systemic inflammation.*, Immunity, Vol. 38, No. 4, pp. 669–680, Apr 2013.
- [240] **Linterman, M. A., Rigby, R. J., Wong, R., Silva, D., Withers, D., Anderson, G., Verma, N. K., Brink, R., Hutloff, A., Goodnow, C. C. and Vinuesa, C. G.**, *Roquin differentiates the specialized functions of duplicated T cell costimulatory receptor genes CD28 and ICOS.*, Immunity, Vol. 30, No. 2, pp. 228–241, Feb 2009.

- [241] Bertossi, A., Aichinger, M., Sansonetti, P., Lech, M., Neff, F., Pal, M., Wunderlich, F. T., Anders, H.-J., Klein, L. and Schmidt-Supprian, M., *Loss of Roquin induces early death and immune deregulation but not autoimmunity.*, J Exp Med, Vol. 208, No. 9, pp. 1749–1756, Aug 2011.
- [242] Ellyard, J. I., Chia, T., Rodriguez-Pinilla, S.-M., Martin, J. L., Hu, X., Navarro-Gonzalez, M., Garcia, J. F., Delfau-Larue, M.-H., Montes-Moreno, S., Gaulard, P., Cook, M. C., Walters, G., Piris, M. A. and Vinuesa, C. G., *Heterozygosity for Roquin-san leads to angioimmunoblastic T-cell lymphoma-like tumors in mice.*, Blood, Vol. 120, No. 4, pp. 812–821, Jul 2012.
- [243] Siess, D. C., Vedder, C. T., Merkens, L. S., Tanaka, T., Freed, A. C., McCoy, S. L., Heinrich, M. C., Deffebach, M. E., Bennett, R. M. and Hefeneider, S. H., *A human gene coding for a membrane-associated nucleic acid-binding protein.*, J Biol Chem, Vol. 275, No. 43, pp. 33655–33662, Oct 2000.
- [244] Li, W., Gao, B., Lee, S.-M., Bennett, K. and Fang, D., *RLE-1, an E3 ubiquitin ligase, regulates C. elegans aging by catalyzing DAF-16 polyubiquitination.*, Dev Cell, Vol. 12, No. 2, pp. 235–246, Feb 2007.
- [245] Athanasopoulos, V., Barker, A., Yu, D., Tan, A. H.-M., Srivastava, M., Contreras, N., Wang, J., Lam, K.-P., Brown, S. H. J., Goodnow, C. C., Dixon, N. E., Leedman, P. J., Saint, R. and Vinuesa, C. G., *The ROQUIN family of proteins localizes to stress granules via the ROQ domain and binds target mRNAs.*, FEBS J, Vol. 277, No. 9, pp. 2109–2127, May 2010.
- [246] Leppek, K., Schott, J., Reitter, S., Poetz, F., Hammond, M. C. and Stoecklin, G., *Roquin promotes constitutive mRNA decay via a conserved class of stem-loop recognition motifs.*, Cell, Vol. 153, No. 4, pp. 869–881, May 2013.
- [247] Schaefer, J. S., Montufar-Solis, D., Vigneswaran, N. and Klein, J. R., *Selective upregulation of microRNA expression in peripheral blood leukocytes in IL-10^{-/-} mice precedes expression in the colon.*, J Immunol, Vol. 187, No. 11, pp. 5834–5841, Dec 2011.
- [248] Hieronymus, H. and Silver, P. A., *A systems view of mRNP biology.*, Genes Dev, Vol. 18, No. 23, pp. 2845–2860, Dec 2004.
- [249] Moore, M. J., *From birth to death: the complex lives of eukaryotic mRNAs.*, Science, Vol. 309, No. 5740, pp. 1514–1518, Sep 2005.
- [250] Dreyfuss, G., Kim, V. N. and Kataoka, N., *Messenger-RNA-binding proteins and the messages they carry.*, Nat Rev Mol Cell Biol, Vol. 3, No. 3, pp. 195–205, Mar 2002.

- [251] **Oeffinger, M.**, *Two steps forward—one step back: advances in affinity purification mass spectrometry of macromolecular complexes.*, Proteomics, Vol. 12, No. 10, pp. 1591–1608, May 2012.
- [252] **Keene, J. D.**, *Minireview: global regulation and dynamics of ribonucleic Acid.*, Endocrinology, Vol. 151, No. 4, pp. 1391–1397, Apr 2010.
- [253] **Licatalosi, D. D., Mele, A., Fak, J. J., Ule, J., Kayikci, M., Chi, S. W., Clark, T. A., Schweitzer, A. C., Blume, J. E., Wang, X., Darnell, J. C. and Darnell, R. B.**, *HITS-CLIP yields genome-wide insights into brain alternative RNA processing.*, Nature, Vol. 456, No. 7221, pp. 464–469, Nov 2008.
- [254] **König, J., Zarnack, K., Rot, G., Curk, T., Kayikci, M., Zupan, B., Turner, D. J., Luscombe, N. M. and Ule, J.**, *iCLIP reveals the function of hnRNP particles in splicing at individual nucleotide resolution.*, Nat Struct Mol Biol, Vol. 17, No. 7, pp. 909–915, Jul 2010.
- [255] **Hafner, M., Landthaler, M., Burger, L., Khorshid, M., Hausser, J., Berninger, P., Rothballer, A., Ascano, Jr, M., Jungkamp, A.-C., Munschauer, M., Ulrich, A., Wardle, G. S., Dewell, S., Zavolan, M. and Tuschl, T.**, *Transcriptome-wide identification of RNA-binding protein and microRNA target sites by PAR-CLIP.*, Cell, Vol. 141, No. 1, pp. 129–141, Apr 2010.
- [256] **Ule, J., Jensen, K. B., Ruggiu, M., Mele, A., Ule, A. and Darnell, R. B.**, *CLIP identifies Nova-regulated RNA networks in the brain.*, Science, Vol. 302, No. 5648, pp. 1212–1215, Nov 2003.
- [257] **König, J., Zarnack, K., Luscombe, N. M. and Ule, J.**, *Protein-RNA interactions: new genomic technologies and perspectives.*, Nat Rev Genet, Vol. 13, No. 2, pp. 77–83, Feb 2011.
- [258] **Ceman, S., Brown, V. and Warren, S. T.**, *Isolation of an FMRP-associated messenger ribonucleoprotein particle and identification of nucleolin and the fragile X-related proteins as components of the complex.*, Mol Cell Biol, Vol. 19, No. 12, pp. 7925–7932, Dec 1999.
- [259] **Niranjanakumari, S., Lasda, E., Brazas, R. and Garcia-Blanco, M. A.**, *Reversible cross-linking combined with immunoprecipitation to study RNA-protein interactions in vivo.*, Methods, Vol. 26, No. 2, pp. 182–190, Feb 2002.
- [260] **Lingner, J. and Cech, T. R.**, *Purification of telomerase from Euplotes aediculatus: requirement of a primer 3' overhang.*, Proc Natl Acad Sci U S A, Vol. 93, No. 20, pp. 10712–10717, Oct 1996.
- [261] **Mitchell, S. F., Jain, S., She, M. and Parker, R.**, *Global analysis*

- of yeast mRNPs., *Nat Struct Mol Biol*, Vol. 20, No. 1, pp. 127–133, Jan 2013.
- [262] **Castello, A., Fischer, B., Eichelbaum, K., Horos, R., Beckmann, B. M., Strein, C., Davey, N. E., Humphreys, D. T., Preiss, T., Steinmetz, L. M., Krijgsveld, J. and Hentze, M. W.**, *Insights into RNA biology from an atlas of mammalian mRNA-binding proteins.*, *Cell*, Vol. 149, No. 6, pp. 1393–1406, Jun 2012.
- [263] **Mogridge, J., Mah, T. F. and Greenblatt, J.**, *A protein-RNA interaction network facilitates the template-independent cooperative assembly on RNA polymerase of a stable antitermination complex containing the lambda N protein.*, *Genes Dev*, Vol. 9, No. 22, pp. 2831–2845, Nov 1995.
- [264] **Czaplinski, K., Köcher, T., Schelder, M., Segref, A., Wilm, M. and Mattaj, I. W.**, *Identification of 40LoVe, a Xenopus hnRNP D family protein involved in localizing a TGF-beta-related mRNA during oogenesis.*, *Dev Cell*, Vol. 8, No. 4, pp. 505–515, Apr 2005.
- [265] **Carey, J., Cameron, V., de Haseth, P. L. and Uhlenbeck, O. C.**, *Sequence-specific interaction of R17 coat protein with its ribonucleic acid binding site.*, *Biochemistry*, Vol. 22, No. 11, pp. 2601–2610, May 1983.
- [266] **Beach, D. L. and Keene, J. D.**, *Ribotrap : targeted purification of RNA-specific RNPs from cell lysates through immunoaffinity precipitation to identify regulatory proteins and RNAs.*, *Methods Mol Biol*, Vol. 419, pp. 69–91, 2008.
- [267] **Bardwell, V. J. and Wickens, M.**, *Purification of RNA and RNA-protein complexes by an R17 coat protein affinity method.*, *Nucleic Acids Res*, Vol. 18, No. 22, pp. 6587–6594, Nov 1990.
- [268] **Fouts, D. E., True, H. L. and Celander, D. W.**, *Functional recognition of fragmented operator sites by R17/MS2 coat protein, a translational repressor.*, *Nucleic Acids Res*, Vol. 25, No. 22, pp. 4464–4473, Nov 1997.
- [269] **Valegård, K., Murray, J. B., Stonehouse, N. J., van den Worm, S., Stockley, P. G. and Liljas, L.**, *The three-dimensional structures of two complexes between recombinant MS2 capsids and RNA operator fragments reveal sequence-specific protein-RNA interactions.*, *J Mol Biol*, Vol. 270, No. 5, pp. 724–738, Aug 1997.
- [270] **Lim, F., Downey, T. P. and Peabody, D. S.**, *Translational repression and specific RNA binding by the coat protein of the Pseudomonas phage PP7.*, *J Biol Chem*, Vol. 276, No. 25, pp. 22507–22513, Jun 2001.
- [271] **Lim, F. and Peabody, D. S.**, *RNA recognition site of PP7 coat protein.*, *Nucleic Acids Res*, Vol. 30, No. 19, pp. 4138–4144, Oct 2002.

- [272] **Chao, J. A., Patskovsky, Y., Almo, S. C. and Singer, R. H.**, *Structural basis for the coevolution of a viral RNA-protein complex.*, Nat Struct Mol Biol, Vol. 15, No. 1, pp. 103–105, Jan 2008.
- [273] **Bertrand, E., Chartrand, P., Schaefer, M., Shenoy, S. M., Singer, R. H. and Long, R. M.**, *Localization of ASH1 mRNA particles in living yeast.*, Mol Cell, Vol. 2, No. 4, pp. 437–445, Oct 1998.
- [274] **Lykke-Andersen, J., Shu, M. D. and Steitz, J. A.**, *Human Upf proteins target an mRNA for nonsense-mediated decay when bound downstream of a termination codon.*, Cell, Vol. 103, No. 7, pp. 1121–1131, Dec 2000.
- [275] **Baron-Benhamou, J., Gehring, N. H., Kulozik, A. E. and Hentze, M. W.**, *Using the lambdaN peptide to tether proteins to RNAs.*, Methods Mol Biol, Vol. 257, pp. 135–154, 2004.
- [276] **Coller, J. and Wickens, M.**, *Tethered function assays using 3' untranslated regions.*, Methods, Vol. 26, No. 2, pp. 142–150, Feb 2002.
- [277] **SenGupta, D. J., Zhang, B., Kraemer, B., Pochart, P., Fields, S. and Wickens, M.**, *A three-hybrid system to detect RNA-protein interactions in vivo.*, Proc Natl Acad Sci U S A, Vol. 93, No. 16, pp. 8496–8501, Aug 1996.
- [278] **Slobodin, B. and Gerst, J. E.**, *A novel mRNA affinity purification technique for the identification of interacting proteins and transcripts in ribonucleoprotein complexes.*, RNA, Vol. 16, No. 11, pp. 2277–2290, Nov 2010.
- [279] **Lee, N., Pimienta, G. and Steitz, J. A.**, *AUF1/hnRNP D is a novel protein partner of the EBER1 noncoding RNA of Epstein-Barr virus.*, RNA, Vol. 18, No. 11, pp. 2073–2082, Nov 2012.
- [280] **Yoon, J.-H., Srikantan, S. and Gorospe, M.**, *MS2-TRAP (MS2-tagged RNA affinity purification): tagging RNA to identify associated miRNAs.*, Methods, Vol. 58, No. 2, pp. 81–87, Oct 2012.
- [281] **Gong, C., Popp, M. W.-L. and Maquat, L. E.**, *Biochemical analysis of long non-coding RNA-containing ribonucleoprotein complexes.*, Methods, Vol. 58, No. 2, pp. 88–93, Oct 2012.
- [282] **Said, N., Rieder, R., Hurwitz, R., Deckert, J., Urlaub, H. and Vogel, J.**, *In vivo expression and purification of aptamer-tagged small RNA regulators.*, Nucleic Acids Res, Vol. 37, No. 20, pp. e133, Nov 2009.
- [283] **Corcoran, C. P., Rieder, R., Podkaminski, D., Hofmann, B. and Vogel, J.**, *Use of aptamer tagging to identify in vivo protein binding partners of small regulatory RNAs.*, Methods Mol Biol, Vol. 905, pp. 177–200, 2012.

- [284] **Rieder, R., Reinhardt, R., Sharma, C. and Vogel, J.**, *Experimental tools to identify RNA-protein interactions in Helicobacter pylori.*, RNA Biol, Vol. 9, No. 4, pp. 520–531, Apr 2012.
- [285] **Tsai, B. P., Wang, X., Huang, L. and Waterman, M. L.**, *Quantitative profiling of in vivo-assembled RNA-protein complexes using a novel integrated proteomic approach.*, Mol Cell Proteomics, Vol. 10, No. 4, pp. M110.007385, Apr 2011.
- [286] **Hogg, J. R. and Collins, K.**, *RNA-based affinity purification reveals 7SK RNPs with distinct composition and regulation.*, RNA, Vol. 13, No. 6, pp. 868–880, Jun 2007.
- [287] **Hogg, J. R. and Goff, S. P.**, *Upf1 senses 3'UTR length to potentiate mRNA decay.*, Cell, Vol. 143, No. 3, pp. 379–389, Oct 2010.
- [288] **Lee, H. Y., Haurwitz, R. E., Apffel, A., Zhou, K., Smart, B., Wenger, C. D., Laderman, S., Bruhn, L. and Doudna, J. A.**, *RNA-protein analysis using a conditional CRISPR nuclease.*, Proc Natl Acad Sci U S A, Vol. 110, No. 14, pp. 5416–5421, Apr 2013.
- [289] **Bachler, M., Schroeder, R. and von Ahsen, U.**, *StreptoTag: a novel method for the isolation of RNA-binding proteins.*, RNA, Vol. 5, No. 11, pp. 1509–1516, Nov 1999.
- [290] **Hartmuth, K., Urlaub, H., Vornlocher, H.-P., Will, C. L., Gentzel, M., Wilm, M. and Lührmann, R.**, *Protein composition of human prespliceosomes isolated by a tobramycin affinity-selection method.*, Proc Natl Acad Sci U S A, Vol. 99, No. 26, pp. 16719–16724, Dec 2002.
- [291] **Srisawat, C. and Engelke, D. R.**, *Streptavidin aptamers: affinity tags for the study of RNAs and ribonucleoproteins.*, RNA, Vol. 7, No. 4, pp. 632–641, Apr 2001.
- [292] **Li, Y. and Altman, S.**, *Partial reconstitution of human RNase P in HeLa cells between its RNA subunit with an affinity tag and the intact protein components.*, Nucleic Acids Res, Vol. 30, No. 17, pp. 3706–3711, Sep 2002.
- [293] **Green, N. M.**, *Avidin and streptavidin.*, Methods Enzymol, Vol. 184, pp. 51–67, 1990.
- [294] **Srisawat, C. and Engelke, D. R.**, *RNA affinity tags for purification of RNAs and ribonucleoprotein complexes.*, Methods, Vol. 26, No. 2, pp. 156–161, Feb 2002.
- [295] **Lemay, V., Hossain, A., Osheim, Y. N., Beyer, A. L. and Dragon, F.**, *Identification of novel proteins associated with yeast snR30*

- small nucleolar RNA.*, Nucleic Acids Res, Vol. 39, No. 22, pp. 9659–9670, Dec 2011.
- [296] **Leonov, A. A., Sergiev, P. V., Bogdanov, A. A., Brimacombe, R. and Dontsova, O. A.**, *Affinity purification of ribosomes with a lethal G2655C mutation in 23 S rRNA that affects the translocation.*, J Biol Chem, Vol. 278, No. 28, pp. 25664–25670, Jul 2003.
- [297] **Dienstbier, M., Boehl, F., Li, X. and Bullock, S. L.**, *Egalitarian is a selective RNA-binding protein linking mRNA localization signals to the dynein motor.*, Genes Dev, Vol. 23, No. 13, pp. 1546–1558, Jul 2009.
- [298] **Iioka, H., Loisel, D., Haystead, T. A. and Macara, I. G.**, *Efficient detection of RNA-protein interactions using tethered RNAs.*, Nucleic Acids Res, Vol. 39, No. 8, pp. e53, Apr 2011.
- [299] **Dix, C. I., Soundararajan, H. C., Dzhinzhev, N. S., Begum, F., Suter, B., Ohkura, H., Stephens, E. and Bullock, S. L.**, *Lissencephaly-1 promotes the recruitment of dynein and dynactin to transported mRNAs.*, J Cell Biol, Vol. 202, No. 3, pp. 479–494, Aug 2013.
- [300] **Butter, F., Scheibe, M., Mörl, M. and Mann, M.**, *Unbiased RNA-protein interaction screen by quantitative proteomics.*, Proc Natl Acad Sci U S A, Vol. 106, No. 26, pp. 10626–10631, Jun 2009.
- [301] **Scheibe, M., Butter, F., Hafner, M., Tuschl, T. and Mann, M.**, *Quantitative mass spectrometry and PAR-CLIP to identify RNA-protein interactions.*, Nucleic Acids Res, Vol. 40, No. 19, pp. 9897–9902, Oct 2012.
- [302] **Xiao, S., Day-Storms, J. J., Srisawat, C., Fierke, C. A. and Engelke, D. R.**, *Characterization of conserved sequence elements in eukaryotic RNase P RNA reveals roles in holoenzyme assembly and tRNA processing.*, RNA, Vol. 11, No. 6, pp. 885–896, Jun 2005.
- [303] **Leppek, K. and Stoecklin, G.**, *An optimized streptavidin-binding RNA aptamer for purification of ribonucleoprotein complexes identifies novel ARE-binding proteins.*, Nucleic Acids Res, Oct 2013.
- [304] **Stoecklin, G., Stoeckle, P., Lu, M., Muehlemann, O. and Moroni, C.**, *Cellular mutants define a common mRNA degradation pathway targeting cytokine AU-rich elements.*, RNA, Vol. 7, No. 11, pp. 1578–1588, Nov 2001.
- [305] **Oeffinger, M., Wei, K. E., Rogers, R., DeGrasse, J. A., Chait, B. T., Aitchison, J. D. and Rout, M. P.**, *Comprehensive analysis of diverse ribonucleoprotein complexes.*, Nat Methods, Vol. 4, No. 11, pp. 951–956, Nov 2007.

- [306] **Xu, D.** and **Shi, H.**, *Composite RNA aptamers as functional mimics of proteins.*, Nucleic Acids Res, Vol. 37, No. 9, pp. e71, May 2009.
- [307] **Boersema, P. J., Raijmakers, R., Lemeer, S., Mohammed, S.** and **Heck, A. J. R.**, *Multiplex peptide stable isotope dimethyl labeling for quantitative proteomics.*, Nat Protoc, Vol. 4, No. 4, pp. 484–494, 2009.
- [308] **Rousseau, S., Morrice, N., Peggie, M., Campbell, D. G., Gaestel, M.** and **Cohen, P.**, *Inhibition of SAPK2a/p38 prevents hnRNP A0 phosphorylation by MAPKAP-K2 and its interaction with cytokine mRNAs.*, EMBO J, Vol. 21, No. 23, pp. 6505–6514, Dec 2002.
- [309] **Morton, S., Yang, H.-T., Moleleki, N., Campbell, D. G., Cohen, P.** and **Rousseau, S.**, *Phosphorylation of the ARE-binding protein DAZAP1 by ERK2 induces its dissociation from DAZ.*, Biochem J, Vol. 399, No. 2, pp. 265–273, Oct 2006.
- [310] **Negishi, Y., Nishita, Y., Saegusa, Y., Kakizaki, I., Galli, I., Kihara, F., Tamai, K., Miyajima, N., Iguchi-Ariga, S. M.** and **Ariga, H.**, *Identification and cDNA cloning of single-stranded DNA binding proteins that interact with the region upstream of the human c-myc gene.*, Oncogene, Vol. 9, No. 4, pp. 1133–1143, Apr 1994.
- [311] **Niki, T., Galli, I., Ariga, H.** and **Iguchi-Ariga, S. M.**, *MSSP, a protein binding to an origin of replication in the c-myc gene, interacts with a catalytic subunit of DNA polymerase alpha and stimulates its polymerase activity.*, FEBS Lett, Vol. 475, No. 3, pp. 209–212, Jun 2000.
- [312] **Niki, T., Izumi, S., Saegusa, Y., Taira, T., Takai, T., Iguchi-Ariga, S. M.** and **Ariga, H.**, *MSSP promotes ras/myc cooperative cell transforming activity by binding to c-Myc.*, Genes Cells, Vol. 5, No. 2, pp. 127–141, Feb 2000.
- [313] **Vitour, D., Lindenbaum, P., Vende, P., Becker, M. M.** and **Poncet, D.**, *RoXaN, a novel cellular protein containing TPR, LD, and zinc finger motifs, forms a ternary complex with eukaryotic initiation factor 4G and rotavirus NSP3.*, J Virol, Vol. 78, No. 8, pp. 3851–3862, Apr 2004.
- [314] **Harb, M., Becker, M. M., Vitour, D., Baron, C. H., Vende, P., Brown, S. C., Bolte, S., Arold, S. T.** and **Poncet, D.**, *Nuclear localization of cytoplasmic poly(A)-binding protein upon rotavirus infection involves the interaction of NSP3 with eIF4G and RoXaN.*, J Virol, Vol. 82, No. 22, pp. 11283–11293, Nov 2008.
- [315] **Regulski, E. E.** and **Breaker, R. R.**, *In-line probing analysis of riboswitches.*, Methods Mol Biol, Vol. 419, pp. 53–67, 2008.

- [316] **Zuker, M.**, *Mfold web server for nucleic acid folding and hybridization prediction.*, Nucleic Acids Res, Vol. 31, No. 13, pp. 3406–3415, Jul 2003.
- [317] **Collart, M. A.** and **Panasenko, O. O.**, *The Ccr4–not complex.*, Gene, Vol. 492, No. 1, pp. 42–53, Jan 2012.
- [318] **Fujita, P. A.**, **Rhead, B.**, **Zweig, A. S.**, **Hinrichs, A. S.**, **Karolchik, D.**, **Cline, M. S.**, **Goldman, M.**, **Barber, G. P.**, **Clawson, H.**, **Coelho, A.**, **Diekhans, M.**, **Dreszer, T. R.**, **Giardine, B. M.**, **Harte, R. A.**, **Hillman-Jackson, J.**, **Hsu, F.**, **Kirkup, V.**, **Kuhn, R. M.**, **Learned, K.**, **Li, C. H.**, **Meyer, L. R.**, **Pohl, A.**, **Raney, B. J.**, **Rosenbloom, K. R.**, **Smith, K. E.**, **Haussler, D.** and **Kent, W. J.**, *The UCSC Genome Browser database: update 2011.*, Nucleic Acids Res, Vol. 39, No. Database issue, pp. D876–D882, Jan 2011.
- [319] **Liu, H.**, **Zhang, S.**, **Lin, H.**, **Jia, R.** and **Chen, Z.**, *Identification of microRNA-RNA interactions using tethered RNAs and streptavidin aptamers.*, Biochem Biophys Res Commun, Vol. 422, No. 3, pp. 405–410, Jun 2012.
- [320] **Walker, S. C.**, **Scott, F. H.**, **Srisawat, C.** and **Engelke, D. R.**, *RNA affinity tags for the rapid purification and investigation of RNAs and RNA-protein complexes.*, Methods Mol Biol, Vol. 488, pp. 23–40, 2008.
- [321] **Park-Lee, S.**, **Kim, S.** and **Laird-Offringa, I. A.**, *Characterization of the interaction between neuronal RNA-binding protein HuD and AURich RNA.*, J Biol Chem, Vol. 278, No. 41, pp. 39801–39808, Oct 2003.
- [322] **Mili, S.** and **Steitz, J. A.**, *Evidence for reassociation of RNA-binding proteins after cell lysis: implications for the interpretation of immunoprecipitation analyses.*, RNA, Vol. 10, No. 11, pp. 1692–1694, Nov 2004.
- [323] **Michlewski, G.** and **Cáceres, J. F.**, *RNase-assisted RNA chromatography.*, RNA, Vol. 16, No. 8, pp. 1673–1678, Aug 2010.
- [324] **Lai, W. S.**, **Parker, J. S.**, **Grissom, S. F.**, **Stumpo, D. J.** and **Blackshear, P. J.**, *Novel mRNA targets for tristetraprolin (TTP) identified by global analysis of stabilized transcripts in TTP-deficient fibroblasts.*, Mol Cell Biol, Vol. 26, No. 24, pp. 9196–9208, Dec 2006.
- [325] **Karima, R.**, **Matsumoto, S.**, **Higashi, H.** and **Matsushima, K.**, *The molecular pathogenesis of endotoxic shock and organ failure.*, Mol Med Today, Vol. 5, No. 3, pp. 123–132, Mar 1999.
- [326] **Anderson, P.**, *Post-transcriptional regulation of tumour necrosis factor alpha production.*, Ann Rheum Dis, Vol. 59 Suppl 1, pp. i3–i5, Nov 2000.

- [327] **Shyu, A. B.** and **Wilkinson, M. F.**, *The double lives of shuttling mRNA binding proteins.*, Cell, Vol. 102, No. 2, pp. 135–138, Jul 2000.
- [328] **Wilusz, C. J.**, **Wormington, M.** and **Peltz, S. W.**, *The cap-to-tail guide to mRNA turnover.*, Nat Rev Mol Cell Biol, Vol. 2, No. 4, pp. 237–246, Apr 2001.
- [329] **Brook, M.**, **Sully, G.**, **Clark, A. R.** and **Saklatvala, J.**, *Regulation of tumour necrosis factor alpha mRNA stability by the mitogen-activated protein kinase p38 signalling cascade.*, FEBS Lett, Vol. 483, No. 1, pp. 57–61, Oct 2000.
- [330] **Goodarzi, H.**, **Najafabadi, H. S.**, **Oikonomou, P.**, **Greco, T. M.**, **Fish, L.**, **Salavati, R.**, **Cristea, I. M.** and **Tavazoie, S.**, *Systematic discovery of structural elements governing stability of mammalian messenger RNAs.*, Nature, Vol. 485, No. 7397, pp. 264–268, May 2012.
- [331] **Marzluff, W. F.**, **Wagner, E. J.** and **Duronio, R. J.**, *Metabolism and regulation of canonical histone mRNAs: life without a poly(A) tail.*, Nat Rev Genet, Vol. 9, No. 11, pp. 843–854, Nov 2008.
- [332] **Mullen, T. E.** and **Marzluff, W. F.**, *Degradation of histone mRNA requires oligouridylation followed by decapping and simultaneous degradation of the mRNA both 5' to 3' and 3' to 5'.*, Genes Dev, Vol. 22, No. 1, pp. 50–65, Jan 2008.
- [333] **Su, W.**, **Slepenkov, S. V.**, **Slevin, M. K.**, **Lyons, S. M.**, **Ziemiak, M.**, **Kowalska, J.**, **Darzynkiewicz, E.**, **Jemielity, J.**, **Marzluff, W. F.** and **Rhoads, R. E.**, *mRNAs containing the histone 3' stem-loop are degraded primarily by decapping mediated by oligouridylation of the 3' end.*, RNA, Vol. 19, No. 1, pp. 1–16, Jan 2013.
- [334] **Hoefig, K. P.**, **Rath, N.**, **Heinz, G. A.**, **Wolf, C.**, **Dameris, J.**, **Schepers, A.**, **Kremmer, E.**, **Ansel, K. M.** and **Heissmeyer, V.**, *Eri1 degrades the stem-loop of oligouridylated histone mRNAs to induce replication-dependent decay.*, Nat Struct Mol Biol, Vol. 20, No. 1, pp. 73–81, Jan 2013.
- [335] **Aviv, T.**, **Lin, Z.**, **Lau, S.**, **Rendl, L. M.**, **Sicheri, F.** and **Smibert, C. A.**, *The RNA-binding SAM domain of Smaug defines a new family of post-transcriptional regulators.*, Nat Struct Biol, Vol. 10, No. 8, pp. 614–621, Aug 2003.
- [336] **Gong, C.** and **Maquat, L. E.**, *lncRNAs transactivate STAU1-mediated mRNA decay by duplexing with 3' UTRs via Alu elements.*, Nature, Vol. 470, No. 7333, pp. 284–288, Feb 2011.
- [337] **Kim, Y. K.**, **Furic, L.**, **Desgroseillers, L.** and **Maquat, L. E.**,

- Mammalian Staufen1 recruits Upf1 to specific mRNA 3'UTRs so as to elicit mRNA decay.*, Cell, Vol. 120, No. 2, pp. 195–208, Jan 2005.
- [338] **Iwasaki, H., Takeuchi, O., Teraguchi, S., Matsushita, K., Uehata, T., Kuniyoshi, K., Satoh, T., Saitoh, T., Matsushita, M., Standley, D. M. and Akira, S.**, *The I β B kinase complex regulates the stability of cytokine-encoding mRNA induced by TLR-IL-1R by controlling degradation of regnase-1.*, Nat Immunol, Vol. 12, No. 12, pp. 1167–1175, Dec 2011.
- [339] **Rouault, T. A.**, *The role of iron regulatory proteins in mammalian iron homeostasis and disease.*, Nat Chem Biol, Vol. 2, No. 8, pp. 406–414, Aug 2006.
- [340] **Muckenthaler, M. U., Galy, B. and Hentze, M. W.**, *Systemic iron homeostasis and the iron-responsive element/iron-regulatory protein (IRE/IRP) regulatory network.*, Annu Rev Nutr, Vol. 28, pp. 197–213, 2008.
- [341] **Hentze, M. W., Muckenthaler, M. U., Galy, B. and Camaschella, C.**, *Two to tango: regulation of Mammalian iron metabolism.*, Cell, Vol. 142, No. 1, pp. 24–38, Jul 2010.
- [342] **Mandal, M. and Breaker, R. R.**, *Gene regulation by riboswitches.*, Nat Rev Mol Cell Biol, Vol. 5, No. 6, pp. 451–463, Jun 2004.
- [343] **Wilkinson, K. A., Merino, E. J. and Weeks, K. M.**, *Selective 2'-hydroxyl acylation analyzed by primer extension (SHAPE): quantitative RNA structure analysis at single nucleotide resolution.*, Nat Protoc, Vol. 1, No. 3, pp. 1610–1616, 2006.
- [344] **Spitale, R. C., Crisalli, P., Flynn, R. A., Torre, E. A., Kool, E. T. and Chang, H. Y.**, *RNA SHAPE analysis in living cells.*, Nat Chem Biol, Vol. 9, No. 1, pp. 18–20, Jan 2013.
- [345] **Lucks, J. B., Mortimer, S. A., Trapnell, C., Luo, S., Aviran, S., Schroth, G. P., Pachter, L., Doudna, J. A. and Arkin, A. P.**, *Multiplexed RNA structure characterization with selective 2'-hydroxyl acylation analyzed by primer extension sequencing (SHAPE-Seq).*, Proc Natl Acad Sci U S A, Vol. 108, No. 27, pp. 11063–11068, Jul 2011.
- [346] **Shu, Z. and Bevilacqua, P. C.**, *Isolation and characterization of thermodynamically stable and unstable RNA hairpins from a triloop combinatorial library.*, Biochemistry, Vol. 38, No. 46, pp. 15369–15379, Nov 1999.
- [347] **Ji, Y. R., Kim, H. J., Yu, D. H., Bae, K. B., Park, S. J., Yi, J. K., Kim, N., Park, S. J., Oh, K. B., Hwang, S. S., Lee,**

- S., Kim, S.-H., Kim, M. O., Lee, J. W. and Ryoo, Z. Y.**, *Enforced expression of roquin protein in T cells exacerbates the incidence and severity of experimental arthritis.*, J Biol Chem, Vol. 287, No. 50, pp. 42269–42277, Dec 2012.
- [348] **Han, J. H., Beutler, B. and Huez, G.**, *Complex regulation of tumor necrosis factor mRNA turnover in lipopolysaccharide-activated macrophages.*, Biochim Biophys Acta, Vol. 1090, No. 1, pp. 22–28, Aug 1991.
- [349] **Raabe, T., Bukrinsky, M. and Currie, R. A.**, *Relative contribution of transcription and translation to the induction of tumor necrosis factor- α by lipopolysaccharide.*, J Biol Chem, Vol. 273, No. 2, pp. 974–980, Jan 1998.
- [350] **Carballo, E., Lai, W. S. and Blackshear, P. J.**, *Evidence that tristetraprolin is a physiological regulator of granulocyte-macrophage colony-stimulating factor messenger RNA deadenylation and stability.*, Blood, Vol. 95, No. 6, pp. 1891–1899, Mar 2000.
- [351] **Chekulaeva, M., Mathys, H., Zipprich, J. T., Attig, J., Colic, M., Parker, R. and Filipowicz, W.**, *miRNA repression involves GW182-mediated recruitment of CCR4-NOT through conserved W-containing motifs.*, Nat Struct Mol Biol, Vol. 18, No. 11, pp. 1218–1226, Nov 2011.
- [352] **Fabian, M. R., Cieplak, M. K., Frank, F., Morita, M., Green, J., Srikumar, T., Nagar, B., Yamamoto, T., Raught, B., Duchaine, T. F. and Sonenberg, N.**, *miRNA-mediated deadenylation is orchestrated by GW182 through two conserved motifs that interact with CCR4-NOT.*, Nat Struct Mol Biol, Vol. 18, No. 11, pp. 1211–1217, Nov 2011.
- [353] **Teixeira, D., Sheth, U., Valencia-Sanchez, M. A., Brengues, M. and Parker, R.**, *Processing bodies require RNA for assembly and contain nontranslating mRNAs.*, RNA, Vol. 11, No. 4, pp. 371–382, Apr 2005.
- [354] **Arlt, A. and Schäfer, H.**, *Role of the immediate early response 3 (IER3) gene in cellular stress response, inflammation and tumorigenesis.*, Eur J Cell Biol, Vol. 90, No. 6-7, pp. 545–552, 2011.
- [355] **Renner, F. and Schmitz, M. L.**, *Autoregulatory feedback loops terminating the NF- κ B response.*, Trends Biochem Sci, Vol. 34, No. 3, pp. 128–135, Mar 2009.
- [356] **Stoecklin, G., Tenenbaum, S. A., Mayo, T., Chittur, S. V., George, A. D., Baroni, T. E., Blackshear, P. J. and Anderson,**

- P.**, *Genome-wide analysis identifies interleukin-10 mRNA as target of tristetraprolin.*, J Biol Chem, Vol. 283, No. 17, pp. 11689–11699, Apr 2008.
- [357] **Xu, N., Loffin, P., Chen, C. Y. and Shyu, A. B.**, *A broader role for AU-rich element-mediated mRNA turnover revealed by a new transcriptional pulse strategy.*, Nucleic Acids Res, Vol. 26, No. 2, pp. 558–565, Jan 1998.
- [358] **Winkler, G. S., Mulder, K. W., Bardwell, V. J., Kalkhoven, E. and Timmers, H. T. M.**, *Human Ccr4-Not complex is a ligand-dependent repressor of nuclear receptor-mediated transcription.*, EMBO J, Vol. 25, No. 13, pp. 3089–3099, Jul 2006.
- [359] **Rothbauer, U., Zolghadr, K., Muyldermans, S., Schepers, A., Cardoso, M. C. and Leonhardt, H.**, *A versatile nanotrap for biochemical and functional studies with fluorescent fusion proteins.*, Mol Cell Proteomics, Vol. 7, No. 2, pp. 282–289, Feb 2008.
- [360] **Ryder, S. P., Recht, M. I. and Williamson, J. R.**, *Quantitative analysis of protein-RNA interactions by gel mobility shift.*, Methods Mol Biol, Vol. 488, pp. 99–115, 2008.

5 Supplemental Data

5.1 Supplemental Figures

The following supplemental figures include data that support and complete the data shown in the Results.

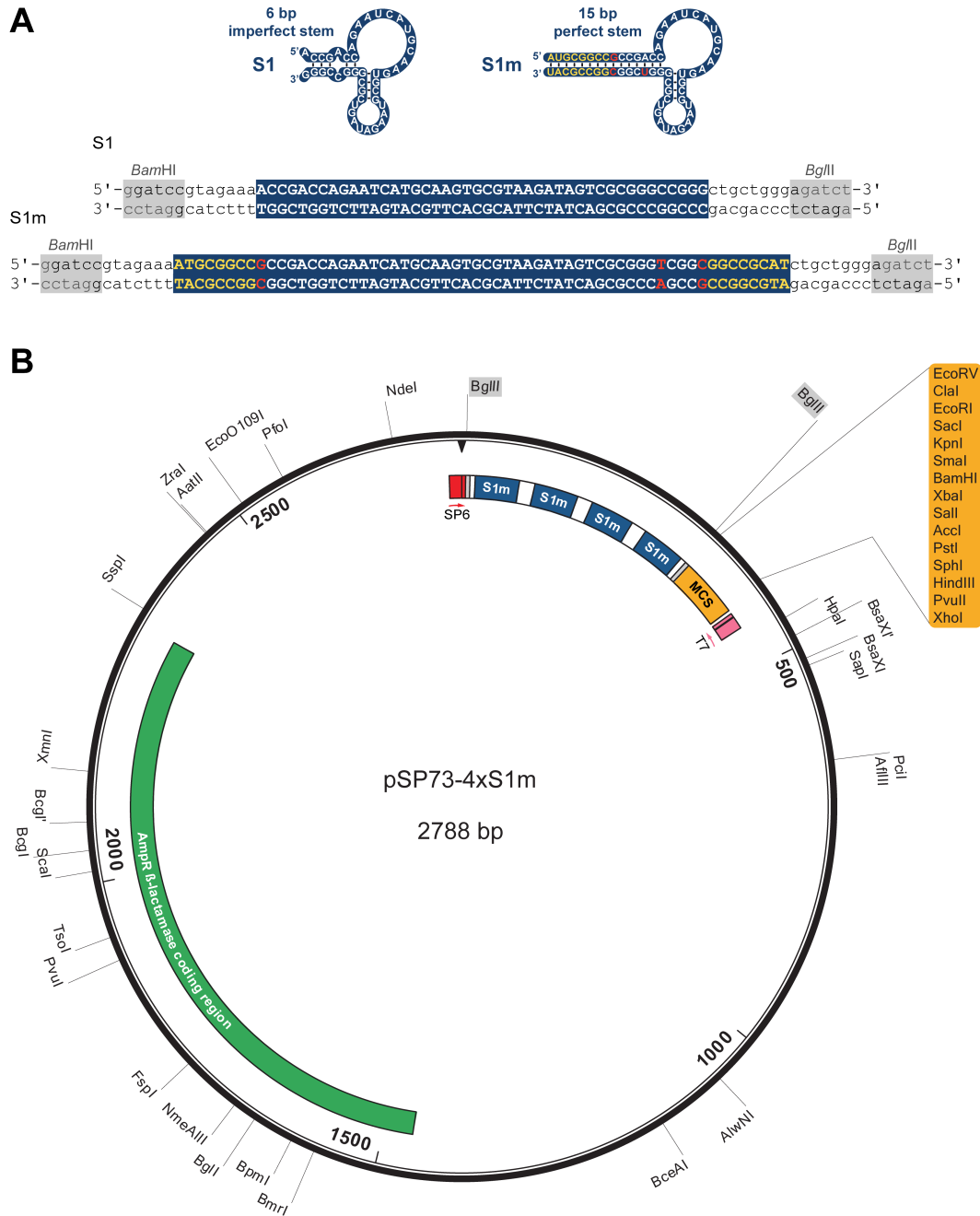


Figure 5.1: S1m Sequence and pSP73-4xS1m Plasmid Map. (A) Sequence of the S1 and S1m aptamers as designed for cloning of tandem repeats. Linear sequences are shown below the predicted secondary structures. Nucleotides mutated in S1m (red), nucleotides added to prolong the stem (yellow), core aptamer (blue). (B) Plasmid map of pSP73-4xS1m (p2880) used for *in vitro* transcription of RNA for S1m-mediated RNP purification. The plasmid was linearized with *EcoRV* downstream of the 3' *BglII* site, column-purified and used as template for run-off transcription by SP6. Alternatively, the template was excised by *NdeI/EcoRV* digest and gel-purified. 4xS1m can be excised with *BglII*. Reproduced with permission from Nucleic Acids Research, Oxford Journals.

5.1 Supplemental Figures

pSP73-4xS1m plasmid sequence (nt 1-2788)

```

GAACCagatctgtagaaaATGCGGCCGCCGACCAGAATCATGCAAGTGCCTAAGATAGTCGCGGGTCGGCG
GCCGCATctgctgggagatccgtagaaaATGCGGCCGCCGACCAGAATCATGCAAGTGCCTAAGATAGTCG
CGGGTCGGCGGCCGCATctgctgggagatccgtagaaaATGCGGCCGCCGACCAGAATCATGCAAGTGCCT
AAGATAGTCGCGGGTCGGCGGCCGCATctgctgggagatccgtagaaaATGCGGCCGCCGACCAGAATCAT
GCAAGTGCCTAAGATAGTCGCGGGTCGGCGGCCGCATctgctgggagatctGATATCATCGATGAATTCCA
GCTCGGTACCCGGGGATCCTCTAGAGTCGACCTGCAGGCATGCAAGCTTCAGCTGCTCGAGGCCGGTCTCC
CTATAGTGAGTCGTATTAATTTTCGATAAGCCAGGTTAACCTGCATTAATGAATCGGCCAACGCGCGGGGAG
AGGGGTTTTGCGTATTGGGCGCTCTTCCGCTTCCTCGCTCACTGACTCGCTGCGCTCGGTTCGTTCCGCTGC
GGCGAGCGGTATCAGCTCACTCAAAGGCGGTAATACGGTTATCCACAGAATCAGGGGATAACGCAGGAAAG
AACATGTGAGCAAAAGGCCAGCAAAAGGCCAGAACCGTAAAAAGGCCGCGTTGCTGGCGTTTTTCCATAG
GCTCCGCCCCCTGACGAGCATCACAAAAATCGACGCTCAAGTCAGAGGTGGCGAAACCCGACAGGACTAT
AAAGATACCAGGCGTTTTCCCTTGGAAAGCTCCCTCGTGCCTCTCCTGTTCCGACCCGTCGCTTACCGGA
TACCTGTCCGCTTTCTCCCTTCGGGAAGCGTGGCGCTTCTCATAGCTCAGCTGTAGGTATCTCAGTTT
GGTGTAGTTCGTTTCGCTCAAGCTGGGCTGTGTGCACGACCCCGGTCAGCCCCGACCCGCTCGCGTTT
CCGGTAACTATCGTCTTGGTCCAACCCGGTAAGACACGACTTATCGCCACTGGCAGCAGCCACTGGTAAC
AGGATTAGCAGAGCGAGGTATGTAGGCGGTGCTACAGAGTCTTGAAGTGGTGGCCTAACTACGGCTACAC
TAGAAGAACAGTATTTGGTATCTGCGCTCTGCTGAAGCCAGTTACCTTCGAAAAAGAGTTGGTAGCTCTT
GATCCGGCAAAACAAACCACCGCTGGTAGCGGTGTTTTTTTTGTTTGAAGCAGCAGATTACGCGCAGAAAA
AAAGGATCTCAAGAAGATCCTTTGATCTTTTCTACGGGGTCTGACGCTCAGTGGAACGAAAACTCACGTTA
AGGGATTTTGGTTCATGAGATTATCAAAAAGGATCTTACCTAGATCCTTTTAAATTAATAAATGAAGTTTTA
AATCAATCTAAAGTATATATGAGTAACTTGGTCTGACAGTTACCAATGCTTAATCAGTGAGGCACCTATC
TCAGCGATCTGTCTATTTTCGTTTCATCCATAGTTGCCTGACTCCCCGTCGTGTAGATAAATCAGATAACGGGA
GGGCTTACCATCTGGCCCCAGTGTGCAATGATACCGCGAGACCCACGCTCACCGGCTCCAGATTTATCAG
CAATAAACAGCCAGCCGGAAGGGCCGAGCGCAGAAGTGGTCTTCAACTTTATCCGCCTCCATCCAGTCT
ATTAATTGTTGCCGGGAAGCTAGAGTAAGTAGTTGCCAGTTAATAGTTTGCAGCAACGTTGTTGCCATTGC
TACAGGCATCGTGGTGTACGCTCGTCTGTTGGTATGGCTTCATTACGCTCCCGTTCCCAACGATCAAGGC
GAGTTACATGATCCCCATGTTGTGCAAAAAAGCGGTTAGCTCCTTCGGTCCCTCCGATCGTTGTCAGAAGT
AAGTTGGCCGCGAGTGTATCACTCATGGTTATGGCAGCACTGCATAATTTCTTACTGTCAATGCCATCCGT
AAGATGCTTTTCTGTGACTGGTGTGACTCAACCAAGTCATTCTGAGAATAGTGTATGCGGGCAGCGAGTT
GCTCTTGCCCGCGTCAATACGGGATAATACCCGCCACATAGCAGAACTTAAAGTGCATCATTGGA
AAACGTTCTTCGGGGCGAAAACTCTCAAGGATCTTACCGCTGTTGAGATCCAGTTCGATGTAACCCACTCG
TGCACCAACTGATCTTACGATCTTTTACTTTACCAGCGTTTCTGGGTGAGCAAAAAACAGGAAGGCAAAA
ATGCCCAAAAAAGGGAATAAGGGCGACACGGAATGTTGAATACTCATACTCTTCTTTTCAATATTAT
TGAAGCATTTATCAGGGTTATGTCTCATGAGCGGATACATATTTGAATGTATTTAGAAAAATAAACAAAT
AGGGGTTCCGCGCACATTTCCCGAAAAGTGCCACCTGACGCTTAAGAAACCATTATTATCATGACATTAA
CCTATAAAAAATAGGCGTATCAGGAGCCCTTTCGCTCGCGCGTTTCGGTGTGACGGTGAACCCCTCTGA
CACATGCAGCTCCCGGAGACGGTACAGCTTGTCTGTAAGCGGATGCCGGGAGCAGACAAGCCCGTCAGGG
CGCGTCAGCGGGTGTGGCGGGTGTGGGGCTGGCTTAACTATGCGGCATCAGAGCAGATTGTACTGAGAG
TGCACCATATGGACATATTGTCGTTAGAACGGCTACAATTAATACATAACCTTATGTATCATACACATA
CGATTAGGTGACACTATA

```

SP6 promoter
BglII-site
4xS1m aptamer repeats with spacers
BamHI/BglII-fusion site
Multiple Cloning Site
T7 promoter
β-lactamase coding region (AmpR)

Figure 5.2: Sequence of the pSP73-4xS1m Plasmid. The four S1m aptamer sequences, separated by 21 nt long spacers, are highlighted in dark blue. The SP6 promoter is marked in red, *BglII* sites in grey, *BamHI/BglII* fusion sites in light blue, the multi cloning sequence in yellow, the T7 promoter in pink, and the β-lactamase coding region in green. Reproduced with permission from Nucleic Acids Research, Oxford Journals.

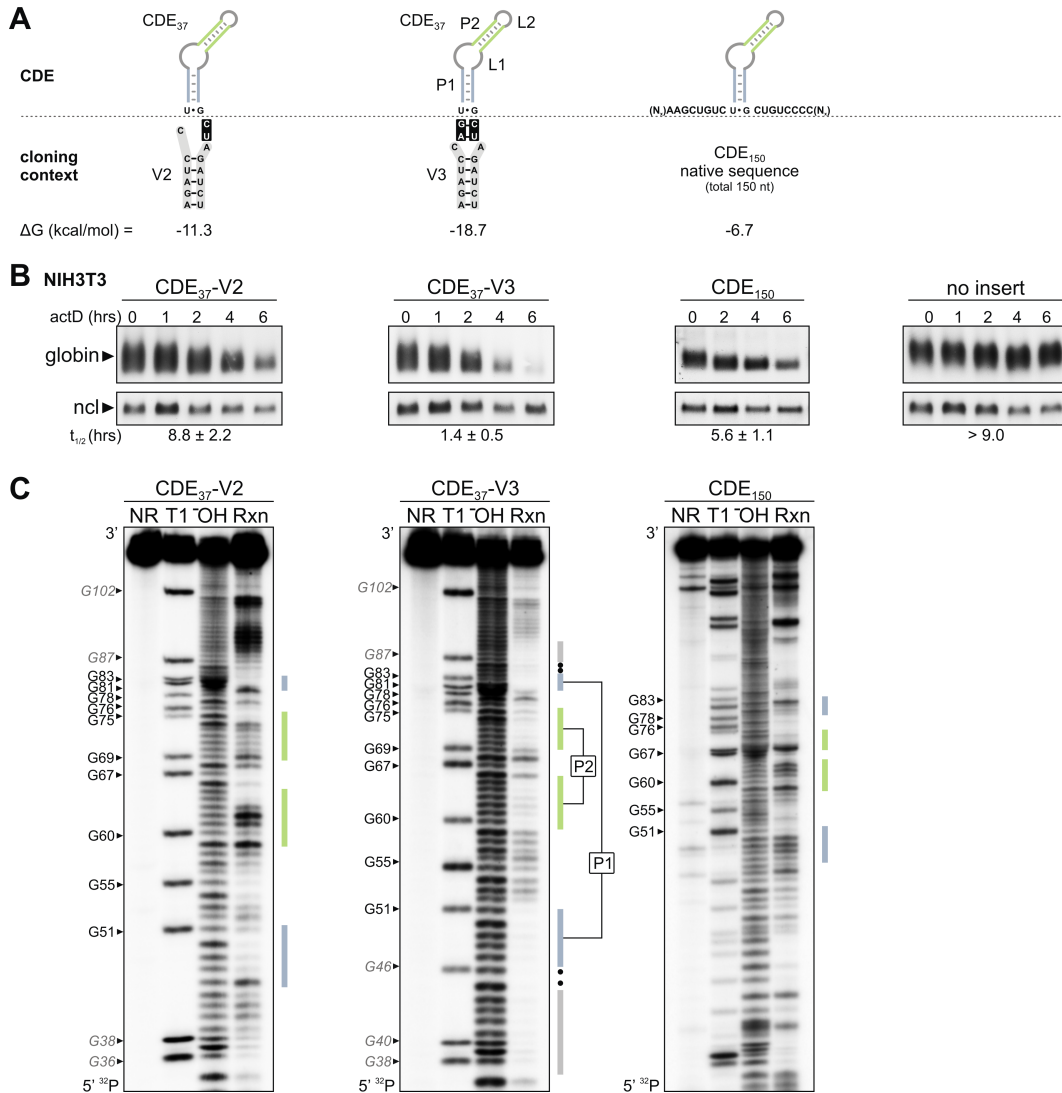


Figure 5.3: Secondary Structure Determination and Comparison of TNF α CDE Variants. (A) Schematic representation of mouse TNF α CDE₃₇ variants V2 and V3, which differ only in the cloning context, and CDE₁₅₀ spanning a 150 nt region of the mouse TNF α 3'UTR. The gain in free energy, ΔG , was calculated for the proposed structures at 37°C using Mfold version 3.5. (B) Globin reporter genes containing TNF α CDE₃₇ variants V2 and V3, CDE₁₅₀ and a control globin reporter lacking an insert were transiently transfected into NIH3T3 cells. Reporter mRNA degradation was measured as described for Figure 2.11D. mRNA half-lives are given as average values \pm SD, $n \geq 3$. (C) In-line probing analysis of *in vitro* synthesized, 5'-³²P-labeled CDE₃₇-V2, CDE₃₇-V3 and CDE₁₅₀ RNAs. The RNAs were either loaded directly (NR, no reaction), subjected to cleavage by RNase T1 or alkaline hydrolysis (-OH), or incubated for 45 hours at room temperature and pH 8.3 (in-line reaction, Rxn) prior to urea-PAGE. The in-line analysis was performed by Ming Hammond. Reproduced with permission from Cell, Elsevier.

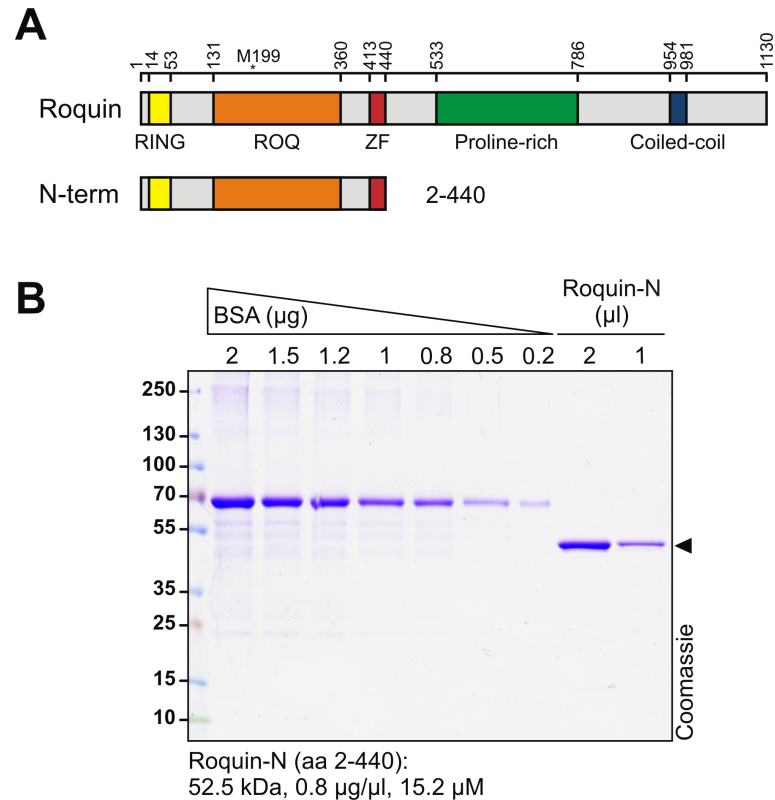


Figure 5.4: Purification of Recombinant Roquin-N. (A) Schematic representation of mouse Roquin domains; ZF, zinc finger. The sequence shows the N-terminal Roquin fragment used for purification. Numbers refer to amino acid positions. (B) Roquin-N (amino acids 2–440) was expressed as a His-tagged protein in *E. coli* and purified via nickel-Sepharose beads. To determine its purity and concentration, the protein was resolved by SDS-PAGE next to a dilution series of bovine serum albumin (BSA), and stained with Coomassie blue. Reproduced with permission from Cell, Elsevier.

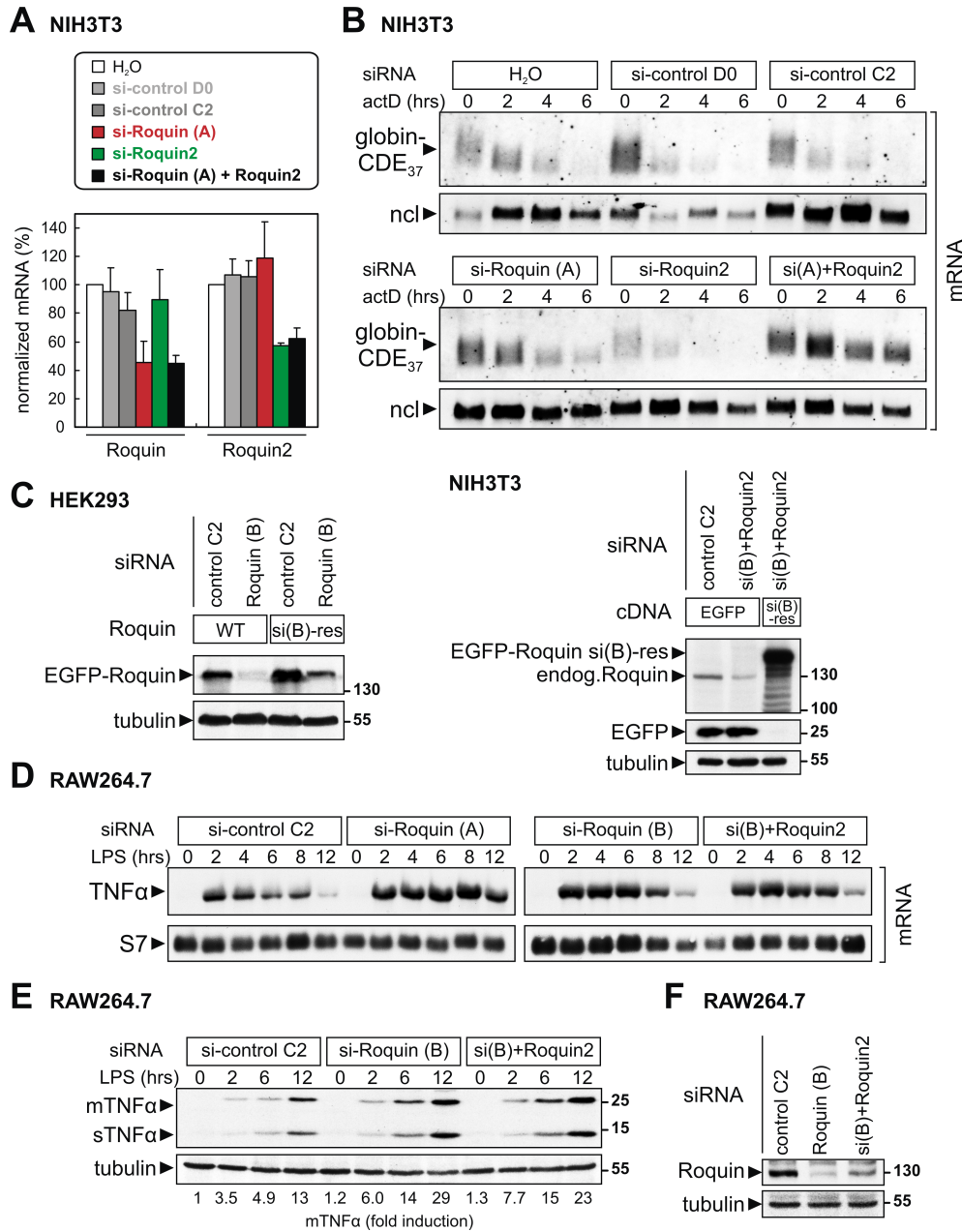


Figure 5.5: Knockdown of Roquin and Roquin2 Prevents CDE-mRNA Degradation. (A) For kd of Roquin and Roquin2, NIH3T3 cells were transfected twice over a period of four days with either water (H₂O), control siRNAs (D0 or C2), or siRNAs against Roquin (A) or Roquin2, either alone or in combination. Roquin and Roquin2 mRNA levels were measured by RT-qPCR, normalized to ncl mRNA levels, and plotted as % of the water control (average \pm SD, $n \geq 4$). (B) Roquin and Roquin2 kd in NIH3T3 cells as in A. The globin-TNF α -CDE₃₇-V3 reporter gene was included in the second transfection, and reporter mRNA decay was measured by Northern blot analysis as described for Figure 2.11D. Quantification of $n \geq 3$ repeat experiments is shown in Figure 2.9A. (Figure legend continued on next page)

5.1 Supplemental Figures

Figure legend continued: (C) Left panel, expression of EGFP-Roquin (WT) and the siRNA-resistant EGFP-Roquin si(B)-res was examined in HEK293 cells. The Roquin expressing plasmids were transfected together with the control siRNA C2 or the Roquin-siRNA (B). Cells were lysed after two days for Western blot analysis using an anti-GFP antibody. Right panel, EGFP or EGFP-Roquin-si(B)-res were transfected into NIH3T3 cells one day after transfection of the control siRNA C2 or the Roquin-siRNA (B). Cells were lysed on day two and Western blot analysis was carried out using an anti-Roquin antibody. (D) TNF α mRNA expression in response to LPS (100 ng/ml) was analyzed by Northern blot in RAW264.7 cells transfected twice over a period of two days with control siRNA (C2), Roquin-siRNA (A), Roquin-siRNA (B) or Roquin-siRNA (B) together with Roquin2-siRNA. (E) TNF α production was analyzed in RAW264.7 cells transfected twice over a period of two days with control siRNA C2, Roquin-siRNA (B) or Roquin-siRNA (B) together with Roquin2-siRNA. Cells were stimulated with LPS (100 ng/ml), and total protein was extracted after 0, 2, 6 and 12 hours. Western blot analysis using an anti-TNF α antibody shows membrane-bound (m)TNF α and soluble (s)TNF α . The first 8 lanes of this plot are the same as in Figure 2.9F. (F) Roquin expression was examined in protein lysates from cells shown in panel E by Western blot analysis. The Data in C was obtained by Fabian Pötz. Reproduced with permission from Cell, Elsevier.

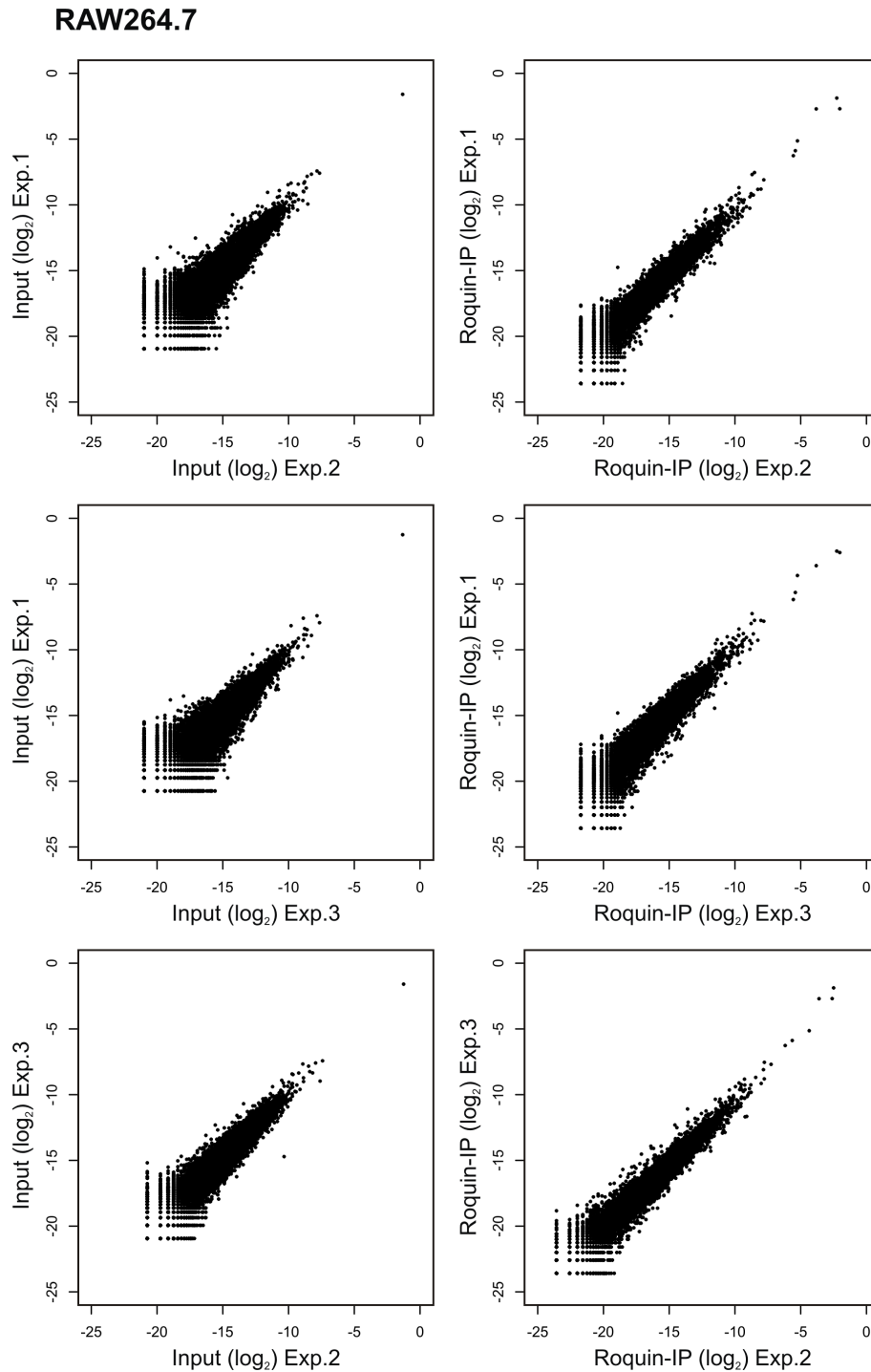
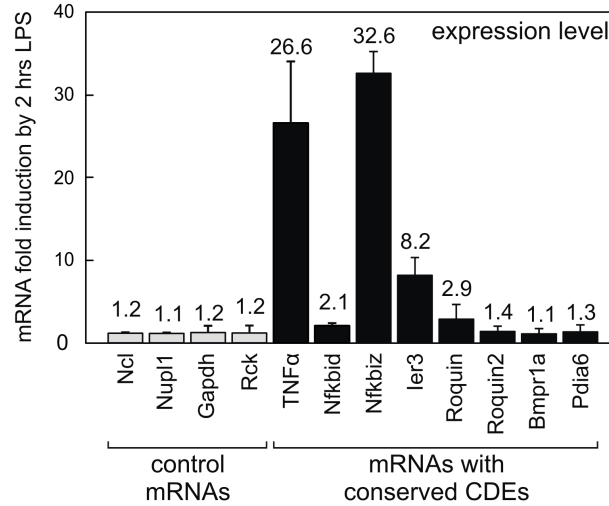


Figure 5.6: Reproducibility of Roquin-IPs for RNA-Seq. Following IP of Roquin from LPS-stimulated RAW264.7 macrophages, mRNAs in the Roquin-IP, control-IP and input material were identified by RNA-Seq in three biological repeat experiments. To assess reproducibility, log₂ of (read counts per gene / total read counts) in the Roquin-IP and input samples was plotted as a pairwise comparison between the three experiments. Analysis performed by Johanna Schott. Reproduced with permission from Cell, Elsevier.

A RAW264.7



B RAW264.7

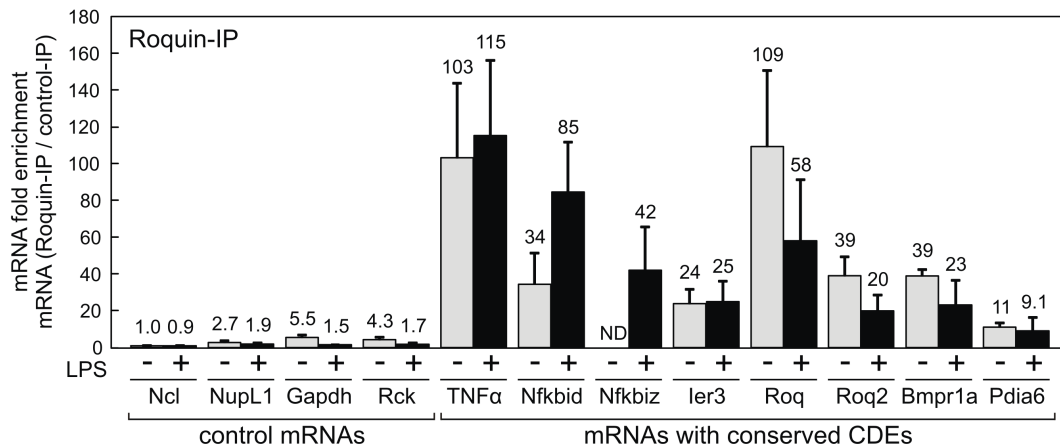


Figure 5.7: Induction of mRNAs Containing Putative CDEs and Roquin Target mRNA Validation. (A) Induction of endogenous TNF α , Nfkbid, Nfkbiz, Ier3, Roquin, Roquin2, Bmpr1a, and Pdia6 CDE-containing mRNAs in comparison to control mRNAs lacking a CDE (Ncl, NupL1, Gapdh, and Rck) in RAW264.7 macrophages stimulated for 2 hours with LPS (100 ng/ml). mRNA levels were measured by RT-qPCR and are shown relative to the mRNA levels in unstimulated cells as average values \pm SE, $n \geq 3$. (B) Binding of control mRNAs and CDE-harboring mRNAs to Roquin by RNA-IP. RAW264.7 macrophages were stimulated with LPS (100 ng/ml) for 2 hours, and Roquin was IP-ed using anti-Roquin antibodies (Roq). HA-antibody was used for control IP. mRNA amounts were quantified by RT-qPCR in the Roquin IP, divided by the amount of mRNA in the control IP, and expressed as average fold enrichment \pm SE, $n \geq 3$.

5.2 Supplemental Tables

The following supplemental tables include data that support and complete the data shown in the Results.

5.2 Supplemental Tables

Table 5.1: CDE Sequences and Globin Reporter mRNA Half-lives in NIH3T3 Cells. CDE sequences that were cloned into the β -globin reporter genes are listed together with corresponding mRNA half-lives. Reporter mRNA decay was measured in transiently transfected NIH3T3 cells or, where indicated by an asterisk, in stably transfected NIH3T3 cells. Reproduced with permission from Cell, Elsevier.

Construct	Sequence	$t_{1/2} \pm SD$ (hrs)	n
TNF α -CDE ₃₇ -V2	AGATCCTTCAGACAGACATGTTTTCTGTGAAAACGGAGCTGAGCTAGATCT	8.8 \pm 2.2	3
TNF α -CDE ₃₇ -V3	AGATCCAGTTCAGACAGACATGTTTTCTGTGAAAACGGAGCTGAGCTAGATCT	1.4 \pm 0.5	7
human TNF α -CDE ₃₇ -V3	AGATCCCTGTTGGCTCAGACATGTTTTCCGTGAAAACGGAGCTGAAACAAGATCT	2.0 \pm 0.7	3
TNF α -CDE ₃₇ -V3-M1	AGATCCAGTTCAGAG-----TTTTCTGTGAAAACGGAGCTGAGCTAGATCT	> 9.0*	1
TNF α -CDE ₃₇ -V3-M2	AGATCCAGTTCAGACAGACATGTTTT-----GCTGAGCTAGATCT	> 9.0*	2
TNF α -CDE ₃₇ -V3-M3	AGATCCAGTAGTGACAGACATGTTTTCTGTGAAAACGGAGCTGAGCTAGATCT	1.5 \pm 0.1	3
TNF α -CDE ₃₇ -V3-M4	AGATCCAGTTCAGACAGACATGTTTTCTGTGAAAACGGAGCAGCTAGATCT	2.5 \pm 0.3	3
TNF α -CDE ₃₇ -V3-M5	AGATCCAGTAGTGACAGACATGTTTTCTGTGAAAACGGAGCAGCTAGATCT	1.1*	2
TNF α -CDE ₃₇ -V3-M6	AGATCCAGTTCAGAGTGACATGTTTTCTGTGAAAACGGAGCTGAGCTAGATCT	1.4 \pm 0.4	3
TNF α -CDE ₃₇ -V3-M7	AGATCCAGTTCAGACAGACAAGTTTTCTGTGAAAACGGAGCTGAGCTAGATCT	> 9.0	3
TNF α -CDE ₃₇ -V3-M8	AGATCCAGTTCAGAGTGACAAGTTTTCTGTGAAAACGGAGCTGAGCTAGATCT	> 9.0*	2
TNF α -CDE ₃₇ -V3-M9	AGATCCAGTTCAGACAGACATGTTTTAGGCTGAAAACGGAGCTGAGCTAGATCT	> 9.0	4
TNF α -CDE ₃₇ -V3-M10	AGATCCAGTTCAGACAGACATGTTTTCTGTGAAAACCTCTGCTGAGCTAGATCT	> 9.0*	1
TNF α -CDE ₃₇ -V3-M11	AGATCCAGTTCAGACAGACATGTTTTAGGCTGAAAACCTCTGCTGAGCTAGATCT	> 9.0*	1
TNF α -CDE ₃₇ -V3-M12	AGATCCAGTTCAGACAGACATGTTTTCTGTGAAAACGCTGCTGAGCTAGATCT	1.3 \pm 0.2	3
TNF α -CDE ₃₇ -V3-M13	AGATCCAGTTCAGACAGACATGTTTTAGTGTGAAAACGCTGCTGAGCTAGATCT	> 9.0	2
TNF α -CDE ₃₇ -V3-M14	AGATCCAGTTCAGACAGACATGTTTTCTGTGAAAACCTGAGCTGAGCTAGATCT	> 9.0	5
TNF α -CDE ₃₇ -V3-M15	AGATCCAGTTCAGACAGACATGTTTTCTGCTGAAAACCTGAGCTGAGCTAGATCT	> 9.0	2
TNF α -CDE ₃₇ -V3-M16	AGATCCAGTTCAGACAGACATGTTTTCTGTGAAAACGGAGCTGAGCTAGATCT	> 9.0	5
TNF α -CDE ₃₇ -V3-M17	AGATCCAGTTCAGACAGACATGTTTTCTGAGAAAACGGAGCTGAGCTAGATCT	> 9.0	2
TNF α -CDE ₃₇ -V3-M18	AGATCCAGTTCAGACAGAGTGTGTTTTCTGTGAAAACGGAGCTGAGCTAGATCT	2.0 \pm 0.7	3
TNF α -CDE ₃₇ -V3-M19	AGATCCAGTTCAGACAGACATCATTTTTCTGTGAAAACGGAGCTGAGCTAGATCT	> 9.0	3
TNF α -CDE ₃₇ -V3-M20	AGATCCAGTTCAGACAGACATCATTTTTCTGTGAAAACGGAGCTGAGCTAGATCT	2.7 \pm 0.8	5
TNF α -CDE ₃₇ -V3-M21	AGATCCAGTTCAGACAGACATGTTTTAGTGTGAAAACGGAGCTGAGCTAGATCT	> 9.0	3
TNF α -CDE ₃₇ -V3-M22	AGATCCAGTTCAGACAGACATGTTTTCTGTGCTAAACGGAGCTGAGCTAGATCT	> 9.0	4
TNF α -CDE ₃₇ -V3-M23	AGATCCAGTTCAGACAGACATGTTTTAGTGTCTAAACGGAGCTGAGCTAGATCT	> 9.0	4
TNF α -CDE ₃₇ -V3-M24	AGATCCAGTTCAGACAGACATGTTTTCTATGAAAACGGAGCTGAGCTAGATCT	2.2 \pm 0.4	4
TNF α -CDE ₃₇ -V3-M25	AGATCCAGTTCAGACAGACATGTTTTCTACA GAAAACGGAGCTGAGCTAGATCT	> 9.0	4
TNF α -CDE ₃₇ -V3-M26	AGATCCAGTTCAGACAGACATGATTTCTGTGAAATACGGAGCTGAGCTAGATCT	5.0 \pm 0.8	3
TNF α -CDE ₃₇ -V3-M27	AGATCCAGTTCAGACAGACATGTTATCTGTGAAATACGGAGCTGAGCTAGATCT	> 9.0	3
TNF α -CDE ₁₇ -ds	AGATCCAGTGTGTTTTCTGTGAAAACGGCTAGATCT	> 9.0	3
TNF α -CDE ₁₇ -ss	TCTAGATGTTTTCTGTGAAAACGACCGGT	1.1 \pm 0.4	5
ICOS-CDE ₁₇ -ss	TCTAGAAAATTTCTGTGAAATAAACCGGT	4.8 \pm 2.5	4
TNF α -CDE ₁₅₀	AGATCCTTTGGAAGCCGGGGTGTCTTGAGGACCCAGTGTGGGAAGCTGCTTTCAGACAG ACATGTTTTCTGTGAAAACGGAGCTGAGCTGTCCCACCTGGCCTCTCTACCTTGTTCCT CCTCTTTGCTTATGTTTAAACAAAATATTTATAGATCT	5.6 \pm 1.1	3
TNF α -CDE ₁₅₀ -M16	AGATCCTTTGGAAGCCGGGGTGTCTTGAGGACCCAGTGTGGGAAGCTGCTTTCAGACAG ACATGTTTTCTGTGAAAACGGAGCTGAGCTGTCCCACCTGGCCTCTCTACCTTGTTCCT CCTCTTTGCTTATGTTTAAACAAAATATTTATAGATCT	> 9.0	3
TNF α -CDE ₁₅₀ -M20	AGATCCTTTGGAAGCCGGGGTGTCTTGAGGACCCAGTGTGGGAAGCTGCTTTCAGACAG ACATCATTTCTGTGAAAACGGAGCTGAGCTGTCCCACCTGGCCTCTCTACCTTGTTCCT CCTCTTTGCTTATGTTTAAACAAAATATTTATAGATCT	5.6 \pm 2.5	3

XXX CDE sequence
 XXX nucleotides introduced into cloning context
 XXX mutation
 --- deletion
 XXX cloning sites
 XXX flanking TNF α 3'UTR sequence in CDE₁₅₀
 XXX primer sites
 * mRNA half-lives determined upon stable transfection

Table 5.2: mRNAs Significantly Enriched by Roquin-IP. RNA was extracted after IP of endogenous Roquin from RAW264.7 macrophages and subjected to RNA-Seq in three biological replicates. Beads alone served as control-IP. The table shows all mRNAs significantly enriched by Roquin-IP ($p \leq 0.005$, Roquin-IP vs control-IP) and fold enrichment (Roquin-IP / control-IP) > 8.0 . Reproduced with permission from Cell, Elsevier.

Name	GeneID	CDE	p-value (Roquin-IP vs control-IP)	fold enrichment (Roquin-IP / control-IP)	fold enrichment (Roquin-IP / Input)
Nfkbid	243910	3'UTR, conserved (2)	2.1E-32	475.1	172.1
Tnf (TNF α)	21926	3'UTR, conserved	1.1E-09	191.8	120.2
Irf4	16364	–	1.7E-15	179.2	69.2
Gm527	217648	–	5.3E-20	179.0	114.0
D5Erttd579e	320661	ORF (2)	3.7E-36	112.4	131.1
Rc3h1 (Roquin)	381305	3'UTR, conserved	1.8E-32	99.8	71.4
Tcf7l2	21416	–	6.7E-21	76.4	68.2
Csf3 (G-CSF)	12985	–	2.3E-03	72.8	45.4
Id1	15901	–	2.3E-04	71.6	122.2
Slc39a14	213053	–	8.6E-05	67.1	34.0
Zfp408	381410	–	4.6E-24	59.1	62.1
Calcr1	54598	–	7.3E-06	58.0	32.8
Rc3h2 (Roquin2)	319817	3'UTR, conserved	6.0E-16	44.2	27.3
Ptger4	19219	–	8.0E-16	41.7	22.7
Ptpre	19267	–	4.6E-17	41.4	24.5
Id3	15903	–	2.1E-23	40.7	52.0
Mgat5	107895	–	5.8E-11	40.7	19.4
Adamts1	11504	–	2.3E-05	39.1	40.3
Clk1	12747	–	4.7E-19	33.4	6.3
Nfkbi2	80859	3'UTR, conserved	4.9E-07	32.7	33.6
Ap1g1	11765	–	1.5E-09	31.7	29.8
Usp53	99526	–	6.4E-18	29.2	15.4
B630005N14Rik	101148	–	1.2E-16	29.1	30.6
Map3k8	26410	–	1.5E-16	28.2	16.4
Id2	15902	–	4.1E-03	27.7	13.2
Pex1	71382	–	1.1E-09	26.8	17.2
Smek2	104570	–	4.3E-16	26.5	14.0
4732418C07Rik	230648	–	1.0E-19	26.1	28.3
Bmpr1a	12166	3'UTR, conserved	1.5E-16	26.1	22.5
Icos	54167	3'UTR, conserved	1.7E-05	25.0	13.1
Zbtb43	71834	–	7.4E-15	24.5	18.5
Ier3	15937	3'UTR, conserved	8.1E-04	24.0	30.6
Fbxo33	70611	–	1.9E-17	22.2	16.5
Pik3ca	18706	–	2.5E-05	21.7	20.4
Rybp	56353	–	6.4E-13	21.6	21.9
Tigd5	105734	–	1.1E-03	21.2	31.2
Ss18l1	269397	–	4.7E-05	21.1	5.2
Lfng	16848	–	5.6E-08	19.7	17.5
Pptc7	320717	–	4.1E-06	19.1	25.3
Rsf1	233532	–	1.8E-13	17.1	10.1
Lysmd4	75099	–	2.4E-03	16.8	5.4
Mlec	109154	–	4.7E-08	16.8	20.9
Fam160b1	226252	–	3.2E-13	16.5	11.0
D030056L22Rik	225995	–	7.9E-04	15.8	23.5
Sec24c	218811	–	2.5E-15	15.8	13.8
Tmem2	83921	–	4.6E-09	15.7	5.3
5830415F09Rik	74753	–	1.3E-09	15.1	19.8
Cenpf	108000	–	1.4E-03	15.0	7.3
Etaa1	68145	–	1.1E-12	14.8	11.5
Nedd1	17997	–	4.4E-13	14.8	10.5
Ipo11	76582	ORF (2)	9.3E-05	14.7	8.7

5.2 Supplemental Tables

Ppan	235036	–	5.1E-06	14.7	13.1
Ppp1r10	52040	3'UTR, conserved	2.1E-05	14.5	13.7
Tm2d3	68634	–	2.2E-03	14.5	11.6
Ndst2	17423	–	3.2E-12	14.3	14.8
Slc35e3	215436	–	3.6E-07	13.4	11.3
Prr3	75210	3'UTR, conserved	5.6E-13	13.1	32.8
Agbl3	76223	–	1.2E-03	13.0	11.0
Msl2	77853	–	5.4E-06	12.4	12.4
Hinfp	102423	–	9.9E-09	12.3	6.9
Kctd6	71393	–	7.0E-08	11.9	33.3
Nuf2	66977	–	1.7E-12	11.9	6.8
Cgrrf1	68755	–	2.0E-07	11.8	7.8
Rbm33	381626	–	7.4E-12	11.2	7.8
Aggf1	66549	3'UTR, conserved	3.7E-05	11.2	14.8
Pole2	18974	ORF	2.2E-06	11.0	10.4
Pap0lg	216578	–	2.3E-10	11.0	8.1
Tfap4	83383	–	9.2E-06	10.7	5.9
Fam76b	72826	–	1.3E-04	10.7	5.3
Cdc7	12545	–	5.3E-09	10.6	7.6
2410042D21Rik	72425	–	5.0E-08	10.4	12.2
Dnajc10	66861	–	1.8E-03	10.4	6.6
Cdon	57810	–	4.0E-03	10.3	4.5
Ap1s3	676051	–	2.1E-03	10.0	11.3
Nfxl1	100978	–	1.6E-08	9.9	7.9
Sacm11	83493	–	7.3E-11	9.8	8.7
Zfp367	238673	–	1.8E-10	9.5	7.5
Hcst	23900	–	4.4E-05	9.4	9.4
Dcun1d1	114893	–	6.4E-06	9.3	5.8
Fbxo11	225055	3'UTR, conserved	8.8E-09	9.3	5.7
B4galt5	56336	ORF	7.4E-10	8.9	10.4
Mthfd2	17768	–	1.6E-10	8.9	13.0
Mrps33	14548	–	4.4E-08	8.8	6.2
Rbbp5	213464	3'UTR, conserved	2.9E-08	8.8	7.7
Ube2q2	109161	–	1.6E-06	8.7	7.2
0610030E20Rik	68364	–	1.9E-08	8.6	10.6
4732471D19Rik	319719	–	4.1E-08	8.6	7.8
Rabl2	68708	–	1.4E-04	8.5	6.3
Hmgxb3	106894	3'UTR, conserved	1.6E-08	8.5	8.6
Lig4	319583	–	1.0E-03	8.4	4.9
Fam84b	399603	–	3.1E-08	8.2	8.5
Epc1	13831	3'UTR, conserved	7.0E-04	8.1	9.3
Dpy19l4	381510	–	9.3E-05	8.1	8.0
AI597479	98404	–	9.8E-08	8.1	6.0
Pik3cb	74769	–	8.8E-09	8.0	8.4

Purple: mRNA significantly enriched by Roquin-IP that contains a conserved CDE in the 3'UTR

Green: mRNA significantly enriched by Roquin-IP that contains a CDE in the ORF

5.3 Roquin Protein Sequence Alignment

In the following alignment, the protein sequence of Roquin of 16 different species, as annotated in NCBI, were aligned using ClustalW. The specific domains are color-coded and deletion mutants used in this study are indicated. The alignment was done by Fabian Pötzt.

```

|----- ΔRING -----|
Mammalia M. Musculus (1) MPVQAPQWTFPLS PICTQTPFDETIRKPISLGCGHTVCKMCLNKLHRKAPFFDQTTINTD 60
Aves G. Gallus (2) MPVQAPQWTFPLS PICTQTPFDETIRKPISLGCGHTVCKMCLNKLHRKAPFFDQTTINTD
Amphibia X. laevis (3) MPVQAPQWTFPLS PICTQTPFDETIRKPISLGCGHTVCKMCLNKLHRKAPFFDQTTINTD
Pisces D. rerio (4) MPVQAPQWT+FL+ PICTQTF+E++R+PISLGCGHTVCKMCLNKLHRKACPFDQT+INTD
Cephalo. B. floridae (5) MP+QAPQWTFPLS PICT+++F+E++RKPISLGCGHTVC++CL+++H+KCPFDQTTI++D
Tunicata C. intest (6) +P+Q+PQW++FL+ C+++F++T+R+PISLGCGHTVC++CL++L+++C+FDQ++I++D
Echinod. S. purpurat (7) MPVQ+PQW++LS CP+C+++F+++R+P+SL+CGHT+C+MCL+KLHR++CPFDQTI++D
Insecta T. castan (8) MP+QAPQWT+FLS CP+C+++F+++R+PISLGCGHTVCK+CL++LHRK+CPFDQTTI++D
Insecta D. melanog. (9) MP+QAP+WTDFL+ PICT+++F+++R+P+SLGCGHT+CK+CL++L+++CPFDQTI++D
Crustac. D. pulex (10) MP+QAPQWT+FLS PICT+++F+++R+PISL+CGHT+CK+CL+KLHR++CPFDQ+++++
Arachn. I. scapular (11) MPVQAPQWT+FLS CP+C+++F+++R+P+SLGCGHT+C++CL++L+R++CPFDQ++I+++
Nematoda A. suum (12) +++Q+++W+++L+ CP+C+Q+F+++++P++L+CGH+V++CL++L+++CP+DQTI+++
Nematoda C. elegans (13) +++Q+++W+++L+ C+I+++F+ET+++P+SL+CGH+C++C++K+++KCP+D+++++
Cnidaria N. vecten (14) MP+Q+PQW+FL+ PICT+++F+++R+PISL+CGHT+CK+CL++LH+++CPFDQT+NTD
Cnidaria H. magna (15) MP+QAPQWTFD++ CP+C+++F+++++PISLGCGH++CK+CL++L+++CPFDQ++I++D
Porifera A. queensl (16) +++QAP+WTDFL+ C+++T+++++T+++P+SL+C+CGH+CK+CL++L+++KCP+D+++I+++
* * * * *

(1) IELLPVNSALLQLVGAQIPEQQPITLCSGVEDTKHYEEAKKCVBEELALYLKPLSSARGVG 120
(2) IELLPVNSALLQLVGAQ+PEQQPIT+CSG+EDTKHYEE+KCKVEELALYLKPLSSARGVG
(3) IELLPVNSALLQLVGAQ+PEQQ+ITLC+G+EDTKHYEEA+KCVBEELALYLKPLS+ARGVG
(4) IE+LPVNSALLQLVG+Q+P+QOP++L+++EDTKHY+EA++CVEELALYLKPLSSARGVG
(5) +++LPVN+A+LQLV+++++Q+++++GVE+T++Y+EA++C+EELALYLK+P+S++G+G
(6) I++LPVNSALL+LV+++++G+E++K+Y+++K++EELAL+L+P+++++
(7) +++LP+N+A+LQLV++Q+P++++I+++++Y+++++EELALYLK+L+++++
(8) IE+LPVN+ALLQLV+G+I+++++V+++++Y+++KCVBEELALYLK+P+++++G
(9) I++LP+N+ALLQLV+++++P+++++E++K+Y++++C+EELAL+LK+++++G+G
(10) +E+LPVN+ALLQL+G++++E+++++E++H+++++CVEELAL+LK+++++GV+
(11) +++LP+N+ALLQLV+++++P+++++G+E+++++A++CV+E+AL+L+P+++++
(12) +++LPVN+ALL+++++P+++C+++++A+++++Y+++++S+RG++
(13) +++P+N+ALL+++++P++Q++TL++V+++++EA+K+V++L+++++S+RG++
(14) I++LPVN+ALLQLVGA+++++E+++++Y++A++++EELALYLK+P+S++G+G
(15) I++LPVN+ALL+L+G++IP+++++K++A++++E+LA++L+++++
(16) +++P+N+A+L+L+G+Q+PE+++++V+++++Y+++++E+LA++LKP+++++G++
* * *

|----- ΔROQ -----|
(1) LNSTTQSVLSRPMQRKLVTLVHCQLVEEEGRIRAMRAARSLGERTVTELIHQHNPQOLS 180
(2) LNSTTQSVLSRPMQRKLVTLVHCQLVEEEGRIRAMRAARSLGERTVTELIHQHNPQOLS
(3) LNSTTQSVLSRPMQRKLVTLVHCQLVEEEGRIRAMRAARSLGERTVTELIHQHNPQOLS
(4) L++++QS+LSRPMQRKLVTLVHCQLVEEEGR+RAMRAARSLGERTVTELIHQHNPQOLS
(5) +NST++++LSRPMQRKLVTLV+CQLVE+EGR+RAMRAARSLGERTVTELIHQHNPQOLS
(6) ++++++LSRPMQRKLV+L++CQLVEEEGR+RA+RA+R+LGER++TELIHQHNP+LS
(7) LN+T++++LSRP+QRKLVTLV+CQL+E+EGR+R++RAARSLGER+VTELIHQHNPQOLS
(8) ++++++S+LSRPMQRKLVTL++CQLVE+EGR+RAMRAARSLGERTVTELIHQHNPQOLS
(9) +++T+++++RPM+RKLVTLV+CQL+EEGR+RA+RAARSLGERTVTELIHQHNPQOLS
(10) L+++++LSRPMQRKLVTL++CQL+E+EGR+RA+RAARSLGERTVTELIHQHNPQOLS
(11) ++++++RKLVTLVHCQL+E+EGR+RA+RAARSLGER++EL+HQH++QOLS
(12) ++S+++++SRP+QRKL+TL++QL+EEGR+RA++AR+L+ER++EL++HQH+++S
(13) ++S+++++SR++QRK+++L+++Q+E+GR+++++R+++ER+++E+IL++Q++++S
(14) L+S+T+++L+RPMQRKLVTLV+CQL+EEGR+RAMRAARSLGERTVTELIHQHNPQOLS
(15) ++++++L+RPMQRK+V+++HCQL+E+EG+RAMRAARS+GER+V+ELI+HQ+PQ+LS
(16) L++T+++++RP+++KL++L+++Q+++EGR++A+AA+S++ER++TEL++HQN++Q+S
* * *

----- ΔROQ -----
(1) SNLWAAVRARGCQFLGPAMQEEALKLVLLALEEDGSALSARKVLVLFVVQRLEPRFPQASKT 240
(2) SNLWAAVRARGCQFLGPAMQEEALKLVLLALEEDGSALSARKVLVLFVVQRLEPRFPQASKT
(3) SNLWAAVRARGCQFLGPAMQEEALKLVLLALEEDGSALSARKVLVLFVVQRLEPRFPQASKT
(4) SNLWAAVRARGCQFLGPAMQEEALKLVLLALEEDGSALSARKVLVLFVVQRLEPRFPQASKT
(5) +NLWAAVRARGCQFLGPAMQEE+LKL+LLALEEDGSALSARKVLV+VVQRLE++P+QASKT
(6) ++LWAAVRARGCQFLGPAMQEEALKL++++EDGS+LSRKVLV++VV++L+++P+QASKT
(7) +NLWAAVRARGCQFLGPAMQEE+LKLVLLEEDG++LSRKVLV+VVQ+LE++P+QASKT
(8) +NLWAAVRARGCQFLGPAMQEE+LKLVLLEEDGSALSARKVLV+VVQRLEP+P+QASKT
(9) SNLWAAVR+RGCQFLGPAMQEE+LKLVLLEALE+GSALSARKVLV+VVQRLEP+P+QASKT
(10) +NLWAAVRARGCQFLGPAMQEE+L+LVLLEEDGSALSARKVLV+VVQRLEP+P+QASKT
(11) ++LWAAVRARGCQFLGP+MQEE+L+LVLLEEDGS+LSRKVLVLFVVQRLEP+P+QASKT
(12) SNLW+AVRARGCQFLGPAMQEE+L+L+L+L+G+++RK+LV+++VQ+L+++PQ+SKT
(13) S+LW+AVRARGCQFLGPAMQ+++L+L+L+L+LE+G+++RK+LV+++VQ+L+++PQ+SKT
(14) +NLWAAVRARGCQFLGPAMQEEALKL+LLAL++G++LSRKVLV+VVQ+LEP+P+QASKT
(15) ++LWAAVR+RGCQFLGPAMQEE+L+L+L+L+LEDG++LSRKVLVLFVVQRLE++P+QASKT
(16) S+LW+AVR+RGCQFLGP+MQEEALKL+L+ALE+++LSRK++V++VVQ+L+P+P+QASKT
* * * * *

```

5.3 Roquin Protein Sequence Alignment

```

----- ΔROQ -----
(1)  SIGHVVQLLYRASCFKVTKRDESSLMQLKEEFRTYEALRREHDSQIVQIAMEAGLRIAP 300
(2)  SIGHVVQLLYRASCFKVTKRDESSLMQLKEEFRTYEALRREHDSQIVQIAMEAGLRIAP
(3)  SIGHVVQLLYRASCFKVTKRDESSLMQLKEEFRTYEALRREHDSQIVQIAMEAGLRIAP
(4)  SIGHVVQLLYRASCFKVTKRDESSLMQLKEEFRTYEALRREHDSQIVQIAMEAGLRIAP
(5)  SIGHVVQLLYRASCFKVTKRDESSLMQLKEEFRTYEALRREHDSQIVQIAMEAGLRIAP
(6)  SIGHVVQLLYRASCFKVTKR+++SSLM+LK+EF++YE+LRREHD+QIV+IA+EAGLRIAP
(7)  S+GHVVQLLYRASCFKVTKR+E+SSLMQLKEEFR+Y++LRREHD+QIVQIA+EAGLRIAP
(8)  SIGHVVQLLYRASCFKVTKR++DSSLMQLKEEFRTYEALRREHD+QIVQIA+EAGLRIAP
(9)  SIGHVVQLLYRASCFKVTKR++DSSLMQLKEEFRTY+ALRREHD+QIVQIA+EAGLRIAP
(10) SIGHVVQLLYRASCFKVTKR++DSSLMQLK+EFRTY++LRREHD+QIVQIA+EAGLRIAP
(11) SIGHVVQLLYRASCFKVTKR++DSSLMQLKEEF+TYEALRREHD+QIVQIA+EAGLRIAP
(12) ++GHVVQLLYRASCF+V+KRD++SSLMQLK+EFR+Y++LRREHD+QIVQIA+EAGLRIAP
(13) ++GHVVQLLYRASCF+V+KRD++SSLMQLKEEFRTYE+LRREHDSQIVQIA+EAGLRIAP
(14) SIGHVVQLLYRASCFKVTKR++SSLMQLKE+FRTYE+LR+EHD+QIVQIAMEAGLRIAP
(15) SIGHVVQLLYRASCFKVTKR++DSSL+QL+E++RTY+ALR+EHD+QIVQIAMEAGLRIAP
(16) +IGHVVQLLYRASCF+V+KRD++DSSLMQLKEE++TYEALRREHDSQI++IAMEAGLRIAP
      ***** * ** *** * ** ** ** ** * ** * ** *

----- ΔROQ -----|
(1)  DQWSSLLYGDQSHKSHMQSIIDKLQTPASFAQSVQELTIALQRTGDPANLNRLRPHLELL 360
(2)  DQWSSLLYGDQSHKSHMQSIIDKLQTPASFAQSVQELTIALQRTGDPANLNRLRPHLELL
(3)  DQWSSLLYGDQSHKSHMQSIIDKLQTPASFAQSVQELTIALQRTGDPANLNRLRPHLELL
(4)  DQWSSLLYGDQSHKSHMQSIIDKLQTPASFAQSVQELTIALQRTGDPANLNRLRPHLELL
(5)  +QWSSLLYGD++HKSHMQSIIDKLQTPASFAQSV+EL+IALQR+GDPANL+R+P+L
(6)  DQWS+LLYGDQSHKS+MQSIID+L++++SF+++++
(7)  +QWSSLLYGD++HKSHMQSIIDKLQTPASF++S+QELTI+LQR+GDP++L++L++LE+L
(8)  DQWS+LLYGD++HKSHMQSIIDKLQTP+SFAQSVQEL+IALQRTGDP++L++L++LE+L
(9)  +QWSSLLYGD++HKSHMQSIIDKLQTP+SFAQSVQEL+IALQRT+DPA+L++L++HL++L
(10) DQWSSLLYGD++HKSHMQSIIDKLQTP+SF+QSVQEL+IALQRTGDP+NL++L+R+L+LELL
(11) +QWSSLLYGD++HKSHMQSIIDKLQ+P+SF+QSVQEL+IALQRTGDP++L++L+R+L+LELL
(12) DQWSSLLYGDQSH+SHMQSIIDKLQ+P++F+Q+VQEL++ALQR+DP++L++++HLE++
(13) DQWS+LLY+DQSH+SHMQSIIDKLQ+++S++Q+V+EL++A+++T++PA++++L+P+LE++
(14) DQWSSLLYGD+++KSHMQSIIDKLQ+P+SF+QS+QEL+I+LQR++DP++L+R+L+H+E+L
(15) +QWS+LLYGD++HKSHMQSIIDKLQTPASF++S+QEL+IALQRT+DP+NL++L++HLE+L
(16) ++WSS+LYG++++KS+MQSIIDKL+++++EL++A++R++D++NLNRL++HL++L
      ** ** * ***** *

(1)  ANIDPSPDAPPTWEQLENGLVAVRTVVHGLVDYIQNHSSKKGADQQPPQHSHKYKTYMCR 420
(2)  ANIDPSPDAPPTWEQLENGLVAVRTVVHGLVDYIQNHSSKKG+DQQPPQHSHKYKTYMCR
(3)  ANIDPSPDAPPTWEQL++GLVAV+TVVHGLVDYIQNHSSKKG+DQQPPQHSHKYKTYMCR
(4)  ANIDPSPDAPPTWEQLE+GLVAV+TVVHGLVD+IQNHSSKKGAD+QPPQHSHKYKTYMCR
(5)  A+IDPSPD+++P+W++++G++AV++VV+G+VD+IQN+S+++++K+YKT+MCR
(6)  ++++++
(7)  A+IDPSP+A++++WE++++L++VR+V++GL++++Q+N+S+K+D+Q+++Q++K+YKT++CR
(8)  A+IDPSP++++P+W++++L+AVR+VV+GLV++I++H+++++PQH+K+YK++MCR
(9)  ANIDP++++P+W++L++L+AVR++V+GLV+++Q+H++++A+++++K+YK++CR
(10) A++DP+PDA++P+W++++L+A+R++V+GL+D+++H+++G++Q++++H+K+YKT++CR
(11) +++DPSP++++WE++++A+++VHGLV+++++G++++PPQ++K+YKT++CR
(12) A++D++++A++P+W+++++V+++V++I+++S+++A+++++YKT++CR
(13) A+I+++++
(14) ++ID++PDA+PP+W++LE+++AV++VV+GLV+++++K+++++PPQ+SK+KT+MCR
(15) A+IDP+P+A+PP+W+++E+++++VV+GL+++++K+++++Q++K+Y+T+MCR
(16) ++IDP+P++P+++WE+++++L+++++D++Q++S+++++YKT+MCR

(1)  DMKQRGGCPRGASCTFAHSQEELKFRKMNKRLVPRRPLSASLGQLENEVGLPSAPILSDE 480
(2)  DMKQRGGCPRGASCTFAHSQEELKFRKMNKRLVPRRPLSASLGQLENEVGLPS++ILSDE
(3)  DMKQRGGCPRGASCTFAHSQEELKFRKMNKRLVPRRPLSASLGQLENEVGLP+AP+++DE
(4)  DMKQ+GGCPRGASCTFAHSQEELK+RKMNKRL+R+P++++L+L+E+++P++P+++
(5)  D+++GGCPRG++CTFAHS+EE+++R++N+++V+++++
(6)  ++++++
(7)  D+ Q+GGCPRG+SCTFAHS+EELEK+R+++++L+++++
(8)  D+++RG+CPRG++CTFAHS+EELEK+++++
(9)  D+++R++CPRG+SCTFAHSQEE+E++R++N+++++PL+++++
(10) D+++RG+CPRG++CTFAHS+EE+++R+++++
(11) D+++QRG+CPRG++CTFAHSQ+E+++++
(12) D+++++CPRG++CT+AH+S++EL+++++
(13) ++++++
(14) D+++GGCPRG+A+C+FAHS++ELEK+++++
(15) D+++Q+++CPRG+A+C+FAHS+EELE+++++
(16) ++++++GGCPRG+A+C+AH++EE++K+++M+K+++++

```

(1) SAVDLSNRKPPALPNGIASSGSTVTQLIPRGTDPSFDSSLKPKVDHLSSSAPGSPDLL 540
(2) ++VDL+NRK++ALPNGI+S+GSTVTQLIPRGT+++++LKP+K+DHLSSSAPGSPDLL
(3) +++DL++RKP+L+PNGI+++GS+VTQLI+R+TD++F+S+LKPVKLDHLSSSAPGSP+LL
(4) ++++++RK++++NG+++++QLIPRGTD+S++D+LKP+K+D++S+SAPGSPD+L
(5) ++++++
(6) ++++++
(7) ++++++
(8) ++++++
(9) ++++++
(10) ++++++
(11) ++++++
(12) ++++++
(13) ++++++
(14) ++++++
(15) ++++++
(16) ++++++

(1) ESAPKSI SALPVNHPVPRPTDLPMPVTKPIQMVPRGSQLYPAQQADVYYQDPRGSA 600
(2) ES+PKSISALPVN+HPVPR++PTDLP+++VTK++QMVPRGSQLY++QQAD++YQD+RG+A
(3) +S+PKS+SALPVN+HP+++R+++DLPP+PV+K+IQMVPRGSQ+Y+++AD+YQ+RG++
(4) +++++++L+++PHVPRP+T+++MP++K+++VPRG+Q+YP+QQ+++Y++P++++
(5) ++++++
(6) ++++++
(7) ++++++
(8) ++++++
(9) ++++++
(10) ++++++
(11) ++++++
(12) ++++++
(13) ++++++
(14) ++++++
(15) ++++++
(16) ++++++

(1) PAFETAPYQQGMYTTPPCVSRFVRPPPSAPEPGPPYLDHYSPLYQDRVINSYQGTQPQQ 660
(2) P+FE+APYQQG+YY+P+++SRFVRPPPSAPEPGPPYLDHYSPLYQDRV+++QY+TQPQQ
(3) P+F++APY+QG+YY+P+++CVSRFVRPP+A+EP+++YLDHY+PLYQDRV+++QYGT++QQ
(4) P++++A+Y++G++Y+PP++VSR++R+PP+++PG+++++Y+++++SQY+++++
(5) ++++++
(6) ++++++
(7) ++++++
(8) ++++++
(9) ++++++
(10) ++++++
(11) ++++++
(12) ++++++
(13) ++++++
(14) ++++++
(15) ++++++
(16) ++++++

(1) YPPMYP AHYDGRVYPAQS YTREEMFRESPIPIDIPSAAVPSYVPESRERYQQVEGYYPV 720
(2) YPPMYP+HYD+RRVYP+Q+Y+REE++R+SP+PI+IP+A+VPSYVPESR+RY+Q+EGY+PV
(3) YP++Y++HYD+RR+YP+++Y+REE++R+SP+P+++P+AAV++YV+ESRERYQ++EGY++
(4) Y+P++P+HY++RR+YP++++R+++R+SP+P+D+P+AA+P++++SR+RY+++GYYP+
(5) ++++++
(6) ++++++
(7) ++++++
(8) ++++++
(9) ++++++
(10) ++++++
(11) ++++++
(12) ++++++
(13) ++++++
(14) ++++++
(15) ++++++
(16) ++++++

5.3 Roquin Protein Sequence Alignment

```
(1) APHPAQIRPSYPRDPPYSRLPPPQPHPSLDELHRRRKEIMAEERKVISPPPFAPSPPTL 780
(2) APH++QIRPS+++++++L+++QPHPSLDELHRRRKEIMAEERKVISPPPFAPSPPTL
(3) ++HP+QIRPSY+R++PY+RLPP+QPHPSLD+LHRRRKEIMAEER+VISPPPFAPSPPTL
(4) +PH++Q+R+S++RDP++S+++++++PSLD+LHRRRKE+++QLEERKVISPPPF+A-SPTL
(5) ++++++
(6) ++++++
(7) ++++++
(8) ++++++
(9) ++++++
(10) ++++++
(11) ++++++
(12) ++++++
(13) ++++++
(14) ++++++
(15) ++++++
(16) ++++++
```

```
(1) PPAFHPEEFLDEDLKVAGKYKANDYSQYSPWSCDTIGSYIGTKDAKPKDVVAAGSVEVMN 840
(2) P++FH+EE+LDEDLKVAGKYK+NDYSQYSPWSCDTIGSYIGTKDAKPKDVVA+SVEM+N
(3) P++FHPPEE+LDE+LK++G++K+NDYSQYSPWSC+DT+G+YIGTKD+K+KDV+A+G+VE++N
(4) PP+++P+E+L+++K++G+++++++QYSPWSCDTIGSYIG+KDAKPKDV++A++VEM+
(5) ++++++
(6) ++++++
(7) ++++++
(8) ++++++
(9) ++++++
(10) ++++++
(11) ++++++
(12) ++++++
(13) ++++++
(14) ++++++
(15) ++++++
(16) ++++++
```

```
(1) VESKGTREQLDLQRRAVETSDDDLIPFGDRPTVSRFGAISRTSKTYQGAGPLQAIAPQ 900
(2) V+SK++R+QLD+QRR+A+E++DDDLIPFGDRPTVSRFGAISRTSK++YQ++G+PQA+A+Q
(3) V++K++R+QR++LQRR+A+E++DDDLIPFGDRPTVSRFGAISRTSK+LYQ++GP++QA+A+
(4) +E+K++RE++LD+QRR++E++DDD+IPFG++PTVS+FGAISRTSKTYQ++GP+QAIA+Q
(5) ++++++
(6) ++++++
(7) ++++++
(8) ++++++
(9) ++++++
(10) ++++++
(11) ++++++
(12) ++++++
(13) ++++++
(14) ++++++
(15) ++++++
(16) ++++++
```

```
(1) GAPTKSINISDYSAYGAHGGWGDSPYSPHANIPQGHFIEREKMSMAEVASHGKPLLSAE 960
(2) GA+TKSI+ISDYS+YG+HGGWG+SPYSPH+NIP+QG+F++RE++SM++VA+HGK+L+SAE
(3) +GA+S++I+DYS+Y++H+G+++++Y++H+N+P+QGH++ERE++S+++++++KPL+++E
(4) +++K+++++++YG+H+CWG+++Y++H++I++QGHF+ERE+++++++P+++++
(5) ++++++
(6) ++++++
(7) ++++++
(8) ++++++
(9) ++++++
(10) ++++++
(11) ++++++
(12) ++++++
(13) ++++++
(14) ++++++
(15) ++++++
```


6 Appendix

6.1 Materials Used in this Study

6.1.1 Disposable Material and Kits

The following disposable material was used in this study.

Table 6.1: Disposable Material and Kits Used in this Study.

Disposables / Kits	Company
1.5 ml, 2 ml Reaction Tubes	Eppendorf
15 ml, 50 ml Falcon Tubes	Falcon, Greiner, Nunc
1.5 mL DNA LoBind Tubes	Eppendorf
2 ml Cryotubes	Nunc
Cellscraper CoStar	Corning Inc.
CellStar Tissue culture flasks (T75, T25)	Greiner Bio-One
CellStar Tissue culture dishes (6, 10, 15cm)	Greiner Bio-One
CellStar Cell culture plates (6-well, 12-well, 24-well)	Greiner Bio-One
DIG labelling Kit	Ambion
Filter paper Whatman 3MM	Whatman
Filter tips	StarLab
Gloves	Meditrade
MegaClear RNA purification Kit	Amersham
MegaScript SP6 RNA Polymerase Kit	Ambion
Mini quick spin RNA column	Roche
Nitrocellulose membrane	Peqlab
Pipette tips Steinbrenner	Starlab
PureLink HiPure Plasmid Maxiprep Kit	Life Technologies
PureLink HiPure Plasmid Midiprep Kit	Life Technologies
QIAquick Gel Extraction Kit	QIAGEN
QIAquick Nucleotide Removal Kit	QIAGEN
QIAprep Spin Miniprep Kit	QIAGEN
QIAquick PCR Purification Kit	QIAGEN
Rapid DNA Ligation Kit	Fermentas

Disposables / Kits	Company
RNA Isolation Kit (tissue culture)	EURx, Roboklon
Transcriptor First Strand cDNA Synthesis Kit	Roche
Xray films	FujiFilm

6.1.2 Chemicals and Enzymes

The following chemicals and enzymes were used in this study.

Table 6.2: Chemicals and Enzymes Used in this Study.

Chemicals	Company
10x Taq Polymerase Buffer	QIAGEN
10x Northern Blot Blocking Solution	Roche
10x RNaseH Buffer	New England Biolabs
2-Mercaptoethanol (2-ME)	Sigma
5x Rapid Ligation Buffer	Fermentas
5x Transcription Buffer	Promega
Acetic Acid	Fluka
Acetone	Sigma
Actinomycin D	AppliChem
Adenosine triphosphate (ATP)	Fermentas
Agar	Roth
Agarose	Biozym Scientific GmbH
Ammoniumpersulfate	AppliChem
Ampicillin	Applichem
Avidin-agarose beads	Pierce, Thermo
Biotin, approx.99%, TLC	Sigma-Aldrich
Biotin, 50 mM stock	Life Technologies
Bovine serum albumine (BSA)	New England Biolabs
Bovine serum albumine (BSA)	PAA Laboratories
Bradford	Sigma-Aldrich
Bromphenol blue	Applichem
Calf Intestine Phosphatase (CIP)	New England Biolabs
CDP-Star Reagent	New England Biolabs
Chloroform	VWR
Chloroquine diphosphate salt	Sigma
Complete Protease Inhibitor Cocktail Tablets, EDTA-free	Roche
Coomassie Brilliant Blue R250	Roth
Coomassie Brilliant Blue R250	AppliChem
Cytidine triphosphate (CTP)	Fermentas

6.1 Materials Used in this Study

Chemicals	Company
Desoxyadenosine triphosphate (dATP)	Fermentas
Desoxycytidine triphosphate (dCTP)	Fermentas
Desoxyguanosine triphosphate (dGTP)	Fermentas
Desoxythymidine triphosphate (dTTP)	Fermentas
Dextrane sulphate sodium salt from <i>Leuconostoc spp.</i>	Sigma
DH5 α competent <i>E. coli</i> cells	Life Technologies
DIG easy hyb solution	Roche
DIG labelling mix	Roche
Dimethylsulfoxid (DMSO)	Serva Electrophoresis
Disodiumhydrogenphosphate	Roth
Dithiothreitol (DTT)	Applichem
Dulbecco's Modified Eagle Medium	Life Technologies
Ethanol	Riedel-de-Haen
Ethidium bromide (EtBr)	Applichem
Ethylenediaminetetraacetic acid (EDTA)	Roth
Fetal calf serum (FCS) superior	Biochrom AG
Fetal Bovine Serum (FBS) tetracycline negative	PAA Laboratories
Formaldehyde	Merck
Formamide	AppliChem
Gamma-[³² P]-ATP	Perkin Elmer
Gene Ruler 1 kb Ladder Plus	Fermentas
Glutathione (GSH, reduced)	Sigma-Aldrich
Glutathione-sepharose 4G beads	GE Healthcare
Glycerol	Roth
Glycine	Gerbu
Guanosine triphosphate (GTP)	Fermentas
Heparin sulfate	Sigma
HEPES	Roth
Horse serum	PAA Laboratories
Isopropanol	Sigma-Aldrich
Imidazole	Sigma-Aldrich
Isopropyl- β -D-thiogalactopyranosid (IPTG)	AppliChem, Roth
Isopropanol	Sigma-Aldrich
Kanamycinesulfate	Roth
L-glutamine	PAN
Lipofectamine 2000	Life Technologies
Lipofectamine RNAimax	Life Technologies
Magnesium chloride	Merck
Maleic acid	Fluka
Methanol	Fluka

Chemicals	Company
Milk powder	Roth
MOPS	Roth
Ni sepharose 6 Fast Flow	GE Healthcare
Nonidet P-40 (NP-40)	US Biological
O'GeneRuler 100bp Plus DNA Ladder	Fermentas
PageRuler Prestained Protein Ladder	Fermentas
Penicillin-streptomycin	PAN
Pfu DNA Polymerase	Stratagene
Polyethyleneimine (PEI)	Polysciences Europe
Ponceau S	MD
Potassiumacetate	Roth
Potassiumchloride	Roth
Puromycin	AppliChem
Protein A/G Ultra Link Resin	Thermo Scientific
Random hexamers	Fermentas
Restriction enzymes	New England Biolabs
RNase A	Genomed
RNase H	New England Biolabs
RNase H 10x Reaction Buffer	New England Biolabs
RNase inhibitor RNasin	Promega
Roti-Phenol/Chloroform/Isoamyl alcohol (25/24/1)	Roth
Rotiphorese Acrylamide Solution	Roth
RQ1 DNase	Promega
RQ1 DNase 5x Reaction Buffer	Promega
RQ1 DNase Stop Solution	Promega
SP6 RNA polymerase	Fermentas
Sodium azide	AppliChem
Sodium chloride	Sigma-Aldrich
Sodium dodecyl sulphate (SDS)	Gerbu
Sodium hydroxide pellets	Riedel-de-Haen
Sodiumfluoride	Sigma-Aldrich
Sodiumvanadate	Sigma-Aldrich
Streptavidin-Sepharose High Performance beads	GE Healthcare
Taq DNA polymerase	QIAGEN
TEMED	AppliChem
Thermo RNA polymerase buffer	New England Biolabs
Transcriptor Reverse Transcriptase	Roche
Transcriptor Reverse transcriptase 5x Reaction Buffer	Roche
Trichloroacetic acid	AppliChem
T4 DNA Ligase	Fermentas

6.1 Materials Used in this Study

Chemicals	Company
T4 Polynucleotide Kinase	New England Biolabs
T7 RNA Polymerase	New England Biolabs
TriFast	PeqLab
Trisodiumcitrate	VWR
Triton-X-100	Appllichem
Trizma base	Sigma-Aldrich
Tryptone	AppliChem
Trypsin/EDTA	PAN
Tween-20	Sigma-Aldrich
Uridine triphosphate (TTP)	Fermentas
Vanadyl ribonucleoside complex (VRC) RNase inhibitor	New England Biolabs
Western Lightning enhanced chemiluminescence substrate	Perkin Elmer
Xylenexanol	AppliChem
Yeast Pyrophosphatase	Sigma
Yeast tRNA	Ambion

6.1.3 Technical Equipment

The following technical equipment was used in this study.

Table 6.3: Technical Equipment Used in this Study.

Technical Equipment	Company
CCD-camera	Andor
Cell Culture Incubator	Hera cell
Centrifuge (5417R)	Eppendorf
Centrifuge (J2-MC, rotor JA-17)	Beckman
Centrifuge (Labofuge M)	Heraeus Sepatech
Centrifuge (Multifuge 1S)	Thermo
Centrifuge (Pico17)	Thermo
EM-CCD camera	Hamamastu
Epson Perfection V700 Photo	EPSON
Film Development Apparatus (HyperProcessor)	Amersham
Freezer -20°C	Liebherr
Freezer -80°C x	Liebherr
Fridge 4°C	Liebherr
GeneAmp PCR System 9700	Applied Biosystems
Heating Block (neoBlock 1)	NeoLab
Intelli-mixer	NeoLab
Laminar Flow Cabinet	Hera cell

Technical Equipment	Company
Magnetic Stirrer (MR3001)	NeoLab
Micropipettes	Gilson
Microwave	Privileg
Mini Protean 3 Cell	BIORAD
Mini Trans Blot Cell	BIORAD
Nanodrop ND 1000	PeqLab
pH Meter (766 Calimetic)	Knick
Phosphoimager (FLA-7000)	FujiFilm
Poly-Prep column	Biorad
Power Supply (powerpack300)	Biorad
Scale (440-47N)	Kern
Scintillation counter (LS 6000IC)	Beckman
Shaker (DOS-20S)	NeoLab
Shaker (PMR-30)	Grant-bio
Sorvall Discovery 90SE	Thermo Scientific
Speedvac	Eppendorf
Stainless Steel Beads, 5 mm (200)	QIAGEN
TurboBlotter (Northern Blot)	Whatman
TissueLyzer II	QIAGEN
UV Gel Documentation System	Raytest IDA
UV Table (TVL-312A)	Spektroline
Vortex	NeoLab
Waterbath	GFL
Waterbath	memmert
Waterbath	huber

6.1.4 Antibodies

The following antibodies were used in this study.

Table 6.4: Antibodies Used in this Study.

Antigen	Clonality	Species	Company (Ordering Number)	Dilution (Method)
α -tubulin	monoclonal	rat	Abcam (ab6160)	1:10,000 (WB)
Caf1a	polyclonal	rabbit	Ann-Bin Shyu (UTexas)	1:1,000 (WB)
cNot1	polyclonal	rabbit	Proteintech (14276-1-AP)	1:x (WB)
Flag M2	monoclonal	mouse	Sigma (F-3165)	1:1,000 (WB)
G3BP1 (TT-Y)	monoclonal	mouse	Santa Cruz (sc-81940)	1:1,000 (IF)
GFP	polyclonal	rabbit	Abcam (ab290)	1:1.000 (WB)
GFP	monoclonal	mouse	Roche (11814460001)	1:1000 (WB)
GST	polyclonal	goat	GE Healthcare (27-4577.1)	1:1,000 (WB)
GST	polyclonal	rabbit	Ludger Hengst (Innsbruck)	1:5,000 (WB)
HuR (3A2)	monoclonal	mouse	Santa Cruz (sc-5261)	1:500 (WB)
myc (A-14)	polyclonal	rabbit	Santa Cruz (sc-789)	1:1,000 (WB)
Rbms1	monoclonal	rabbit	Abcam (ab150353)	1:x (WB)
Rck/p54	polyclonal	rabbit	Bethyl (A300-443A)	1:1,000 (WB)
Roquin	polyclonal	rabbit	Bethyl (A300-514A)	1:500 (WB)
Roquin	polyclonal	rabbit	Bethyl (A300-515A)	1:500 (WB)
T7-Tag	monoclonal	mouse	Novagen (69522-3)	1:1,000 (WB)
TNF α	polyclonal	goat	Santa Cruz (sc-1351)	1:500 (WB)
HRP-coupled 2nd ab	rabbit, mouse, goat	donkey	Jackson ImmunoResearch	1:10,000 (WB)
α -DIG-Fab-AP	-	sheep	Roche (11093274910)	1:4.000 (NB)

6.1.5 Plasmids

The following plasmids were generated in this study.

Table 6.5: Plasmids Generated in this Study. All plasmids mediate ampicillin resistance; O: origin, person cloning the original plasmid: KL: Kathrin Leppek; JS: Johanna Schott; SR: Sonja Reitter; FP: Fabian Pötz.

Code	Name	O	Description
p2772	pGEX-4T-3-TEV	KL	TEV insert (G1875/G1876, ENLYFQG) with <i>Bam</i> HI/ <i>Eco</i> RI sites, in <i>Bam</i> HI/ <i>Eco</i> RI-digested pGEX-4T-3 (p2763)
p2773	pGEX-4T-3-TEV-PP7cp	KL	PP7cp insert (G1859/G1860, <i>Eco</i> RI/ <i>Xho</i> I) from p2211 (D. Peabody) and TEV insert (G1875/G1876, <i>Bam</i> HI/ <i>Eco</i> RI) into pGEX-4T-3 (p2763)
p2774	pGEX-4T-3-TEV-oPP7cp	KL	oPP7cp insert (G1860/1861, <i>Xho</i> I/ <i>Eco</i> RI) from p2770 (K. Collins) and TEV insert (G1875/G1876, <i>Bam</i> HI/ <i>Eco</i> RI) into pGEX-4T-3 (p2763)
p2810	pGEX-2T-TEV-TEV-MS2cp	KL	two TEV inserts (G1852/G1853, <i>Bam</i> HI/ <i>Bgl</i> II) in <i>Bam</i> HI-digested pGEX-2T-MS2cp (p2809)
p2775	pTet-7B-TNF(ARE)-1xS1	KL	1xS1 aptamer insert (G1779/G1780) with <i>Bam</i> HI/ <i>Bgl</i> II sites into <i>Bgl</i> II-digested pTet-7B-TNF-ARE (ARE 53) (p2260)
p2776	pTet-7B-TNF(ARE)-2xS1	KL	2xS1 aptamer insert, see p2775
p2777	pTet-7B-TNF(ARE)-3xS1	KL	3xS1 aptamer insert, see p2775
p2778	pTet-7B-TNF(ARE)-4xS1	KL	4xS1 aptamer insert, see p2775
p2779	pTet-7B-TNF(ARE)-5xS1	KL	5xS1 aptamer insert, see p2775
p2780	pTet-7B-TNF(ARE)-6xS1	KL	6xS1 aptamer insert, see p2775
p2788	pTet-7B-TNF(ARE)-7xS1	KL	7xS1 aptamer insert, see p2775
p2781	pTet-7B-TNF(ARE)-1xS1m	KL	1xS1m aptamer insert (G1850/G1851) with <i>Bam</i> HI/ <i>Bgl</i> II sites into <i>Bgl</i> II-digested pTet-7B-TNF-ARE (ARE 53) (p2260)
p2782	pTet-7B-TNF(ARE)-2xS1m	KL	2xS1m aptamer insert, see p2781
p2783	pTet-7B-TNF(ARE)-3xS1m	KL	3xS1m aptamer insert, see p2781
p2784	pTet-7B-TNF(ARE)-4xS1m	KL	4xS1m aptamer insert, see p2781
p2785	pTet-7B-TNF(ARE)-5xS1m	KL	5xS1m aptamer insert, see p2781
p2786	pTet-7B-TNF(ARE)-6xS1m	KL	6xS1m aptamer insert, see p2781
p2787	pTet-7B-TNF(ARE)-7xS1m	KL	7xS1m aptamer insert, see p2781

6.1 Materials Used in this Study

Code	Name	O	Description
p2811	pTet-7B-CDE	KL	CDE insert (<i>EcoRI/BglII</i> , from Johanna Schott) into <i>EcoRI/BglII</i> -digested pTet-7B (p2254)
p2812	puroMX β -CDE	KL	CDE insert (<i>EcoRI/BglII</i> , from Johanna Schott) into <i>EcoRI/BglII</i> -digested puroMX β (p2220)
p2813	puroMX β -CDE _{37-V1}	KL	CDE _{37-V1} (-CT) (G1911/G1912, 5' <i>BglII/BamHI</i> , 3' <i>BglII</i> site) into <i>BglII</i> -digested puroMX β (p2220)
p2814	puroMX β -CDE _{37-V2}	KL	CDE _{37-V2} (+CT) (G1913/G1914) into puroMX β
p2823	puroMX β -CDE _{37-V3}	KL	CDE _{37-V3} (+CT-AG) (G1915/G1916) into puroMX β
p2825	puroMX β -CDE _{37-V3-M1}	KL	CDE _{37-V3} M1 (5' <i>BglII/BamHI</i> , 3' <i>BglII</i> site) insert into <i>BglII</i> -digested puroMX β (p2220)
p2826	puroMX β -CDE _{37-V3-M2}	KL	CDE _{37-V3} M2 into puroMX β
p2827	puroMX β -CDE _{37-V3-M3}	KL	CDE _{37-V3} M3 into puroMX β
p2828	puroMX β -CDE _{37-V3-M4}	KL	CDE _{37-V3} M4 into puroMX β
p2829	puroMX β -CDE _{37-V3-M5}	KL	CDE _{37-V3} M5 into puroMX β
p2830	puroMX β -CDE _{37-V3-M6}	KL	CDE _{37-V3} M6 into puroMX β
p2831	puroMX β -CDE _{37-V3-M7}	KL	CDE _{37-V3} M7 into puroMX β
p2832	puroMX β -CDE _{37-V3-M8}	KL	CDE _{37-V3} M8 into puroMX β
p2833	puroMX β -CDE _{37-V3-M9}	KL	CDE _{37-V3} M9 into puroMX β
p2834	puroMX β -CDE _{37-V3-M10}	KL	CDE _{37-V3} M10 into puroMX β
p2835	puroMX β -CDE _{37-V3-M11}	KL	CDE _{37-V3} M11 into puroMX β
p2836	puroMX β -CDE _{37-V3-hCDE}	KL	CDE _{37-V3} human CDE into puroMX β
p2859	puroMX β -CDE _{37-V3-M12}	KL	CDE _{37-V3} M12 into puroMX β
p2860	puroMX β -CDE _{37-V3-M13}	KL	CDE _{37-V3} M13 into puroMX β
p2861	puroMX β -CDE _{37-V3-M14}	KL	CDE _{37-V3} M14 into puroMX β
p2862	puroMX β -CDE _{37-V3-M15}	KL	CDE _{37-V3} M15 into puroMX β
p2863	puroMX β -CDE _{37-V3-M16}	KL	CDE _{37-V3} M16 into puroMX β
p2864	puroMX β -CDE _{37-V3-M17}	KL	CDE _{37-V3} M17 into puroMX β
p2944	puroMX β -CDE _{37-V3-M18}	SR	CDE _{37-V3} M18 into puroMX β
p2945	puroMX β -CDE _{37-V3-M19}	SR	CDE _{37-V3} M19 into puroMX β
p2946	puroMX β -CDE _{37-V3-M21}	SR	CDE _{37-V3} M21 into puroMX β
p2947	puroMX β -CDE _{37-V3-M22}	SR	CDE _{37-V3} M22 into puroMX β
p2948	puroMX β -CDE _{37-V3-M25}	SR	CDE _{37-V3} M25 into puroMX β
p2959	puroMX β -CDE _{37-V3-M20}	SR	CDE _{37-V3} M20 into puroMX β
p2960	puroMX β -CDE _{37-V3-M23}	SR	CDE _{37-V3} M23 into puroMX β
p2961	puroMX β -CDE _{37-V3-M24}	SR	CDE _{37-V3} M24 into puroMX β

Code	Name	O	Description
p2967	puroMX β -CDE ₃₇ -V3-M26	SR	CDE ₃₇ -V3 M26 into puroMX β
p2968	puroMX β -CDE ₃₇ -V3-M27	SR	CDE ₃₇ -V3 M27 into puroMX β
p2965	puroMX β -CDE ₁₇ -ss	SR	CDE ₁₇ -ss into puroMX β (minCDE)
p2966	puroMX β -CDE ₁₇ -ds	SR	CDE ₁₇ -ds into puroMX β (minCDE-V3)
p2969	puroMX β -CDE ₁₅₀	SR	CDE ₁₅₀ in native mouse 3'UTR context, cloned via <i>Bam</i> HI/ <i>Bgl</i> II (G2495/G2496) from p2914 into puroMX β
p2970	puroMX β -CDE ₁₅₀ -M16	SR	CDE ₁₅₀ -M16 in native mouse 3'UTR context, cloned via <i>Bam</i> HI/ <i>Bgl</i> II from p2915 into puroMX β
p2971	puroMX β -CDE ₁₅₀ -M19	SR	CDE ₁₅₀ -M19 in native mouse 3'UTR context, cloned via <i>Bam</i> HI/ <i>Bgl</i> II from p2916 into puroMX β
p2972	puroMX β -CDE ₁₅₀ -M20	SR	CDE ₁₅₀ -M20 in native mouse 3'UTR context, cloned via <i>Bam</i> HI/ <i>Bgl</i> II from p2917 into puroMX β
p2824	puroMX β -4xS1m	KL	4xS1m insert amplified with <i>Bgl</i> II-mismatch repair primer (G1919/G1918; <i>Bgl</i> II-site at both ends) from p2784 into <i>Bgl</i> II-digested puroMX β (p2220)
p2856	puroMX β -CDE ₃₇ -V3-4xS1m	KL	4xS1m insert amplified with <i>Bgl</i> II-mismatch repair primer (G1919/G1918; <i>Bgl</i> II-site at both ends) from p2784 into <i>Bgl</i> II-digested puroMX β -CDE ₃₇ -V3 (p2823)
p2857	puroMX β -CDE ₃₇ -V3-M7-4xS1m	KL	4xS1m insert amplified with <i>Bgl</i> II-mismatch repair primer (G1919/G1918; <i>Bgl</i> II-site at both ends) from p2784 into <i>Bgl</i> II-digested puroMX β -CDE ₃₇ -V3-M7 (p2831)
p2858	puroMX β -CDE ₃₇ -V3-M9-4xS1m	KL	4xS1m insert amplified with <i>Bgl</i> II-mismatch repair primer (G1919/G1918; <i>Bgl</i> II-site at both ends) from p2784 into <i>Bgl</i> II-digested puroMX β -CDE ₃₇ -V3-M9 (p2833)
p2880	pSP73-4xS1m (SP6 orientation)	KL	4xS1m insert amplified with <i>Bgl</i> II-mismatch repair primer (G1919/G1918; <i>Bgl</i> II-site at both ends) from p2784 into <i>Bgl</i> II-digested pSP73 (p2008); pSP- <i>Bgl</i> II-4xS1m- <i>Bgl</i> II- <i>Eco</i> RV, IVT: linearize with <i>Eco</i> RV

6.1 Materials Used in this Study

Code	Name	O	Description
p2881	pSP73-TNF(ARE)-4xS1m (SP6 orientation)	KL	ARE-4xS1m insert amplified with <i>Bam</i> HI-mismatch repair primer (G2247/G2235) from p2891 into <i>Bgl</i> II-digested pSP73 (p2008); pSP- <i>Bam</i> HI/ <i>Bgl</i> II fusion site-TNF(ARE)- <i>Bam</i> HI/ <i>Bgl</i> II fusion site-4xS1m- <i>Bgl</i> II- <i>Eco</i> RV, IVT: linearize with <i>Bgl</i> II or <i>Eco</i> RV
p3278	pSP73-4xS1 (SP6 orientation)	KL	4xS1 insert amplified with <i>Bgl</i> II-mismatch repair primer (G1919/G1918; <i>Bgl</i> II-site at both ends) from p2778 into <i>Bgl</i> II-digested pSP73 (p2008)
p3279	pSP73-TNF(ARE)-4xS1 (SP6 orientation)	KL	ARE-4xS1 insert amplified with <i>Bam</i> HI-mismatch repair primer (G2247/G2235) from p2778 into <i>Bgl</i> II-digested pSP73 (p2008); pSP- <i>Bam</i> HI/ <i>Bgl</i> II fusion site-TNF(ARE)- <i>Bam</i> HI/ <i>Bgl</i> II fusion site-4xS1- <i>Bgl</i> II- <i>Eco</i> RV, IVT: linearize with <i>Bgl</i> II or <i>Eco</i> RV
p2882	TOPO-pCRII-4xS1m (SP6 orientation)	KL	pSP- <i>Bam</i> HI-4xS1m- <i>Bgl</i> II- <i>Eco</i> RV, IVT: linearize with <i>Eco</i> RV (gives additional 100 bp)
p2883	TOPO-pCRII-CDE ₃₇ -V3-4xS1m (SP6 orientation)	KL	pSP- <i>Bam</i> HI-CDE ₃₇ -V3- <i>Bgl</i> II-4xS1m- <i>Bgl</i> II- <i>Eco</i> RV, IVT: linearize with <i>Eco</i> RV (gives additional 100 bp)
p2884	TOPO-pCRII-CDE ₃₇ -V3-M7-4xS1m (SP6 orientation)	KL	pSP- <i>Bam</i> HI-CDE ₃₇ -V3-M7- <i>Bgl</i> II-4xS1m- <i>Bgl</i> II- <i>Eco</i> RV, IVT: linearize with <i>Eco</i> RV (gives additional 100 bp)
p2885	TOPO-pCRII-CDE ₃₇ -V3-M9-4xS1m (SP6 orientation)	KL	pSP- <i>Bam</i> HI-CDE ₃₇ -V3-M9- <i>Bgl</i> II-4xS1m- <i>Bgl</i> II- <i>Eco</i> RV, IVT: linearize with <i>Eco</i> RV (gives additional 100 bp)
p2886	TOPO-pCRII-TNF(ARE)-4xS1m (T7 orientation)	KL	pT7- <i>Bam</i> HI-ARE- <i>Bam</i> HI/ <i>Bgl</i> II-fusion-4xS1m- <i>Bgl</i> II- <i>Eco</i> RV
p2891	puroMX β -TNF(ARE)-4xS1m	KL	4xS1m insert amplified with <i>Bgl</i> II-mismatch repair primer (G1919/G1918; <i>Bgl</i> II-site at both ends) from p2784 into <i>Bgl</i> II-digested puroMX β -TNF α -ARE (p2225)
p2914	puroMX β -TNF α -3'UTR (mouse)	JS	complete 3'UTR of mouse TNF α into puroMX β

Code	Name	O	Description
p2915	pCRII-Topo-TNF α -3'UTR (human)	KL	complete 3'UTR of human TNF α (from Hela gDNA)
p2991	puroMX β -ICOS-CDE ₁₇ -ss	KL	minimal ICOS-CDE element (ICOS-minCDE), <i>AgeI/XbaI</i> -site cloned, <i>EcoRI/BglII</i> -transferred into puroMX β
p2992	puroMX β -ICOS-minCDE-nc	KL	minimal ICOS-CDE element in native context (ICOS-minCDE-nc), <i>AgeI/XbaI</i> -site cloned, <i>EcoRI/BglII</i> -transferred into puroMX β
p2985	pLNCX2-EGFP-RC3H2	SR	full-length Roquin2 cDNA cloned via <i>SalI/ClaI</i> into pLNCX2 (Clontech), EGFP was <i>SalI</i> -cloned from p2838 into pLNCX2-Roquin2 (p2984)
p3090	pLNCX2-EGFPA-RC3H1	FP	EGFP was <i>SalI</i> -exsized from p2838 and replaced with PCR-amplified EGFP with a unique 3' <i>AgeI</i> site into pLNCX2-EGFP-Roquin (p2838)
p3101	pLNCX2-EGFPA-RC3H1-S60r	FP	four silent point mutations in the RC3H1 N-terminus were introduced by cloning a PCR fragment into <i>AgeI/MfeI</i> of p3090; resistant to siRNA S060

6.1.6 DNA Oligonucleotides

The following oligonucleotides were used in this study.

Table 6.6: DNA Oligonucleotides Used in this Study. All DNA oligonucleotides used for cloning and RT-qPCR are listed in the table. F, forward primer; R, reverse primer.

Name	Sequence	Description
G014	GTGCTGGTTATTGTGCTG	sequencing β -globin exon 3, F
G37	AATTGAATTCGGATCCCTAAGTCCAAC	F, forward primer for cloning of 6xMS2bs (Jens Lykke-Andersen)
G38	AATTGAATTCAGATCTCCCACTAGACAGC	R, reverse primer for cloning of 6xMS2bs (Jens Lykke-Andersen)
G95	GATCTCCCAGCAGTAAGGGTTTCCATATAAA CTCCTTATTTCTACG	PP7bs F, <i>BamHI</i> and <i>BglIII</i> compatible
G96	GATCCGTAGAAATAAGGAGTTTATATGGAAA CCCTTACTGCTGGGA	PP7bs R, <i>BamHI</i> and <i>BglIII</i> compatible

6.1 Materials Used in this Study

Name	Sequence	Description
G078	GGTGGTCGGAAAGCTATC	S7 probe F
G083	TTACAAAGTCACTCAGGATG	Ncl probe R
G311	AAGCTATCCCACAAATTG	sequencing out of GST, F
G314	TTAAGCTAGCAGGGAATGGG	mouse TNF α probe F
G316	GCCGATTTAGGTGACACTATAGAATACTGGCTCTGTGAGG	mouse TNF α probe R
G1000	GTGCATCTGTCCAGTG	globin probe R
G1001	GCCGATTTAGGTGACACTATAGAATACCCTGAAGTTCTC	globin probe F
G1008	GCCGATTTAGGTGACACTATAGAATACTATAGACACCAG	S7 probe R
G1009	GCCGATTTAGGTGACACTATAGAATACTTAGCGTCTTCG	Ncl probe F
G1612	CCCAAGCTTGATATCATCCACCATGGTGAGCAAG	EGFP F, <i>HindIII-EcoRV</i>
G1613	TTAAGGTACCCTTGACAGCTCGTCCATGCCGAG	EGFP R, <i>KpnI</i>
G1706	AGGGGGCAGAAATTGATGGACGAT	mouse Ncl qPCR F
G1707	TGGGTTCTGGGGCACTTTG	mouse Ncl qPCR R
G1712	GAGCGGGCCGTGGTGTC	mouse Ier3 qPCR F
G1713	CTTGGCAATGTTGGGTTCCCTC	mouse Ier3 qPCR R
G1779	gatccgtagaaaACCGACCAGAATCATGCAAGTGCGTAAGATAGTCCGGGCCGGGctgctggga	S1 aptamer F, <i>BamHI</i> and <i>BglII</i> compatible
G1780	gatctcccagcagCCCGCCCCGCGACTATCTTACGCACTTGCATGATTCTGGTCCGGTtttctacg	S1 aptamer R, <i>BamHI</i> and <i>BglII</i> compatible
G1844	TGCCTATGTCTCAGCCTCTTC	mouse TNF α qPCR F
G1845	GAGGCCATTTGGGAACCTCT	mouse TNF α qPCR R
G1850	gatccgtagaaaATGCGGCCCGCCGACCAGAATCATGCAAGTGCCTAAGATAGTCCGGGTCGGCGGCCGCATctgctggga	S1m aptamer F (15 bp stem, mismatch repair), <i>BamHI</i> and <i>BglII</i> compatible
G1851	gatctcccagcagATGCGGCCCGCCGACCCGCGACTATCTTACGCACTTGCATGATTCTGGTCCGGCGGCCGCATtttctacg	S1m aptamer R (15 bp stem, mismatch repair), <i>BamHI</i> and <i>BglII</i> compatible
G1852	gatccGAAAACCTCTACTTCCAAGGGa	TEV cleavage site F, <i>BamHI</i> and <i>BglII</i> compatible
G1853	gatctCCCTTGGAAGTAGAGGTTTTTCg	TEV cleavage site R, <i>BamHI</i> and <i>BglII</i> compatible
G1854	TTGAGATGAGGATAAAATACTCTGAGTCC	β -globin exon 3 For (in single intron region, for colony-PCR)
G1855	ATATGTCCTTCCGAGTGAGAGACAC	β -globin 3'UTR R (colony-PCR)
G1859	atgcGAATTCATGTCCAAAACCATCGTTCTTTTC	F, PP7cp (David Peabody), <i>EcoRI</i>
G1860	atgcCTCGAGTTAACGGCCAGCGGC	R, PP7cp (David Peabody), <i>XhoI</i>

Name	Sequence	Description
G1861	atgcGAATTCATGGCCAAAACCATCGTTCTT	F, oPP7cp (Kathleen Collins), <i>EcoRI</i>
G1875	gatccGAGAACCTCTACTTCCAGGGCg	TEV cleavage site F, <i>BamHI</i> and <i>EcoRI</i> compatible
G1876	aattcGCCCTGGAAGTAGAGGTTCTCg	TEV cleavage site R, <i>BamHI</i> and <i>EcoRI</i> compatible
G1899	atgcGAATTCATGGCTTCTAACTTTACTCAGTTTCGTT	MS2cp F, <i>EcoRI</i> -site attached
G1900	atgcCTCGAGTTAGTAGATGCCGAGTTTGCT	MS2cp R, <i>XhoI</i> -site attached
G1918	GGGCTTCATGATGTCCCC	R, reverse primer for S1m cloning into puroMX8, downstream of aptamer tags
G1919	CTTATTATTTATTATTATTATTATTATTATT GAGATCTGTAG	F, mismatch repair forward primer reconstituting <i>BglII</i> site
G2053	ACTCCACTCACGGCAAATTC AACG	mouse <i>Gapdh</i> qPCR F
G2054	AAGACACCAGTAGACTCCACGACA	mouse <i>Gapdh</i> qPCR R
G2181	CAGGTGAACACCACGGATT	mouse <i>Nfkbiz</i> qPCR F
G2182	CTCACAGCTCCCTTCTGGAT	mouse <i>Nfkbiz</i> qPCR R
G2199	ATATTCGTGAACATAAAGGCAAGA	mouse <i>Nfkbid</i> qPCR F
G2200	TCAGTGGCGTTAGGCTCTG	mouse <i>Nfkbid</i> qPCR R
G2234	CCAAGTAATACGACTCACTATAGGCCTGGCTCACA AATACCACTG	pT7-in-line F
G2235	AATTTTTGGCAGAGGGAAAAAG	in-line R
G2247	CTCACAAATACCACTGGGATCC	F, <i>BamHI</i> repair forward primer
G2332	CCAAGTAATACGACTCACTATAGGTTTGGAAAGGCC GGGGT	pT7-CDE ₁₅₀ mouse in-line F
G2333	ATAAATATTTGTTTTAAACATAAGCAAAAGAG	CDE ₁₅₀ mouse in-line R
G2364	CATGGCTGCAACACTTACACAGCA	mouse <i>Nupl1</i> qPCR F
G2365	ATTGCAAGCCAGTGCCAATACCTG	mouse <i>Nupl1</i> qPCR R
G2392	TTGTACCTGAAGCCACTCAGCAGT	mouse <i>Roquin</i> qPCR F
G2393	TCCACTAGCTGGCAATGAACCAGA	mouse <i>Roquin</i> qPCR R
G2394	TGCCATTCTCAGGAAGAGCTTGA	mouse <i>Roquin2</i> qPCR F
G2395	GCTGTGGTTGTGACAGTGCTGTTT	mouse <i>Roquin2</i> qPCR R
G2421	TGGACACAGTATCATACCCAGAAAACACCTGT CTCTTCAACTCTTCTGTGGCCA	mouse <i>Roquin2</i> cDNA F
G2427	GATCATCGATTTCAGCTGTTAACCATCTTCCCA	mouse <i>Roquin2-ClaI</i> cDNA R
G2495	GATCGGATCCTTTGGAAAGCCGGGGT	CDE ₁₅₀ - <i>BamHI</i> -outF
G2496	GATCAGATCTATAAATATTTGTTTTAAACATAA GCAAAAGAG	CDE ₁₅₀ -outR- <i>BglII</i>
G2497	TTCTGTGAAATGGGAGCTGAG	CDE ₁₅₀ -M16 F
G2498	TTTCACAGAAAACATGTCTGTCTGA	CDE ₁₅₀ -M16 R
G2501	GACAGACATCATTCTGTGAAATGGGA	CDE ₁₅₀ -M20 F

6.2 Permission Statements

Name	Sequence	Description
G2502	ATGTCTGTCTGAAGACAGCTTCC	CDE ₁₅₀ -M20 R
G2554	AAACTAGTATGCGCCGAGATTTACGA	Roquin2 cDNA C413R F
G2555	CATACTAGTTTTTATACTTGCTGTTTGGCTG	Roquin2 cDNA C413R R
G2556	GATCCAATTGTTTTGCAGCGAACTG	Roquin2-MfeI cDNA F
G2576	AACATACATGCGTCGAGATATGAAG	Roquin cDNA C419R F
G2577	CATGTATGTTTTGTATTTGCTATGCTGT	Roquin cDNA C419R R
G2579	GATCCACATGGTGGTGGAGTATAGTACATACC	Roquin- <i>Dra</i> III cDNA R
G2592	TTCCCCCTGTTGAAGTTCC	mouse Ppp1r10 qPCR F
G2593	CTTGCGAGTCAGCTGGTTG	mouse Ppp1r10 qPCR R
G2622	GATACTGTGTCCACTGATCTGGC	<i>Bst</i> XI-Roquin2 cDNA R
G2623	TCATTTGCACAGAGTGTTCAGG	Roquin- <i>Dra</i> III cDNA F
G2723	TGACCTGGGCCTAGCTGTTA	mouse Bmpr1a qPCR F
G2724	TTCAGGCTTTCATCCAGCA	mouse Bmpr1a qPCR R
G2729	CTCACATCCTGGACACTGGA	mouse Pdia6 qPCR F
G2730	ACTGGGCTCCAGCTTCTGT	mouse Pdia6 qPCR R
G2737	TGTTGGCCCTCTATGAATCTG	mouse Hmgxb3 qPCR F
G2738	TGGAACCACAGACCACCTG	mouse Hmgxb3 qPCR R
G2747	TTCATCGTATTGGAAGATCAGG	mouse Rck qPCR F
G2748	TTGGGATGGGTTTGATCTCT	mouse Rck qPCR R
G2788	AGGGACCGGTGTCGACC	<i>Age</i> I- <i>Sal</i> I-Roquin flanking fr1 F
G2789	AGAGCAATTGTTAGCTCCTGAACA	<i>Mfe</i> I-Roquin flanking fr2 R
G2790	GTGACCGAACTGATTCTCCAGCACCAG	siRNA-resistant Roquin fr2 F
G2791	CAGTTCGGTCACTGTGCGTTCACCTAAAG	siRNA-resistant Roquin fr1 R
G2840	ATTAATCGATCTATTCCCTGTGAATGTG	<i>Cla</i> I-Stop-N-term R
G2842	TTATACCGGTGGAAGTGGAAAAG	Roquin C-term F
G2843	GTCCCACGTGGAATCAGTTG	Roquin C-term R
G2855	TTATACCGGTGCGCCCAATGCAGAGGAA	ROQ- <i>Age</i> I F
G2856	TATAATCGATGAGTAACTCCAAATGGGGTCTTAG	ROQ- <i>Cla</i> I R

6.2 Permission Statements

The following License Agreements were obtained from Cell Press, Elsevier and Nucleic Acids Research, Oxford University Press, respectively. These permission statements document that I have the right to use the material (figures and text) for the purpose of reproduction in this thesis from two respective publications in Cell and Nucleic Acids Research, of both of which I am the first author.

6.2.1 Permission from Cell Press, Elsevier

Publication: Kathrin Leppek, Johanna Schott, Sonja Reitter, Fabian Poetz, Ming C. Hammond, and Georg Stoecklin. Roquin promotes constitutive mRNA decay via a conserved class of stem-loop recognition motifs. *Cell*, Elsevier; 153(4):869–881, May 2013.

ELSEVIER LICENSE TERMS AND CONDITIONS

Sep 18, 2013

This is a License Agreement between Kathrin Leppek ("You") and Elsevier ("Elsevier") provided by Copyright Clearance Center ("CCC"). The license consists of your order details, the terms and conditions provided by Elsevier, and the payment terms and conditions.

All payments must be made in full to CCC. For payment instructions, please see information listed at the bottom of this form.

Supplier	Elsevier Limited The Boulevard, Langford Lane Kidlington, Oxford, OX5 1GB, UK
Registered Company Number	1982084
Customer name	Kathrin Leppek
Customer address	Im Neuenheimer Feld 280 Heidelberg, None 69120
License number	3225391062647
License date	Sep 10, 2013
Licensed content publisher	Elsevier
Licensed content publication	Cell
Licensed content title	Roquin Promotes Constitutive mRNA Decay via a Conserved Class of Stem-Loop Recognition Motifs
Licensed content author	Kathrin Leppek, Johanna Schott, Sonja Reitter, Fabian Poetz, Ming C. Hammond, Georg Stoecklin
Licensed content date	9 May 2013
Licensed content volume number	153
Licensed content issue number	4
Number of pages	13
Start Page	869
End Page	881
Type of Use	reuse in a thesis/dissertation
Portion	full article
Format	both print and electronic
Are you the author of this Elsevier article?	Yes
Will you be translating?	No
Order reference number	None
Title of your thesis/dissertation	Roquin Promotes Constitutive mRNA Decay via a Conserved Class of Stem-Loop Recognition Motifs
Expected completion date	Dec 2013
Estimated size (number of pages)	100
Customer Tax ID	32082-01782
Elsevier VAT number	GB 494 6272 12
Permissions price	0.00 EUR
VAT/Local Sales Tax	0.0 USD / 0.0 GBP

6.2 Permission Statements

Total

0.00 EUR

Terms and Conditions

INTRODUCTION

1. The publisher for this copyrighted material is Elsevier. By clicking "accept" in connection with completing this licensing transaction, you agree that the following terms and conditions apply to this transaction (along with the Billing and Payment terms and conditions established by Copyright Clearance Center, Inc. ("CCC"), at the time that you opened your Rightslink account and that are available at any time at <http://myaccount.copyright.com>).

GENERAL TERMS

2. Elsevier hereby grants you permission to reproduce the aforementioned material subject to the terms and conditions indicated.
3. Acknowledgement: If any part of the material to be used (for example, figures) has appeared in our publication with credit or acknowledgement to another source, permission must also be sought from that source. If such permission is not obtained then that material may not be included in your publication/copies. Suitable acknowledgement to the source must be made, either as a footnote or in a reference list at the end of your publication, as follows:
"Reprinted from Publication title, Vol /edition number, Author(s), Title of article / title of chapter, Pages No., Copyright (Year), with permission from Elsevier [OR APPLICABLE SOCIETY COPYRIGHT OWNER]." Also Lancet special credit - "Reprinted from The Lancet, Vol. number, Author(s), Title of article, Pages No., Copyright (Year), with permission from Elsevier."
4. Reproduction of this material is confined to the purpose and/or media for which permission is hereby given.
5. Altering/Modifying Material: Not Permitted. However figures and illustrations may be altered/adapted minimally to serve your work. Any other abbreviations, additions, deletions and/or any other alterations shall be made only with prior written authorization of Elsevier Ltd. (Please contact Elsevier at permissions@elsevier.com)
6. If the permission fee for the requested use of our material is waived in this instance, please be advised that your future requests for Elsevier materials may attract a fee.
7. Reservation of Rights: Publisher reserves all rights not specifically granted in the combination of (i) the license details provided by you and accepted in the course of this licensing transaction, (ii) these terms and conditions and (iii) CCC's Billing and Payment terms and conditions.
8. License Contingent Upon Payment: While you may exercise the rights licensed immediately upon issuance of the license at the end of the licensing process for the transaction, provided that you have disclosed complete and accurate details of your proposed use, no license is finally effective unless and until full payment is received from you (either by publisher or by CCC) as provided in CCC's Billing and Payment terms and conditions. If full payment is not received on a timely basis, then any license preliminarily granted shall be deemed automatically revoked and shall be void as if never granted. Further, in the event that you breach any of these terms and conditions or any of CCC's Billing and Payment terms and conditions, the license is automatically revoked and shall be void as if never granted. Use of materials as described in a revoked license, as well as any use of the materials beyond the scope of an unrevoked license, may constitute copyright infringement and publisher reserves the right to take any and all action to protect its copyright in the materials.
9. Warranties: Publisher makes no representations or warranties with respect to the licensed material.
10. Indemnity: You hereby indemnify and agree to hold harmless publisher and CCC, and their respective officers, directors, employees and agents, from and against any and all claims arising out of your use of the licensed material other than as specifically authorized pursuant to this license.
11. No Transfer of License: This license is personal to you and may not be sublicensed, assigned, or transferred by you to any other person without publisher's written permission.
12. No Amendment Except in Writing: This license may not be amended except in a writing signed by both parties (or, in the case of publisher, by CCC on publisher's behalf).
13. Objection to Contrary Terms: Publisher hereby objects to any terms contained in any purchase order, acknowledgment, check endorsement or other writing prepared by you, which terms are inconsistent with these terms and conditions or CCC's Billing and Payment terms and conditions. These terms and conditions, together with CCC's Billing and Payment terms and conditions (which are incorporated herein), comprise the entire agreement between you and publisher (and CCC) concerning this licensing transaction. In the event of any conflict between your obligations established by these terms and conditions and those established by CCC's Billing and Payment terms and conditions, these terms and conditions shall control.
14. Revocation: Elsevier or Copyright Clearance Center may deny the permissions described in this License at their sole discretion, for any reason or no reason, with a full refund payable to you. Notice of such denial will be made using the contact information provided by you. Failure to receive such notice will not alter or invalidate the denial. In no event will Elsevier or Copyright Clearance Center be responsible or liable for any costs, expenses or damage incurred by you as a result of a denial of your permission request, other than a refund of the amount(s) paid by you to Elsevier and/or Copyright Clearance Center for denied permissions.

LIMITED LICENSE

The following terms and conditions apply only to specific license types:

15. **Translation:** This permission is granted for non-exclusive world **English** rights only unless your license was granted for translation rights. If you licensed translation rights you may only translate this content into the languages you requested. A professional translator must perform all translations and reproduce the content word for word preserving the integrity of the article. If this license is to re-use 1 or 2 figures then permission is granted for non-exclusive world rights in all languages.
16. **Website:** The following terms and conditions apply to electronic reserve and author websites:
Electronic reserve: If licensed material is to be posted to website, the web site is to be password-protected and made

available only to bona fide students registered on a relevant course if:

This license was made in connection with a course.

This permission is granted for 1 year only. You may obtain a license for future website posting.

All content posted to the web site must maintain the copyright information line on the bottom of each image.

A hyper-text must be included to the Homepage of the journal from which you are licensing at <http://www.sciencedirect.com/science/journal/xxxx> or the Elsevier homepage for books at <http://www.elsevier.com> , and

Central Storage: This license does not include permission for a scanned version of the material to be stored in a central repository such as that provided by Heron/XanEdu.

17. **Author website** for journals with the following additional clauses:

All content posted to the web site must maintain the copyright information line on the bottom of each image, and the

permission granted is limited to the personal version of your paper. You are not allowed to download and post the published

electronic version of your article (whether PDF or HTML, proof or final version), nor may you scan the printed edition to

create an electronic version. A hyper-text must be included to the Homepage of the journal from which you are licensing at

<http://www.sciencedirect.com/science/journal/xxxx> . As part of our normal production process, you will receive an e-mail

notice when your article appears on Elsevier's online service ScienceDirect (www.sciencedirect.com). That e-mail will include

the article's Digital Object Identifier (DOI). This number provides the electronic link to the published article and should be

included in the posting of your personal version. We ask that you wait until you receive this e-mail and have the DOI to do

any posting.

Central Storage: This license does not include permission for a scanned version of the material to be stored in a central

repository such as that provided by Heron/XanEdu.

18. **Author website** for books with the following additional clauses:

Authors are permitted to place a brief summary of their work online only.

A hyper-text must be included to the Elsevier homepage at <http://www.elsevier.com> . All content posted to the web site must

maintain the copyright information line on the bottom of each image. You are not allowed to download and post the published

electronic version of your chapter, nor may you scan the printed edition to create an electronic version.

Central Storage: This license does not include permission for a scanned version of the material to be stored in a central

repository such as that provided by Heron/XanEdu.

19. **Website** (regular and for author): A hyper-text must be included to the Homepage of the journal from which you are

licensing at <http://www.sciencedirect.com/science/journal/xxxx> . or for books to the Elsevier homepage at

<http://www.elsevier.com>

20. **Thesis/Dissertation**: If your license is for use in a thesis/dissertation your thesis may be submitted to your institution in

either print or electronic form. Should your thesis be published commercially, please reapply for permission. These

requirements include permission for the Library and Archives of Canada to supply single copies, on demand, of the complete

thesis and include permission for UMI to supply single copies, on demand, of the complete thesis. Should your thesis be

published commercially, please reapply for permission.

21. **Other Conditions**:

v1.6

If you would like to pay for this license now, please remit this license along with your payment made payable to "COPYRIGHT CLEARANCE CENTER" otherwise you will be invoiced within 48 hours of the license date. Payment should be in the form of a check or money order referencing your account number and this invoice number RLNK501109416.

Once you receive your invoice for this order, you may pay your invoice by credit card. Please follow instructions provided at that time.

Make Payment To:

Copyright Clearance Center

Dept 001

P.O. Box 843006

Boston, MA 02284-3006

For suggestions or comments regarding this order, contact RightsLink Customer Support:

customercare@copyright.com or +1-877-622-5543 (toll free in the US) or +1-978-646-2777.

Gratis licenses (referencing \$0 in the Total field) are free. Please retain this printable license for your reference. No payment is required.

6.2 Permission Statements

6.2.2 Permission from Oxford University Press

Publication: Kathrin Leppek and Georg Stoecklin. An optimized streptavidin-binding RNA aptamer for purification of ribonucleoprotein complexes identifies novel ARE-binding proteins. *Nucleic Acids Research*, Oxford Journals; doi: 10.1093/nar/gkt956, October 2013.

OXFORD UNIVERSITY PRESS LICENSE TERMS AND CONDITIONS

Oct 24, 2013

This is a License Agreement between Kathrin Leppek ("You") and Oxford University Press ("Oxford University Press") provided by Copyright Clearance Center ("CCC"). The license consists of your order details, the terms and conditions provided by Oxford University Press, and the payment terms and conditions.

All payments must be made in full to CCC. For payment instructions, please see information listed at the bottom of this form.

License Number	3255321358583
License date	Oct 24, 2013
Licensed content publisher	Oxford University Press
Licensed content publication	Nucleic Acids Research
Licensed content title	An optimized streptavidin-binding RNA aptamer for purification of ribonucleoprotein complexes identifies novel ARE-binding proteins:
Licensed content author	Kathrin Leppek, Georg Stoecklin
Licensed content date	10/23/2013
Type of Use	Thesis/Dissertation
Institution name	None
Title of your work	Roquin Promotes Constitutive mRNA Decay via a Conserved Class of Stem-Loop Recognition Motifs
Publisher of your work	n/a
Expected publication date	Dec 2013
Permissions cost	0.00 EUR
Value added tax	0.00 EUR
TotalTotal	0.00 EUR
TotalTotal	0.00 EUR
Terms and Conditions	

STANDARD TERMS AND CONDITIONS FOR REPRODUCTION OF MATERIAL FROM AN OXFORD UNIVERSITY PRESS JOURNAL

1. Use of the material is restricted to the type of use specified in your order details.
2. This permission covers the use of the material in the English language in the following territory: world. If you have requested additional permission to translate this material, the terms and conditions of this reuse will be set out in clause 12.
3. This permission is limited to the particular use authorized in (1) above and does not allow you to sanction its use elsewhere in any other format other than specified above, nor does it apply to quotations, images, artistic works etc that have been reproduced from other sources which may be part of the material to be used.
4. No alteration, omission or addition is made to the material without our written consent. Permission must be re-cleared with Oxford University Press if/when you decide to reprint.
5. The following credit line appears wherever the material is used: author, title, journal, year, volume, issue number, pagination, by permission of Oxford University Press or the sponsoring society if the journal is a society journal. Where a journal is being published on behalf of a learned society, the details of that society must be included in the credit line.
6. For the reproduction of a full article from an Oxford University Press journal for whatever purpose, the corresponding author of the material concerned should be informed of the proposed use. Contact details for the corresponding authors of all Oxford University Press journal contact can be found alongside either the abstract or full text of the article concerned, accessible from www.oxfordjournals.org Should there be a problem clearing these rights, please contact journals.permissions@oup.com
7. If the credit line or acknowledgement in our publication indicates that any of the figures, images or photos was reproduced, drawn or modified from an earlier source it will be necessary for you to clear this permission with the original publisher as well. If this permission has not been obtained, please note that this material cannot be included in your publication/photocopies.

8. While you may exercise the rights licensed immediately upon issuance of the license at the end of the licensing process for the transaction, provided that you have disclosed complete and accurate details of your proposed use, no license is finally effective unless and until full payment is received from you (either by Oxford University Press or by Copyright Clearance Center (CCC)) as provided in CCC's Billing and Payment terms and conditions. If full payment is not received on a timely basis, then any license preliminarily granted shall be deemed automatically revoked and shall be void as if never granted. Further, in the event that you breach any of these terms and conditions or any of CCC's Billing and Payment terms and conditions, the license is automatically revoked and shall be void as if never granted. Use of materials as described in a revoked license, as well as any use of the materials beyond the scope of an unrevoked license, may constitute copyright infringement and Oxford University Press reserves the right to take any and all action to protect its copyright in the materials.
9. This license is personal to you and may not be sublicensed, assigned or transferred by you to any other person without Oxford University Press's written permission.
10. Oxford University Press reserves all rights not specifically granted in the combination of (i) the license details provided by you and accepted in the course of this licensing transaction, (ii) these terms and conditions and (iii) CCC's Billing and Payment terms and conditions.
11. You hereby indemnify and agree to hold harmless Oxford University Press and CCC, and their respective officers, directors, employs and agents, from and against any and all claims arising out of your use of the licensed material other than as specifically authorized pursuant to this license.
12. Other Terms and Conditions:
v1.4

If you would like to pay for this license now, please remit this license along with your payment made payable to "COPYRIGHT CLEARANCE CENTER" otherwise you will be invoiced within 48 hours of the license date. Payment should be in the form of a check or money order referencing your account number and this invoice number RLNK501143028.

Once you receive your invoice for this order, you may pay your invoice by credit card. Please follow instructions provided at that time.

**Make Payment To:
Copyright Clearance Center
Dept 001
P.O. Box 843006
Boston, MA 02284-3006**

**For suggestions or comments regarding this order, contact RightsLink Customer Support:
customercare@copyright.com or +1-877-622-5543 (toll free in the US) or +1-978-646-2777.**

Gratis licenses (referencing \$0 in the Total field) are free. Please retain this printable license for your reference. No payment is required.
